



HAL
open science

Cyclodextrin-based photoactive liposomal nanoparticles for tumor targeting

Ilya Yakavets

► **To cite this version:**

Ilya Yakavets. Cyclodextrin-based photoactive liposomal nanoparticles for tumor targeting. Life Sciences [q-bio]. Université de Lorraine; Belarusian State University (Minsk, Biélorussie), 2019. English. NNT : 2019LORR0138 . tel-02461205

HAL Id: tel-02461205

<https://hal.univ-lorraine.fr/tel-02461205v1>

Submitted on 30 Jan 2020

HAL is a multi-disciplinary open access archive for the deposit and dissemination of scientific research documents, whether they are published or not. The documents may come from teaching and research institutions in France or abroad, or from public or private research centers.

L'archive ouverte pluridisciplinaire **HAL**, est destinée au dépôt et à la diffusion de documents scientifiques de niveau recherche, publiés ou non, émanant des établissements d'enseignement et de recherche français ou étrangers, des laboratoires publics ou privés.



AVERTISSEMENT

Ce document est le fruit d'un long travail approuvé par le jury de soutenance et mis à disposition de l'ensemble de la communauté universitaire élargie.

Il est soumis à la propriété intellectuelle de l'auteur. Ceci implique une obligation de citation et de référencement lors de l'utilisation de ce document.

D'autre part, toute contrefaçon, plagiat, reproduction illicite encourt une poursuite pénale.

Contact : ddoc-theses-contact@univ-lorraine.fr

LIENS

Code de la Propriété Intellectuelle. articles L 122. 4

Code de la Propriété Intellectuelle. articles L 335.2- L 335.10

http://www.cfcopies.com/V2/leg/leg_droi.php

<http://www.culture.gouv.fr/culture/infos-pratiques/droits/protection.htm>

ACKNOWLEDGEMENTS

I would like to express my sincere gratitude to my advisor **Dr. Vladimir Zorin** for intellectual encouragement, scientific advice and discussions and guidance, and for steering me in the right direction. We have worked together for 7 long years, - 3 years at the university, my Master's degree, and PhD years, which in totality were the making years for me as a researcher.

My sincere thanks also goes to my advisor **Dr. Lina Bolotina**, for giving me the opportunity to join their team as intern, for her time and for long discussions of the research problems as well as of the research articles in the process of writing, and for directing me to the exciting world of the European science. I could not have imagined having a better advisor and mentor for my Ph.D study.

My research benefited significantly from the help of **Dr. Henri-Pierre Lassalle**, for the continuous support of my Ph.D study and related research. His guidance helped me continuously during my research and writing of this thesis.

I am indebted to **Prof. Sandy MacRobert** for accepting to review my thesis manuscript. His big experience in bio- and photophysics, formidable commentaries and questions has greatly contributed to the finalization of this work. I thank you for your keen interest in this thesis, and for giving me a wonderful opportunity to discuss it with you.

I am very grateful to **Dr. Andrey Klymchenko** for reviewing my thesis manuscript. It was an honor for me to have my work evaluated by this distinguished scientist, and I have profited greatly from his insightful and profound questions on the work.

I would like to thank the rest of my thesis committee: **Prof. Geneviève Ubeaud-Sequier**, **Prof. Vladimir Kostyuk**, and **Dr. Ariane Boudier**, for their kind and gracious acceptance to take part in the thesis defense as a member of the jury, for their insightful comments and fundamental discussion that we have had during the defense.

During my PhD years, I had the pleasure of working with several outstanding researchers, to whom I would like to express my gratitude. I thank **Ms. Aurélie François** and **Mrs. Laureline Lamy** for the indispensable experience in cell cultures and animal experimentation. I am very grateful to the members of the Research Laboratory of Biophysics and Biotechnology of Belarusian State University – **Dr. Tatiana Zorina**, **Mrs. Irina Kravchenko** and **Dr. Ivan Khludkev**. They were actively involved in teaching me the fundamentals of laboratory research work, spectroscopy and chromatography experiments. I will always remember the warm atmosphere of the laboratory created by these devoted scientists.

I thank my fellow labmates **Dr. Marie Millard** and **Dr. Tristan Mangeolle** for the stimulating discussions, my friends **Dr. Igor Yankovsky** and **Dr. Estelle Bastien** for the sleepless nights we were working together before deadlines, and for all the fun we have had working together. Besides, I am also very grateful to **Mrs. Dominique Leprince** for her assistance throughout my dissertation.

Last but not the least, I would like to thank my family: my parents **Vladimir** and **Sviatlana** and wife **Vera** for supporting me spiritually throughout writing this thesis and my life in general.

TABLE OF CONTENTS

ACKNOWLEDGEMENTS.....	2
TABLE OF CONTENTS	4
ABBREVIATIONS	5
LIST OF FIGURES.....	6
LIST OF TABLES.....	7
GENERAL INTRODUCTION.....	8
CHAPTER I. INTRODUCTION.....	10
1. Photodynamic therapy.....	10
1.1. History and basic principles.....	10
1.2. Basis of PDT therapy	11
1.3. Mechanisms of PDT action.....	13
1.4. Light sources.....	16
1.5. Photosensitizers.....	18
2. Meta-tetra(hydroxyphenyl)chlorin.....	21
2.1. General properties and usage	21
2.2. Uptake and localization	23
2.3. Biodistribution and pharmacokinetic properties	24
2.4. Nanoscale delivery systems.....	26
3. Drug-in-cyclodextrin-in-liposome (DCL) nanoplatfom	47
3.1. Liposomes.....	47
3.2. Cyclodextrin-based inclusion complexes.....	51
3.3. DCL.....	57
OBJECTIVES.....	62
CHAPTER II. CD INCLUSION COMPLEXES	64
4. Characterization of inclusion complex formation.....	64
5. Development of spectral techniques for monitoring the distribution of inclusion complexes	74
6. Nanoshuttle mechanism of mTHPC delivery.....	83
CHAPTER III. MTHPC-IN-CYCLODEXTRINS-IN-LIPOSOME	92
7. Development and optimization of mTHPC-DCL	92
8. Double loaded mTHPC-DCL	108
GENERAL DISCUSSION.....	126
CONCLUSION AND PERSPECTIVES	130
REFERENCES.....	128
SCIENTIFIC OUTPUT.....	150
SYNTHESE DES TRAVAUX DE THESE	154

ABBREVIATIONS

5-ALA	– 5-Aminolevulinic Acid
AIPCS ₄	– sulfonated aluminum phthalocyanines
ATMPn	– 9-Acetoxy-2,7,12,17-tetrakis-(β-methoxyethyl)-porphycene
CD	– cyclodextrin
Chl e ₆	– chlorin e ₆
DCL	– drug-in-CD-in-liposome
DL-DCL	– double-loaded drug-in-CD-in-liposome
DLI	– drug-light interval
DS	– degree of substitution
ε	– extinction coefficient
EE	– encapsulation efficiency
EPR	– enhanced permeability and retention
FDA	– Food and Drug Administration
GUV	– giant unilamellar vesicles
HAL	– hethyl aminolevulinate
HDL	– high-density lipoproteins
Hp-β-CD	– hydroxypropyl-β-cyclodextrin
IV	– intravenous
K	– association constant
LUV	– large unilamellar vesicles
LDL	– low-density lipoprotein
logP	– octanol-water partition coefficient
MAL	– methyl aminolevulinate
MD	– methyl-β-cyclodextrin-based DL-DCL
Me-β-CD	– methyl-β-cyclodextrin
MLV	– multilamellar vesicles
MPS	– mononuclear phagocyte system
mTHPC	– meta-tetra(hydroxyphenyl)chlorin
¹ O ₂	– singlet oxygen
³ O ₂	– molecular (triplet) oxygen
Pd-Bpheid	– palladium-bacteriopheophorbide
PDT	– photodynamic therapy
PEG	– polyethylene glycol
PS	– photosensitizer
QY	– quantum yield
RES	– reticuloendothelial system
ROS	– reactive oxygen species
SUV	– small unilamellar vesicles
S ₁	– first singlet excited electron orbital
S _n	– singlet n excited electron orbital
T ₁	– first excited triplet state
T _M	– phase transition temperature
TD	– trimethyl-β-cyclodextrin-based DL-DCL
TM-β-CD	– trimethyl-β-cyclodextrin
VD	– volume of distribution

LIST OF FIGURES

Figure 1.1 Schematic illustration of PDT treatment process.....	11
Figure 1.2 Photosensitization Processes Illustrated by a Modified Jablonski Diagram. Reprinted from (Agostinis et al., 2011).	12
Figure 1.3 The main cell death subroutines induced by PDT. Reprinted from (Agostinis et al., 2011).....	13
Figure 1.4 Mechanisms of PDT-mediated photoeradication of tumor mass (from Agostinis et al. 2011)	15
Figure 1.5 Light propagation through the tissues.	17
Figure 1.6 Structural skeletons of porphyrinoid-based PSs (Ben Mihoub et al., 2018)	20
Figure 2.1 (A) Chemical structure of mTHPC. (B) Steric mTHPC conformation.....	21
Figure 3.1 Schematic structure of DCL	47
Figure 3.2 Typical supramolecular equilibria of inclusion complexes with 1:1, 1:2, 2:1 and 2:2 stoichiometries.	54
Figure 3.3 Preparation of DCL by (A) thin-film hydration, (B) ethanol injection, (C) reverse phase evaporation and (D) dehydration-rehydration methods (Gharib et al., 2015).....	58

LIST OF TABLES

Table 1.1. Photosensitizers approved for clinics for PDT (from Agostinis et al., 2011; Dos Santos et al., 2019; Lucky et al., 2015; Ormond and Freeman, 2013)	19
Table 2.1 Photophysical properties of mTHPC in methanol (Bautista-Sanchez et al., 2005; Bonnett et al., 1989)	22
Table 3.1 General CD structures (Ben Mihoub et al., 2018; Stella and He, 2008)	52

GENERAL INTRODUCTION

Photodynamic therapy (PDT) is an alternative cancer treatment which offers a more targeted and less invasive treatment regimen compared to traditional modalities. Over the last decades, it has been demonstrated that the combination of PDT drugs (photosensitizers, PSs) with nanomaterial platforms enable precise delivery of PS to the target tissues improving the PDT effectiveness. Since the most effective PSs tend to be insoluble hydrophobic molecules with a high tendency to aggregate, their encapsulation into nanocarriers could improve their pharmacokinetic properties. Additionally, nanoparticles provide the opportunity for active targeting, control release and multimodal combined therapies.

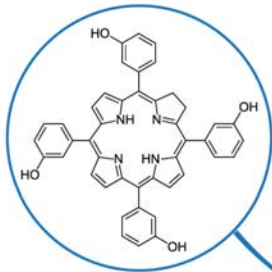
Temoporfin (mTHPC, medicinal product name: Foscan[®]), is one of the most potent clinically approved PS. However, its poor solubility in aqueous medium caused several complications of its administration. Thus, many attempts were done in the application of nanoscale delivery systems for temoporfin delivery. Over the last 25 years, many nanoplateforms such as host-guest inclusion complexes, lipid-and polymer-based nanoparticles and carbon nanotubes were loaded with temoporfin. In particular, liposomal formulation offers an excellent opportunity to achieve selective drug targeting which is expected to optimize the pharmacokinetic parameters, prevent local irritation, and reduce drug toxicity. While, cyclodextrin-based inclusion complexes provide alteration of temoporfin biodistribution.

To improve the transport of mTHPC to target tissue and to strengthen its intra-tissue accumulation, the coupling of two these independent delivery systems was proposed. Thus, the main objective of present work was to develop and optimize temoporfin-loaded drug-in-cyclodextrin-in-liposomes (DCL) nanoconstruct with the aim to achieve synergetic combination of both delivery systems for efficient delivery of mTHPC in the target tumor tissue. With this purpose, the complexation of mTHPC with CDs and behavior of these complexes in 3D tumor tissue *in vitro* model have been studied. In addition, new approaches for analyzing mTHPC release from CDs have been developed to characterize the structure of mTHPC-DCL. *In fine*, the composition of developed mTHPC-DCL have been optimized according to the studies on 2D and 3D *in vitro* tumor models.

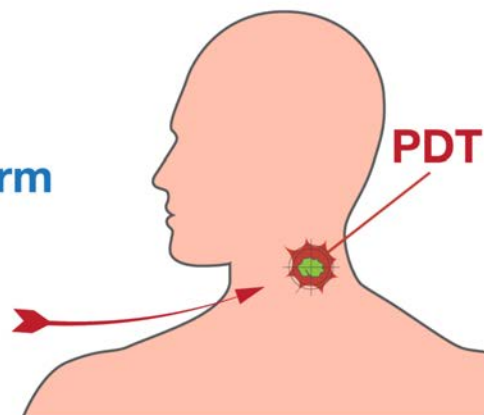
CHAPTER I.

INTRODUCTION

Temoporfin



Nanoplatform



1. Photodynamic therapy

1.1. History and basic principles

Photodynamic therapy (PDT) employs a combination of photosensitizer, light, and molecular oxygen to selectively target cells like tumor cells via cytotoxic activity (Agostinis et al., 2011). Since the Ancient, Indian and Chinese civilizations, PDT has now been in application for the treatment of various diseases including vitiligo, rickets, psoriasis, and skin cancer (Daniell and Hill, 1991). Nowadays, PDT has been clinically utilized for more than 25 years as a cancer treatment. In 1972 Diamond *et al.* published the first medical study on PDT for cancer and introduced hematoporphyrin as a powerful agent for the selective light-mediated killing of glioma cells *in vitro* and tumors *in vivo* (Diamond et al., 1972). In 1960–1970s when new generations of less toxic drugs were developed for diagnosis and treatment of solid tumors, PDT became a hot scientific area attracting many researchers to the field. Already in 1999, PDT was the first drug-device combination approved by the US Food and Drug Administration (FDA) to treat pre-cancerous skin lesions of the face or scalp. Nowadays, numerous clinical studies show potential of PDT, especially in multimodal approach, while preclinical studies indicate there still is a room for improvement on multiple fronts (van Straten et al., 2017).

The action of PDT consists in the interaction of three principal components: (i) a light-absorbing compound that initiates the photochemical reaction, namely photosensitizer (PS), (ii) the light of a specific wavelength and (iii) tissue/molecular oxygen (Dolmans et al., 2003). All together they initiate a photochemical reaction that culminates in the generation of toxic reactive oxygen species (ROS), while individually none of these components is toxic. The ROS can rapidly cause significant toxicity leading to cell death via apoptosis or necrosis (Castano et al., 2005). PDT is a complex procedure which includes the following steps (Figure 1.1). Firstly, PS is administrated topically, locally or systemically (e.g., intravenously, IV). Then, PS redistributes into the body and selectively accumulates into the target tissue. Afterward, the localized illumination of the tumor region is carried out with a light source at emission wavelength corresponding to PS absorbance spectrum. Absorption of this light by tumor-localized sensitizer leads to ROS generation, which finally results in the destruction of malignant tissue (Agostinis et al., 2011). There are three interconnected mechanisms of PDT-mediated tissue destruction: the direct killing of target cells, damage to the vasculature, and induction of an inflammatory reaction that can lead to the immune response (Castano et al., 2006). It worth noting that collateral PDT-damage to healthy tissue can be minimized by the selective PS accumulation in the target tissue, as well as by delivering the light in a

spatially confined and focused manner. This concept of dual selectivity is one of the chief benefits of PDT compared to other treatment modalities.

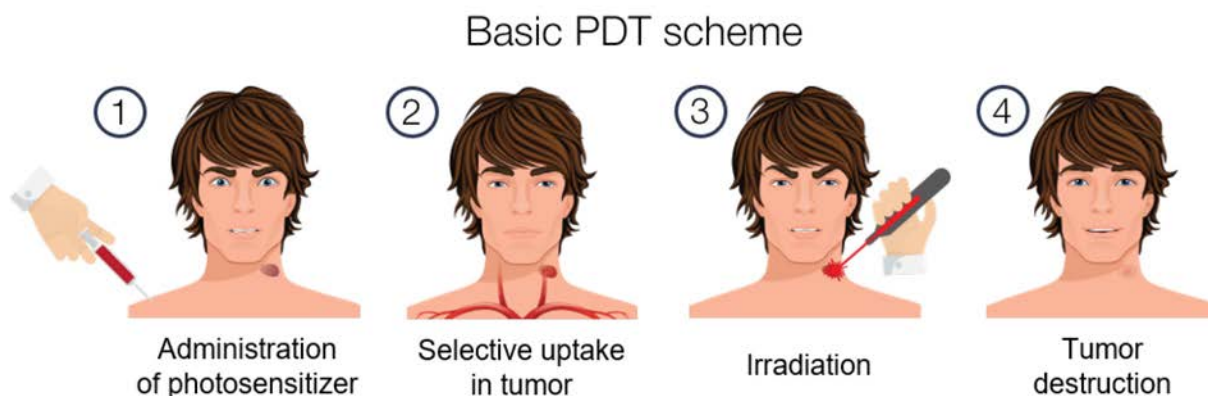


Figure 1.1 Schematic illustration of PDT treatment process

1.2. Basis of PDT therapy

The biological effects of PDT are a consequence of basic photophysical and photochemical reactions involving PS, light, and oxygen, which can be illustrated using a modified Jablonski diagram (Figure 1.2). Most PSs initially are in the ground state (usually singlet) that corresponds to two electrons with opposite spins in the low energy molecular orbital. The initial step of all photoreactions is the absorption of a photon with appropriate wavelength by PS molecule. Following the absorption of the photons, one of the electrons is boosted into a high-energy orbital (S_n , where n depending on the PS and excitation wavelength used) but keeps its spin (excited singlet state). Excited PS molecule will finally fall from a higher excited state S_n to the first excited singlet state S_1 by internal conversion. This process is very fast and takes a fraction of a nanosecond between 10^{-14} and 10^{-11} s, therefore we consider only S_1 on the diagram. The upper excited states may be filled only under the special conditions of multiphoton absorption (short pulse, high intensities of irradiation) leading to the complex photophysical and photochemical processes (Smith et al., 1994). In turn, this singlet state is very unstable and can rapidly return to the ground state level S_0 emitting this excess energy as light (fluorescence) and/or heat (internal conversion). The probability of emitting the energy through the fluorescence pathway is described by the value of quantum yield (QY) of fluorescence as a ratio between emitted photons to the total absorbed photons. It worth noting that fluorescence is widely used for PS detection in photodiagnosis applications (Matoba et al., 2018).

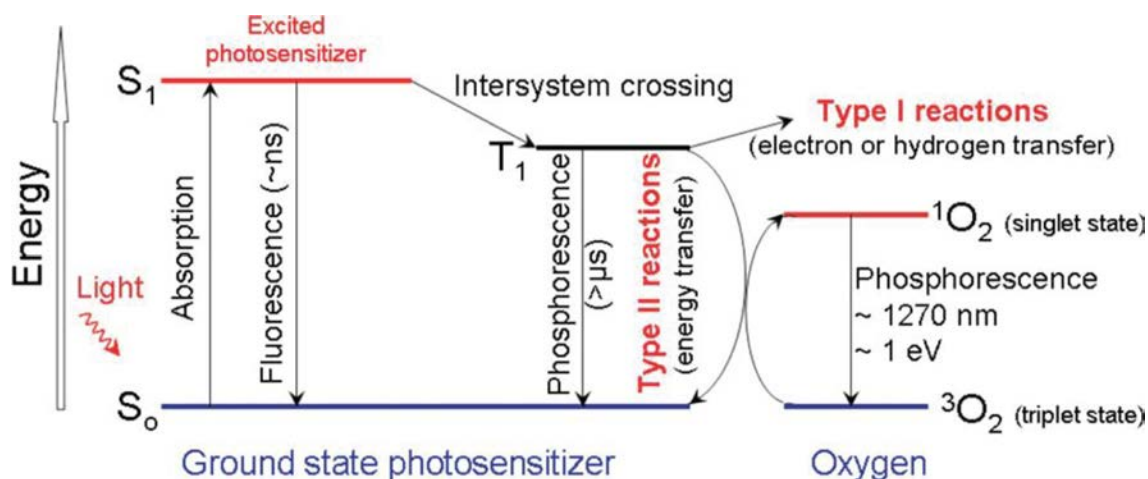


Figure 1.2 Photosensitization Processes Illustrated by a Modified Jablonski Diagram. Reprinted from (Agostinis et al., 2011).

The excited singlet PS' state may also undergo as intersystem crossing whereby the spin of the excited electron inverts forming an excited triplet state (T_1). This triplet state has electron spins parallel and is more stable than singlet one: the lifetime of T_1 is $\tau > 10^{-4}$ s, while $\tau \sim 10^{-9}$ s for the singlet S_1 state. As well as for excited singlet state, PS molecules tend to return to the ground state level S_0 from triplet state T_1 by emitting a photon (phosphorescence) or undergoing non-radiative intersystem crossing followed by vibrational relaxation. The relatively long lifetime of excited triplet state (T_1) increases the probability of a reaction with neighboring substrate molecules making possible the collisional transfer of energy to surrounding oxygen molecules.

There are two various types of photochemical reactions which simultaneously occur during PDT (Figure 1.2). Type I reaction involves the direct reaction of PS with an organic molecule resulting in forming a radical by a hydrogen atom or electron transfer (Henderson and Dougherty, 1992). Type I reactions result in the generation of superoxide anion radical ($O_2^{\cdot-}$), hydrogen peroxide (H_2O_2), oxidant hydroxyl-radical (HO^{\cdot}), etc., which could subsequently participate in different kinds of oxidation reactions.

Type II photochemistry is much simpler. In Type II process, the reaction proceeds via energy transfer from the excited triplet-state PS to the molecular oxygen in its triplet state (3O_2). As a result, highly reactive singlet oxygen (1O_2) is generated. Most PSs are believed to operate via a Type II rather than Type I mechanism. However, only PSs which possessed an energy gap between the ground state and the excited triplet state higher than the energy needed to excite oxygen into its excited singlet state (94.29 kJ/mol according to van Lier & Spikes, 1989) can generate singlet oxygen. The energy limit of 94.29 kJ/mol corresponds to the photon wavelength of 1270 nm, however only PSs which absorb photons with wavelengths longer than 800 nm could generate 1O_2 (Juzeniene et al., 2006).

1.3. Mechanisms of PDT action

The distance of photodynamic damage is limited to the immediate intracellular localization of the PS (Moan et al., 1989) due to the short lifetime $^1\text{O}_2$ (approximately 10-320 ns) and limited diffusion in biological media (up to 100 nm) (Dysart and Patterson, 2005). Singlet oxygen is a very reactive species, much more electrophilic than its ground state, and very rapidly oxidizes closest biomolecules such as proteins and lipids. Hundred nanometers range of its oxidation determined the subcellular level of PDT damage. Thus, intracellular localization is crucial for effective PDT and PSs displaying a higher cellular uptake are usually more cytotoxic (Jensen et al., 2010).

Direct tumor cell death effects

PS accumulates in various intracellular compartments and can induce multiple cell death subroutines at the cellular level (Figure 1.3). There are two main types of cell death subroutines: accidental (necrosis) and regulated (apoptosis, autophagy, etc). Necrosis is an uncontrollable form of cell death characterized by the disruption of the plasma membrane, cytoplasm swelling, and destruction of organelles. Necrosis has been associated with incidental cell death, caused by extreme physical, chemical, or mechanical cues.

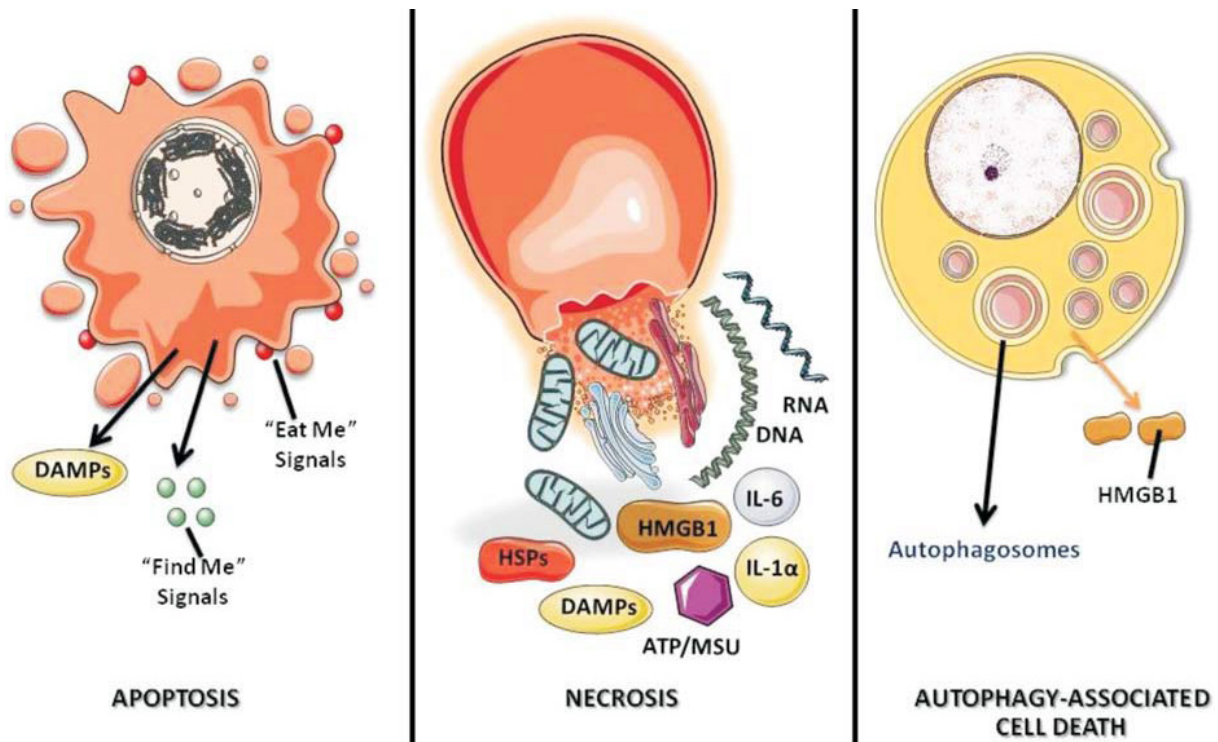


Figure 1.3 The main cell death subroutines induced by PDT. Reprinted from (Agostinis et al., 2011)

In turn, regulated cell death subroutines could be pharmacologically or genetically modulated through the one or more signal transduction modules. Regulated cell death

subroutines, which could be induced upon PDT mainly include apoptosis and autophagy. Apoptosis or programmed cell death is identified in single cells, and morphologically characterized by cell shrinkage, chromatin condensation, cleavage of chromosomal DNA into internucleosomal fragments, blebbing of the plasma membrane, and the formation of apoptotic bodies without plasma membrane breakdown (Agostinis et al., 2004; Almeida et al., 2004). It was identified that among all subcellular structures mitochondria plays the most critical role in the initiation of PDT-mediated apoptosis (Castano et al., 2005; Kessel and Luo, 1999). PDT-induced damage of mitochondria results in a cascade of reactions including the rapid release of mitochondrial cytochrome c into the cytosol followed by activation of the apoptosome and procaspase-3 that eventually cause the apoptosis (Oleinick et al., 2002).

Autophagy, as one of the regulated cell death subroutines, is a specific type of cell damage which relies on degradation redundant or damaged cell's elements. This subroutine is characterized by a massive vacuolization of the cytoplasm and can be stimulated by various stress signals, including oxidative stress (Dewaele et al., 2010). During autophagy, normal cell functions used to degrade components of the cytoplasm are involved and characterized by appearance autophagosomes, autolysosomes, electron-dense membranous autophagic vacuoles, myelin whorls, multivesicular bodies, as well as engulfment of entire organelles (Castano et al., 2005). Autophagy is upregulated in response to extra- or intracellular stress and signals such as starvation, growth factor deprivation, ER stress and pathogen infection (Kessel and Oleinick, 2009). Along with the mentioned cell death mechanisms, the subroutines such as mitotic cell death (Castedo et al., 2004), cathepsin-mediated lysosomal death pathway (Leist and Jäätelä, 2001), programmed necrosis (Bizik et al., 2004; Vanlangenakker et al., 2008) were also reported for PDT.

Mechanism of cell death depends on cell and PS type, treatment protocol, and photodynamic dose (Agostinis et al., 2011). PS localization within or on the cell surface is critical to determine the mode of cell death induction and thus the cellular response to photodamage. Apoptosis is preferable for PDT treatment because the cells undergoing apoptosis release the "find me" and "eat me" signals in the interstitial medium which are required for the clearance of the remaining apoptotic bodies by phagocytes that usually prevents inflammation response. On the other hand, during necrosis, the release of cellular contents and pro-inflammatory molecules into the intracellular media also caused an intense inflammatory reaction. Nevertheless, non-homogenous distribution of PS within the tumor, insufficient depth of light penetration into the tumor or distance of tumor cells from the vessels (Korbelik and Krosi, 1994) as well as availability of oxygen (Tromberg et al., 1990) make difficulties to achieve the tumoricidal effect *in vivo* only through direct damage of tumor cells. Along with direct tumor cell damage, PDT could also damage the tumor-associated

vasculature and could induce robust inflammatory reactions activating an immune response against tumor (Figure 1.4).

Antivascular effects of PDT

According to the literature, tumor blood vessels are fundamentally different from normal vasculature (Eberhard et al., 2000; Siemann, 2011). Tumor vasculature is characterized by the vessels that are immature in nature with poorly developed, chaotic growing architecture and discontinuous endothelial linings (Eberhard et al., 2000). Photodamage of endothelium cells lining tumor vessels could incite the modifications in cytoskeleton proteins organization with consecutive induction of a signal to the platelets and neutrophils activation which adhere on the vessel wall (Senge and Radomski, 2013). It was demonstrated, that endothelial cells accumulate more PS and possess higher sensitivity to PDT compared to muscle cells (West et al., 1990). Finally, the combination of vessel constriction, thrombus formation, and increased interstitial pressure leads to tumor tissue ischemia (Fingar et al., 2000; Henderson et al., 1985) and restricts nutrient supply to the proliferating tumor cells inhibiting tumor growth, making the tumor vasculature a promising target for anticancer treatment. Moreover, PDT vascular destruction may be accompanied by an inflammatory response (Korbelik, 1996).

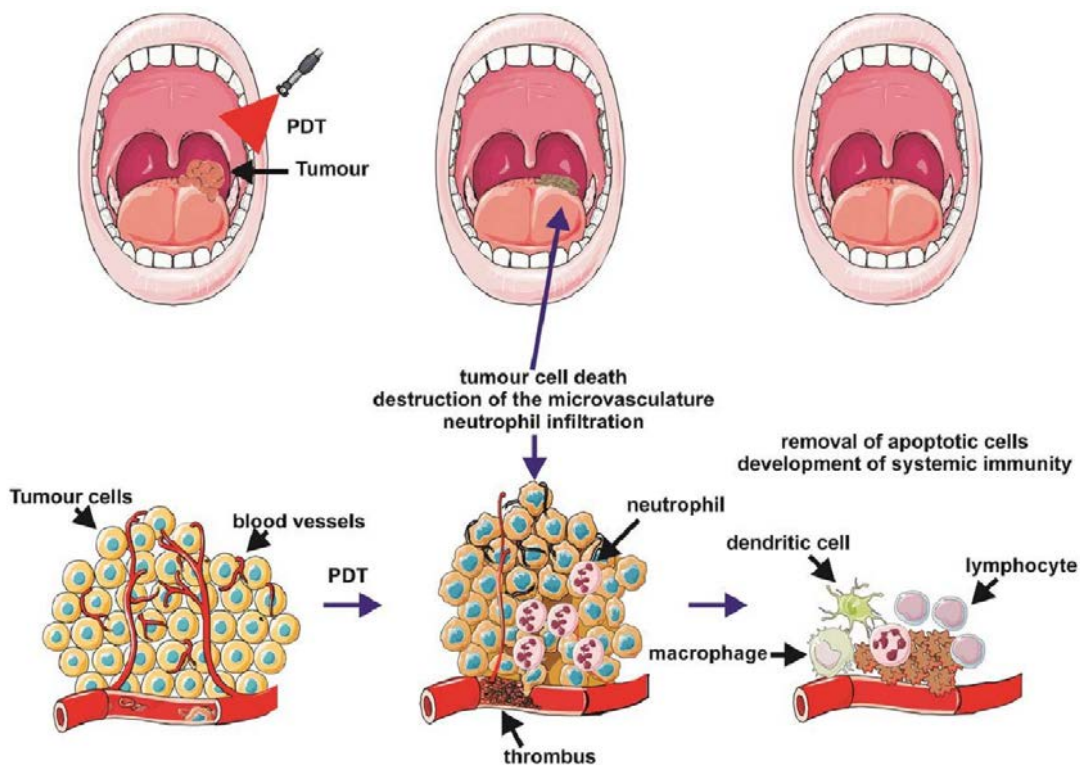


Figure 1.4 Mechanisms of PDT-mediated photoeradication of tumor mass (from Agostinis et al. 2011)

PDT and the immune response

PDT-response is closely connected with the immune system. It could be said that photosensitizers, vascular and immune system together create a group to fight with tumor cells (Oniszczyk et al., 2016). To date, it was established that PDT could stimulate both innate immunity and adaptive immunity (Castano et al., 2006). Preclinical studies have shown that low-dose PDT regimens can induce anti-tumor immunity (Shams et al., 2015). The oxidative stress induced by PDT could incite a strong acute inflammatory response observed as localized edema at the target site (Dougherty, 2002). Inflammatory response promotes local healing with the restoration of normal tissue function after the disruption of homeostasis and the removal of damaged cells. PDT treatment stimulates the regulation of the release of pro- or anti-inflammatory cytokines by macrophages (Korbelik and Krosi, 1994; Lynch et al., 1989). Furthermore, the lysates generated after PDT can activate dendritic cells and increase the ability to stimulate T-cells, which play an essential role in the development of a cellular immune response (Gollnick et al., 2002). Finally, removal of inflammatory cells or inhibition of their activity demonstrated significant reducing of the total therapeutic effect of PDT (Agostinis et al., 2011).

However, PDT-mediated immune response depends on the many factors, such as the type PS, features of pharmacokinetic and location within tumor and surrounding cells (especially immune cells), the area treated and treatment regimen (e.g., drug-light interval (DLI) and settings of irradiation) (Kousis et al., 2007; Reinhard et al., 2015). So, the regimens that result in rapid cell death (within 1h of treatment) and maximal tissue damage were demonstrated to cause minimal acute inflammation, presumably because of the vascular shutdown, which would prevent neutrophil infiltration and systemic release of cytokines. In contrast, regimens that cause diffuse tumor damage should allow neutrophil infiltration followed by induction of expression and release of inflammatory mediators critical for enhancement of anti-tumor immunity (Henderson et al., 2004). In summary, the cytotoxic effects mediated by PDT are strongly depended on the localization of PSs. Thus, the distribution processes of PSs could be considered as key factors of successful PDT alongside the PS photophysical properties and treatment regimen.

1.4. Light sources

As it was mentioned above, the contribution of tumor eradication mechanisms as well as PDT efficiency strongly depends on the settings of irradiation and light source used. To date, with various light sources including lasers, incandescent light, laser emitting diodes, and daylight were applied for PDT (Agostinis et al., 2011; Fitzmaurice and Eisen, 2016). Nowadays, the diode lasers are widely used due to their compact size, cost-effectiveness,

automated dosimetry and calibration, simple installation and long operational life. Light-emitting diodes are alternative light sources with relatively narrow spectral bandwidths and high fluence rates (Juzeniene et al., 2006). To deliver the light to the hard-to-reach places (e.g., urinary bladder and the digestive tract) lasers beams are coupled into fibers with diffusing tips. Moreover, there are already in the market inflatable balloons, covered on the inside with a strongly scattering material and formed to fit an organ (Beyer, 1996).

No single light source is ideal for all PDT indications, even with the same PS. The choice of the light source should, therefore, be based on PS absorption (fluorescence excitation and action spectra), disease (location, size of lesions, accessibility, and tissue characteristics), cost and size. Preferably, the light should efficiently penetrate the tissue to be delivered across the whole tumor mass. Due to light scattering and absorption of tissue chromophores, shorter wavelengths (< 600 nm) have less tissue penetration and are mostly absorbed. Blue light penetrates only several hundred micrometers, whereas red and infrared radiations penetrate more deeply (up to 1 cm) (Figure 1.5). The most effective for the human organism is wavelength above 630 nm (Castano et al., 2004). The light in this range can penetrate human tissue on the appropriate required level, which provides the success of the therapy. More precise tuning of laser excitation wavelength is performed for certain PSs according to its action spectra. However, the longer the excitation wavelength, the less energy the PS will absorb, and the longer the exposure time will be (Henderson et al., 2004). The clinical efficacy of PDT is dependent on complex dosimetry: total light dose, light exposure time, and light delivery mode (single vs fractionated or even metronomic).

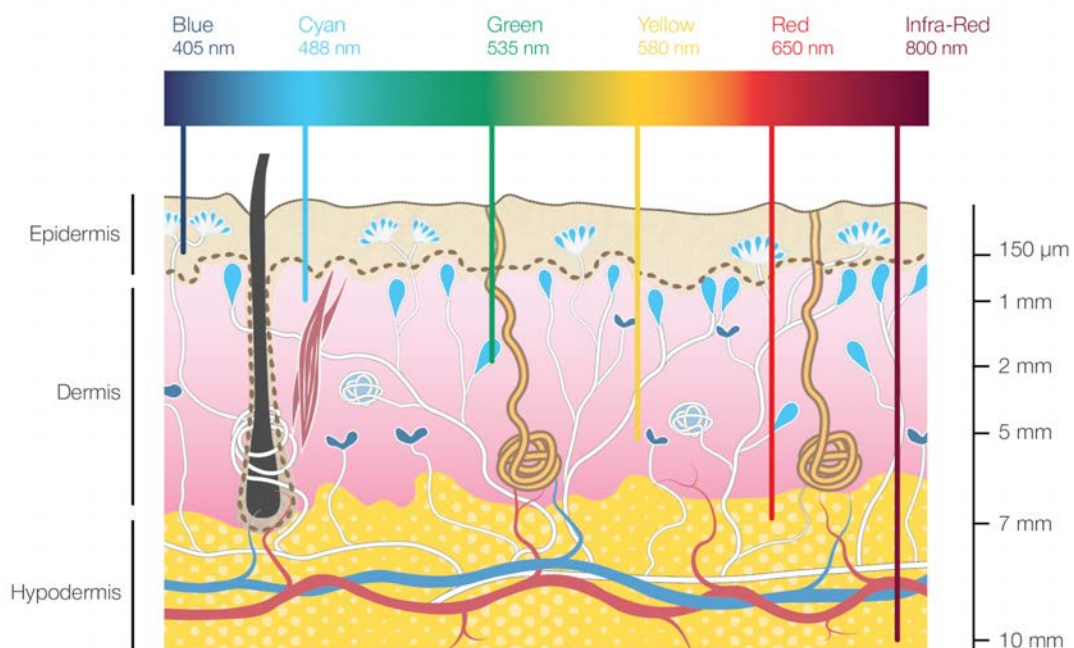


Figure 1.5 Light propagation through the tissues.

1.5. Photosensitizers

PS is the most significant component having an influential impact on the PDT process. Appropriate choice of the compound is a guarantee of success. The main characteristics of PS are selectivity for tumor cells, formation a long-lived triplet excited state in reaction, activation with wavelength appropriate for tissue and high chemical purity (Robertson et al., 2009; Zhang et al., 2018). To date, more than 400 compounds are known as PSs, which are used in various fields such as medicine, cosmetics, chemicals, etc. (Robertson et al., 2009). The most significant groups of the substances are tetrapyrrolic compounds (porphyrins, chlorins, phthalocyanines, etc) (Josefsen and Boyle, 2012; O'Connor et al., 2009), non-porphyrin PS (5-aminolevulinic acid, xanthenes, phenothiazines, triarylmethanes, curcumin, hypericin) (Craig et al., 2015; Kübler, 2005), and other classes of compounds such as synthetic dyes (e.g., phenothiazinium, squaraine), transition metal complexes, and natural products (e.g., hypericin, riboflavin, curcumin) (Abrahamse and Hamblin, 2016).

To be considered as an efficient PS, the substance concurrently should match the following criteria (Pushpan et al., 2002):

- Strong absorption (high extinction coefficient, ϵ) of light in the red or far-red region;
- The high QY of ROS generation;
- Low photobleaching (self-oxidation) rate;
- Low dark toxicity for both photosensitizer and its metabolites;
- Selectively accumulates in tumor tissues and cellular compartments;
- Rapid clearance from healthy tissues upon completion of treatment.

Additionally, PS should be in a pure form (known chemical composition) and stable compound with relatively easy and low cost synthesis. From a clinical point of view, the substance should be commercially available, reliable, and pain-free upon activation, acceptable for outpatient treatment with versatile and easy administration.

PDT drugs are generally classified as first, second or third generation PSs. Currently, only a few PSs, have official approval worldwide and are being used clinically for cancer treatments (Table 1.1). Photofrin[®] and Photogem[®], the first-generation PDT sensitizers, are porphyrin-based PS which have been for a very long time the only PSs used in clinical PDT. They consist of a mixture of monomers, dimers, and oligomers of hematoporphyrin derivatives. However, due to the complex composition, non-optimal photophysical properties, lack of tumor selectivity, poor bioavailability and prolong patient photosensitivity (poor clearance) their application in PDT was limited (Macdonald and Dougherty, 2001).

Table 1.1. Photosensitizers approved for clinics for PDT (from Agostinis et al., 2011; Dos Santos et al., 2019; Lucky et al., 2015; Ormond and Freeman, 2013)

PS	Trademark	Approved	λ_{ex} , (nm)	Application
<i>Porphyrins</i>				
Porfimer sodium	Photofrin [®] , Photogem [®] , Photosan-3 [®]	WW	630	Bladder, esophageal, lung, cervical, endobronchial, and gastric cancers
<i>Porphyrin precursors</i>				
5-ALA ¹	Levulan [®] , Ameluz [®]	WW	400	Treatment of actinic keratosis, basal cell carcinoma, head and neck, and gynecological tumors; diagnosis of bladder, brain, head & neck cancers
MAL ²	Metvix [®] , Metvixia [®]	USA, EU, New Zealand & Australia)	630	Actinic keratosis, Bowen's disease, and basal cell carcinoma
HAL ³	Hexvix [®] , Cysview [®]	USA	635	Diagnosis of bladder and colon cancers
<i>Benzoporphyrin</i>				
Verteporfin	Visudyne [®]	USA, EU, Canada	689	Treatment for wet age-related macular degeneration, pathologic myopia, histoplasmosis
<i>Chlorins</i>				
Temoporfin	Foscan [®]	EU	652	Head and neck cancers
Talaporfin or MACE	Aptocine [®] , Laserphyrin [®]	Japan	664	Lung cancer
Chl e ₆ ⁴	Fotolon [®] , Radachlorin [®] , Photodithazine [®]	Belarus, Russia, Ukraine	665	Nasopharyngeal, sarcoma, brain, skin cancer
<i>Phthalocyanines</i>				
AIPCS ₄ ⁵	Photosens [®]	Russia	675	Stomach, skin, oral cavity, tongue, and breast cancers
<i>Texaphyrins</i>				
Lutetium texaphyrin	Lutex [®]	USA	732	Breast cancer and malignant melanomas
<i>Pheophorbides</i>				
Pd-Bpheid ⁶	Tookad [®]	EU	538/762	Prostate cancer
<i>Porphycenes</i>				
ATMPn ⁷	ATMPn	Germany	630	Psoriasis and non-melanoma skin cancer

¹ 5-Aminolevulinic Acid; ² Methyl aminolevulinic acid; ³ Hethyl aminolevulinic acid; ⁴ Chlorin e6 derivatives; ⁵ Sulfonated aluminum phthalocyanines; ⁶ Palladium-bacteriopheophorbide; ⁷ 9-Acetoxy-2,7,12,17-tetrakis-(β -methoxyethyl)-porphycene

Compared with the first generation, the composition and structure of the second-generation PSs are definite; the photosensitivity, absorption spectrum and tissue selectivity have significantly been improved. As a result, the variety of new PS molecules such as metalloporphyrins or texaphyrins (Lutrin[®] and Lutex[®]) (Magda and Miller, 2006; Young et al., 1996); benzoporphyrins (Visudyne[®]) (Battaglia Parodi et al., 2016); chlorins (Fotolon[®], Radachlorin[®], Photodithazine[®], Aptocine[®], Foscan[®]) (Kochneva et al., 2010; Miki et al., 2014; Senge and Brandt, 2011; Shliakhtsin et al., 2009; Wen et al., 2011); porphycenes (Guardiano et al., 1989; Szeimies et al., 1996); pheophorbides (Tookad[®]) (Taneja et al., 2016; Trachtenberg et al., 2008); purpurins (Purlytin[®]) (Forsyth et al., 1995); phthalocyanines (Photosens[®]) (Miller et al., 2007; Muehlmann et al., 2015; Trushina et al., 2011), protoporphyrin-IX precursors (Hexvix[®], Metvix[®] and Levulan[®]) (Kennedy et al., 1990; Sachar et al., 2016) have been developed and approved for clinical applications (Figure 1.6).

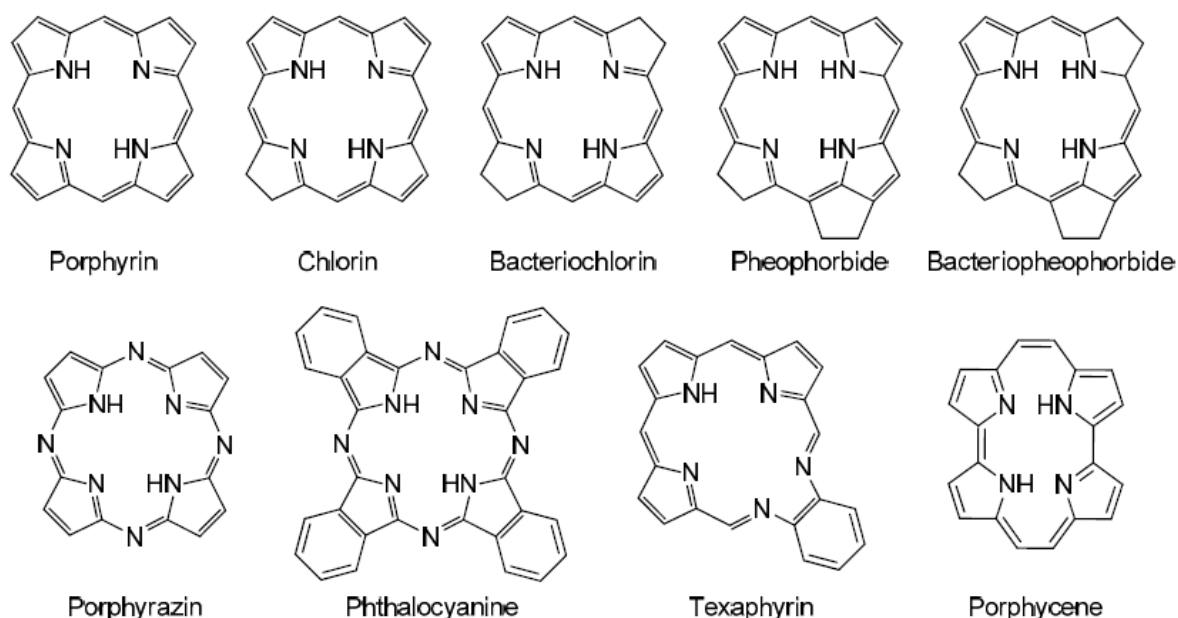


Figure 1.6 Structural skeletons of porphyrinoid-based PSs (Ben Mihoub et al., 2018)

Moreover, along with clinically approved PSs, phenothiazines (methylene blue and toluidine blue) (Tardivo et al., 2005); cyanines (merocyanine540, indocyanine green) (Delaey et al., 2000; Shirata et al., 2017); dipyrromethenes (BODIPYs) (Awuah and You, 2012); hypericin (Garg et al., 2012); xanthenes (RoseBengal) (Panzarini et al., 2014) and curcumin (Ellerkamp et al., 2016) have been also considered as good second-generation PSs for experimental PDT.

However, the second generations PSs are still poorly selective for tumors and require the improvements in their delivery to the target site due to the hydrophobic nature of many of them. Third-generation PS are now being developed to improve the PDT outcomes using

nanotechnology approaches. Considerable efforts have been devoted to developing specific carriers for delivery of PSs in order to improve the selectivity of PS uptake in the target tissue and to avoid phototoxicity to healthy tissues, such as skin (Marchal et al., 2015). The first and second-generation PSs, covalently attached to various biological modifiers like oligosaccharides, lipoproteins, antibodies and amino acids, or formulated into drug delivery systems like liposomes, polymeric nanoparticles, cyclodextrins, and emulsions are classified as third-generation PSs.

Of particular interest for this study is temoporfin (Foscan[®]), which is an extremely potent PS (approximately 100 times more photoactive than Photofrin[®]) (Mitra and Foster, 2005; Senge and Brandt, 2011). Senge MO raised the question on the ways of development of third-generation PS on the example of temoporfin (Senge, 2012), the properties of which will be described in detail in the next chapter.

2. Meta-tetra(hydroxyphenyl)chlorin

2.1. General properties and usage

5,10,15,20-Tetra(m-hydroxyphenyl)chlorin (mTHPC, Figure 2.1) was discovered and synthesized by the group of professor Raymond Bonnett in 1989 as a second-generation PS (Berenbaum et al., 1986; Bonnett et al., 1989). mTHPC (generic name temoporfin, proprietary name Foscan[®]) possesses pure-compound preparation, hence efficient light tissue penetration, certain selectivity of tumor uptake, a low administration dose and attractive photophysical characteristics (Senge and Brandt, 2011).

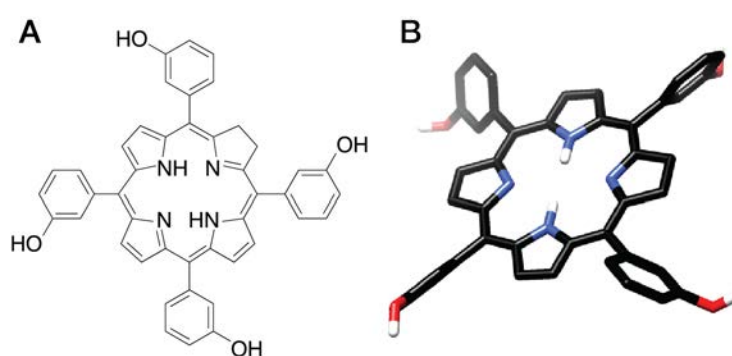


Figure 2.1 (A) Chemical structure of mTHPC. (B) Steric mTHPC conformation

Photophysical properties of mTHPC were well investigated (Bautista-Sanchez et al., 2005; Bonnett et al., 1989, 1999) and the main characteristics are summarized in Table 2.1. Temoporfin possesses an extinction coefficient of $29,600 \text{ M}^{-1}\text{cm}^{-1}$ in the red region of spectra (650 nm). Furthermore, triplet state QY formation is 0.89, hence QY singlet oxygen is 0.43 in

aerated methanol (Bonnett et al., 1999). There are however compounds superior to it in terms of in certain photophysical properties. For example, bacteriochlorin-type **TOOKAD[®]** exhibits extinction coefficient $90,000 \text{ M}^{-1}\text{cm}^{-1}$ at 763 nm (Koudinova et al., 2003), while tin ethyl etiopurpurin (**Purlytin[™]**), possess the highest quantum yield of singlet oxygen $\Phi_{\Delta} = 0.7$ (Pogue et al., 1998).

Table 2.1 Photophysical properties of mTHPC in methanol (Bautista-Sanchez et al., 2005; Bonnett et al., 1989)

Property	Value
Absorption maximum, nm	650
Extinction coefficient, $\text{M}^{-1} \text{cm}^{-1}$	29 600
Fluorescence maximum, nm	652
Fluorescence QY	0.18
Triplet QY	0.32
Singlet oxygen generation QY (air-saturated)	0.31
Singlet oxygen generation QY (oxygen-saturated)	0.42

Nevertheless, mTHPC is considered as one of the most potent PSs due to both a very low drug dose (0.15 mg kg^{-1}) and light intensity (order of 10 J cm^{-2}) applied in clinical PDT. So, the resulting total PDT dose (light dose \times PS dose) is more than 100 times lower compared to other clinically approved first-generation PSs, such as haematoporphyrin derivatives (Savary et al., 1997, 1997) and Photofrin (Ball et al., 1999). In 2001, mTHPC was approved in the EU and used as a solvent-based formulation (**Foscan[®]**; Biolitec Research GmbH, Jena, Germany) for the palliative treatment of head and neck cancers (Senge and Brandt, 2011). In addition, mTHPC has been successfully utilized for the clinical treatment of other types of cancers such as early squamous cell carcinoma (Jerjes et al., 2011; de Visscher et al., 2013), basal cell carcinoma (Betz et al., 2012), biliary tract carcinoma (Wagner et al., 2015), prostate (Swartling et al., 2010, 2016), pancreatic cancer (Bown et al., 2002) and nonmelanoma skin cancers (Horlings et al., 2015). Furthermore, there are reports in preclinical models on mTHPC-PDT application in antibacterial therapy (Ossmann et al., 2015), rheumatoid arthritis (Hansch et al., 2008), ulcerate colitis and prevention of colitis-associated carcinogenesis (Reinhard et al., 2015). Taking into account moderate photophysical characteristics, it was supposed that the potency of mTHPC-PDT should mainly rely on the features of mTHPC behavior during its distribution in biological systems.

2.2. Uptake and localization

First of all, the biological behavior of drugs is determined by the physical-chemical properties of PS. Temoporfin molecules have a highly hydrophobic nature characterized by octanol-water partition coefficient (logP) of 8.8, according to Pubchem database (PubChem), thus forming large aggregates in an aqueous environment (Kruijt et al., 2009; Tikhomirov et al., 2009). As a rule, mTHPC is administrated intravenously and formation of non-photoactive aggregates in blood flow after its injection distorts the pharmacokinetics and reduces drug bioavailability. Molecular aggregates of mTHPC slowly dissociates in the presence of serum proteins redistributing PS to the lipoproteins or cellular membranes due to the high lipophilicity of mTHPC (Melnikova et al., 1999; Sasnouski et al., 2005; Triesscheijn et al., 2007). According to the literature data, about 95% of mTHPC in plasma is associated with high-density lipoproteins (HDL) and low-density lipoproteins (LDL), and the binding with HDL is twice higher than that with LDL (Reshetov et al., 2012; Triesscheijn et al., 2007).

However, as compared with other hydrophobic drugs, the kinetics of mTHPC redistribution between serum proteins and/or other biomembrane is very slow (Sasnouski et al., 2005, 2006). The redistribution process takes hours, thus making intracellular uptake of mTHPC very sluggish. For instance, time-dependent mTHPC accumulation in A431 human epidermoid carcinoma cells reaches a plateau only at 24 h (Berlanda et al., 2010). High lipophilicity of mTHPC also determines a high affinity to lipid microenvironment of cellular membranes. It worth noting that temoporfin is strongly confined to model biomembranes (Kachatkou et al., 2009), demonstrating tight binding in the cells without remarkable release (Ball et al., 1999; Berlanda et al., 2010; Mitra and Foster, 2005). Overall, the cellular uptake of mTHPC could be affected by various factors. As discussed above, due to the high affinity of mTHPC to lipoproteins, HDL-mediated endocytosis was proposed as the main mode of temoporfin transport into the cells (Sasnouski et al., 2006). At the same time, tumor cells could internalize mTHPC in its aggregated form, followed by slow monomerization (Rezzoug et al., 1998), attested by fluorescence lifetime imaging microscopy data (Lassalle et al., 2008). In addition, photosensitivity of cells increased with decreasing pH, while uptake of mTHPC in tumor cells has been identified as pH-independent in the range of pH 6.8-7.8 (Ma et al., 1999). Overall, all these factors lead to the heterogeneity of mTHPC distribution in the tumor tissue. Indeed, *in vitro* studies in multicellular tumor spheroid model demonstrated that mTHPC did not penetrate deeper than 50 μm and was localized only in the peripheral cell layers of spheroids (Marchal et al., 2005; Millard et al., 2018; Mitra and Foster, 2005; Mitra et al., 2005).

As have been described above, the mechanism of PDT cell death strongly depend on the PS intracellular localization (Castano et al., 2005). The analysis of preferential sites of

mTHPC localization in cells demonstrated the presence of PS in cellular organelles, except perinuclear space (Melnikova et al., 1999). Teiten *et al.* (2003) reported preferential mTHPC accumulation in the Golgi apparatus and endoplasmic reticulum in MCF-7 human adenocarcinoma cells. On the other hand, mitochondrial damage and cytochrome *c* release after mTHPC-PDT have been described for various cancer cells (Marchal et al., 2004; Yow et al., 2000). An apoptotic response after mTHPC-PDT *in vitro* has been observed by Kessel due to the mitochondrial damage and subsequent activation of caspase cascade caused by the release of cytochrome *c* (Kessel, 1999). Although mitochondria are not affected directly, apoptotic signals originating in the endoplasmic reticulum and/or Golgi apparatus converge on mitochondria triggering afterward apoptotic cell death (Marchal et al., 2007). Photoinduced mode of cell death varies widely depending on the cell type. Indeed, mTHPC-PDT in human colon cancer cells was shown to be a strong inducer of necrosis with a negligible percentage of apoptotic cells (Marchal et al., 2005). Alternatively, the recent study of mTHPC-PDT on other human cell lines (lung, oral cavity, esophagus, bladder and cervix) reported mainly apoptotic cellular death and autophagy after mTHPC-PDT with a minor role of necrosis (Lange et al., 2019).

2.3. Biodistribution and pharmacokinetic properties

The issues of mTHPC pharmacokinetics were studied in detail in various preclinical models. It was reported that temoporfin's half-life in plasma was estimated in a range of 26–45 h depending on the animal model (Campbell et al., 2002; Glanzmann et al., 1998; Ronn et al., 1996; Triesscheijn et al., 2007). It was demonstrated that the mean values for plasma drug concentrations were in good agreement with the injected dose of mTHPC. Pharmacokinetics of radiolabeled mTHPC in tumor-bearing rats was described using a tri-exponential model with a half-time of 0.46, 6.91 and 82.5 h, respectively (Jones et al., 2003). At the same time, the pharmacokinetics in mice and humans is quite different (Campbell et al., 2002; Triesscheijn et al., 2007; Whelpton et al., 1996). In humans the mean plasma concentration of mTHPC was constant at high level for several hours after IV administration (Triesscheijn et al., 2007). The authors suggested that the prolonged plateau in drug concentrations in human plasma is the result of the formation of drug depot, probably in the vascular compartment immediately after IV injection. In addition, it was shown that neither drug distribution over the lipoproteins nor the metabolism of lipoproteins influenced plasma pharmacokinetics of mTHPC (Triesscheijn et al., 2007). Recently, Jablonka and co-workers confirmed these suggestions simulating *in silico* pharmacokinetics and biodistribution of Foscan® in humans assuming precipitated mTHPC in the injection site (drug depot) (Jablonka et al., 2019).

The biodistribution studies demonstrated that the uptake of mTHPC depends on the perfusion degree of the organ. So, highly perfused organs (liver, spleen, kidney and lung) contained higher amount of the drug compared with less perfused organs (Campbell et al., 2002; Whelpton et al., 1996), while the maximum level of mTHPC varies in different animal models and depends on the administration doses (Ronn et al., 1996, 1997). mTHPC is not metabolized and is excreted unchanged via the biliary route in the feces in a murine model (Cai et al., 1999a, 1999b). Nearly 40% of the drug was excreted by the feces during the first day, and less than 0.2% of the administered dose was observed in the urine (Whelpton et al., 1996).

The intratumoral distribution of mTHPC was studied in detail by Mitra and co-workers using high-resolution confocal fluorescence imaging (Mitra et al., 2005). The authors simultaneously mapped microscopic intratumoral mTHPC localization with respect to perfused vasculature in the function of time after injection and demonstrated the maximal mTHPC fluorescence in the perivascular region 3h after injection. Localization of mTHPC in tumor parenchyma was observed only at 24h post-administration. It corresponds to the results of Jones with co-workers (Jones et al., 2003), where mTHPC had a small initial volume of distribution with strong retention in the vasculature together with two peaks of PDT efficacy (2 and 24h) in rats. As it is known for the majority of PSs, PDT at the early time of irradiation could result mainly in the destruction of the microvasculature of the tumor, while at DLI of 24h it affects the tumor tissue. Similarly, mTHPC exhibits two peaks of PDT efficacy (2 and 24h) in rats (Jones et al., 2003). In fact, a fractionated double injection (3 and 24h prior to PDT) should be superior to cumulative single administration, the fact was confirmed in mice bearing EMT6 tumors (Garrier et al., 2010). *In fine*, although direct cells damage is predominant in tumor destruction by mTHPC-PDT, other mechanisms play an important role in the complete tumor destruction and prolonged PDT-effect. Early pre-clinical studies have demonstrated the depth of necrosis of 3.79 ± 0.28 mm for mTHPC-PDT in PC6 tumor-bearing mice (Bonnett et al., 1989). Also, it was shown that mTHPC mediates cell photodamage, principally through singlet oxygen formation (Melnikova et al., 1999) and its efficacy is sensitive to oxygenation conditions (Coutier et al., 2002). However, several authors observed the absence of correlation between mTHPC concentration in tumor and PDT efficiency (Garrier et al., 2010; Ris et al., 1998; Veenhuizen et al., 1997).

Nevertheless, mTHPC exhibits several side effects. The major issue in the clinical management of mTHPC is poor-selectivity and prolong post-treatment skin photosensitivity (Senge, 2012). Skin and eye photosensitivity of mTHPC is less than that of Photofrin® (van Geel et al., 1995; Wagnieres et al., 1998). However, it persists for up to 6 weeks (usually 2-3 weeks) after mTHPC administration (Allison and Sibata, 2010). Usually, Foscan-based PDT

resulted in mild to moderate skin photosensitivity and caused neither functional nor cosmetic impairments after treatment of early oral squamous cell carcinoma (O'Connor et al., 2009). Most common side effects of Foscan[®] include headache, hemorrhage, dysphagia and edema (Baskaran et al., 2018). Moreover, there is evidence indicating a mild to moderate pain in the treated area (Allison and Sibata, 2010). Nevertheless, temoporfin remains one of the most potent PSs on the market, while most side effects are caused by non-optimal mTHPC distribution in the organism and could be significantly reduced using nanoparticle-based delivery platforms.

2.4. Nanoscale delivery systems

The era of nanoparticle-based mTHPC-PDT started in 1995 (Westermann et al., 1995) when mTHPC was covalently linked with polyethylene glycol (PEG) to increase its solubility and improve its bioavailability. Currently, there are numerous nano-platforms developed for efficient and targeted mTHPC delivery. The information on the features of each nano-platform for mTHPC was summarized in the scientific review below.



Contents lists available at ScienceDirect

Journal of Controlled Release

journal homepage: www.elsevier.com/locate/jconrel

Review article

Current state of the nanoscale delivery systems for temoporfin-based photodynamic therapy: Advanced delivery strategies

Ilya Yakavets^{a,b,c}, Marie Millard^{a,b}, Vladimir Zorin^{c,d}, Henri-Pierre Lassalle^{a,b}, Lina Bezdetnaya^{a,b,*}

^a Centre de Recherche en Automatique de Nancy, Centre National de la Recherche Scientifique UMR 7039, Université de Lorraine, Campus Sciences, Boulevard des Aiguillettes, 54506 Vandoeuvre-lès-Nancy, France

^b Research Department, Institut de Cancérologie de Lorraine, 6 avenue de Bourgogne, 54519 Vandoeuvre-lès-Nancy, France

^c Laboratory of Biophysics and Biotechnology, Belarusian State University, 4 Nezavisimosti Avenue, 220030 Minsk, Belarus

^d International Sakharov Environmental Institute, Belarusian State University, Dauhahrodskaja 23, 220030 Minsk, Belarus



ARTICLE INFO

Keywords:

Drug delivery
Hybrid nanodelivery systems
Nanoparticles
Photodynamic therapy
Temoporfin

ABSTRACT

Enthusiasm for photodynamic therapy (PDT) as a promising technique to eradicate various cancers has increased exponentially in recent decades. The majority of clinically approved photosensitizers are hydrophobic in nature, thus, the effective delivery of photosensitizers at the targeted site is the main hurdle associated with PDT. Temoporfin (mTHPC, medicinal product name: Foscan®), is one of the most potent clinically approved photosensitizers, is not an exception. Successful temoporfin-PDT requires nanoscale delivery systems for selective delivery of photosensitizer. Over the last 25 years, the number of papers on nanoplatforms developed for mTHPC delivery such as conjugates, host-guest inclusion complexes, lipid- and polymer-based nanoparticles and carbon nanotubes is burgeoning. However, none of them appeared to be “ultimate”. The present review offers the description of different challenges and achievements in nanoparticle-based mTHPC delivery focusing on the synergetic combination of various nano-platforms to improve temoporfin delivery at all stages of biodistribution. Furthermore, the association of different nanoparticles in one nanoplatform might be considered as an advanced strategy allowing the combination of several treatment modalities.

1. Introduction

Photodynamic therapy (PDT) is a promising minimally invasive treatment, commonly used in medical disciplines, such as dermatology, oncology, gynecology and urology [1]. PDT has been approved for palliative treatment of head and neck tumors, basal-cell carcinoma, biliary tract cancer, lung cancer, T-cell lymphoma and age-related macular degeneration [2]. Currently, clinical trials with PDT are proposed for a wide range of solid tumors, including the brain, breast, lung, pancreas, and prostate. Good therapeutic results and the possibility of combining PDT with other therapeutic modalities in cancerology defines its attractiveness [3].

Phototherapeutics termed photosensitizers (PSs), exhibit the properties such as (i) photo-reactivity; (ii) not-toxicity in the absence of light; (iii) specific accumulation in tumor tissues; (iv) selectivity conferred by a light beam; (v) photocytotoxic activity against targeted cells. Upon light excitation, these molecules generate cytotoxic reactive

oxygen species (ROS), inducing cell death and tissue destruction. The efficiency of ROS generation is mainly determined by photophysical properties of PS and penetration ability of excitation light across the tissue. Thus, to be effective PS should possess a high quantum yield of ROS generation and strong absorption in the red and/or infra-red spectral regions [4]. The effectiveness of PDT is also determined by PS pharmacodynamics and biodistribution. Inasmuch as the main intermediate, singlet oxygen, a highly reactive species with a short half-life in biological systems (< 40 ns) [5], directly affects only molecules and structures that are proximal to the area of its production [6]. Therefore, precise delivery and accurate localization of PS at target sites are required for effective PDT.

Over the last decades, it has been demonstrated that the combination of photosensitizers with nanomaterial platforms enable precise delivery of PS to the target tissues improving the PDT effectiveness. Nanoparticles (NPs) can have numerous advantages as a PS delivery system, such as (i) protection of the PS against enzymatic degradation;

* Corresponding author at: Institut de Cancérologie de Lorraine, 6 Avenue de Bourgogne – CS 30519, 54519 Vandoeuvre-lès-Nancy, Cedex, France.

E-mail addresses: ilya.yakavets@nancy.unicancer.fr (I. Yakavets), marie.millard@nancy.unicancer.fr (M. Millard), zorin@bsu.by (V. Zorin), h.lassalle@nancy.unicancer.fr (H.-P. Lassalle), l.bolotina@nancy.unicancer.fr (L. Bezdetnaya).

<https://doi.org/10.1016/j.jconrel.2019.05.035>

Received 10 April 2019; Received in revised form 21 May 2019; Accepted 23 May 2019

Available online 25 May 2019

0168-3659/ © 2019 Elsevier B.V. All rights reserved.

(ii) the control release of PS allowing a constant and uniform concentration into the target cells; (iii) the ability to penetrate target tissues due to their submicron size; (iv) biocompatibility and resorbability through natural pathways and (v) photostability. Moreover, since the most effective PSs tend to be insoluble hydrophobic molecules with a high propensity to aggregate, their encapsulation into nanocarriers could improve their pharmacokinetic properties. Additionally, nanotechnology-based drug delivery systems provide the opportunity for active targeting and for application of multimodal combined therapies.

The present review focuses on the nanoparticle-based delivery systems of potent clinically approved PS temoporfin. Among other second-generation photosensitizers, temoporfin possesses unique biopharmaceutical properties defining its high PDT potency. Since the last decade, about 10 reports per year on temoporfin nanoparticles have been published and this number is constantly increasing. However, a state-of-the-art review of *in vitro* and *in vivo* aspects of nanovehicle-based temoporfin delivery, along with a critical discussion of nanoformulations design parameters, perspectives, and challenges regarding *in vivo* drug distribution is not currently available. Therefore, we have attempted to provide the comprehensive review, aiming to guide future research in photonanomedicine using temoporfin. The successive sections summarize the investigations on the strategies aiming the development of nanotechnology-based temoporfin delivery systems in PDT.

2. Temoporfin

5,10,15,20-Tetrakis(3-hydroxyphenyl)chlorin (mTHPC, temoporfin), the standard chlorin-based photosensitizer (PS) since its discovery in the 1980s, is one of the most potent second generation photosensitizers currently available in clinical PDT. In 2011, Senge and Brandt comprehensively reviewed the general aspects of mTHPC application in clinics [7]. Temoporfin was already clinically approved in European Union in 2001 for the treatment of head and neck squamous cell carcinoma using an ethanol anhydrous/propylene glycol-based commercial formulation (Foscan®; biolitec pharma Ltd., Jena, Germany) [8,9]. In clinical PDT mTHPC is applied at both a very low drug dose (0.15 mg/kg) and light intensity (order of 10 J/cm²) resulting in a total PDT dose (light dose × PS dose) > 100 times lower compared with other clinically approved PSs, such as haematoporphyrin derivatives [10,11] and Photofrin [12].

Photophysical properties of mTHPC were intensively investigated [13,14] and it appears that they solely cannot account for the high mTHPC-PDT efficacy. Other PS as bacteriochlorin-type TOOKAD® or tin ethyl etiopurpurin (Purlytin™) are also characterized by a high extinction coefficient (90,000/M/cm at 763 nm) [15] or high quantum yield of singlet oxygen $\Phi_{\Delta} = 0.7$ [16]. Therefore, the moderate values of both extinction coefficient (30,000/M/cm) and quantum yield of singlet oxygen ($\Phi_{\Delta} = 0.43$), as well as the long wavelength of absorbance at 652 nm, could not be the only responsible for high PDT efficiency (Fig. 1). Thus, it was supposed that the benefits of mTHPC application mainly rely on the capacity of mTHPC to sequester tightly in cells along with its photophysical properties [17].

Nevertheless, mTHPC-PDT is still not optimal, leaving a much room for improvement. The essential challenge of mTHPC delivery is its poor water-solubility. As a rule, mTHPC is intravenously introduced to the patients as a solution for i.v. injection (Foscan®) containing 1 mg of temoporfin in a 1 ml of a mixture of ethanol anhydrous and propylene glycol [9] in order to palliate its high hydrophobic nature. mTHPC molecules possess octanol-water partition coefficients ($\log P$) > 3 [18], thus hydrophobic nature defines its pharmacokinetics and biodistribution behavior. Administration of mTHPC as Foscan® formulation prevents the effective formation of non-photoactive aggregates in blood flow after its injection resulting in distorting the pharmacokinetics and reducing drug bioavailability. Foscan® formulation should be injected slowly to avoid drug precipitation at the injection site, however, its administration is accompanied by pain [7].

More importantly is that mTHPC molecule is highly lipophilic. Lipophilic nature determines its high affinity for lipid microenvironment as lipoproteins or cellular membranes [20–22]. Thus, complete or partial disaggregation could happen in the circulation upon interaction with blood components, mostly cells and serum lipoproteins [20]. Nevertheless, high mTHPC lipophilicity hampers its diffusion through aqueous surrounding making the redistribution process of PS between binding sites extremely slow [2]. Hereby, a considerable amount of PS moves from aggregates to blood components and further slowly redistributes to target cells. This is why the drug-light interval (DLI) for Foscan® is up to several days [7,24], while Verteporfin-PDT may be performed at a dozen minutes after the PS administration [24]. Even when mTHPC reaches the tumor tissue, high lipophilicity leads to the limited PS penetration into the tumor stroma, as was demonstrated on multicellular tumor spheroids and *in vivo* pre-clinical models [17,25,26]. This could be a reason for tumor relapse sometimes observed after PDT. Finally, mTHPC noticeably accumulates in the skin that together with the extremely slow release of mTHPC from the cells [17] results in a prolong post-treatment skin photosensitivity [27]. Eye and skin preservation for 6 weeks after mTHPC injection should be also considered in clinical settings. Most common side effects of Foscan®-based PDT are headache, hemorrhage, dysphagia and edema [28]. Overcoming the mentioned challenges in PS biodistribution could be possible by application of nanomedicine facilities. The use of nanocarriers based on polymers, lipids or non-organic materials provides the opportunity to facilitate administration of hydrophobic drugs as mTHPC and to tune its pharmacokinetics.

3. Nanodelivery systems for temoporfin

The attempts of NP-based mTHPC delivery have been made since 1995 [29,30]. Currently, numerous nano-platforms based on a variety of organic and inorganic nanomaterials have been studied for efficient and targeted mTHPC delivery (Fig. 2). Various strategies of passive and active transport of mTHPC were conducted. Hereafter we review in details all nanoscale-based mTHPC formulations in terms of structural, photophysical and biopharmaceutical properties. The nanoparticles will be present in function of their size and complexity for easy following this review. We will describe the conjugates, inclusion complexes, polymeric and lipid-based NPs, ending up with carbon-based nanostructures. In conclusion, hybrid delivery systems for mTHPC will be reviewed.

The main observations on temoporfin nanocarriers, which achieved *in vitro* and *in vivo* evaluation in pre-clinical models, are presented in the Table 1.

3.1. Conjugates

Chemical conjugation of therapeutics with active molecules is one of the oldest strategies of biopharmaceutical improvement. This strategy was applied to introduce the third generation photosensitizers and was comprehensively reviewed by Senge [27]. There are many types of common biomolecules which are suggested to be conjugated with mTHPC to improve its solubility, *i.e.* polymers [31,32], to increase drug selectivity against tumor, *i.e.* glucose [18,100], folic acid (FA) [35], monoclonal antibodies [36,37] or to overcome the post-treatment side effects using anti-inflammatory agents *i.e.* ibuprofen [38] (Fig. 3). It should be noted, that covalent linkage may be subjected to damage in biological media and may also affect photophysical properties of dyes.

The simplest way to solubilize drug is to prevent the interaction between its molecules. Poly(ethylene)glycol (PEG) is considered as a common solubilizing molecule, which could be covalently bound to mTHPC, according to the patent of Sinn & co-workers in 1991 [101]. The hydrodynamic diameter of PEG depends on the polymerization degree (*i.e.* 3 and 5 nm for PEG-2000 and PEG-5000, respectively) [102]. Following the optimization of conjugates, the degree of PEG

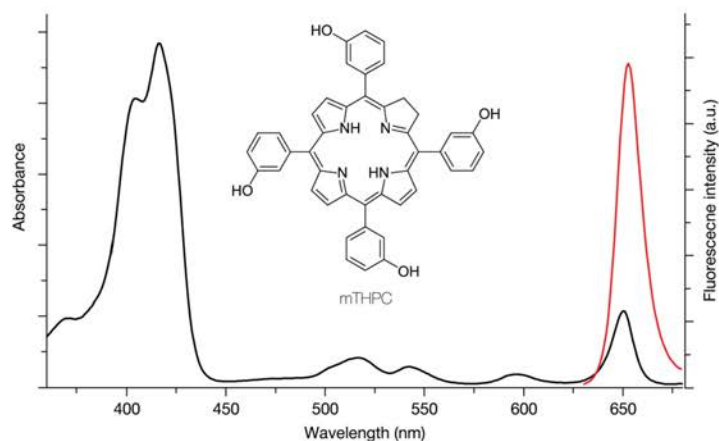


Fig. 1. Absorbance (black) and fluorescence (red) spectra of mTHPC in methanol. Adapted and reprinted with permission from ref. [19]. (For interpretation of the references to colour in this figure legend, the reader is referred to the web version of this article.)

polymerization varied and mTHPC-PEG-2000 was pre-selected for further *in vitro* studies due to its stability in biological media and a lowest dark toxicity in Colo26 colorectal tumor cells [32]. Obviously, PEG conjugates prevent mTHPC aggregation as well as the PS interactions with lipoproteins. Moreover, PEG molecules commonly have a limited intracellular accumulation that theoretically could reduce PDT efficiency. Practically, solubilization of mTHPC due to conjugation with PEG prolongs 2 times its half-time in murine plasma [103] and significantly improves selectivity, demonstrating a better accumulation in human LS174T colon carcinoma xenografts (tumor-to-muscle ratio up

to 20) and a lower level in liver compared with free mTHPC [29]. Nevertheless, the photodynamic efficiency of mTHPC-PEG compounds did not exceed that of free mTHPC in xenografts [29–31,33,34].

Another strategy is to use small active molecules as solubilizers for mTHPC. For example, glucose [18] and FA [35] (the size is < 1 nm [104]) were conjugated with mTHPC and modulated its water solubility by creating a balance between hydrophilicity and hydrophobicity. Additionally, in the case of glucose, it has been hypothesized that targeting of glucose metabolism may provide a selective targeting of cancer due to the Warburg effect [105]. However, *in vitro* studies performed using

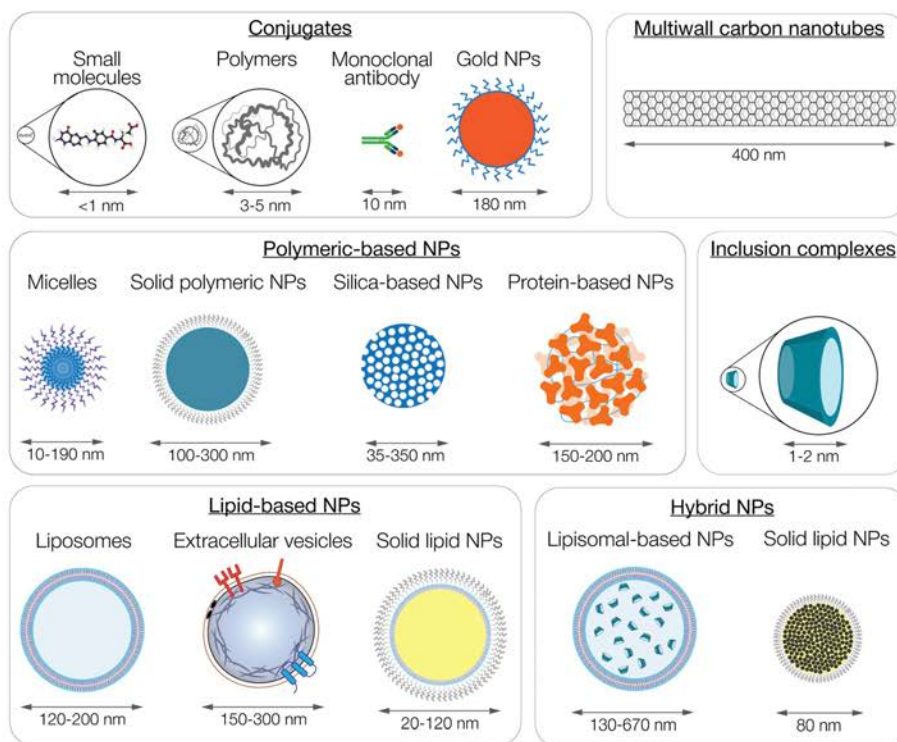


Fig. 2. Nanoplatfoms already applied for mTHPC delivery.

Table 1
Temoporfin-loaded nanoplatfoms in biological studies.

NP	Targets	Observations	Ref.
Conjugates PEG	Nude mouse bearing xenografts LS174T, chinese hamster with induced early squamous cell carcinoma in the cheekpouch mucosa	Compared with free mTHPC: longer plasma half-time and lower liver uptake; lower penetration depth in the tumor tissue <i>in vivo</i> ; higher the maximal tumor-to-muscle ratio <i>in vivo</i> ; no selectivity in early squamous carcinoma cells <i>in vivo</i> (hamster mucosa); no significant difference after PDT.	[29,30]
	Nude mice bearing xenografts Colo26	Compared with free mTHPC: increased plasma half-time; lower tumor necrosis depth <i>in vivo</i> ; no significant muscle damages; PEG chain length had relatively little effect on the patterns of mTHPC bioactivity.	[31,32]
	Nude mouse bearing human squamous cell carcinoma and adenocarcinoma xenografts; minipig	Larger tumor necrosis in squamous cell carcinoma, but not in adenocarcinoma xenografts in mice <i>in vivo</i> compared with free mTHPC. No visible normal tissue alterations after mTHPC-PEG administration in minipigs <i>in vivo</i> .	[33]
Glycose	Female RAG-2-mice bearing xenografts XF-354 HT29 monolayer cells	No significant therapeutic effect observed <i>in vivo</i> . The asymmetric TPC(m-O-GluOH) ₃ exhibited higher phototoxicity <i>in vitro</i> compared to free mTHPC. An active receptor-mediated endocytosis mechanism of conjugates' internalization. Intracellular localization in mitochondria.	[34] [18]
Folic acid	HT29 and KB monolayer cells; nude mouse bearing xenografts HT29 and KB	Active targeted accumulation in KB tumors <i>in vivo</i> compared with free mTHPC	[35]
Monoclonal antibodies	UM-SCC-22A, UM-SCC-22B, HNX-OE monolayer cells; nude mouse bearing xenografts HNX-OE	Stable in serum. Low dark toxicity along with decreased intracellular accumulation and PDT efficiency <i>in vitro</i> . Selective targeting of the sensitizer to the tumor <i>in vivo</i> .	[36,37]
Non-steroidal anti-inflammatory drugs	SKGT-4, OE33 monolayer cells	All conjugates successfully entered the cells and whilst no cytotoxicity <i>in vitro</i> was observed.	[38]
Gold nanoparticles (180 nm)	SH-SY5Y monolayer cells	Internalization in cells <i>in vitro</i> was confirmed. Lower dark toxicity and increased phototoxicity <i>in vitro</i> compared to free mTHPC.	[39]
Inclusion complexes β-cyclodextrin derivatives	Monolayer HT29 cells; multicellular HT29 spheroids; nude mouse bearing xenografts HT29	Compared with free mTHPC: enhanced uptake and phototoxicity in cells <i>in vitro</i> ; increased accumulation and deeper penetration in spheroids <i>in vitro</i> ; higher tumor-to-skin and tumor-to-muscle ratios <i>in vivo</i> .	[40,41]
Micelles	14C monolayer cells	The uptake and phototoxicity of mTHPC in cells <i>in vitro</i> were observed only after degradation of micelles	[42]
mPEG750 polymers (10 nm)	HT29 monolayer cells	mTHPC oil/water nanoemulsion displays lower cellular uptake <i>in vitro</i> compared with Foscan®	[43]
pH-responsive PEO2-b-PLA (180–190 nm)	HT29 monolayer cells; nude mouse bearing xenografts HT29	Low cellular uptake and phototoxicity <i>in vitro</i> compared to free mTHPC. Similar to free mTHPC antitumor effects <i>in vivo</i> significantly reduced skin photosensitivity <i>in vivo</i> .	[44]
pH-responsive PEO2-b-PLA (77 nm)	HT29 monolayer cells	Lower cellular uptake <i>in vitro</i> with preferable localization in lysosomes. Comparable with free mTHPC phototoxicity <i>in vitro</i>	[45]
pH-responsive PEGMA-co-DPA (132–156 nm)	U87MG monolayer cells	VES-g-GSO/TPGS/RGD/K nanparticles exhibit higher cellular uptake and phototoxicity <i>in vitro</i> .	[46]
Chitosan oligosaccharide nanoparticles (130–145 nm)	U87MG monolayer cells; multicellular U87MG spheroids; nude mouse bearing xenografts U87MG	Deeper penetration and better photodynamic effect in spheroids <i>in vitro</i> . Enhanced antitumor efficiency <i>in vivo</i> .	[47]
Lipid-DNA polymer (8–10 nm)	A431, HT29, L929, J744A1.1, CAL27 monolayer cells	Compared with free mTHPC, lower dark cytotoxicity and higher PDT efficiency in cells <i>in vitro</i>	[48]
Ben-PCL-mPEG (16–57 nm)	RAW264.7, C166 C166 monolayer cells; nude mouse; LDIR-/- ApoB100/100 mouse	Selective phototoxicity in macrophages compared with endothelial cells <i>in vitro</i> . Similar to free mTHPC pharmacokinetics in plasma <i>in vivo</i>	[48]
Solid polymeric nanoparticles	C6 monolayer cells	PDT efficacy <i>in vitro</i> similar to free mTHPC PDT	[49]
Ultrafine hydrogel nanoparticles (2–3 nm)	HT29 monolayer cells	Similar to free mTHPC both accumulation in cells and penetration into spheroids <i>in vitro</i> . Reduction of dark cytotoxicity. Time- and concentration-dependent decrease in cell proliferation and viability <i>in vitro</i> after PDT similar to free mTHPC.	[50]
PLGA nanoparticles (283 nm)	A549, MCF10A U937, nude mouse bearing xenografts HCT-116-luc	PEGylation reduced mTHPC uptake in cells <i>in vitro</i> . Reduced dark cytotoxicity along with equal PDT efficacy <i>in vitro</i> as for free mTHPC. The therapeutically favorable tissue distribution <i>in vivo</i> .	[51]
PLGA-PEG nanoparticles (145–180 nm)	J774.AI, HT29 monolayer cells; male CD-11 ChCD1(ICR) mouse	Reduced dark cytotoxicity along with equal PDT efficacy <i>in vitro</i> compared with free mTHPC. Improved <i>in vivo</i> distribution after injection.	[52]
PLGA-PEG nanoparticles (97 nm)			
Silica based nanoparticles	KYSE 510 monolayer cells	Reduced intracellular uptake, however similar to free mTHPC phototoxicity <i>in vitro</i> .	[53]
Organically modified silica nanoparticles (33 nm)			

(continued on next page)

Table 1 (continued)

NP	Targets	Observations	Ref.
Calcium phosphate nanoparticles (170–205 nm)	CAL-27 monolayer cells; nude mouse bearing xenografts CAL-27	Calcium phosphate nanoparticles/teniporfin/RGDfK peptide/DY682-NHS platform. RGDfK targeting decreased intratumoral accumulation and enhanced uptake in the lungs <i>in vivo</i> . Therapeutic success was achieved with 3 of 4 mice <i>in vivo</i> .	[54]
Silica-based nanoparticles (160–350 nm)	4T1, MDA-MB-231 monolayer cells; nude mouse bearing xenografts MDA-MB-231	Comparable with free mTHPC intracellular uptake <i>in vitro</i> . Higher antitumor PDT effect <i>in vivo</i> compared to Foscan*. Penetration through the blood-brain barrier was confirmed.	[55]
Protein-based nanoparticles	Junkar monolayer cells	The single oxygen generation inside Junkar cells <i>in vitro</i> was confirmed. Similar cellular uptake and phototoxicity <i>in vitro</i> as free mTHPC. Preferable intracellular localization in lysosomes.	[56,57]
HSA nanoparticles (150–200 nm)	Fertilized chicken eggs	Significant vascular damage in chick chorioallantoic membrane <i>in ovo</i> at high drug dose (1 mg/kg b.w.) and at a minimally effective light dose $> 25 \text{ J/cm}^2$.	[58]
Liposomes	Nude mouse with induced skin carcinoma	High selectivity <i>in vivo</i> : the average tumor-to-muscle and the tumor-to-skin selectivity were 6.6 and 2, respectively. Rapid biodistribution and clearance from the bloodstream.	[59]
Foslip* (135 nm)	Nude mouse bearing xenografts HT29	Lower accumulation and dark toxicity in cells <i>in vitro</i> compared to Foscan*. Almost identical behavior of both formulations in the presence of serum.	[60]
	GBC, BDC monolayer cells	Slow mTHPC release from liposomes and inhomogeneous distribution in the tumor <i>in vivo</i> after intratumoral administration. Optimal, albeit partial, cure rates at 24 h post-administration.	[61]
	Nude mouse bearing xenografts EMT6	Similar to Foscan* uptake in tumor cells <i>in vitro</i> . The decrease of mTHPC fluorescence life-times during incubation.	[62]
	Hela monolayer cells	Tumor-to-muscle ratio <i>in vivo</i> was 3.6 from 6 to 15 h DLI. Illumination intervals at 6 and 15 h were the most effective in terms of growth delay.	[63]
	Female Foxn1 ^{nu/nu} mouse bearing xenografts EMT6	Significant acceleration of wound healing after PDT <i>in vivo</i> .	[64]
	Nude female SKH-1 mouse	Foslip*-based PDT resulted in severe damage of both RNA and DNA <i>in vitro</i> .	[65]
	PC-3 monolayer cells	Higher bioavailability <i>in vivo</i> than Foscan*.	[66]
	Female Fisher-344 rat bearing xenografts R3230AC	Comparable to Foscan* fluorescence in the subepithelial stroma <i>in vivo</i> . Higher fluorescence in the tumor <i>in vivo</i> at 2, 4, and 8 h compared to Foscan*.	[67]
	Male Wistar rats with induced carcinoma of oral epithelium	Quick destruction of liposomes in blood in chick chorioallantoic membrane <i>in ovo</i> . The destruction and occlusion of the smaller vessel at 1 h DLI and total occlusion of the treated area at 3 h DLI after PDT <i>in ovo</i> .	[68]
	Free and EMT6 xenografted fertilized chicken eggs	Tumor necrosis was 30% at 15 min as well as at 1 h DLI.	[69]
	Nude mouse bearing xenografts HT29	Quick drug efflux from Foslip* in plasma <i>in vivo</i> . High elimination rate from the skin <i>in vivo</i> . Release from vasculature to tumor stroma at 15 h. Tumor growth delay was 44.4 days at 24 h DLI.	[70]
	Nude mouse bearing xenografts CAL-27	PDT-induced apoptosis and tumor vascularization damage <i>in vivo</i> at 2 days after treatment. Decrease of tumor volume at 20 days after PDT.	[71]
	Female C57BL/6 mouse with induced acute colitis	Reduced intestinal tumor growth <i>in vivo</i> . Prevention of a dysbiotic microbiota in colitis-associated cancer <i>in vivo</i> model.	[72]
	Hela monolayer cells; multiceellular HeLa spheroids	Higher uptake and lower dark cytotoxicity in monolayer cells <i>in vitro</i> compared to free mTHPC. Less homogeneous distribution in spheroids <i>in vitro</i> than free mTHPC. Slightly better PDT efficiency in monolayer cells and in spheroids <i>in vitro</i> than free mTHPC.	[73]
	Nude mouse bearing xenografts CAL-33	The increased tumor-to-skin ratio <i>in vivo</i> compared to free mTHPC. Enhanced accumulation of mTHPC in all tissues. The better therapeutic antitumor effect <i>in vivo</i> than free mTHPC.	[74]
	143B, K7M2L2 monolayer cells; female SCID mouse bearing xenografts 143B; female BALB/c mouse bearing xenografts K7M2L2	No significant difference, lower dark cytotoxicity and higher PDT efficiency in cells <i>in vitro</i> compared to Foscan*. Enhanced uptake in tumor and slightly higher antitumor efficiency <i>in vivo</i> compared to Foscan*.	[75]
	Multiceellular HT29 spheroids	Similar to Foscan* effect on pulmonary metastases and tumor perfusion <i>in vivo</i> .	[76]
	HT29 monolayer cells; multiceellular HT29 spheroids	Limited penetration of mTHPC in spheroids <i>in vitro</i> .	[76]
		Lower accumulation in cells <i>in vitro</i> compared to free mTHPC. Low penetration ability of mTHPC in spheroids <i>in vitro</i> .	

(continued on next page)

Table 1 (continued)

NP	Targets	Observations	Ref.
Fospeg* (125 nm)	Cats bearing cutaneous squamous cell carcinoma xenografts	Several times higher tumor accumulation, therapeutic ratio, plasma concentration and bioavailability in cats <i>in vivo</i> compared to Foscan*	[77]
	Fertilized chicken egg	Higher vascular damage in chick chorioallantoic membrane <i>in ovo</i> compared to Foslip*	[58]
	A431 monolayer cells	Similar uptake and retention in cells <i>in vitro</i> . Reduced dark and photoinduced cytotoxicity effects <i>in vitro</i> .	[78]
	A549, CCD-34Hu monolayer cells	Lower accumulation, dark cytotoxicity and photocytotoxicity in cells <i>in vitro</i> compared to free mTHPC.	[79]
	Female Fisher-344 rat bearing xenografts R2230AC	Higher bioavailability <i>in vivo</i> than Foscan*. The highest tumor fluorescence <i>in vivo</i> at the earlier time points compared to Foslip* and Foscan*.	[66]
	Female Wistar rat bearing xenografts MC28	Decreased plasma clearance and lower skin photosensitivity <i>in vivo</i> compared to Foscan*. Increased accumulation in the tumor <i>in vivo</i> and the tumor-to-skin ratio was 6. A greater percentage of tumor necrosis at low dose PDT.	[80]
	LNcap monolayer cells	Enhanced intracellular uptake and photodynamic activity in cells <i>in vitro</i> .	[81]
	Male Wistar rats with induced carcinoma of oral epithelium	Higher fluorescence in normal and tumor tissue <i>in vivo</i> compared to both Foscan* and Foslip*.	[67]
	Free and EMT6 xenografted fertilized chicken eggs	Significantly higher stability, slower drug release, better tumoricidal effect and lower damage to the normal vasculature in chick chorioallantoic membrane <i>in ovo</i> at already 1 h DLI as compared to Foslip*.	[68]
	Nude mouse bearing xenografts HT29	Higher levels for the first 6 h in plasma <i>in vivo</i> compared to Foslip*. Slow release form vasculature <i>in vivo</i> .	[69]
	Nude mouse bearing xenografts HT29	Higher <i>in vivo</i> PDT efficiency at shorter DLI compared to Foslip*.	[82]
	C666–1, HK1, CNE2 monolayer cells	The rapid uptake of mTHPC in the liver <i>in vivo</i> followed by a fast clearance. Tumor-to-skin ratio was 3.8 at 2 h.	[83]
	HeLa monolayer cells; multicellular HeLa spheroids	No P-gp-mediated efflux in cells <i>in vitro</i> . Induction of over-expression of MDR1 gene transcript and P-gp proteins after PDT.	[83]
	COLO206, LN229, U118, A172, DBTRG, C6 monolayer cells	No significant differences in penetration and PDT efficiency in spheroids <i>in vitro</i> compared to Foslip*.	[72]
	Nude mouse bearing xenografts HT29	Cationic gemini surfactant increased mTHPC cellular uptake and resulted in a high grade of photocytotoxic effect <i>in vitro</i> .	[84–87]
	Human female abdominal skin	Treatment with mTHPC-loaded invasomes with 1% terpene mixture resulted in a slower increase in tumor size <i>in vivo</i> .	[88]
	Human abdominal skin	The increase of mTHPC amount in deep stratum corneum and deeper skin layers <i>in vitro</i> compared to free mTHPC.	[89]
	CT26 monolayer cells; multicellular CT26 spheroids	Cationic liposomes delivered the highest mTHPC amount to stratum corneum and deeper skin layers compared to anionic and neutral ones.	[90]
	HT29 monolayer cells; multicellular HT29 spheroids	Enhanced uptake in cancer cells and equivalent penetration potential in spheroids <i>in vitro</i> compared to free mTHPC and Foslip*.	[91]
	MCF-7 monolayer cells	Increased stability in plasma compared Foslip*. Enhanced accumulation and photocytotoxicity in cells <i>in vitro</i> . Deeper penetration and higher PDT efficiency in spheroids <i>in vitro</i> .	[76]
	CAL-33 monolayer cells; multicellular CAL-33 spheroids; nude mouse bearing xenografts CAL-33	Mild dark and photoinduced cytotoxicity <i>in vitro</i> for naked lipid nanodroplets.	[92]
	4T1, MDA-MB-231 monolayer cells; nude mouse bearing xenografts MDA-MB-231	Lower uptake in cells and deeper penetration in spheroids <i>in vitro</i> compared with free mTHPC. Reduced dark cytotoxicity in cells and spheroids <i>in vitro</i> . Increased mTHPC uptake in all tissues <i>in vivo</i> compared to Foscan*.	[73, 93]
	SKOV3 monolayer cells	Comparable tumor volume reduction with Foscan*.	[94]
	SKOV3 monolayer cells	Carbon nanotubes internalized in the cells <i>in vitro</i> with subsequent mTHPC release to the cellular compartments. Synergic impact of the combined photothermal/photodynamic therapy <i>in vitro</i> .	[95]
	SKOV-3, PC3, TC-1 monolayer cells; nude mouse bearing xenografts SKOV-3	Enhanced uptake by cancer cells and cellular death due to the magnetic targeting <i>in vitro</i> . The increased antitumor effect <i>in vivo</i> .	[96, 97]
	SKOV-3 monolayer cells; nude mouse bearing xenografts A431	Synergistic antitumor PDT efficacy <i>in vitro</i> . Complete eradication of the tumor <i>in vivo</i> by combined magnetic/photodynamic therapy.	[98]
	ALTS1C1, bEnd.3 monolayer cells, male C57BL/6 J mice bearing orthotopic ALTS1C1 tumor	Upconversion nanoparticles/IR-780/mTHPC/C-PEG-maleimide nanoparticles. Higher accumulation in cells <i>in vitro</i> compared to free mTHPC. Synergistic antitumor efficacy <i>in vitro</i> after photothermal/photodynamic therapy. Overcoming a blood-brain barrier and enhanced mTHPC accumulation in brain tumor <i>in vivo</i> . Increased median survival after combined therapy <i>in vivo</i> .	[99]
	HT29 monolayer cells; multicellular HT29 spheroids	Similar to Foslip* accumulation in cells and spheroids <i>in vitro</i> . Complete penetration and homogeneous distribution of mTHPC across the spheroid <i>in vitro</i> .	[75]

glucosylated mTHPC demonstrated less intracellular uptake in human colorectal adenocarcinoma (HT29) monolayer cells than that of the free drug [18]. Nevertheless, photodynamic efficiency was increased in the case of (TPC(*m*-O-Glu)₃) compared with symmetrical (TPC(*m*-O-Glu)₄) and free mTHPC. At the same time, water-soluble vitamin B9 or FA could be used as targeting agents for cancers that overexpress folate receptor (FR- α) on their cellular membrane, like ovarian, breast and lung cancers [106]. In 2008, Gravier et al. tested FA-conjugated mTHPC in a mouse xenograft model *in vivo* using KB cells rich in FR- α and HT29 cells as a negative control [35]. This study indeed demonstrated that FA-mTHPC conjugates were strongly accumulated in the KB tumors with a tumor/normal tissue ratio > 5.0, compared with that of 2.1 for free mTHPC; equal accumulation was noted for both formulations in HT29 tumors.

The selectivity of the drug against a specific cancer type could be achieved using tumor-selective monoclonal antibodies. With this aim, Vrouenraets and co-workers conjugated mTHPC with neck squamous cell carcinoma-selective chimeric monoclonal antibody (cMAb) U36 [36,37]. The size of cMAb is about 10 nm, as was estimated for IgG [102]. Despite the optimistic *in vitro* results on serum stability and immunoreactivity, mTHPC loading ratio was only several molecules per cMAb that was not enough for efficient PDT treatment of U36 monolayer cells *in vitro*. The experiments *in vivo* in tumor-bearing mice demonstrated that the tumor/skin ratio was 3.5 times higher compared with mTHPC, nevertheless it was concluded that successful PDT application of mTHPC-MAb conjugates requires a high level of total conjugate binding and is possible only for internalized MABs.

To go further in order to improve PDT therapeutic efficacy, the combined therapy using non-steroidal anti-inflammatory drugs was proposed. Rogers and co-workers theorized that a conjugate will undergo biological cleavage to deliver the PS and anti-inflammatory drug at the tumor site [38]. With this aim, they successfully synthesized the library of “iPorphyrins” composed of mTHPC conjugates with non-steroidal anti-inflammatory drugs to specifically target the tumor microenvironment. However, the covalent linking of mTHPC to non-steroidal anti-inflammatory drugs significantly reduced the efficiency of singlet oxygen production. Therefore, it is not surprising that the phototoxic effect was not observed in the esophageal carcinoma OE33 and SKGT-4 cells despite the successful intracellular accumulation of conjugates. It is one of the examples of how covalent binding of mTHPC

with biomolecules influences photophysical properties of PS thus complicating the prediction of photodynamic response of such compounds using standard uptake studies *in vitro*.

Finally, mTHPC could be conjugated with nanoplatforms such as gold nanoparticles (AuNPs). AuNPs are non-toxic, biocompatible and provide a relatively long circulation time of drug bound to their surface [107]. Haimov with co-workers synthesized 180-nm mTHPC-AuNPs allowing to passively target the hyper-permeable tumors taking the benefits of enhanced permeability and retention (EPR) effect [39]. This also offered an opportunity to use mTHPC-AuNPs as contrast agents for computed tomography imaging *in vitro* and *in vivo* [108]. Surprisingly but photophysical properties of mTHPC remain almost unchanged after the conjugation with AuNPs, probably due to the low loading of mTHPC per NP. The studies *in vitro* demonstrated the potency of mTHPC-AuNPs, namely NPs internalization in human neuroblastoma cells SH-SY5Y and a better PDT effect of conjugates compared with free mTHPC.

It should be also noted that other biomolecules were proposed for conjugation with PSs. For example, the association of PSs with peptides and proteins is recognized as a successful method for enhancing the selectivity and efficacy of photodynamic treatment. Giuntini et al. have already described in the review paper the advances of various peptide-appended porphyrin systems [109]. To date, the focus of investigations is shifted to nanoparticle-based systems, which are non-covalently bound to mTHPC.

3.2. Host-guest supramolecular complexes

Supramolecular systems are one of the most versatile strategies in PS delivery [110]. Initially, in 1999, cyclodextrins (CDs) were proposed only as an approach for mTHPC detection in blood [111] and only in 2016 the first report on CD-based independent delivery of mTHPC was published [41]. Since that time, it has been demonstrated that mTHPC efficiently forms supramolecular non-covalent complexes of few nanometers in size with one or two CD molecules (Fig. 4), causing the monomerization of PS molecules in the aqueous surrounding in the presence of CDs [100,111–113]. It should be noted that the complex formation process strongly depends on the type of CD and especially on its substitutes [111,114].

Deep investigations of CDs as pharmaceutical agents demonstrated that depending on the affinity to the drug, the CD could act as a drug

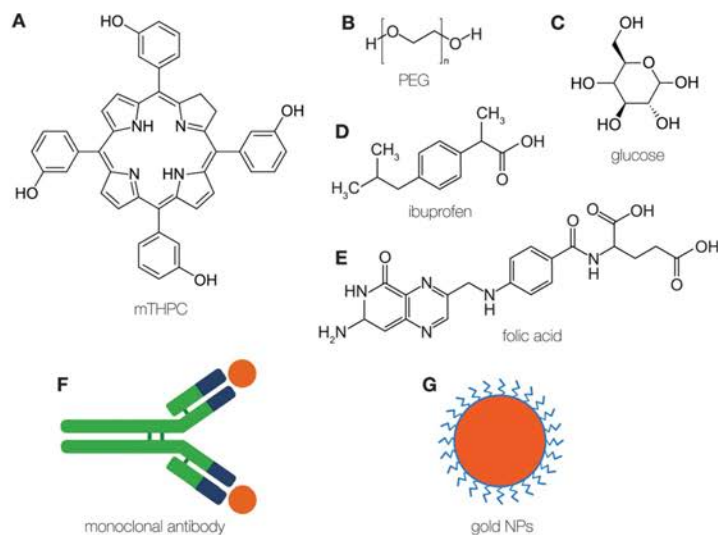


Fig. 3. Active molecules, which could covalently bound to (A) mTHPC; (B) poly(ethylene-glycol) (PEG), (C) glucose, (D) ibuprofen, (E) folic acid, (F) monoclonal antibody, (G) gold NPs. (For interpretation of the references to colour in this figure legend, the reader is referred to the web version of this article.)

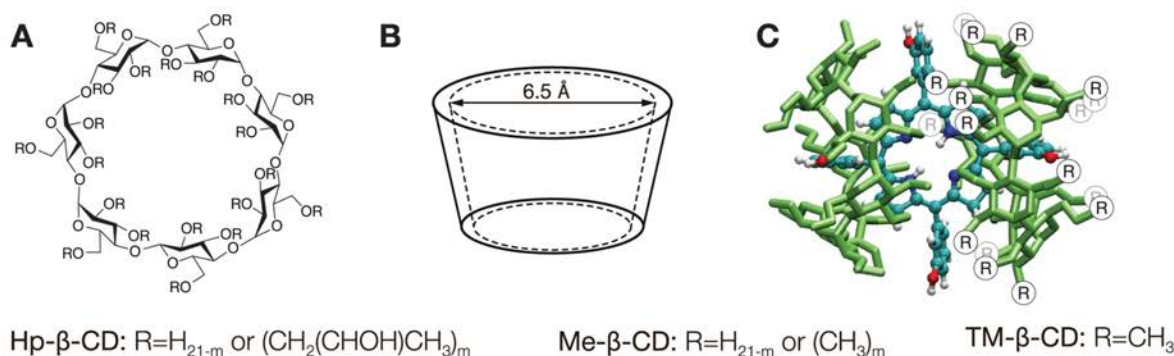


Fig. 4. The schematic representation of (A,B) CD structure and (C) inclusion complexes with CDs. Adapted and reprinted with permission from ref. [114].

solubilizer only (binding constant (K) is $< 10^4 \text{ M}^{-1}$) and/or as drug biodistribution modulator, when K value is higher than 10^5 M^{-1} [115]. In the case of mTHPC, K values are huge reaching $1 \times 10^7 \text{ M}^{-1}$ for completely methylated β -CD [114] and as such determining the unique properties of β -CDs as mTHPC nanoshuttles [40,41]. Overall, co-administration of β -CDs/mTHPC complexes could solve several mTHPC drawbacks at once:

- 1) mTHPC is monomeric from the onset of administration and during the whole circulation time [41]. Additionally, such high affinity allows using CD concentrations as low as 0.5–5 mg/kg being much lower than toxicity limits (estimated as 40–100 mg/kg and higher) [115]. Even after dilution of complexes in blood, their dissociation resulted in a quick mTHPC redistribution to transport proteins instead of PS self-aggregation.
- 2) Distribution of mTHPC in serum is modulated by both concentration and type of CD [41]. The presence of a large amount of β -CD results in mTHPC sequestration in inclusion complexes. This also leads to the shift of equilibrium distribution of PS in serum to the inclusion complexes. The high affinity of CDs to mTHPC determines the formation of complexes in serum even in the presence of many potential mTHPC binding sites.
- 3) The CD-mediated nanoshuttle mechanism for mTHPC offers the opportunity to accelerate mTHPC redistribution between transport proteins themselves and between transporters and cellular membranes (Fig. 5A). In the presence of CDs, mTHPC almost completely redistributes between lipoproteins *in vitro* within 30 min [41], while in CD free medium this process takes > 20 h [20].
- 4) Intratumoral mTHPC distribution is improved. CD nanoshuttles accelerate accumulation in tumor cells and strongly improve mTHPC penetration in multicellular tumor spheroids (Fig. 5B). This is possibly due to the small size of CD nanoshuttles (1–2 nm), which easily diffuse into the interstitial medium [40]. These observations were confirmed in xenografted tumors *in vivo*, where the maximal level of mTHPC fluorescence from the surface of HT29 tumor was achieved at already 2 h post-administration of mTHPC/CD complexes [41]. Finally, *ex vivo* fluorescence analysis of isolated tumors at 24 h after injection demonstrated that co-administration of mTHPC with methyl- β -CD increases the total fluorescence signal 1.3 times from isolated tumors compared with free mTHPC (from 196 ± 26 a.u. to 247 ± 30 a.u., $p < .05$) [41].
- 5) Biodistribution of mTHPC is favorably modified [41]. The application of β -CDs decreased the level of mTHPC 1.5–3 times in skin and muscle tissues that together with better PS accumulation in tumor results in the increased therapeutic ratio (tumor/skin or tumor/muscles) up to 2 times (Fig. 5C). Moreover, the small size of CDs and strong binding to mTHPC leads to the changes of mTHPC excretion routes: the level of mTHPC in the liver is reduced 1.5 times and

increased in kidneys 1.8 times compared to free mTHPC administration.

Overall, the application of CDs significantly improves the delivery of mTHPC at all stages of PS distribution, making CDs powerful nanocarriers for mTHPC. Further, CDs are supposed not to penetrate into cells [116], therefore they modulate only transportation of PS to the tumor cells keeping intact favorable photobiological properties of PS. Nevertheless, the supramolecular complex lacks long-term stability that together with a strong dependence of CDs effects on their concentration complicates the control of PS delivery at the target site. Moreover, individual application of the supramolecular complex *in vivo* is problematic due to the dilution of CD-mTHPC complexes and a rapid CD excretion from the circulating system after intravenous injection [117].

3.3. Polymeric NPs

To date, macromolecular-based nanocarriers attract the most attention in terms of PS delivery [118]. These nanocarriers possess beneficial advantages, which mainly reside in their excellent colloid dispersity in water enabling solubilization of hydrophobic PS in physiological conditions. Moreover, compared to supramolecular complexes, the size of macromolecular NPs is easily modulated in the nanometer range providing tumor targeting by EPR effect [119]. Although the limitations of EPR are now acknowledged [120], it remains the main process of passive targeting of NPs to tumors. Phospholipids or polymers including FDA-approved synthetic polymers or biopolymers are popular materials for the creation of organic NPs. Polymeric NPs can be formed by self-assembly of biodegradable polymers, which spontaneously assemble into a core-shell structure in an aqueous environment minimizing the system's free energy. Additionally, their surface properties, morphology, and composition can be easily modified to control NP degradation and kinetics of drug release. Next part of this review related to polymeric NPs will be divided into several items according to NP structure: micelles, solid NPs, silica- and protein-based NPs.

3.3.1. Micelles

Micelles are the example of colloidal nanocarriers, micro/nanospheres, polymer-drug conjugates and liposomes [119,121]. Generally, micelles are fabricated based on the self-assembly of amphiphilic blocks or graft *co*-polymers. The hydrophobic core of micelles can accommodate hydrophobic drugs, whereas their hydrophilic shell ensures the possibility for active targeting or additional protection of NPs with PEG molecules. It is worth noting that polymeric micelles are resistant to dilution effects, for example, they keep initial structure intact upon intravenous administration of the drug formulation due to the very low critical micelle concentration of polymeric surfactants. There are

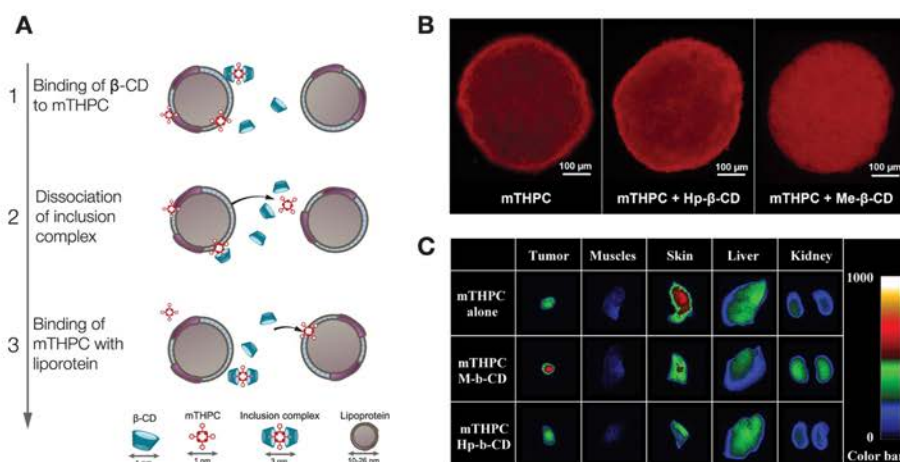


Fig. 5. (A) Schematic representation of nanoshuttle mechanism of CD action. (B) Improvement of mTHPC distribution in HT29 multicellular tumor spheroids by CDs. (C) Biodistribution of mTHPC in HT29 tumor bearing mice after co-administration with CDs. Adapted and reprinted with permission from ref. [40,41].

several possibilities to encapsulate hydrophobic drugs, such as physical entrapment to the hydrophobic core and/or covalent binding to the polymer molecules. Still, in the case of mTHPC, the latter may not be preferred due to the significant changes of photophysical properties and uptake limitations. Thus all micellar formulations of mTHPC encapsulate PS within the hydrophobic core (Fig. 6).

The evolution of mTHPC micellar formulations includes several stages. In 2008, Hofman et al. were the first to report the use of biodegradable mPEG750-b-oligo(ϵ -caprolactone)₅ micelles (10 nm in size) loaded with mTHPC in 15% (w/w) feed ratio (loading efficacy was 90%) [42]. However, the authors reported the necessity of site-specific enzymatic micelle degradation and subsequent mTHPC release for effective cellular mTHPC uptake as an explanation of comparable with free mTHPC photocytotoxicity in 14C cells. That is why in 2017 they proposed the updated mTHPC-loaded micelles as an approach to treat atherosclerotic lesions using PDT modality [48]. The next step was to change the mechanism of mTHPC release in order to increase the accumulation of PS for efficient PDT. It has been proposed to use pH-responsive poly(2-ethyl-2-oxazoline)-b-poly(D,L-lactide) (PEOz-b-PLA) as well as poly(ethylene-glycol)-methacrylate-co-2-diisopropylamine (PEGMA-co-DPA) di-block co-polymers in micelles formation to achieve control drug release at the tumor site [44,45]. The obtained micelles were about 100 nm in size (77 nm for PEOz-b-PLA and 140 nm for PEGMA-co-DPA) and possessed a high loading efficiency (a percentage of drug loaded in NP) of mTHPC (92.5% and > 80% for PEOz-b-PLA and PEGMA-co-DPA, respectively). It was hypothesized that NP with such size will passively target tumor and that mTHPC will be released in the tumor microenvironment, which is characterized by low pH 5.0. However, despite not optimistic *in vitro* results [44,45], in HT29 tumor bearing mice, the authors demonstrated reduced skin photosensitivity of micellar mTHPC formulation alongside with the similar to free mTHPC antitumor PDT efficiency. The successful PDT using micellar mTHPC was achieved in the case of integrin-rich U87MG tumors [46].

Using the mixture of chitosan-vitamin E succinate conjugates and D- α -tocopheryl-PEG conjugates grafted with cyclic RGD peptide Wu and co-workers prepared 145-nm micelles and loaded them with mTHPC with a loading efficiency 50%. Such active targeting improved accumulation and PDT efficiency in monolayer cells and increased mTHPC penetration depth in multicellular tumor spheroids *in vitro*, while *in vivo* RGD-modification resulted in inhibition of the growth of U87MG tumors without any toxicity to other tissues.

Recently, the concept of polymeric micelles was updated with new amphiphilic DNA-based co-polymers [122]. Thus, Liu and co-workers efficiently incorporated mTHPC in 11-nm lipid-DNAs micelles (loading capacity 11.7%, w/w) [47]. *In vitro* studies demonstrated better biocompatibility and reduced dark toxicity of mTHPC loaded lipid-DNAs micelles in various cell lines compared with free mTHPC. However, a high loading capacity in DNA-based micelles also has a negative aspect consisting of concentration quenching [47], determining the dependence of PDT efficiency of DNA-based micelles on drug release processes. Immunogenicity of DNA-based micelles was not addressed in this study. An interesting perspective could be offered by the bare DNA self-assembly NPs. Indeed, the previous research on these NPs demonstrated a low level of their immunogenicity, indicating the biosafety of DNA-based materials [123].

3.3.2. Solid polymeric NPs

Solid polymeric nanospheres are defined as colloid stable nanostructures. Such NPs consist mainly of biocompatible and biodegradable components exhibiting controlled drug release through biodegradation after the intracellular accumulation of NPs. Depending on the type of polymers, various size of nanospheres could be obtained, *i.e.* ultrafine 2–3 nm polyacrylamide NPs [49], 145-nm poly(D,L-lactide-co-glycolide) (PLGA) NPs [51], polyplex NPs based on chitosan (ca 498 nm) or chitosan oligomer lactate (ca 728 nm) polymer [124]. The opportunity to synthesize ultrafine NPs for mTHPC delivery was used by Gao De and

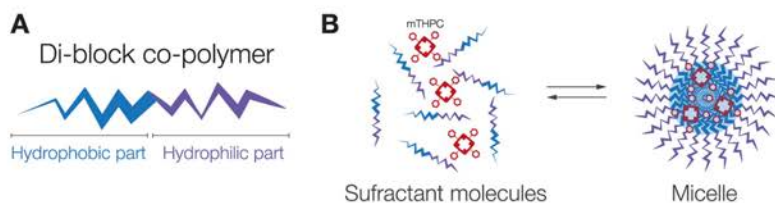


Fig. 6. (A) The structure of di-block co-polymers and (B) principal scheme of micelles formation.

co-authors [49]. The authors supposed that these NPs could be of interest *in vivo* due to their ultrasmall size and potential low protein and macrophage adsorption. To date, *in vitro* studies demonstrated PDT cytotoxicity in C6 rat glioma cells.

The most common polymer used for solid NPs preparation is PLGA. Owing to excellent biocompatibility and biodegradability, PLGA has been approved by the US Food and Drug Administration (FDA) [125]. After cellular uptake, it undergoes hydrolysis generating two monomers (lactic acid and glycolic acid) with very low systemic toxicity. Therefore, in 2011 Low and co-workers proposed PLGA-based nanospheres as an mTHPC delivery system. With this aim, they synthesized PLGA nanospheres of 283.2 ± 20.4 nm and tested their efficiency against HT29 monolayer cells and multicellular tumor spheroids [50]. PLGA nanoparticles successfully delivered mTHPC to HT29 cells, released it into the cytoplasm and caused apoptosis after illumination. However, no further changes in PS accumulation and distribution in both monolayer and spheroid models were observed compared with free mTHPC, probably because of untimely release. Photocytotoxicity in monolayer cells was also comparable with free mTHPC. To prevent adverse interaction of PLGA NPs with proteins and mononuclear phagocytic system, PEGylation of NPs was performed [51,52]. Depending on the preparation technique, the particles from 100 to 170 nm were obtained and loaded with mTHPC. PEGylated mTHPC-PLGA nanospheres were sufficiently stable in serum over the observed time frame [52]. Nevertheless, PEG shell is also the hydrophobic environment and may bind mTHPC, therefore substantial leak of the drug may occur in the presence of serum proteins [51]. Concerning *in vitro* efficiency, PLGA-mTHPC-NPs with PEG shell displayed similar behavior as ultrafine nanospheres. Finally, the study of mTHPC biodistribution upon its delivery by PLGA NPs demonstrated similar to Foscan® tumor selectivity raising the question on the possible improvement of PLGA platform with active targeting molecules or stimuli-response moieties. Recently, PLGA-nanospheres were upgraded using light-degradable aliphatic polycarbonate moieties for the controlled release of mTHPC [126]. To date, no *in vitro* data on the interaction of synthesized NPs with cells are available, however, the proposed NPs are activated at 365 nm suggesting significant limitations of its *in vivo* application due to the small penetration depth of UV light.

Along with the conventional materials for polymeric NPs as PLGA, some specific nanomaterials were applied such as chitosan polymer or chitosan oligomer lactate [124]. These natural biodegradable polymers are nontoxic, biocompatible, biodegradable, can be easily chemically modified, have a relatively low cost and certain flexibility to respond to pH changes [127]. Thus, chitosan polymer or chitosan oligomer lactate were used for the preparation of biodegradable polyplex nanospheres [124]. These NPs possessed the size of > 300 nm and at pH = 5.0 they were unfolded increasing in size up to 500 nm. However, as many strategies, such NPs passed only the basic release experiments, so additional *in vitro* and *in vivo* experiments are needed to assess the applicability of natural biodegradable nanospheres in mTHPC-PDT.

3.3.3. Silica-based NPs

Silica-based NPs (SiNPs) represent porous nanospheres which can be loaded with organic molecules by covalent links to the silica matrix or by simple entrapping as in the case of hydrophobic mTHPC. SiNPs are transparent to light and photochemically inert. The first studies on mTHPC-SiNPs were performed by Yan and Kopelman in 2007 [128]. The authors hypothesized that SiNPs may decrease mTHPC photodegradation and further demonstrated the reasonable generation of singlet oxygen by 180-nm mTHPC-SiNPs. However, this approach works only when entrapped mTHPC is delivered to cells in association with the silica matrix. As was mentioned above, the drug release mechanism is usually essential for such nanoplateforms, nevertheless, the balance is needed. For example, SiNPs were organically modified to deliver mTHPC to human oesophageal squamous carcinoma KYSE 510 cells [53]. The authors successfully entrapped mTHPC in feed ratio of

1% (w/w) into 41-nm organic-modified SiNPs (ORMOSIL NPs). However, without PEG coating, mTHPC is completely released from ORMOSIL to serum proteins in 1 h making NPs inefficient as nanocarriers. Silica NPs with delayed mTHPC release demonstrated PDT potency *in vivo* in MDA-MB-231 – bearing Nu/Nu mice compared with conventional mTHPC formulation Foscan® [55]. Moreover, the authors reported that mTHPC-loaded SiNPs could pass through the blood-brain barrier [55], as was already demonstrated for PEGylated SiNPs [129,130], perhaps, due to the receptor-mediated endocytosis by the endothelial cells of the brain capillary followed by transcytosis and specific-transporters support [131]. Based on that, the authors suggested SiNPs as a potent delivery system for mTHPC against brain metastases [55].

In fine, silica-modified calcium phosphate NPs were used as a multifunctional theranostic platform that regroups near-infrared fluorescence optical imaging with optimized tumor targeting and PDT. With this aim, Haedicke and co-workers embedded mTHPC into synthesized 200-nm CaP/PEI/SiO₂ and attached near-infrared fluorescence agent DY682 along with RGDfK-peptide for active targeting of CAL-27 tumor (Fig. 7) [54]. SiNPs-RGD loaded with mTHPC were selectively accumulated in the tumor tissue *in vivo* (Fig. 7B). PDT with these NPs was rather efficient (75% of cured mice) (Fig. 7C). In addition, the authors demonstrated PDT-induced damage of tumor vasculature using IRDye® 800CW RGD and detected apoptotic tumor cells already 2 days post-PDT (Fig. 7D).

3.3.4. Protein-based NPs

Protein nanoparticles have better biocompatibilities, biodegradability, non or low -antigenicity and thus could be also attractive material for drug delivery platforms [132]. For instance, human serum albumin (HSA) is one of the most known natural transporters of PS in serum [133] and has been proposed for the preparation of protein-based nanocarriers for PSs. mTHPC molecules, however, possess low affinity to HSA binding sites [20], thus mTHPC encapsulation requires chemical cross-linking of HSA to obtain porous NP structure (Fig. 8). Chemical cross-linking of HSA units results in the formation of 150–200 nm porous NPs [56,134]. Such microenvironment is supposed to induce non-covalent adsorption of drug molecules to the surface of HSA and can be altered by varying the cross-linking degree between HSA units as was performed for mTHPC [57]. *In vitro* studies of mTHPC-HSA NPs on Jurkat cells demonstrated efficient intracellular accumulation and similar to free mTHPC total phototoxicity. The *in vivo* potency of HSA-NPs is questionable, however, the opportunity to adjust drug release and size by varying cross-linking degree makes such platforms very flexible.

3.4. Lipid-based NPs

In the range of natural biomaterials, lipids as one of the main components of biological membranes and lipoproteins as serum transporters are particularly attractive. Lipid-based drug delivery systems have shown effective size-dependent properties together with a high degree of biocompatibility and versatility [135]. Moreover, lipid-based NPs should be very capacious due to the high affinity of mTHPC to lipid microenvironment. Finally, phospholipids are major components of biological membranes and could be easily incorporated in membrane structures providing required drug release upon the fusion with biomembranes. In the next chapters, we shall review several types of lipid-based NPs used for mTHPC delivery, including vesicular (liposomes and extracellular vesicles) and solid lipid nanoparticulate systems.

3.4.1. Liposomes

Among various lipid-based formulations, classical “liposomes,” which primarily consist of phospholipids (basic components of cellular membranes) were extensively studied as mTHPC nanocarriers [136]. Liposomes represent bilayered phospholipid nanocapsules which could

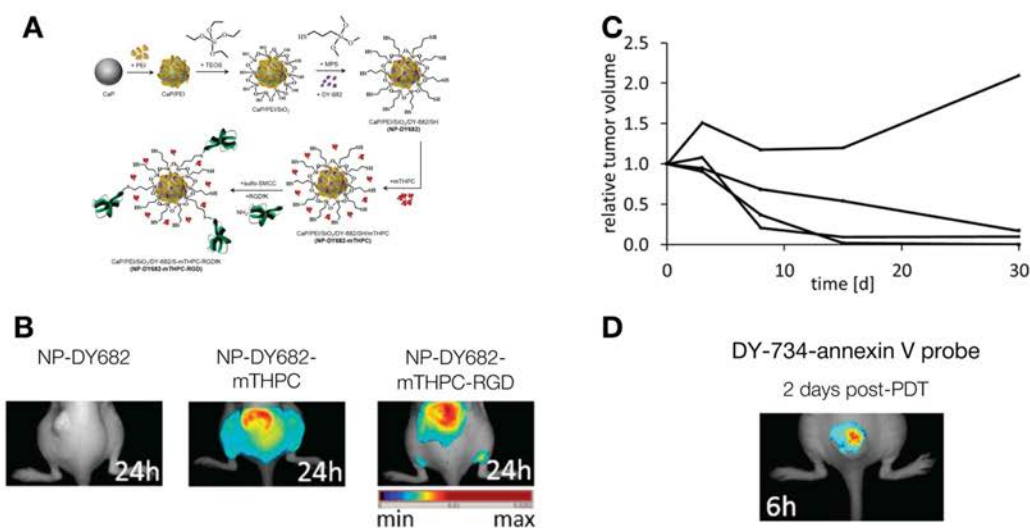


Fig. 7. (A) Schematic representation of RGDfK-conjugated silica-modified calcium phosphate NPs loaded with DY682 fluorescent dye and mTHPC. (B) The representative composite images illustrate the fluorescence of the NPs in mice bearing CAL-27 tumors at 24 h after injection. (C) The kinetics of relative volume of CAL-27 tumors (related to the volume before PDT) in mice after nanoparticle-based PDT ($n = 4$). (D) Representative composite image showing the fluorescence of DY-734-annexin-V in CAL-27 tumor-bearing mice at 2 days after PDT with mTHPC-SiNP-RGD. Adapted and reprinted with permission from ref. [54].

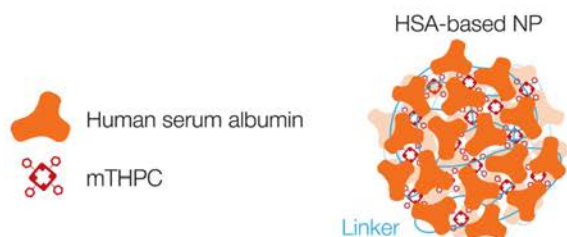


Fig. 8. Schematic representation of HSA-based mTHPC NPs.

be loaded with hydrophobic compounds in the lipid bilayer (Fig. 9). Liposomes could contain a lot of mTHPC molecules in the monomeric state without destabilization of the lipid bilayer (up to 1:13 drug to lipid ratio) due to the hydrogen bonding between lipids and mTHPC molecules [137]. Biolitec AG (Jena, Germany) proposed a commercial mTHPC liposomal formulation Foslip® which is based on the conventional dipalmitoylphosphatidylcholine (DPPC) liposomes (ca 120 nm) with the addition of 10% negative charged dipalmitoylphosphatidylglycerol (DPPG) lipid to the bilayer for colloidal stability [138]. After two decades of investigation, we can state that Foslip® is one of the most successful and the most studied mTHPC nanoformulation. Since the first report in 2005, over 25 papers have been published reporting various aspects of Foslip® characterization and application in mTHPC-PDT (Table 1).

Briefly, liposomes were successfully internalized into cellular membranes ensuring efficient mTHPC accumulation in many types of cancer cells [23,62,65,72,74]. After internalization, the liposomal membrane is simply fused with cellular membranes and mTHPC is redistributed between cellular compartments. Thus, no apparent difference in intracellular localization of Foslip® and free mTHPC was observed. The most important is that Foslip® overcomes almost all drawbacks of free mTHPC during its biodistribution, namely:

1. Lipid microenvironment provides complete monomerization of mTHPC during all stages of its distribution *in vivo* [58,60,63]. Moreover, Foslip® is administrated in the water-buffer solution thus

reducing the pain and negative effects upon injection.

2. Foslip® demonstrated higher bioavailability [66] and tumor selectivity than free mTHPC at shorter post-injection times [60,67]. Indeed tumor-to-muscle ratios were up to 9 already after 15 h post-administration compared with 24 h and more for Foscan® [69]. Significant selectivity of Foslip® between the lesion and normal surrounding skin at 4 h was observed in a non-melanotic skin tumor model [59]. Moreover, application of liposomal mTHPC formulations decreased dark cytotoxicity, keeping high phototoxicity of mTHPC *in vitro* [23,65,72] and thus providing the opportunity to decrease general post-PDT photosensitivity.
3. Foslip® showed appropriate PDT-efficiency in xenografted tumor models [69,73,74,80]. It was observed that PDT at very short (1–3 h) drug-light-intervals (DLIs) induces persistent oedema, significant ectoderm hyperplasia and a decreased vessels density *in ovo* in xenografted chick embryo chorioallantoic membrane model [68]. In the case of xenografted mice, DLIs of 6 h and more were effective in terms of growth delay [63,69].

Additionally, Foslip® was successfully applied in a low-dose PDT treatment. Foslip®-based PDT-induced photoimmunomodulation resulted in a considerable acceleration of wound healing [64]. Moreover, low-dose Foslip®-PDT demonstrated promising results as a treatment modality to prevent colitis-associated carcinogenesis in a murine model of ulcerous colitis [71].

Nevertheless, liposomes still present some unsolved drawbacks. In fact, due to their big size and lipid composition, tumor cells internalize liposomes either by fusion or by one of the endocytosis mechanisms [139]. These factors significantly limit the penetration of mTHPC loaded in liposomes across the tumor tissue as was observed in multicellular tumor spheroids *in vitro* [72,75,76]. Inhomogeneous distribution of mTHPC in tumor can result in relapse of tumor growth *in vivo* [70], and was even observed after intratumoral *in vivo* administration of Foslip® [61]. Additionally, intravenously administrated liposomes are rapidly disintegrated in blood upon the interaction with serum components releasing almost all PS [69,140]. Thus, after 6 h post-administration, only 40% of intact liposomes remain in plasma. It is worth noting that liposomes destabilization is mainly the result of lipid

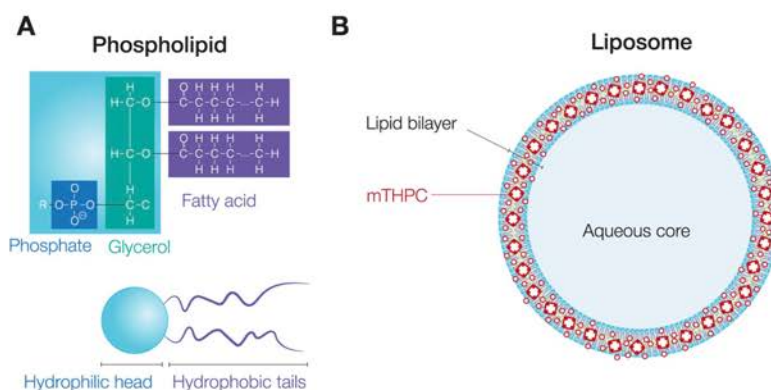


Fig. 9. (A) Chemical structure of phospholipids and (B) schematic representation of mTHPC-loaded liposome.

transfer between lipoproteins and lipid vesicles. This transfer is also accompanied by redistribution of PS to serum proteins [140–143]. Due to both the release and liposome destruction, Foslip® pharmacokinetics after already 6 h post-administration reflects the circulation of free mTHPC released from the liposomes [69].

Sterically protected PEG-modified liposomal formulation mTHPC, Fospeg® (Biolitec Pharma Ltd., Jena, Germany), was proposed to overcome the destruction of liposomes and to increase a plasma half-life. Foremost, Fospeg® exhibited the absence of carrier destruction and due to the PEG steric protection, a significantly higher amount of mTHPC remains in liposomes compared to Foslip® [69]. Fospeg®, as well as Foslip®, demonstrated reduced dark cytotoxicity effects in monolayer cells *in vitro* [78,79,81]. Additionally, incorporation of mTHPC into long-circulating PEGylated liposomes provided a high tumor selectivity and accumulation even at 4 h post-injection compared with 24 h for Foslip® or Foscan® [63,69,77,80,82]. As such, PDT efficiency with Fospeg® was determined as maximal for short DLIs (15 h) and this is the main advantage of sterically stabilized liposomes compared with non-pegylated Foslip® [69,77,82]. Therefore, Pegaz and co-authors proposed Fospeg® as a potentially suitable compound for obtaining more selective killing of choroidal neovascularity for age-related macular degeneration with PDT. Moreover, recent studies related to photodynamic treatment of multidrug-resistant cells suggested that Fospeg® could be used to overcome MDR1-related cancer drug resistance [83]. It should be noted that similar effect was also demonstrated for free mTHPC [144]. Nevertheless, the steric protection does not solve the problem of liposome penetration in tissue making it even worse [72]. It was demonstrated that in the case of Fospeg® up to 30% of encapsulated mTHPC molecules are localized in the PEG shell with easy access to acceptor structures (*i.e.* serum proteins) [140]. Thus, both Fospeg® and Foslip® showed a major efflux of mTHPC from liposomes in the circulation [70,140].

To overcome low percutaneous penetration in the case of topical mTHPC delivery for the cutaneous malignant (basal-cell carcinoma) or non-malignant diseases (psoriasis, acne, etc), flexible liposomes were suggested [88–90]. The authors reported that the addition of ethanol and terpene (invasome) or Tween® 20 (flexosome) into the lipid bilayer makes it flexible and provides a significant enhancement of mTHPC accumulation in the skin compared with conventional liposomes in preclinical models [88–90]. It was found that the highest penetration ability of mTHPC in stratum corneum and deeper skin layers are achieved for cationic flexosomes.

It is worth noting that there were already the attempts to vary the lipid composition of liposomes for mTHPC delivery. The cationic liposomes from dimyristoylphosphatidylcholine (DMPC) containing Gemini surfactant were proposed as a promising tool to overcome the blood-brain barrier and to improve mTHPC delivery to glioblastoma cells

[84–87].

In fine, despite the success of liposomal formulations *in vivo*, their translation into clinical practice is limited perhaps due to the not optimal drug release and limited penetration of drug-loaded liposomes into the tumor tissues. In order to maximize the benefits of liposomal carriers, a balance between drug delivery to the tumor and drug release from the liposomes must be achieved, for example using stimuli-response moieties, making the liposomal carries triggerable.

3.4.2. Extracellular vesicles

While liposomes represent pure lipid bilayer, natural biomembranes consist of a mix of different lipids including peptides, saccharides, receptors, etc. All these components confer membranes' flexibility, providing specific cell-recognition mechanisms and protecting bilayer from undesirable interactions with other biomacromolecules [145]. Thus, it was suggested to use natural liposomes, derived from the cellular membranes, namely extracellular vesicles (EVs), as nanocarriers for PSs [146], including mTHPC [76,91,97]. To encapsulate mTHPC in EVs, precursor endothelial cells were loaded with mTHPC before EVs isolation [76]. As a result, the purified EV suspension was loaded with 3% mTHPC and was slightly heterogeneous in size (from 100 to 500 nm). To increase the loading capacity of mTHPC into EVs, EVs were modified by fusion with mTHPC-loaded liposomes [91]. This approach has allowed increasing the drug encapsulation efficiency up to 90%. In addition, due to the biogenic composition, mTHPC-EVs showed a remarkable increase in stability in the presence of plasma proteins compared with conventional liposomes as Foslip® [76]. Upon the interaction with serum components, EVs kept their integrity, while its size was reduced to 70 nm. In its turn, the small size of serum-treated EVs together with enhanced flexibility of natural membrane caused deep penetration of EVs-based mTHPC into tumor spheroids. It is worth noting that EVs also release mTHPC in the presence of serum but much slower than Foslip® [76]. The opportunity of mTHPC release from EVs promotes PS accumulation. Indeed, the cellular uptake and phototoxicity of mTHPC-EVs were 2 and 4-times higher in 3D tumor spheroids than Foslip® and free mTHPC, respectively. EVs were also used as a theranostic platform, loaded simultaneously with iron NP for diagnosis and mTHPC for therapy [96,97]. Intratumor administration of these NPs showed improved PDT efficacy *in vivo* extending a tumor growth delay. To date, EVs is a novel perspective liposomal-based delivery nanopatform which requires additional studies to fully explore its benefits for drug delivery.

3.4.3. Solid lipid NPs

Solid lipid nanoparticles (SLNPs) are aqueous colloidal dispersions, their matrix is composed of solid biodegradable lipids [147]. While vesicular lipid-based mTHPC formulations consist of the bilayer only,

which is only a small volume of NP, a greater part of SLNPs' volume consists of lipids thus providing the opportunity to encapsulate higher amount of hydrophobic PS molecules [148]. Usually, lipid core is coated with polymeric compounds such as PEG to prevent the dissolution of lipid NPs and a fast drug release in biological fluids. The first report on mTHPC-SLNPs was performed in 2000 when 190-nm oil (Miglyol) reservoirs with PLA-PEG or PLA coated with poloxamer 188 external layers were loaded with mTHPC [43]. However, the choice of polymeric shell had a negative impact on the internalization of NPs and also on PDT efficiency *in vitro*. Then, 14 years later instead of biodegradable PLA, phospholipids (lipoid s75) and pegylated surfactants (Myrj s40) were suggested to coat lipid inner core (soybean oil and Suppocire NB) (Fig. 10) [92]. The authors called it Lipidots and tested this mTHPC-based formulation in various tumor models [73,92,93]. Varying the ratio between components (oily phase: PEG surfactant: phospholipids), the size of Lipidots could be modulated from 20 to 120 nm providing the opportunity to find out the best composition for mTHPC delivery. In advanced 3D cell culture model, the authors demonstrated that small 50-nm Lipidots possess both higher accumulation and penetration ability compared with 120-nm ones. Nevertheless, PS distribution in spheroids, as well as PDT efficiency of 50-nm Lipidots, were close to free mTHPC. A similar tendency was also observed in a CAL33 tumor model in mice. The treatment with conventional liposomal formulation Foslip® was significantly superior to both Foscan® and Lipidots. Thus, the authors emphasized the biocompatibility of Lipidots as the main benefit of this formulation.

In 2016, Brezaniova with co-workers presented liquid droplets based on lipid core stabilized by the nontoxic polymeric surfactant copolymer poly(ethylene oxide-*block*-ε-caprolactone) to deliver mTHPC [94]. Even without active targeting, the obtained 30-nm NPs efficiently delivered mTHPC to the target cells resulting in a 2-fold increase of photocytotoxicity in 4 T1 and human breast carcinoma MDA-MB-231 cell lines. *In vitro* experiments also demonstrated high stability in the serum of mTHPC encapsulated in NPs. The success of formulation *in vitro* was also accompanied with more striking and large necrotic areas compared with Foscan® after PDT in xenografted human breast carcinoma MDA-MB-231 mice. Foremost, the significant advantage of mTHPC loaded SLNP is a considerable decrease in DLI (3 h) with 100% tumor growth inhibition at 3rd day post PDT; nevertheless, the partial tumor relapse on the periphery of the original tumor occurred 35 days after PDT.

Recently, several studies involving mTHPC excitation through fluorescence resonance energy transfer (FRET) from the components of the nanodelivery system were reported. The first study was conducted in 2015, when 13–48 nm SLNPs coated with semiconducting polymers and PEGylated phospholipids demonstrated efficient generation of singlet oxygen by mTHPC upon FRET after excitation of semiconducting polymers at 600 nm (Fig. 11) [149]. However, one can suppose that tumor cells can internalize the NPs without the release of mTHPC. Further, the irradiation at 600 nm vs 650 nm is not beneficial for mTHPC-PDT. Probably, this is the reason why up to moment there are no available *in vitro* and/or *in vivo* data.

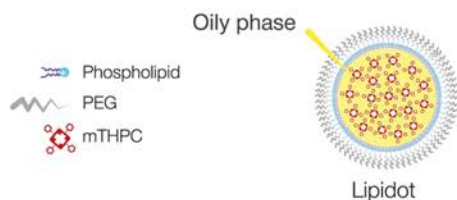


Fig. 10. Schematic representation of mTHPC-loaded Lipidots. Adapted and reprinted with permission from ref. [93].

3.5. Carbon nanotubes (CNTs)

The strategy to use semiconductor materials as components of nanoplatform for mTHPC delivery was introduced recently with CNTs. Semiconducting CNTs generate heat under illumination in a wide spectral range demonstrating an intrinsic photothermal effect [150]. Marangon and co-workers constructed a nanosystem based on multi-walled carbon nanotubes (MWCNTs) loaded with mTHPC using π - π stacking on their surface for cancer treatment by the combination of photodynamic and photothermal therapies [95]. MWCNTs were shortened to increase their water dispersibility and therefore they obtained the size of 39 nm in diameter and 400 nm in length. mTHPC was loaded with a maximum loading of 3.5%wt resulting in a complete quenching of mTHPC emission by nanotubes. According to this, PS is inactivated in the complex with MWCNTs outside the cell and becomes active after cell internalization of the complex and subsequent light irradiation. The authors evidenced different routes of apoptosis in human ovarian tumor cells (SKOV3) depending on the irradiation conditions culminating synergistically in the apoptosis of the whole cell population when combined PDT and photothermal treatment was applied. Nevertheless, the behavior of such complex in blood raises the questions on the bioavailability and selectivity of MWCNTs as well as on the rate of mTHPC released to serum components.

3.6. Hybrid nanodelivery systems

Nanocarriers mainly improve particular mTHPC drawbacks modifying PS behavior at one of the stages of its distribution in the organism. All NPs prevent mTHPC aggregation, while only a few of them improve selectivity and enhance penetration of PS into tumor tissue. In order to maximize the improvement, hybrid nanodelivery systems, which are based on a combination of individual carriers were suggested as an advanced strategy for mTHPC delivery. Thus, a smart choice of hybrid system components could provide a synergetic effect, making mTHPC delivery efficient at all stages.

Due to functional versatility of liposomes, the first example of hybrid system was based on the liposomes which include mTHPC in lipid bilayer while magnetic iron oxide NPs were encapsulated in the inner aqueous core (Fig. 12) [98]. The double cargo was translated into double functionality with photogeneration of singlet oxygen and heat production upon alternating magnetic field stimulation, thus coupling PDT with magnetic hyperthermia (MHT). As a basis, pegylated liposomes (such as Fospeg®) were taken with a slight modification of lipid composition. The authors successfully loaded 200-nm lipid vesicles with mTHPC (the lipid-to-drug ratio was about 7) and iron oxide NPs (about 2400 NPs per vesicle). The authors proved *in vitro* efficacy of such hybrid NPs as PDT agents as well as MHT sensitizers. *In vivo*, each treatment alone was able to inhibit tumor growth, while the combination of both therapies remarkably led to the complete tumor regression.

Similar idea to combine hyperthermia and PDT was recently reported by Tsai and co-workers [99]. Instead of liposomes, a concept of SLNPs was adapted for synergistic treatment of glioblastoma using the combination of photothermal (IR-780) and mTHPC-mediated photodynamic actions (Fig. 13). Hybridization aimed to use oleic acid-coated upconversion NPs (UCNP) as a basis of solid lipid core due to their ability to excite mTHPC through FRET mechanism absorbing near-infrared light (980 nm). Along with near-infrared excitation, the treatment of brain tumors requires penetration across the blood-brain barrier. For this purpose, the PEGylated surface of hybrid NPs was decorated with angiopep-2 as an active targeting agent. The concept was successfully confirmed on astrocytoma ALTS1C1 cells *in vitro* demonstrating pronounced cytotoxicity by combined NIR-triggered photodynamic and photothermal therapies. In consistency with the increased penetration of NPs through endothelial monolayer *in vitro*, the NPs also demonstrated selective accumulation in brain tumor and prominent

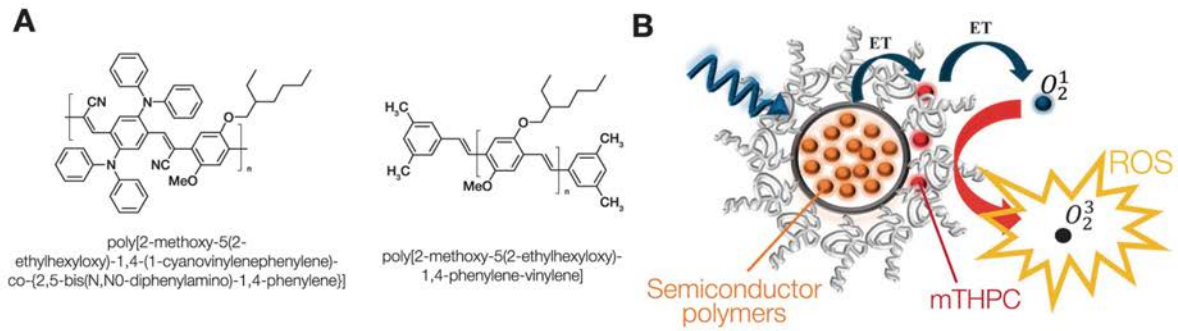


Fig. 11. (A) Chemical structures of semiconductor polymers. (B) Semiconducting polymer dot enhances the singlet oxygen production by FRET to the PS. Adapted and reprinted with permission from ref. [149].

apoptotic and necrotic effects on orthotopic tumors *in vivo* after dual phototherapies (median survival was 24 days). All reported data converge on the idea that proposed NPs are a promising tool against glioblastoma.

It should be noted, that the development of the described hybrid system was focused on the combination of treatment modalities, while the delivery aspects were sometimes neglected. Recently, “drug-in-cyclodextrin-in-liposome” (DCL) hybrid NP was proposed to deliver mTHPC (Fig. 14) [75]. It is worth noting that this approach has been firstly announced by McCormack & Gregoriadis [151] aiming an increase of encapsulation efficiency of hydrophobic drug in liposomes. Due to the unique properties of mTHPC/CDs inclusion complexes, this concept got a second wind. We suppose that liposomes could act as a container while its rapid release and degradation in the biological medium could stimulate the transportation of mTHPC/CD, encapsulated in the aqueous core of liposomes. Moreover, the released mTHPC/CD complexes additionally may increase mTHPC tumor selectivity and improve its penetration into tumor tissues completely refining mTHPC biodistribution. The optimization of drug-loading procedure allows stable and efficient encapsulation of mTHPC bound to β -CDs into conventional liposomes [75]. The synthesized 135-nm mTHPC-DCLs demonstrated a complete penetration of mTHPC and homogeneous PS distribution across the multicellular HT29 tumor

spheroids *in vitro* (Fig. 14 B&C). However, hybrid mTHPC-DCL construct should be additionally optimized for *in vivo* studies expecting critical improvements of mTHPC biodistribution in tumor compared to its liposomal counterparts (Foslip®).

4. Conclusions and perspectives

The rapid growth of nanotechnology is one of the most quickly emerging tendency in cancer therapies, including PDT. Nanotherapeutics are supposed to overcome the major constraints of conventional medicine such as low solubility and stability, non-adequate pharmacokinetic profiles and side effects. To date, many nano-platforms were applied for the delivery of mTHPC, one of the most potent clinically approved PS.

Potent mTHPC-based NPs have been intensively tested in different *in vitro* preclinical models (2D and 3D tumor cell cultures), while complete PDT studies, including biodistribution, pharmacokinetics and PDT efficacy in tumor-bearing *in vivo* animal models are rather sparse. This situation seriously complicates the assessment of the benefits of mTHPC-based NPs against Foscan®. We attempted to summarize the general benefits and limitations of mTHPC-based nanoconstructs compared to free mTHPC (Table 2). In spite of the great disparity of pros and cons for each nanoconstruct, some common elements can be

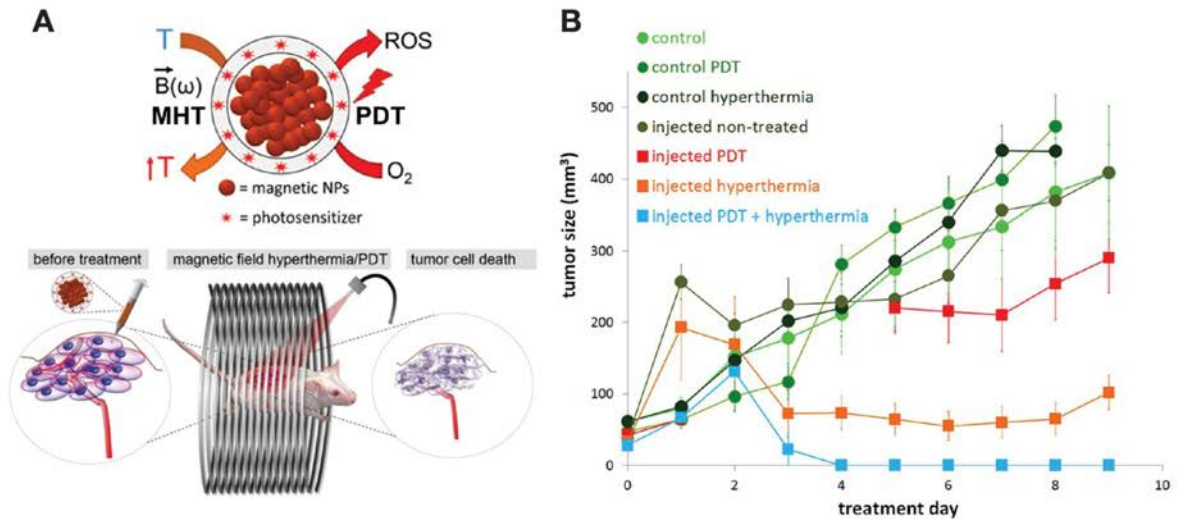


Fig. 12. (A) Schematic description of ultramagnetic photosensitive liposomes structure and therapeutic strategy. (B) Tumor growth curves of different control groups and treatment groups. Adapted and reprinted with permission from ref. [98].

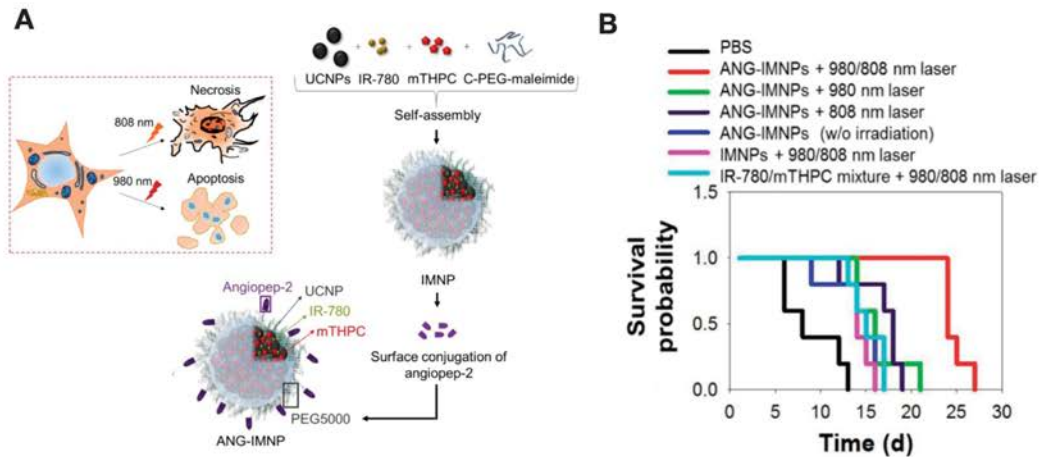


Fig. 13. (A) Schematic representation of hybrid NPs structure and the mechanisms of cancer cell necrosis and apoptosis induced by hybrid NPs with 980/808 nm laser irradiation. (B) Kaplan-Meier survival curves of the glioma-bearing mice ($n = 5$). Adapted and reprinted with permission from ref. [99].

discerned. First of all, nanoplateforms effectively solve the problem of mTHPC aggregation, providing easy administration of PS. Secondly, the dark toxicity of mTHPC delivered by NPs is significantly lower than that of free drug. Further, among mTHPC nanoformulations that were tested in preclinical *in vivo* models, the majority of them demonstrated an improved selectivity and bioavailability. Common drawbacks for mTHPC-based NPs are difficult to list since they greatly depend on individual characteristics of each NP. We can only note a rather poor drug release at the target site. It seems inconsistent but NPs with high stability in plasma lack the efficient drug release at the target tumor site. An optimal balance between NPs' plasma stability and efficient PS release could be achieved with the tailoring of stimuli-response moieties thus providing control drug release.

Due to the variability of processes involved in the drug distribution at various stages (blood circulation, tumor tissue distribution, intracellular accumulation), the algorithms for the design of ideal NPs do not yet exist. We suppose that combining different NPs in one nanoplateform will foster future research avenue in the field of mTHPC delivery. Lipid and polymer nanocapsules could be used for this purpose. To date, several reports on the successful inclusion of various drug-loaded nanoparticles (CDs complexes, micelles) in liposomes [152,153] or inclusion of drug-CDs complexes in PLGA nanocapsules [154] have been published. Recently, hybrid drug-in-cyclodextrin-in-liposome nanoplateform was adapted for mTHPC combining the benefits of both liposomal nanocarriers and CD nanoshuttles [75]. Finally, the association of different nanoparticles in one nanoplateform allow the

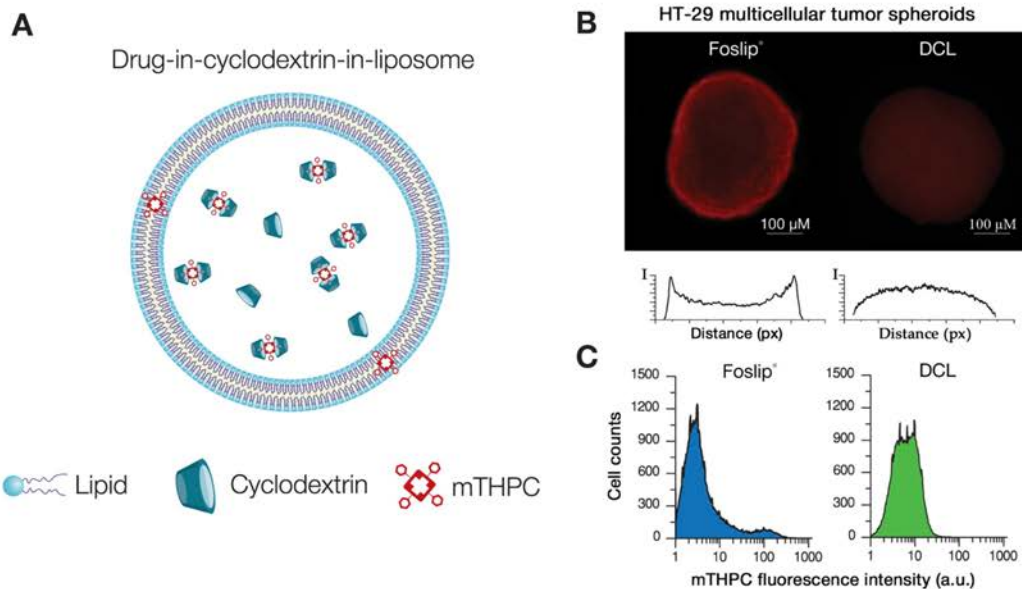


Fig. 14. (A) Schematic representation of the mTHPC-DCL hybrid NP. Improvement of mTHPC distribution in HT29 multicellular tumor spheroids by DCL: (B) fluorescence imaging and (C) flow-cytometry analysis. Adapted and reprinted with permission from ref. [76].

Table 2
The benefits and limitations of nanoplatfrom-based delivery against free mTHPC.

Benefits	Limitations
Conjugates <ul style="list-style-type: none"> • Drug solubility • Lower dark phototoxicity <i>in vitro</i> • Prolonged plasma life-time <i>in vivo</i> • Better selectivity <i>in vivo</i> 	<ul style="list-style-type: none"> • Modification of chemical structure of PSs • Hurdles in uptake in tumor cells <i>in vitro</i> • Active targeting is limited by low loading capacity (several PS molecules)
Inclusion complexes <ul style="list-style-type: none"> • Drug solubility • Alteration of distribution in serum • Accelerated uptake to the cells <i>in vitro</i> • Improved penetration in tumor tissue <i>in vitro</i> • Better selectivity and bioavailability <i>in vivo</i> • Modification of excretion route <i>in vivo</i> 	<ul style="list-style-type: none"> • CDs quickly excreted from blood <i>in vivo</i> • Low complex stability (dynamic equilibrium) • The difficulties to control concentration -dependent on CD effects in the target site <i>in vivo</i>
Micelles <ul style="list-style-type: none"> • Drug solubility • Lower dark phototoxicity <i>in vitro</i> 	<ul style="list-style-type: none"> • Complicated uptake in tumor cells <i>in vitro</i> • Control release mechanisms are mandatory • Low penetration in tumor tissue <i>in vitro</i>
Solid polymer nanoparticles <ul style="list-style-type: none"> • Drug solubility • Lower dark phototoxicity <i>in vitro</i> • Better selectivity <i>in vivo</i> • Better PDT <i>in vivo</i> 	<ul style="list-style-type: none"> • Complicated uptake in tumor cells <i>in vitro</i>
Silica-based NPs <ul style="list-style-type: none"> • Drug solubility • Better selectivity <i>in vivo</i> • Better PDT <i>in vivo</i> • Penetration through the blood-brain barrier <i>in vivo</i> 	<ul style="list-style-type: none"> • Complicated uptake in tumor cells <i>in vitro</i> • Control release mechanisms are essential
Protein-based nanoparticles <ul style="list-style-type: none"> • Drug solubility 	<ul style="list-style-type: none"> • No improvement of mTHPC accumulation and/or PDT efficiency
Liposomes <ul style="list-style-type: none"> • Drug solubility • Lower dark phototoxicity <i>in vitro</i> • Higher drug bioavailability <i>in vivo</i> • Better selectivity <i>in vivo</i> • Better PDT in short DLI <i>in vivo</i> • High vascular PDT damage • Possibility to encapsulate NPs 	<ul style="list-style-type: none"> • Low penetration in tumor tissue <i>in vitro</i> • Complicated uptake in tumor cells <i>in vitro</i> • Low stability in blood <i>in vivo</i> • Quick release of drug <i>in vivo</i>
Extracellular vesicles <ul style="list-style-type: none"> • Drug solubility • Lower dark phototoxicity <i>in vitro</i> • Higher accumulation in tumor cells <i>in vitro</i> • Stability in serum <i>in vitro</i> • Improved penetration in tumor tissue <i>in vitro</i> • Better PDT in cells and spheroids <i>in vitro</i> 	<ul style="list-style-type: none"> • Low efficiency of passive loading
Solid Lipid Nanoparticles <ul style="list-style-type: none"> • Drug solubility • Lower dark phototoxicity <i>in vitro</i> • Stability in serum <i>in vitro</i> • Higher drug bioavailability <i>in vivo</i> 	<ul style="list-style-type: none"> • Complicated uptake in tumor cells <i>in vitro</i>
Carbon nanotubes <ul style="list-style-type: none"> • Drug solubility • Combination of PTT/PDT available 	<ul style="list-style-type: none"> • Complicated uptake in tumor cells <i>in vitro</i>

combination of several treatment modalities improving anti-tumor effect *in vivo* and offering an advanced strategy of anticancer treatment [155].

Acknowledgments

This work was supported by the French “Ligue Nationale contre le Cancer (CCIR-GE)”, the Institut de Cancérologie de Lorraine, Belarusian Republican Foundation for Fundamental Research (BRFFR) [grant number M18MB-002] and the Ministry of Education of the Republic of Belarus.

Disclosures

The authors report no declarations of interest.

Author contributions

IY, MM: Writing – Original Draft; HPL, VZ, LB: Writing – Review & Editing; VZ, LB: Supervision.

References

- [1] S. Kwiatkowski, B. Knap, D. Przystupski, J. Saczko, E. Kędzierska, K. Knap-Czop, J. Kotlińska, O. Michel, K. Kotowski, J. Kulbacka, Photodynamic therapy – mechanisms, photosensitizers and combinations, *Biomed. Pharmacother* 106 (2018) 1098–1107, <https://doi.org/10.1016/j.biopha.2018.07.049>.

- [2] D. van Straten, V. Mashayekhi, H.S. de Bruijn, S. Oliveira, D.J. Robinson, Oncologic photodynamic therapy: basic principles, current clinical status and future directions, *Cancers* 9 (2017), <https://doi.org/10.3390/cancers9020019>.
- [3] D. Luo, K.A. Carter, D. Miranda, J.F. Lovell, Chemophototherapy: an emerging treatment option for solid tumors, *Adv. Sci.* 4 (2017) 1600106, <https://doi.org/10.1002/adv.201600106>.
- [4] A.P. Castano, T.N. Demidova, M.R. Hamblin, Mechanisms in photodynamic therapy: part three-photosensitizer pharmacokinetics, biodistribution, tumor localization and modes of tumor destruction, *Photodiagn. Photodyn. Ther.* 2 (2005) 91–106, [https://doi.org/10.1016/S1572-1000\(05\)00060-8](https://doi.org/10.1016/S1572-1000(05)00060-8).
- [5] J. Moan, K. Berg, The photodegradation of porphyrins in cells can be used to estimate the lifetime of singlet oxygen, *Photochem. Photobiol.* 53 (1991) 549–553.
- [6] R.R. Allison, K. Moghissi, Photodynamic therapy (PDT): PDT mechanisms, *Clin. Endosc.* 46 (2013) 24–29, <https://doi.org/10.5946/ce.2013.46.1.24>.
- [7] M.O. Senge, J.C. Brandt, Temoporfin (Foscan[®], 5,10,15,20-tetra(m-hydroxyphenyl)chlorin) – a second-generation photosensitizer, *Photochem. Photobiol.* 87 (2011) 1240–1296, <https://doi.org/10.1111/j.1751-1097.2011.00986.x>.
- [8] A.E. O'Connor, W.M. Gallagher, A.T. Byrne, Porphyrin and nonporphyrin photosensitizers in oncology: preclinical and clinical advances in photodynamic therapy, *Photochem. Photobiol.* 85 (2009) 1053–1074, <https://doi.org/10.1111/j.1751-1097.2009.00585.x>.
- [9] EMA, Foscan, Eur. Med. Agency, <https://www.ema.europa.eu/en/medicines/human/EPAR/foscan>, (2018) (accessed May 20, 2019).
- [10] J.F. Savary, P. Grosjean, P. Monnier, C. Fontolliet, G. Wagnières, D. Braichotte, H. van den Bergh, Photodynamic therapy of early squamous cell carcinomas of the esophagus: a review of 31 cases, *Endoscopy* 30 (1998) 258–265, <https://doi.org/10.1055/s-2007-1001252>.
- [11] J.F. Savary, P. Monnier, C. Fontolliet, J. Mizeret, G. Wagnières, D. Braichotte, H. van den Bergh, Photodynamic therapy for early squamous cell carcinomas of the esophagus, bronchi, and mouth with m-tetra (hydroxyphenyl) chlorin, *Arch. Otolaryngol. Head Neck Surg.* 123 (1997) 162–168.
- [12] D.J. Ball, D.I. Vernon, S.B. Brown, The high photoactivity of m-THPC in photodynamic therapy. Unusually strong retention of m-THPC by RIF-1 cells in culture, *Photochem. Photobiol.* 69 (1999) 360–363, <https://doi.org/10.1111/j.1751-1097.1999.tb03299.x>.
- [13] R. Bonnett, R.D. White, U.J. Winfield, M.C. Berenbaum, Hydroporphyrins of the meso-tetra(hydroxyphenyl)porphyrin series as tumour photosensitizers, *Biochem. J.* 261 (1989) 277–280.
- [14] R. Bonnett, P. Charlesworth, B.D. Djelal, S. Foley, D.J. McGarvey, T.G. Truscott, Photophysical properties of 5,10,15,20-tetrakis(m-hydroxyphenyl)porphyrin (m-THPP), 5,10,15,20-tetrakis(m-hydroxyphenyl)chlorin (m-THPC) and 5,10,15,20-tetrakis(m-hydroxyphenyl)baacteriochlorin (m-THPBC): a comparative study, *J. Chem. Soc. Perkin Trans. 2* (1999) 325–328, <https://doi.org/10.1039/A805328F>.
- [15] N.V. Koudinova, J.H. Pinthus, A. Brandis, O. Brenner, P. Bendel, J. Ramon, Z. Eshhar, A. Scherz, Y. Salomon, Photodynamic therapy with Pd-bacteriopheophorbide (TOOKAD): successful in vivo treatment of human prostatic small cell carcinoma xenografts, *Int. J. Cancer* 104 (2003) 782–789, <https://doi.org/10.1002/ijc.11002>.
- [16] B.W. Pogue, R.W. Redmond, N. Trivedi, T. Hasan, Photophysical properties of tin ethyl etiopurpurin I (SnEt2) and Tin octaethylbenzochlorin (SnOEBc) in solution and bound to albumin, *Photochem. Photobiol.* 68 (1998) 809–815, <https://doi.org/10.1111/j.1751-1097.1998.tb05288.x>.
- [17] S. Mitra, T.H. Foster, Photophysical parameters, photosensitizer retention and tissue optical properties completely account for the higher photodynamic efficacy of meso-tetra-hydroxyphenyl-chlorin vs photofrin[®], *Photochem. Photobiol.* 81 (2005) 849–859, <https://doi.org/10.1111/j.1751-1097.2005.tb01453.x>.
- [18] I. Laville, T. Figueiredo, B. Looek, S. Pigaglio, P. Maillard, D.S. Grierson, D. Carrez, A. Croisy, J. Blais, Synthesis, cellular internalization and photodynamic activity of glucoconjugated derivatives of tri and tetra(meta-hydroxyphenyl)chlorins, *Bioorg. Med. Chem.* 11 (2003) 1643–1652.
- [19] J.Y. Chen, N.K. Mak, C.M.N. Yow, M.C. Fung, L.C. Chiu, W.N. Leung, N.H. Cheung, The binding characteristics and intracellular localization of Temoporfin (mTHPC) in myeloid leukemia cells: Phototoxicity and mitochondrial damage[®], *Photochem. Photobiol.* 72 (2000) 541–547, [https://doi.org/10.1562/0031-8655\(2000\)0720541TBAIL2.0.CO;2](https://doi.org/10.1562/0031-8655(2000)0720541TBAIL2.0.CO;2).
- [20] S. Sasnouski, V. Zorin, I. Khludayev, M.-A. D'Hallewin, F. Guillemin, L. Bezdetnaya, Investigation of Foscan interactions with plasma proteins, *Biochim. Biophys. Acta* 1725 (2005) 394–402, <https://doi.org/10.1016/j.bbagen.2005.06.014>.
- [21] V.O. Melnikova, L.N. Bezdetnaya, C. Bour, E. Festor, M.P. Gramain, J.L. Merlin, A.Ya Potapenko, F. Guillemin, Subcellular localization of meta-tetra (hydroxyphenyl) chlorin in human tumor cells subjected to photodynamic treatment, *J. Photochem. Photobiol. B* 49 (1999) 96–103.
- [22] M. Triesscheijn, M. Ruevekamp, R. Out, T.J.C. Van Berkel, J. Schellens, P. Baas, F.A. Stewart, The pharmacokinetic behavior of the photosensitizer meso-tetrahydroxyphenyl-chlorin in mice and men, *Cancer Chemother. Pharmacol.* 60 (2007) 113–122, <https://doi.org/10.1007/s00280-006-0356-9>.
- [23] T. Kiesslich, J. Berlanda, K. Plaetzer, B. Krammer, F. Berr, Comparative characterization of the efficiency and cellular pharmacokinetics of Foscan- and Foslip-based photodynamic treatment in human biliary tract cancer cell lines, *Photochem. Photobiol. Sci.* 6 (2007) 619–627, <https://doi.org/10.1039/b617659c>.
- [24] I. Opitz, T. Krueger, Y. Pan, H.-J. Altmatt, G. Wagnières, H.-B. Ris, Preclinical comparison of mTHPC and verteporfin for intracavitary photodynamic therapy of malignant pleural mesothelioma, *Eur. Surg. Res.* 38 (2006) 333–339, <https://doi.org/10.1159/000094028>.
- [25] S. Marchal, A. Fadloun, E. Maugain, M.-A. D'Hallewin, F. Guillemin, L. Bezdetnaya, Necrotic and apoptotic features of cell death in response to Foscan photosensitization of HT29 monolayer and multicell spheroids, *Biochem. Pharmacol.* 69 (2005) 1167–1176, <https://doi.org/10.1016/j.bcp.2005.01.021>.
- [26] S. Mitra, E. Maugain, L. Bolotine, F. Guillemin, T.H. Foster, Temporally and spatially heterogeneous distribution of mTHPC in a murine tumor observed by two-color confocal fluorescence imaging and spectroscopy in a whole-mount model, *Photochem. Photobiol.* 81 (2005) 1123–1130, <https://doi.org/10.1562/2005-03-24-RA-471>.
- [27] M.O. Senge, mTHPC – a drug on its way from second to third generation photosensitizer? *Photodiagn. Photodyn. Ther.* 9 (2012) 170–179, <https://doi.org/10.1016/j.pdpdt.2011.10.001>.
- [28] R. Baskaran, J. Lee, S.-G. Yang, Clinical development of photodynamic agents and therapeutic applications, *Biomater. Res.* 22 (2018) 25, <https://doi.org/10.1186/s40824-018-0140-z>.
- [29] P. Westermann, T. Glanzmann, S. Andrejevic, D.R. Braichotte, M. Forrer, G.A. Wagnières, P. Monnier, H. Van Den Bergh, J.-P. Mach, S. Folli, Long circulating half-life and high tumor selectivity of the photosensitizer meta-tetra-hydroxyphenylchlorin conjugated to polyethylene glycol in nude mice grafted with a human colon carcinoma, *Int. J. Cancer* 76 (1998) 842–850, [https://doi.org/10.1002/\(SICI\)1097-0215\(19980610\)76:6<842::AID-IJC13>3.0.CO;2-4](https://doi.org/10.1002/(SICI)1097-0215(19980610)76:6<842::AID-IJC13>3.0.CO;2-4).
- [30] P. Westermann, T.M. Glanzmann, S. Folli, D. Braichotte, M. Forrer, S. Andrejevic-Blant, J.-P. Mach, P. Monnier, H. van den Bergh, Comparison of the influence of a water-soluble polymer carrier on the tumor localization and biodistribution of mesotetramethoxyphenylchlorin (mTHPC) in two animal models, 5th Int. Photodyn. Assoc. Bienn. Meet. International Society for Optics and Photonics, 1995, pp. 45–51, <https://doi.org/10.1117/12.203361>.
- [31] M.F. Grah, A. Giger, A. McGuinness, M.L. de Jode, J.C. Stewart, H.B. Ris, H.J. Altmatt, N.S. Williams, mTHPC polymer conjugates: the in vivo photodynamic activity of four candidate compounds, *Lasers Med. Sci.* 14 (1999) 40–46, <https://doi.org/10.1007/s101030050019>.
- [32] M.F. Grah, A. McGuinness, M.L. de Jode, A. Giger, A.S. Dhiman, C.-M. Cheung, S. Pavitt, R. Benzie, N.S. Williams, In-vivo photodynamic activity of mTHPC poly (ethylene glycol) conjugates (SCI02), *Photochem. Photodyn. Ther. Modalities III*, International Society for Optics and Photonics, 1997, pp. 180–187, <https://doi.org/10.1117/12.297801>.
- [33] H.B. Ris, Q. Li, T. Krueger, C.K. Lim, B. Reynolds, U. Althaus, H.J. Altmatt, Photosensitizing effects of m-tetrahydroxyphenylchlorin on human tumor xenografts: correlation with sensitizer uptake, tumor doubling time and tumor histology, *Int. J. Cancer* 76 (1998) 872–874.
- [34] T. Reuther, A.C. Kübler, U. Zillmann, C. Flechtenmacher, H. Sinn, Comparison of the in vivo efficiency of photofrin II, mTHPC[®], mTHPC-PEG- and mTHPCnPEG-mediated PDT in a human xenografted head and neck carcinoma, *Lasers Surg. Med.* 29 (2001) 314–322.
- [35] J. Gravier, R. Schneider, C. Frochet, T. Bastogne, F. Schmitt, J. Didelon, F. Guillemin, M. Barberi-Heyob, Improvement of meta-tetra(hydroxyphenyl) chlorin-like photosensitizer selectivity with folate-based targeted delivery. Synthesis and in vivo delivery studies, *J. Med. Chem.* 51 (2008) 3867–3877, <https://doi.org/10.1021/jm800125a>.
- [36] M.B. Vrouenraets, G.W.M. Visser, M. Stigter, H. Oppelaar, G.B. Snow, G.A.M.S. van Dongen, Comparison of aluminum (III) phthalocyanine tetra-sulfonate- and meta-tetrahydroxyphenylchlorin-monoconal antibody conjugates for their efficacy in photodynamic therapy in vitro, *Int. J. Cancer* 98 (2002) 793–798.
- [37] M.B. Vrouenraets, G.W.M. Visser, F.A. Stewart, M. Stigter, H. Oppelaar, P.E. Postmus, G.B. Snow, G.A.M.S. van Dongen, Development of meta-tetra-hydroxyphenylchlorin-monoconal antibody conjugates for photoimmunotherapy, *Cancer Res.* 59 (1999) 1505–1513.
- [38] L. Rogers, N.N. Sergeeva, E. Paszko, G.M.F. Vaz, M.O. Senge, Lead structures for applications in photodynamic therapy. 6. Temoporfin anti-inflammatory conjugates to target the tumor microenvironment for in vitro PDT, *PLoS One* 10 (2015) e0125372, <https://doi.org/10.1371/journal.pone.0125372>.
- [39] E. Haimov, H. Weitman, S. Polani, H. Schori, D. Zitoun, O. Shefi, Meso-tetra-hydroxyphenylchlorin-conjugated gold nanoparticles as a tool to improve photodynamic therapy, *ACS Appl. Mater. Interfaces* 10 (2018) 2319–2327, <https://doi.org/10.1021/acsami.7b16455>.
- [40] I. Yakavets, I. Yankovsky, M. Millard, L. Lamy, H.-P. Lassalle, A. Wiehe, V. Zorin, L. Bezdetnaya, The alteration of temoporfin distribution in multicellular tumor spheroids by β -cyclodextrins, *Int. J. Pharm.* 529 (2017) 568–575, <https://doi.org/10.1016/j.ijpharm.2017.07.037>.
- [41] I. Yankovsky, E. Bastien, I. Yakavets, I. Khludayev, H.-P. Lassalle, S. Gräfe, L. Bezdetnaya, V. Zorin, Inclusion complexation with β -cyclodextrin derivatives alters photodynamic activity and biodistribution of meta-tetra(hydroxyphenyl) chlorin, *Eur. J. Pharm. Sci.* 91 (2016) 172–182, <https://doi.org/10.1016/j.ejps.2016.06.012>.
- [42] J.-W. Hofman, M.G. Carstens, F. van Zeeland, C. Helwig, F.M. Flesch, W.E. Hennink, C.F. van Nostrom, Photocytotoxicity of mTHPC (temoporfin) loaded polymeric micelles mediated by lipase catalyzed degradation, *Pharm. Res.* 25 (2008) 2065–2073, <https://doi.org/10.1007/s11095-008-9590-7>.
- [43] O. Bourdon, V. Mosqueira, P. Legrand, J. Blais, A comparative study of the cellular uptake, localization and phototoxicity of meta-tetra(hydroxyphenyl) chlorin encapsulated in surface-modified submicronic oil/water carriers in HT29 tumor cells, *J. Photochem. Photobiol. B* 55 (2000) 164–171, [https://doi.org/10.1016/S1011-1344\(00\)00043-9](https://doi.org/10.1016/S1011-1344(00)00043-9).
- [44] M.-J. Shieh, C.-L. Peng, W.-L. Chiang, C.-H. Wang, C.-Y. Hsu, S.-J.J. Wang, P.-S. Lai, Reduced skin photosensitivity with meta-tetra(hydroxyphenyl)chlorin-

- loaded micelles based on a poly(2-ethyl-2-oxazoline)-b-poly(D,L-lactide) diblock copolymer in vivo, *Mol. Pharm.* 7 (2010) 1244–1253, <https://doi.org/10.1021/mp10060v>.
- [45] C.-L. Peng, L.-Y. Yang, T.-Y. Luo, P.-S. Lai, S.-J. Yang, W.-J. Lin, M.-J. Shieh, Development of pH sensitive 2-(diisopropylamino)ethyl methacrylate based nanoparticles for photodynamic therapy, *Nanotechnology* 21 (2010) 155103, <https://doi.org/10.1088/0957-4484/21/15/155103>.
- [46] J. Wu, S. Feng, W. Liu, F. Gao, Y. Chen, Targeting integrin-rich tumors with temoporfin-loaded vitamin-E-succinate-grafted chitosan oligosaccharide/d- α -tocopheryl polyethylene glycol 1000 succinate nanoparticles to enhance photodynamic therapy efficiency, *Int. J. Pharm.* 528 (2017) 287–298, <https://doi.org/10.1016/j.ijpharm.2017.06.021>.
- [47] Y. Liu, J.-W. de Vries, Q. Liu, A. Hartman, G. Wieland, S. Wiecezorek, H. Boemer, A. Wiehe, E. Buhler, M. Stuart, W. Browne, A. Herrmann, A.K.H. Hirsch, Lipid-DNAs as solubilizers of mTHPC, *Chem. Eur. J.* (2017), <https://doi.org/10.1002/chem.201705206>.
- [48] J.W.H. Wemink, Y. Liu, P.I. Mäkinen, F. Setaro, A. de la Escosura, M. Bourajjaj, J.P. Lappalainen, L.P. Holappa, J.B. van den Dikkenberg, M. al Fartousi, P.N. Trohopoulos, S. Ylä-Herttua, T. Torres, W.E. Hennink, C.F. van Nostrum, Macrophage selective photodynamic therapy by meta-tetra(hydroxyphenyl)chlorin loaded polymeric micelles: a possible treatment for cardiovascular diseases, *Eur. J. Pharm. Sci.* 107 (2017) 112–125, <https://doi.org/10.1016/j.ejps.2017.06.038>.
- [49] De Gao, Hao Xu, Martin A. Philbert, Raoul Kopelman, Ultrafine hydrogel nanoparticles: synthetic approach and therapeutic application in living cells, *Angew. Chem. Int. Ed.* 46 (2007) 2224–2227, <https://doi.org/10.1002/anie.200603927>.
- [50] K. Löw, T. Knobloch, S. Wagner, A. Wiehe, A. Engel, K. Langer, H. von Briesen, Comparison of intracellular accumulation and cytotoxicity of free mTHPC and mTHPC-loaded PLGA nanoparticles in human colon carcinoma cells, *Nanotechnology* 22 (2011) 245102, <https://doi.org/10.1088/0957-4484/22/24/245102>.
- [51] M. Rojnik, P. Kocbek, F. Moret, C. Compagnin, L. Celotti, M.J. Bovis, J.H. Woodhams, A.J. MacRobert, D. Scheglmann, W. Helfrich, M.J. Verkaik, E. Papini, E. Reddi, J. Kos, In vitro and in vivo characterization of temoporfin-loaded PEGylated PLGA nanoparticles for use in photodynamic therapy, *Nanomedicine* (7) (2012) 663–677, <https://doi.org/10.2217/nmm.11.130>.
- [52] M. Villa Nova, C. Janas, M. Schmidt, T. Ulshoefer, S. Gräfe, S. Schiffmann, N. de Bruin, A. Wiehe, V. Albrecht, M.J. Pamham, M. Luciano Bruschi, M.G. Wacker, Nanocarriers for photodynamic therapy – rational formulation design and medium-scale manufacture, *Int. J. Pharm.* 491 (2015) 250–260, <https://doi.org/10.1016/j.ijpharm.2015.06.024>.
- [53] C. Compagnin, L. Baù, M. Mognato, L. Celotti, G. Miotto, M. Arduini, F. Moret, C. Fede, F. Selvestrel, I.M.R. Echevarria, F. Mancin, E. Reddi, The cellular uptake of meta-tetra(hydroxyphenyl)chlorin entrapped in organically modified silica nanoparticles is mediated by serum proteins, *Nanotechnology* 20 (2009) 345101, <https://doi.org/10.1088/0957-4484/20/34/345101>.
- [54] K. Haedike, D. Kozlova, S. Gräfe, U. Teichgräber, M. Eppe, I. Hilger, Multifunctional calcium phosphate nanoparticles for combining near-infrared fluorescence imaging and photodynamic therapy, *Acta Biomater.* 14 (2015) 197–207, <https://doi.org/10.1016/j.actbio.2014.12.009>.
- [55] I. Brezániová, K. Záruba, J. Králová, A. Sinica, H. Adámková, P. Ulbrich, P. Poučková, M. Hrubý, P. Štěpánek, V. Král, Silica-based nanoparticles are efficient delivery systems for temoporfin, *Photodiagn. Photodyn. Ther.* 21 (2018) 275–284, <https://doi.org/10.1016/j.pdpdt.2017.12.014>.
- [56] K. Chen, M. Wacker, S. Hackbarth, C. Ludwig, K. Langer, B. Röder, Photophysical evaluation of mTHPC-loaded HSA nanoparticles as novel PDT delivery systems, *J. Photochem. Photobiol. B* 101 (2010) 340–347, <https://doi.org/10.1016/j.jphotobiol.2010.08.006>.
- [57] A. Preuß, K. Chen, S. Hackbarth, M. Wacker, K. Langer, B. Röder, Photosensitizer loaded HSA nanoparticles II: in vitro investigations, *Int. J. Pharm.* 404 (2011) 308–316, <https://doi.org/10.1016/j.ijpharm.2010.11.023>.
- [58] B. Pegaz, E. Debeffe, J.-P. Ballini, G. Wagnières, S. Spaniol, V. Albrecht, D.V. Scheglmann, N.E. Nifantiev, H. van den Bergh, Y.N. Konan-Kouakou, Photothermal activity of m-THPC-loaded liposomal formulations: pre-clinical assessment on chick chorioallantoic membrane model, *Eur. J. Pharm. Sci.* 28 (2006) 134–140, <https://doi.org/10.1016/j.ejps.2006.01.008>.
- [59] A. Johansson, J. Svensson, N. Bendsoe, K. Svanberg, E. Alexandratou, M. Kyriazi, D. Yova, S. Gräfe, T. Trebst, S. Andersson-Engels, Fluorescence and absorption assessment of a lipid mTHPC formulation following topical application in a non-melanotic skin tumor model, *J. Biomed. Opt.* 12 (2007) 034026, <https://doi.org/10.1117/1.2743080>.
- [60] J. Svensson, A. Johansson, S. Gräfe, B. Gitter, T. Trebst, N. Bendsoe, S. Andersson-Engels, K. Svanberg, Tumor selectivity at short times following systemic administration of a liposomal temoporfin formulation in a murine tumor model, *Photochem. Photobiol.* 83 (2007) 1211–1219, <https://doi.org/10.1111/j.1751-1097.2007.00146.x>.
- [61] M.A. D'Hallewin, D. Kochetkov, Y. Viry-Babel, A. Leroux, E. Werkmeister, D. Dumas, S. Gräfe, V. Zorin, F. Guillemain, L. Bezdetnaya, Photodynamic therapy with intratumoral administration of lipid-based mTHPC in a model of breast cancer recurrence, *Lasers Surg. Med.* 40 (2008) 543–549, <https://doi.org/10.1002/lsm.20662>.
- [62] H.-P. Lassalle, M. Wagner, L. Bezdetnaya, F. Guillemain, H. Schneckenburger, Fluorescence imaging of Foscan® and Foslip in the plasma membrane and in whole cells, *J. Photochem. Photobiol. B* 92 (2008) 47–53, <https://doi.org/10.1016/j.jphotobiol.2008.04.007>.
- [63] H.-P. Lassalle, D. Dumas, S. Gräfe, M.-A. D'Hallewin, F. Guillemain, L. Bezdetnaya, Correlation between in vivo pharmacokinetics, intratumoral distribution and photodynamic efficiency of liposomal mTHPC, *J. Control. Release* 134 (2009) 118–124, <https://doi.org/10.1016/j.jconrel.2008.11.016>.
- [64] J. Garrier, L. Bezdetnaya, C. Barlier, S. Gräfe, F. Guillemain, M.-A. D'Hallewin, Foslip®-based photodynamic therapy as a means to improve wound healing, *Photodiagn. Photodyn. Ther.* 8 (2011) 321–327, <https://doi.org/10.1016/j.pdpdt.2011.06.003>.
- [65] E.B. Gyenge, S. Hiestand, S. Graefe, H. Walt, C. Maake, Cellular and molecular effects of the liposomal mTHPC derivative Foslipos in prostate carcinoma cells in vitro, *Photodiagn. Photodyn. Ther.* 8 (2011) 86–96, <https://doi.org/10.1016/j.pdpdt.2011.02.001>.
- [66] S.A.H.J. de Visser, S. Kaščáková, H.S. de Bruijn, A.V.D.P. van den Heuvel, A. Amelink, H.J.C.M. Sterenberg, D.J. Robinson, J.L.N. Roodenburg, M.J.H. Witjes, Fluorescence localization and kinetics of mTHPC and liposomal formulations of mTHPC in the window-chamber tumor model, *Lasers Surg. Med.* 43 (2011) 528–536, <https://doi.org/10.1002/lsm.21082>.
- [67] S.A.H.J. de Visser, M.J.H. Witjes, B. van der Veeg, H.S. de Bruijn, A.V.D.P. van den Heuvel, A. Amelink, H.J.C.M. Sterenberg, J.L.N. Roodenburg, D.J. Robinson, Localization of liposomal mTHPC formulations within normal epithelium, dysplastic tissue, and carcinoma of oral epithelium in the 4NQO-carcinogenesis rat model: LOCALIZATION OF LIPOSOMAL mTHPC FORMULATIONS, *Lasers Surg. Med.* 45 (2013) 668–678, <https://doi.org/10.1002/lsm.22197>.
- [68] J. Garrier, V. Reshetov, S. Gräfe, F. Guillemain, V. Zorin, L. Bezdetnaya, Factors affecting the selectivity of nanoparticle-based photoinduced damage in free and xenografted chorioallantoic membrane model, *J. Drug Target.* (2013), <https://doi.org/10.3109/1061186X.2013.860981>.
- [69] V. Reshetov, H.-P. Lassalle, A. François, D. Dumas, S. Hupont, S. Gräfe, V. Filipe, W. Jiskoot, F. Guillemain, V. Zorin, L. Bezdetnaya, Photodynamic therapy with conventional and PEGylated liposomal formulations of mTHPC (temoporfin): comparison of treatment efficacy and distribution characteristics in vivo, *Int. J. Nanomedicine* 8 (2013) 3817–3831, <https://doi.org/10.2147/IJN.S51002>.
- [70] K. Haedike, S. Gräfe, F. Lehmann, I. Hilger, Multiplexed in vivo fluorescence optical imaging of the therapeutic efficacy of photodynamic therapy, *Biomaterials* 34 (2013) 10075–10083, <https://doi.org/10.1016/j.biomaterials.2013.08.087>.
- [71] A. Reinhard, A. Bressenot, R. Dassonneville, A. Loywick, D. Hot, C. Audebert, S. Marchal, F. Guillemain, M. Chamailard, L. Peyrin-Biroulet, L. Bezdetnaya, Photodynamic therapy relieves colitis and prevents colitis-associated carcinogenesis in mice, *Inflamm. Bowel Dis.* 21 (2015) 985–995, <https://doi.org/10.1097/MIB.0000000000000354>.
- [72] E. Gaio, D. Scheglmann, E. Reddi, F. Moret, Uptake and photo-toxicity of Foscan®, Foslip® and Fospeg® in multicellular tumor spheroids, *J. Photochem. Photobiol. B* 161 (2016) 244–252, <https://doi.org/10.1016/j.jphotobiol.2016.05.011>.
- [73] D. Hinger, S. Gräfe, F. Navarro, B. Spingler, D. Pandiarajan, H. Walt, A.-C. Couffin, C. Maake, Lipid nanoemulsions and liposomes improve photodynamic treatment efficacy and tolerance in CAL-33 tumor bearing nude mice, *J. Nanobiotechnology*. 14 (2016) 71, <https://doi.org/10.1186/s12951-016-0223-8>.
- [74] D. Meier, S.M. Botter, C. Campanile, B. Robl, S. Gräfe, G. Pellegrini, W. Born, B. Fuchs, Foscan and foslip based photodynamic therapy in osteosarcoma in vitro and in intratibial mouse models, *Int. J. Cancer* 140 (2017) 1680–1692, <https://doi.org/10.1002/ijc.30572>.
- [75] I. Yakavets, H.-P. Lassalle, D. Scheglmann, A. Wiehe, V. Zorin, L. Bezdetnaya, I. Yakavets, H.-P. Lassalle, D. Scheglmann, A. Wiehe, V. Zorin, L. Bezdetnaya, Temoporfin-in-cyclodextrin-in-liposome – a new approach for anticancer drug delivery: the optimization of composition, *Nanomaterials* 8 (2018) 847, <https://doi.org/10.3390/nano8100847>.
- [76] M. Millard, I. Yakavets, M. Piffoux, A. Brun, F. Gazeau, J.-M. Guigner, J. Jasniewski, H.-P. Lassalle, C. Wilhelm, L. Bezdetnaya, mTHPC-loaded extracellular vesicles outperform liposomal and free mTHPC formulations by an increased stability, drug delivery efficiency and cytotoxic effect in tridimensional model of tumors, *Drug Deliv.* 25 (2018) 1790–1801, <https://doi.org/10.1080/10717544.2018.1513609>.
- [77] J. Buchholz, B. Kaser-Hotz, T. Khan, C. Rohrer Bley, K. Melzer, R.A. Schwendener, M. Roos, H. Walt, Optimizing photodynamic therapy: in vivo pharmacokinetics of liposomal meta-tetra(hydroxyphenyl)chlorin in feline squamous cell carcinoma, *Clin. Cancer Res.* 11 (2005) 7538–7544, <https://doi.org/10.1158/1078-0432.CCR-05-0490>.
- [78] J. Berlanda, T. Kiesslich, V. Engelhardt, B. Krammer, K. Plaetzer, Comparative in vitro study on the characteristics of different photosensitizers employed in PDT, *J. Photochem. Photobiol. B* 100 (2010) 173–180, <https://doi.org/10.1016/j.jphotobiol.2010.06.004>.
- [79] C. Compagnin, F. Moret, L. Celotti, G. Miotto, J.H. Woodhams, A.J. MacRobert, D. Scheglmann, S. Itratni, E. Reddi, Meta-tetra(hydroxyphenyl)chlorin-loaded liposomes sterically stabilised with poly(ethylene glycol) of different length and density: characterisation, in vitro cellular uptake and phototoxicity, *Photochem. Photobiol. Sci.* 10 (2011) 1751–1759, <https://doi.org/10.1039/c1pp05163f>.
- [80] M.J. Bovis, J.H. Woodhams, M. Loizidou, D. Scheglmann, S.G. Bown, A.J. MacRobert, Improved in vivo delivery of m-THPC via pegylated liposomes for use in photodynamic therapy, *J. Control. Release* 157 (2012) 196–205, <https://doi.org/10.1016/j.jconrel.2011.09.085>.
- [81] A. Petri, D. Yova, E. Alexandratou, M. Kyriazi, M. Rallis, Comparative characterization of the cellular uptake and photodynamic efficiency of Foscan® and Fospeg® in a human prostate cancer cell line, *Photodiagn. Photodyn. Ther.* 9 (2012) 344–354, <https://doi.org/10.1016/j.pdpdt.2012.03.008>.
- [82] H. Xie, P. Svenmarker, J. Axelsson, S. Gräfe, M. Kyriazi, N. Bendsoe, S. Andersson-Engels, K. Svanberg, Pharmacokinetic and biodistribution study following systemic administration of Fospeg® – a Pegylated liposomal mTHPC formulation in a

- murine model: pharmacokinetic and biodistribution study following systemic administration of Fospeg[®], *J. Biophotonics* 8 (2015) 142–152, <https://doi.org/10.1002/jbip.201360133>.
- [83] R.W.K. Wu, E.S.M. Chu, Z. Huang, C.S. Xu, C.W. Ip, C.M.N. Yow, Effect of Fospeg[®] mediated photoactivation on P-gp/ABCB1 protein expression in human nasopharyngeal carcinoma cells, *J. Photochem. Photobiol. B* 148 (2015) 82–87, <https://doi.org/10.1016/j.jphotobiol.2015.03.019>.
- [84] C. Bombelli, A. Stringaro, S. Borocci, G. Bozzuto, M. Colone, L. Giansanti, R. Scambato, L. Toccaceli, G. Mancini, A. Molinari, Efficiency of liposomes in the delivery of a photosensitizer controlled by the stereochemistry of a gemini surfactant component, *Mol. Pharm.* 7 (2010) 130–137, <https://doi.org/10.1021/mp900173v>.
- [85] C. Bombelli, G. Caracciolo, P. Di Profio, M. Diociaiuti, P. Luciani, G. Mancini, C. Mazzuca, M. Marra, A. Molinari, D. Monti, L. Toccaceli, M. Venanzi, Inclusion of a photosensitizer in liposomes formed by DMPC/Gemini surfactant: correlation between physicochemical and biological features of the complexes, *J. Med. Chem.* 48 (2005) 4882–4891, <https://doi.org/10.1021/jm050182d>.
- [86] A. Molinari, C. Bombelli, S. Mannino, A. Stringaro, L. Toccaceli, A. Calcabrini, M. Colone, A. Mangiola, G. Maira, P. Luciani, G. Mancini, G. Arancia, m-THPC-mediated photodynamic therapy of malignant gliomas: assessment of a new transfection strategy, *Int. J. Cancer* 121 (2007) 1149–1155, <https://doi.org/10.1002/ijc.22793>.
- [87] A. Molinari, M. Colone, A. Calcabrini, A. Stringaro, L. Toccaceli, G. Arancia, S. Mannino, A. Mangiola, G. Maira, C. Bombelli, G. Mancini, Cationic liposomes, loaded with m-THPC, in photodynamic therapy for malignant glioma, *Toxicol. In Vitro* 21 (2007) 230–234, <https://doi.org/10.1016/j.tiv.2006.09.006>.
- [88] N. Dragicevic-Curic, S. Grafić, V. Albrecht, A. Fahr, Topical application of temoporfin-loaded invasomes for photodynamic therapy of subcutaneously implanted tumours in mice: a pilot study, *J. Photochem. Photobiol. B* 91 (2008) 41–50, <https://doi.org/10.1016/j.jphotobiol.2008.01.009>.
- [89] N. Dragicevic-Curic, D. Scheglmann, V. Albrecht, A. Fahr, Development of different temoporfin-loaded invasomes – novel nanocarriers of temoporfin: characterization, stability and in vitro skin penetration studies, *Colloids Surf. B: Biointerfaces* 70 (2009) 198–206, <https://doi.org/10.1016/j.colsurfb.2008.12.030>.
- [90] N. Dragicevic-Curic, S. Grafić, B. Gitter, S. Winter, A. Fahr, Surface charged temoporfin-loaded flexible vesicles: in vitro skin penetration studies and stability, *Int. J. Pharm.* 384 (2010) 100–108, <https://doi.org/10.1016/j.ijpharm.2009.10.006>.
- [91] M. Piffoux, A.K.A. Silva, C. Wilhelm, F. Gazeau, D. Taresté, Modification of extracellular vesicles by fusion with liposomes for the design of personalized biogenic drug delivery systems, *ACS Nano* 12 (2018) 6830–6842, <https://doi.org/10.1021/acsnano.8b02053>.
- [92] F.P. Navarro, G. Creusat, C. Frochet, A. Moussaron, M. Verhille, R. Vandresse, J.-S. Thomann, P. Boisseau, I. Texier, A.-C. Couffin, M. Barberi-Heyob, Preparation and characterization of m-THPC-loaded solid lipid nanoparticles for photodynamic therapy, *J. Photochem. Photobiol. B* 130 (2014) 161–169, <https://doi.org/10.1016/j.jphotobiol.2013.11.007>.
- [93] D. Hinger, F. Navarro, A. Käch, J.-S. Thomann, F. Mittler, A.-C. Couffin, C. Maake, Photoinduced effects of m-tetrahydroxyphenylchlorin loaded lipid nanoemulsions on multicellular tumor spheroids, *J. Nanobiotechnology* 14 (2016), <https://doi.org/10.1186/s12951-016-0221-x>.
- [94] I. Brezaniova, M. Hruby, J. Kralova, V. Kral, Z. Cernochova, P. Cernoch, M. Slouf, J. Kredatusova, P. Stepanek, Temoporfin-loaded 1-tetradecanol-based thermoresponsive solid lipid nanoparticles for photodynamic therapy, *J. Control. Release* 241 (2016) 34–44, <https://doi.org/10.1016/j.jconrel.2016.09.009>.
- [95] I. Marangon, C. Ménard-Moyon, A.K.A. Silva, A. Bianco, N. Luciani, F. Gazeau, Synergic mechanisms of photothermal and photodynamic therapies mediated by photosensitizer/carbon nanotube complexes, *Carbon* 97 (2016) 110–123, <https://doi.org/10.1016/j.carbon.2015.08.023>.
- [96] A.K.A. Silva, N. Luciani, F. Gazeau, K. Aubertin, S. Bonneau, C. Chauvierre, D. Letoumeur, C. Wilhelm, Combining magnetic nanoparticles with cell derived microvesicles for drug loading and targeting, *Nanomedicine* 11 (2015) 645–655, <https://doi.org/10.1016/j.nano.2014.11.009>.
- [97] A.K.A. Silva, J. Kolosnjaj-Tabi, S. Bonneau, I. Marangon, N. Boggetto, K. Aubertin, O. Clément, M.F. Bureau, N. Luciani, F. Gazeau, C. Wilhelm, Magnetic and photoresponsive theranostics: translating cell-released vesicles into smart nanovectors for cancer therapy, *ACS Nano* 7 (2013) 4954–4966, <https://doi.org/10.1021/nl400269x>.
- [98] R. Di Corato, G. Béalle, J. Kolosnjaj-Tabi, A. Espinosa, O. Clément, A.K.A. Silva, C. Ménager, C. Wilhelm, Combining magnetic hyperthermia and photodynamic therapy for tumor ablation with photoresponsive magnetic liposomes, *ACS Nano* 9 (2015) 2904–2916, <https://doi.org/10.1021/nl506949t>.
- [99] Y.-C. Tsai, P. Vijayaraghavan, W.-H. Chiang, H.-H. Chen, T.-I. Liu, M.-Y. Shen, A. Omoto, M. Kamimura, K. Soga, H.-C. Chiu, Targeted delivery of functionalized upconversion nanoparticles for externally triggered photothermal/photodynamic therapies of brain glioblastoma, *Theranostics* 8 (2018) 1435–1448, <https://doi.org/10.7150/thno.22482>.
- [100] A. Bautista-Sanchez, A. Kasselouri, M.-C. Desroches, J. Blais, P. Maillard, D.M. de Oliveira, A.C. Tedesco, P. Prognon, J. Delaire, Photophysical properties of glucoconjugated chlorins and porphyrins and their associations with cyclodextrins, *J. Photochem. Photobiol. B* 81 (2005) 154–162, <https://doi.org/10.1016/j.jphotobiol.2005.05.013>.
- [101] H.-J. Sinn, H.-H. Schrenk, W. Maier-Borst, E. Friedrich, G. Grashew, D. WÖHRLE, T. Klenner, Polyethersubstituierte Tumormittel, WO1991018630A1 <https://patents.google.com/patent/WO1991018630A1/en?q=WO+91%2F8630>, (1991) accessed March 17, 2019.
- [102] J.K. Armstrong, R.B. Wenby, H.J. Meiselman, T.C. Fisher, The hydrodynamic radii of macromolecules and their effect on red blood cell aggregation, *Biophys. J.* 87 (2004) 4259–4270, <https://doi.org/10.1529/biophysj.104.047746>.
- [103] L.W. Seymour, Passive tumor targeting of soluble macromolecules and drug conjugates, *Crit. Rev. Ther. Drug Carrier Syst.* 9 (1992) 135–187.
- [104] S.G. Schultz, A.K. Solomon, Determination of the effective hydrodynamic radii of small molecules by viscometry, *J. Gen. Physiol.* 44 (1961) 1189–1199, <https://doi.org/10.1085/jgp.44.6.1189>.
- [105] R.B. Hamanaka, N.S. Chandel, Targeting glucose metabolism for cancer therapy, *J. Exp. Med.* 209 (2012) 211–215, <https://doi.org/10.1084/jem.20120162>.
- [106] A. Cheung, H.J. Bax, D.H. Josephs, K.M. Hleva, G. Pellizzari, J. Opzoomer, J. Bloomfield, M. Pittall, A. Grigoriadis, M. Figini, S. Canevari, J.F. Spicer, A.N. Tutt, S.N. Karagiannis, Targeting folate receptor alpha for cancer treatment, *Oncotarget* 7 (2016) 52553–52574, <https://doi.org/10.18632/oncotarget.9651>.
- [107] S. Jain, D.G. Hirst, J.M. O'Sullivan, Gold nanoparticles as novel agents for cancer therapy, *Br. J. Radiol.* 85 (2012) 101–113, <https://doi.org/10.1259/bjr/59448833>.
- [108] R. Meir, K. Shamalov, O. Betzer, M. Motiei, M. Horovitz-Fried, R. Yehuda, A. Popovtzer, R. Popovtzer, C.J. Cohen, Nanomedicine for cancer immunotherapy: tracking cancer-specific T-cells in vivo with gold nanoparticles and CT imaging, *ACS Nano* 9 (2015) 6363–6372, <https://doi.org/10.1021/acsnano.5b01939>.
- [109] F. Giuntini, C.M.A. Alonso, R.W. Boyle, Synthetic approaches for the conjugation of porphyrins and related macrocycles to peptides and proteins, *Photochem. Photobiol. Sci.* 10 (2011) 759–791, <https://doi.org/10.1039/c0pp00366b>.
- [110] A. Ben Mihoub, L. Larue, A. Moussaron, Z. Youssef, L. Colombeau, F. Baros, C. Frochet, R. Vandresse, S. Acherar, Use of cyclodextrins in anticancer photodynamic therapy treatment, *Molecules* 23 (2018) 1936, <https://doi.org/10.3390/molecules23081936>.
- [111] D. Demore, A. Kasselouri, O. Bourdon, J. Blais, G. Mahuzier, P. Prognon, Enhancement of 5,10,15,20-tetra(m-hydroxyphenyl)chlorin fluorescence emission by inclusion in natural and modified cyclodextrins, *Appl. Spectrosc.* 53 (1999) 523–527.
- [112] I. Yakavets, I. Yankovsky, L. Bezdetsnaya, V. Zorin, Soret band shape indicates m-THPC distribution between β -cyclodextrins and serum proteins, *Dyes Pigments* 137 (2017) 299–306, <https://doi.org/10.1016/j.dyepig.2016.11.007>.
- [113] M.-C. Desroches, A. Kasselouri, O. Bourdon, P. Chaminate, J. Blais, P. Prognon, A direct sensitized fluorimetric determination of 5,10,15,20-tetra(m-hydroxyphenyl)chlorin [m-THPC(Foscan)[®]] in human plasma using a cyclodextrin inclusion complex, *Analyst* 126 (2001) 923–927, <https://doi.org/10.1039/B100808K>.
- [114] I. Yakavets, H.-P. Lassalle, I. Yankovsky, F. Ingrassio, A. Monari, L. Bezdetsnaya, V. Zorin, Evaluation of temoporfin affinity to β -cyclodextrins assuming self-aggregation, *J. Photochem. Photobiol. A Chem.* 367 (2018) 13–21, <https://doi.org/10.1016/j.jphotochem.2018.07.046>.
- [115] V.J. Stella, Q. He, Cyclodextrins, *Toxicol. Pathol.* 36 (2008) 30–42, <https://doi.org/10.1177/0192623307310945>.
- [116] N. Sharma, A. Baldi, Exploring versatile applications of cyclodextrins: an overview, *Drug Deliv.* 23 (2016) 729–747, <https://doi.org/10.3109/10717544.2014.938839>.
- [117] V.J. Stella, V.M. Rao, E.A. Zannou, V. Zia, Mechanisms of drug release from cyclodextrin complexes, *Adv. Drug Deliv. Rev.* 36 (1999) 3–16, [https://doi.org/10.1016/S0169-409X\(98\)00052-0](https://doi.org/10.1016/S0169-409X(98)00052-0).
- [118] L. Li, K.M. Huh, Polymeric nanocarrier systems for photodynamic therapy, *Biomater. Res.* 18 (2014) 19, <https://doi.org/10.1186/2055-7124-18-19>.
- [119] C.F. van Nostrum, Polymeric micelles to deliver photosensitizers for photodynamic therapy, *Adv. Drug Deliv. Rev.* 56 (2004) 9–16, <https://doi.org/10.1016/j.addr.2003.07.013>.
- [120] Y. Nakamura, A. Mochida, P.L. Choyke, H. Kobayashi, Nanodrug delivery: is the enhanced permeability and retention effect sufficient for curing cancer? *Bioconjug. Chem.* 27 (2016) 2225–2238, <https://doi.org/10.1021/acs.bioconjchem.6b00437>.
- [121] V.P. Torchilin, Structure and design of polymeric surfactant-based drug delivery systems, *J. Control. Release* 73 (2001) 137–172.
- [122] M. Anaya, M. Kwak, A.J. Musser, K. Müllen, A. Herrmann, Tunable hydrophobicity in DNA micelles: design, synthesis, and characterization of a new family of DNA amphiphiles, *Chem. Eur. J.* 16 (2010) 12852–12859, <https://doi.org/10.1002/chem.201001816>.
- [123] J. Li, H. Pei, B. Zhu, L. Liang, M. Wei, Y. He, N. Chen, D. Li, Q. Huang, C. Fan, Self-assembled multivalent DNA nanostructures for noninvasive intracellular delivery of immunostimulatory CpG oligonucleotides, *ACS Nano* 5 (2011) 8783–8789, <https://doi.org/10.1021/nn202774x>.
- [124] I. Brezaniova, J. Trousil, Z. Cernochova, V. Kral, M. Hruby, P. Stepanek, M. Slouf, Self-assembled chitosan-alginate polyplex nanoparticles containing temoporfin, *Colloid Polym. Sci.* 295 (2017) 1259–1270, <https://doi.org/10.1007/s00396-016-3992-6>.
- [125] J.-M. Lü, X. Wang, C. Marin-Muller, H. Wang, P.H. Lin, Q. Yao, C. Chen, Current advances in research and clinical applications of PLGA-based nanotechnology, *Expert. Rev. Mol. Diagn.* 9 (2009) 325–341, <https://doi.org/10.1586/erm.09.15>.
- [126] J. Sun, W. Birbaumu, J. Anderski, M.-T. Picker, D. Mulac, K. Langer, D. Kuckling, Use of light-degradable aliphatic polycarbonate nanoparticles as drug carrier for photosensitizer, *Biomacromolecules* (2018), <https://doi.org/10.1021/acs.biomac.8b01446>.
- [127] T.A. Debele, S. Peng, H.-C. Tsai, Drug carrier for photodynamic cancer therapy, *Int. J. Mol. Sci.* 16 (2015) 22094–22136, <https://doi.org/10.3390/ijms160922094>.
- [128] Fei Yan, Raoul Kopelman, The embedding of meta-tetra(hydroxyphenyl)-chlorin

- into silica nanoparticle platforms for photodynamic therapy and their singlet oxygen production and pH-dependent optical properties[†], *Photochem. Photobiol.* 78 (2007) 587–591, [https://doi.org/10.1562/0031-8655\(2007\)0780587TEOMIS2.0.CO;2](https://doi.org/10.1562/0031-8655(2007)0780587TEOMIS2.0.CO;2).
- [129] D. Liu, B. Lin, W. Shao, Z. Zhu, T. Ji, C. Yang, In vitro and in vivo studies on the transport of PEGylated silica nanoparticles across the blood–brain barrier, *ACS Appl. Mater. Interfaces* 6 (2014) 2131–2136, <https://doi.org/10.1021/am405219u>.
- [130] S. Hanada, K. Fujioka, Y. Inoue, F. Kanaya, Y. Manome, K. Yamamoto, Cell-based in vitro blood–brain barrier model can rapidly evaluate nanoparticles' brain permeability in association with particle size and surface modification, *Int. J. Mol. Sci.* 15 (2014) 1812–1825, <https://doi.org/10.3390/ijms15021812>.
- [131] J. Kreuter, Influence of the surface properties on nanoparticle-mediated transport of drugs to the brain, *J. Nanosci. Nanotechnol.* 4 (2004) 484–488.
- [132] D. Verma, N. Gulati, S. Kaul, S. Mukherjee, U. Nagaich, Protein based nanostructures for drug delivery, *Aust. J. Pharm.* (2018), <https://doi.org/10.1155/2018/9285854>.
- [133] E. Reddi, Role of delivery vehicles for photosensitizers in the photodynamic therapy of tumours, *J. Photochem. Photobiol. B* 37 (1997) 189–195, [https://doi.org/10.1016/S1011-1344\(96\)07404-0](https://doi.org/10.1016/S1011-1344(96)07404-0).
- [134] M. Wacker, K. Chen, A. Preuss, K. Possemeyer, B. Roeder, K. Langer, Photosensitizer loaded HSA nanoparticles. I: preparation and photophysical properties, *Int. J. Pharm.* 393 (2010) 254–263, <https://doi.org/10.1016/j.ijpharm.2010.04.022>.
- [135] A. Puri, K. Loomis, B. Smith, J.-H. Lee, A. Yavlovich, E. Heldman, R. Blumenthal, Lipid-based nanoparticles as pharmaceutical drug carriers: from concepts to clinic, *Crit. Rev. Ther. Drug Carrier Syst.* 26 (2009) 523–580.
- [136] V.P. Torchilin, Recent advances with liposomes as pharmaceutical carriers, *Nat. Rev. Drug Discov.* 4 (2005) 145–160, <https://doi.org/10.1038/nrd1632>.
- [137] M.D. Vetta, L. González, J.J. Nogueira, Hydrogen bonding regulates the rigidity of liposome-encapsulated chlorin photosensitizers, *ChemistryOpen* 7 (2018) 475–483, <https://doi.org/10.1002/open.201800050>.
- [138] J. Kuntsche, I. Freisleben, F. Steiniger, A. Fahr, Temoporfin-loaded liposomes: physicochemical characterization, *Eur. J. Pharm. Sci.* 40 (2010) 305–315, <https://doi.org/10.1016/j.ejps.2010.04.005>.
- [139] N. Düzgüneş, S. Nir, Mechanisms and kinetics of liposome–cell interactions, *Adv. Drug Deliv. Rev.* 40 (1999) 3–18, [https://doi.org/10.1016/S0169-409X\(99\)00037-X](https://doi.org/10.1016/S0169-409X(99)00037-X).
- [140] V. Reshetov, D. Kachatkou, T. Shmigol, V. Zorin, M.-A. D'Hallewin, F. Guillemin, L. Bezdetnaya, Redistribution of meta-tetra(hydroxyphenyl)chlorin (mTHPC) from conventional and PEGylated liposomes to biological substrates, *Photochem. Photobiol. Sci.* 10 (2011) 911–919, <https://doi.org/10.1039/C0PP00303D>.
- [141] H. Hefesha, S. Loew, X. Liu, S. May, A. Fahr, Transfer mechanism of temoporfin between liposomal membranes, *J. Control. Release* 150 (2011) 279–286, <https://doi.org/10.1016/j.jconrel.2010.09.021>.
- [142] S. Holzschuh, K. Kaeß, G.V. Bossa, C. Decker, A. Fahr, S. May, Investigations of the influence of liposome composition on vesicle stability and drug transfer in human plasma: a transfer study, *J. Liposome Res.* 28 (2018) 22–34, <https://doi.org/10.1080/08982104.2016.1247101>.
- [143] D. Kachatkou, S. Sasnouski, V. Zorin, T. Zorina, M.-A. D'Hallewin, F. Guillemin, L. Bezdetnaya, Unusual photoinduced response of mTHPC liposomal formulation (Foslip), *Photochem. Photobiol.* 85 (2009) 719–724, <https://doi.org/10.1111/j.1751-1097.2008.00466.x>.
- [144] M.H. Teiten, L. Bezdetnaya, J.L. Merlin, C. Bour-Dill, M.E. Pauly, M. Dicato, F. Guillemin, Effect of meta-tetra(hydroxyphenyl)chlorin (mTHPC)-mediated photodynamic therapy on sensitive and multidrug-resistant human breast cancer cells, *J. Photochem. Photobiol. B* 62 (2001) 146–152.
- [145] R. van der Meel, M.H.A.M. Fens, P. Vader, W.W. van Solinge, O. Eniola-Adefeso, R.M. Schiffelers, Extracellular vesicles as drug delivery systems: lessons from the liposome field, *J. Control. Release* 195 (2014) 72–85, <https://doi.org/10.1016/j.jconrel.2014.07.049>.
- [146] G. Fuhrmann, A. Serio, M. Mazo, R. Nair, M.M. Stevens, Active loading into extracellular vesicles significantly improves the cellular uptake and photodynamic effect of porphyrins, *J. Control. Release* 205 (2015) 35–44, <https://doi.org/10.1016/j.jconrel.2014.11.029>.
- [147] R.H. Müller, K. Mäder, S. Gohla, Solid lipid nanoparticles (SLN) for controlled drug delivery – a review of the state of the art, *Eur. J. Pharm. Biopharm.* 50 (2000) 161–177, [https://doi.org/10.1016/S0939-6411\(00\)00087-4](https://doi.org/10.1016/S0939-6411(00)00087-4).
- [148] V.J. Lingayat, N.S. Zarekar, R.S. Shendge, Solid lipid nanoparticles: a review, *Nanosci. Nanotechnol. Res.* 4 (2017) 67–72, <https://doi.org/10.12691/nnr-4-2-5>.
- [149] S. Haupt, I. Lazar, H. Weitman, M.O. Senge, B. Ehrenberg, Pdots, a new type of nanoparticle, bind to mTHPC via their lipid modified surface and exhibit very high FRET efficiency between the core and the sensitizer, *Phys. Chem. Chem. Phys.* 17 (2015) 11412–11422, <https://doi.org/10.1039/C4CP05579A>.
- [150] T. Murakami, H. Nakatsuji, M. Inada, Y. Matoba, T. Uneyama, M. Tsujimoto, S. Isoda, M. Hashida, H. Imahori, Photodynamic and photothermal effects of semiconducting and metallic-enriched single-walled carbon nanotubes, *J. Am. Chem. Soc.* 134 (2012) 17862–17865, <https://doi.org/10.1021/ja3079972>.
- [151] B. McCormack, G. Gregoriadis, Entrapment of cyclodextrin–drug complexes into liposomes: potential advantages in drug delivery, *J. Drug Target.* 2 (1994) 449–454, <https://doi.org/10.3109/10611869408996821>.
- [152] S. Franzè, U.M. Musazzi, P. Minghetti, F. Citarzo, Drug-in-micelles-in-liposomes (DIMIL) systems as a novel approach to prevent drug leakage from deformable liposomes, *Eur. J. Pharm. Sci.* 130 (2019) 27–35, <https://doi.org/10.1016/j.ejps.2019.01.013>.
- [153] J. Chen, W.-L. Lu, W. Gu, S.-S. Lu, Z.-P. Chen, B.-C. Cai, X.-X. Yang, Drug-in-cyclodextrin-in-liposomes: a promising delivery system for hydrophobic drugs, *Expert Opin. Drug Deliv.* 11 (2014) 565–577, <https://doi.org/10.1517/17425247.2014.884557>.
- [154] P. Mura, F. Maestrelli, M. Cecchi, M. Bragagni, A. Almeida, Development of a new delivery system consisting in 'drug-in cyclodextrin-in PLGA nanoparticles, *J. Microencapsul.* 27 (2010) 479–486, <https://doi.org/10.3109/02652040903515508>.
- [155] S. Rawal, M.M. Patel, Threatening cancer with nanoparticle aided combination oncotherapy, *J. Control. Release* 301 (2019) 76–109, <https://doi.org/10.1016/j.jconrel.2019.03.015>.

3. Drug-in-cyclodextrin-in-liposome (DCL) nanoplatform

Due to the high hydrophobicity of many clinically effective drugs, the entrapment of hydrophobic drugs in the form of water-soluble drug-cyclodextrin (CD) complexes in liposomes has been investigated as a new strategy to combine the relative advantages of CDs and liposomes into one system, namely drug-in-CD-in-liposome (DCL) (Figure 3.1). This concept was firstly proposed by McCormack and Gregoriadis in 1994 (McCormack and Gregoriadis, 1994) in an effort to combine the advantages offered by both CDs and liposomes in one nano-plattform. DCL approach can be useful in increasing drug solubility and vesicles stability, in controlling the *in vivo* fate of hydrophobic drugs and in avoiding burst release of drug from the vesicles. Relevant characteristics of liposomes and CDs will be briefly described in the next paragraphs.

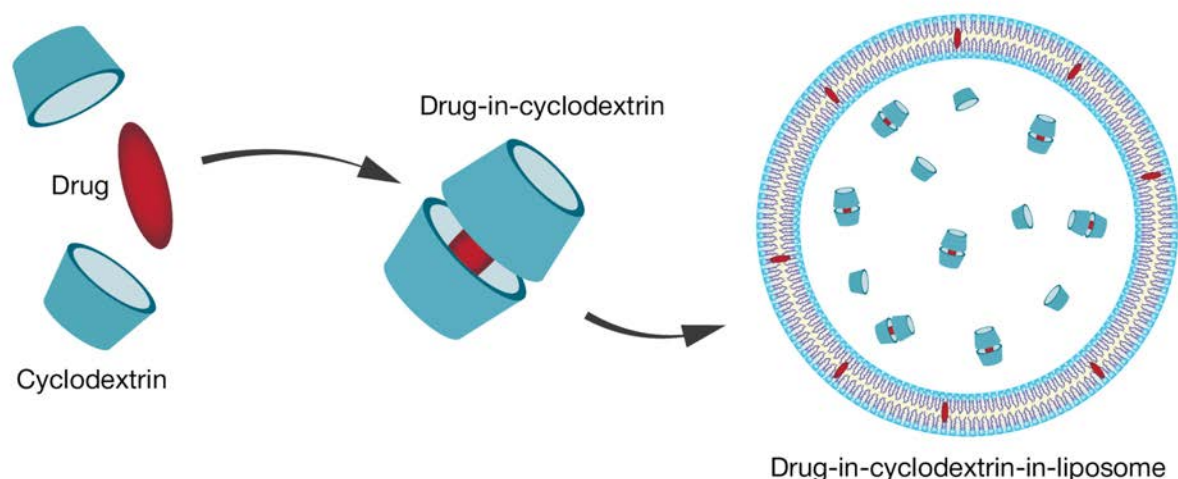


Figure 3.1 Schematic structure of DCL

3.1. Liposomes

The pioneering observation of spherical self-closed bilayered structures formed by phospholipids in aqueous systems was done by Alec Bangham about 55 years ago (Bangham and Horne, 1964). Ten years later, liposomes were already suggested as drug carriers in cancer chemotherapy by Gregoriadis et al. (Gregoriadis et al., 1974). Since then, the interest in lipid vesicles has widely grown and liposomal systems are currently being extensively studied as drug carriers (Olusanya et al., 2018; Torchilin, 2005). Interestingly, a liposomal formulation of doxorubicin (PEGylated liposomal-based doxorubicin, Doxil®) became the first nano-drug approved by the FDA in 1995 (Barenholz, 2012), demonstrating a significant role of liposomes in pharmaceuticals and particular in nanomedicine.

Composition and classification

Briefly, liposomes are spherical vesicles formed of one or more concentric phospholipid bilayers, separated by aqueous compartments (Olusanya et al., 2018; Torchilin, 2005). Lipid vesicle can encapsulate both hydrophilic and hydrophobic agents, protecting the cargo during the circulation in the body. The properties of lipid vesicles strongly depend on the lipid bilayers composition and a wide range of phospholipids with varying physical-chemical properties provide high versatility of liposomes. Liposomes can be made from different natural and/or synthetic phospholipids (Phosphatidylethanolamine, Phosphatidylglycerol, Phosphatidylcholine (DPPC), Phosphatidylserine, Phosphatidylinositol). Phosphatidylcholine (also known as lecithin) and phosphatidylethanolamine constitute two major structural components of most biological membranes.

Varying the composition of lipid mixture, the physical properties of the lipid bilayer, such as permeability and fluidity, which greatly influence the performance of liposomes *in vitro* and *in vivo*, could be specifically tailored (Slingerland et al., 2012). Different natural and synthetic phospholipids have different phase transition temperature (T_M), which is a very important parameter influencing drug encapsulation efficiency and both storage and *in vivo* stability. With increasing temperature, lipids pass from the ordered gel to a disordered liquid-crystalline phase, making easier the permeation of encapsulated drug through the bilayer. Therefore, phospholipids whose T_M is higher than the body temperature are often used to prepare more stable liposomes as drug delivery carriers for *in vivo* use. Stability against leakage may be additionally promoted by adding cholesterol (Samad et al., 2007; Vemuri and Rhodes, 1995). However, while cholesterol may increase the lipid membrane rigidity and stabilize the liposomes, it may also increase the particle size of liposomes in a dose-dependent manner (López-Pinto et al., 2005). The application of physiological lipids, which decrease the danger of acute and chronic toxicity, is a clear advantage of liposomes application.

Liposomes can be categorized in different ways. Generally, liposomes are classified according to their size and number of bilayers (also referred to as lamellae) (Samad et al., 2007). Both the size and the number of lamellae in the liposomal structure are considered to be the most crucial factors affecting the vesicles biological behavior and drug encapsulation efficiency (Akbarzadeh et al., 2013). Liposomes with a single bilayer are called unilamellar vesicles, which are subdivided into the small (SUV, 20-200 nm), large (LUV, 200-1000 nm) and giant (GUV, >1000 nm) ones. The vesicles consisting of one to five bilayers are called oligolamellar vesicles and are characterized by the size of 100-1000 nm. Finally, multilamellar vesicles composed of multiple bilayers (MLV, 5-25 lamella) usually possess the diameter from 500 nm up to 5 μm . Liposomes can be also categorized based on the lipid

surface properties such as the charge, PEGylation, active targeting, etc (Torchilin, 2005) and preparation method (Akbarzadeh et al., 2013). Ideally, the liposome formulations should be optimized in terms of the species and contents of lipids as well as preparation parameters in order to achieve desired properties, such as particle size, surface charge, encapsulation efficiency, and stability.

Methods of liposome preparation

The methods of preparing the liposomes involve the general stages such as (i) drying down the lipids from an organic solvent, (ii) dispersing the lipid suspension in aqueous media and (iii) purification of the resultant liposomes (Akbarzadeh et al., 2013). Drug loading can be attained either passively (i.e., during liposome formation) or actively (i.e., after liposome formation). There are several passive loading techniques, which are used for liposomes preparation: mechanical dispersion (sonication, extrusion, micro-emulsification, etc), solvent dispersion (ether or ethanol injection, reverse phase evaporation) and detergent removal methods (dialysis, chromatography, chemical adsorbers). The preparation of liposomes will be further described on the example of small unilamellar vesicles, as most widely used for the delivery of macromolecules.

Among the methods available for liposome preparation, the most commonly employed one is thin-layer hydration proposed by Bangham et al. (Bangham et al., 1965). According to this method, a suspension of multilamellar lipid vesicles is readily obtained by co-dissolving the desired lipids (including any hydrophobic cargo) in an organic solvent, subsequent drying using rotatory evaporator and finally hydrating under agitation above the lipid phase transition temperature. In order to decrease the lamellarity and heterogeneity of resulting suspension, mechanical dispersion methods such as sonication or membrane extrusion could be applied. The resulting liposomes are characterized by narrow size distribution and are ready to use. Hydrophilic drugs could also be encapsulated within an aqueous compartment of liposomes. In this case, the addition of the active compound is carried out at the step of thin lipid hydration when the drug is dissolved in the hydration buffer. As a result, the drug is encapsulated in the inner aqueous core of liposomes. *In fine*, the resultant suspension is purified by means of dialysis, chromatography or ultracentrifugation techniques.

It worth noting, that the trapping efficiency strongly depends on the solubility and partitioning characteristics of encapsulated drug (Gulati et al., 1998). Hence, highly lipophilic drugs ($\log P > 5$) are entrapped almost completely in the lipid bilayer of the liposomes (trapping efficiency $\approx 100\%$), e.g. mTHPC (Kuntsche et al., 2010). While highly hydrophilic drugs with $\log P < (-0.3)$, are located exclusively in the aqueous compartments of the liposomes. In that case, the efficiency of passive encapsulation of hydrophylic drug is

depends on the preparation technique and lipid concentration (ratio between aqueous volume of liposomes and unentrapped volume left in the void space due to the curvature of liposomes) and generally do not exceed 30% (Akbarzadeh et al., 2013).

The behavior of liposomes in vivo

Liposomal formulations have shown the ability to enhance the pharmacokinetics and pharmacodynamics of encapsulated drugs since these formulations can induce rapid uptake and long retention by the target tissues (Akbarzadeh et al., 2013). The advantages of liposome-mediated drugs also include greater solubility, longer circulation times, greater exposure and targeted delivery of the enclosed drug (Torchilin, 2010). Concerning anticancer therapy, numerous different liposome-based formulations demonstrated lower toxicity than free drugs (Olusanya et al., 2018). Liposomes selectively deliver anticancer drugs to the tumor tissue by means of a passive targeting via the enhanced permeability and retention (EPR) effect of the tumor vasculature. Tumor vessel units are leaky and are characterized by the absence of lymph drainage (Maeda, 2001). Thus, due to the size of hundreds of nanometers, liposomes could permeate into the tumor interstitium (typically over 24–48 h) via leaky tumor vasculature through molecular movement within fluids. However, the EPR effect is relatively modest, offering less than a 2-fold increase in delivery compared with critical normal organs (Matsumura and Maeda, 1986; Nakamura et al., 2016). Advancements in liposomal vesicle development have achieved both controlled drug release and targeted drug delivery (disease-specific localization) by means of the modification of the liposomal surface by active targeting moieties (Torchilin, 2005). Additionally, stimuli-responsive moieties could be embedded in order to control the release of the drug at the preferable sites.

The pharmacokinetics and biodistribution of liposome-encapsulated drugs are controlled by the interplay of two factors: the rate of plasma clearance of the liposome carrier and the stability of the liposome-drug association in the circulation. The clearance of intravenously-injected liposomes is governed by the mononuclear phagocyte system (MPS), or the reticuloendothelial system (RES) (Abra and Hunt, 1981). MPS includes monocytes, macrophages and dendritic cells located primarily in the liver and spleen determining the preferable biodistribution of liposomal cargo. To be recognized by MPS, specific proteins (opsonins) adsorb immediately after the liposomes contact with plasma *in vivo*. Moreover, along with opsonins, serum proteins (i.e., lipoproteins) interact with liposomes causing intensive lipid mass transfer between them. This, in turn, leads to the release of the encapsulated drug from the liposomes to the serum proteins and also could result in liposome disintegration. To avoid the interaction of liposomal vesicles with serum components and RES, the liposomal surface could be modified by the addition of charged (either positive or negative) lipids (Jain et al., 2012) and/or surface-grafted hydrophilic

polymers (i.e., PEG) (Ishida et al., 2005). This unique and flexible variety in the liposomal structure and composition distinguishes liposomes as the preferred nanocarriers for a broad spectrum of therapeutic agents, including anticancer drugs (Akbarzadeh et al., 2013).

In conclusion, liposomes are non-toxic, flexible, biocompatible, completely biodegradable and non-immunogenic drug nanodelivery systems for systemic and non-systemic drugs administrations. Lipid vesicles increase stability and solubility of the hydrophobic drug via encapsulation resulting in the reduced drug toxicity and side effects such as the exposure of sensitive tissues to toxic drugs (Akbarzadeh et al., 2013). The main drawback of liposomes is its hindered penetration into the tissues. Thus, liposomes act well as containers for the hydrophobic drug delivery to the tumor but are not an ultimate nanoplatform. On the other hand, inner aqueous core allows encapsulating of soluble drugs or its formulations (i.e., micelles, CD-based inclusion complexes) forming hybrid nanoplatforms (i.e., drug-in-micelles-in-liposomes, drug-in-cyclodextrin-in-liposomes) (Chen et al., 2014; Franzè et al., 2019). Recently, a similar strategy was also adopted to encapsulate drug-loaded micelles into liposomes making drug-in-micelle-in-liposome (Franzè et al., 2019).

3.2. Cyclodextrin-based inclusion complexes

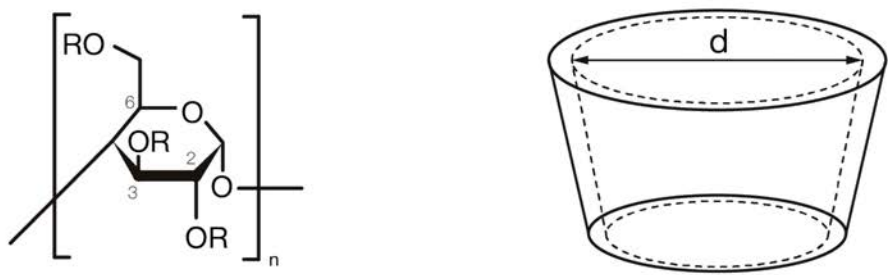
The inclusion complexes of CDs with a wide variety of organic and non-organic compounds refer to the class of the simplest supramolecular systems extensively studied for the last decades (Carneiro et al., 2019). CDs were discovered by French scientist Villiers in 1891 when he noticed that *Bacillus amylobacter* produces a crystalline substance from starch after the digestion (Crini, 2014). However, industrial-scale production of CD in pure form was performed only in 1984, attracting the attention of pharmaceutical and food industries (Szejtli, 1998). CDs belong to the family of cage molecules; that is, the core of their structure is composed of a dimensionally stable hydrophobic cavity that can trap or encapsulate other molecules. To date, CDs are widely used in different areas such as pharmaceuticals, drug delivery systems, cosmetics, food and chemical industries (Carneiro et al., 2019). They can be found in commercially available medications, including tablets, eye drops and ointments (Loftsson and Brewster, 2010). There are above 40 products or formulations containing various CDs, especially β -CD and its derivatives such as sulfobutyl ether of β -cyclodextrin or 2-hydroxypropyl- β -cyclodextrin (HP- β -CD), which are currently used in at least six FDA-approved products (four for sulfobutyl ether of β -cyclodextrin and two for HP- β -CD) (Gidwani and Vyas, 2015). Nowadays, a broad spectrum of CDs containing materials with versatile supramolecular architectures (nanoparticles, nanosponges, nanomicelles, nanovesicles, etc.) has been synthesized to assemble functional platforms for

drug delivery (Duchêne, 2011). Also, CDs have been recently proposed as a perspective nanoplatform for the delivery of PSs (Ben Mihoub et al., 2018; Kryjewski et al., 2015).

Structure and derivatives

CDs are cyclic oligosaccharides, formed by six α -cyclodextrin (α -CD), seven β -cyclodextrin (β -CD), eight γ -cyclodextrin (γ -CD) D-glucopyranose units linked by α -(1,4) bonds (Table 3.1). It worth noting that the formation of CDs with fewer than 6 units cannot be performed due to steric hindrances while the higher CDs homologs with 9 or more glucose units are very difficult to purify (Challa et al., 2005). Generally, the cavity size of α -CD is insufficient for many drugs and γ -CD is expensive, while β -CD is affordable and has cavity size suitable for the widest range of drugs. Thus, β -CD has been more widely used in pharmaceutical applications than other native CDs (Rajewski and Stella, 1996).

Table 3.1 General CD structures (Ben Mihoub et al., 2018; Stella and He, 2008)



Cyclodextrin	Abbreviation	R	DS*	n**	d, Å
α -cyclodextrin	α -CD	H	–	4	4.7-5.3
β -cyclodextrin	β -CD	H	–	5	6.0-6.5
2-hydroxypropyl- β -cyclodextrin	HP- β -CD	CH ₂ (CHOH)CH ₃ or H	3.5-5.5	5	6.0-6.5
randomly methylated β -cyclodextrin	Me- β -CD	CH ₃ or H	11-14	5	6.0-6.5
heptakis(2,3,6-tri-O-methyl)- β -cyclodextrin	TM- β -CD	CH ₃	21	5	6.0-6.5
γ -cyclodextrin	γ -CD	H	–	6	7.5-8.3

* Degree of substitution; ** n+2, number of glucopyranoside units

CDs exhibit the shape of a truncated cone due to the chair conformation of the D-glucopyranose units. Free hydroxyls are on the outside of the CDs, while apolar C₃ and C₅ hydrogens are located in the cavity of CDs (Del Valle, 2004). As result CD molecules have a hydrophilic outside (logP is between (–13) and (–17)), and apolar cavity, which provides a hydrophobic matrix comparable to 60–70% of aqueous ethanol solution (Connors, 1997; Loftsson and Brewster, 2013). The increase in the number of glucopyranose units results in the enlargement of the hydrophobic cavity (Table 3.1). Despite the high hydrophilicity of CD's outer surface, the solubility in water could vary from 18 mg/ml for β -CD to 250 mg/ml for γ -

CD (Duchêne, 2011). The relatively low water solubility of CDs, especially of β -CD, significantly reduces their applicability. CDs are chemically stable under neutral and basic conditions in aqueous solutions (Frömming and Szejtli, 1994) and are quite resistant to light within the ultraviolet-visible spectrum and infrared ranges (Loftsson and Brewster, 1996).

To overcome these problems and extend the physicochemical properties and inclusion capacity of parent CDs, chemically modified CD derivatives were produced by aminations, esterifications or etherifications of primary and secondary hydroxyl groups of the CDs (Szente, 1999). It should be however noted, that the location of substituted groups could vary at different (2, 3 or 6) positions on the parent CD molecule (Blanchard and Proniuk, 1999). The degree of substitution (DS) is defined as the average number of substituents per CD molecule (Table 3.1). Thus, the methylated β -CDs (Me- β -CD, TM- β -CD) possess the water solubility of > 500 mg/ml and hydroxypropyl derivative more than 600 mg/ml. The modification of substitutions changes the hydrophobic cavity volume and can improve solubility, physical and microbiological stability. Such high versatility of CD structure helps to select an optimal CD for each specific drug depending on the size of the guest molecules or its side substituents (Szente and Fenyvesi, 2017). *In fine*, it reduces parenteral toxicity and may help to control the chemical activity of guest molecules (Challa et al., 2005; Davis and Brewster, 2004).

Complex formation

The presence of a hydrophobic interior cavity allows the formation of inclusion host-guest complexes with an extensive range of solid, liquid and gaseous compounds (Del Valle, 2004; Laza-Knoerr et al., 2010; Vyas et al., 2008). There are two key factors influencing the ability of CDs to form an inclusion complex with a guest molecule, namely steric and thermodynamic. Thus, the main quantitative parameters describing the mechanism of formation of the inclusion complexes are the stoichiometry and binding constants. From the steric point of view, the formation of the complex is a dimensional fit between the host cavity and guest molecule (Muñoz-Botella et al., 1995). The stoichiometry displays the number of molecules involved in the formation of the complex and determines the binding model, while the value of the binding constant reflects the degree of affinity between the complexants (Thordarson, 2011). The stoichiometry of the complex varies depending on the combination of CD-drug. Depending on their respective size, one CD molecule can bind more than one drug molecule, as a drug molecule may form complexes with several CD molecules (Figure 3.3). The most common stoichiometry among them is 1:1, but others like 1:2, 2:1, 2:2 can also be encountered (Szejtli, 1998). It worth noting that inclusion complexation with CDs is a reversible process (dynamic equilibrium), i.e., each molecule can dissociate from the

complex. Thus, often, the system with the high stoichiometric ratio is the mixture of the complexes with simple stoichiometry (Thordarson, 2011).

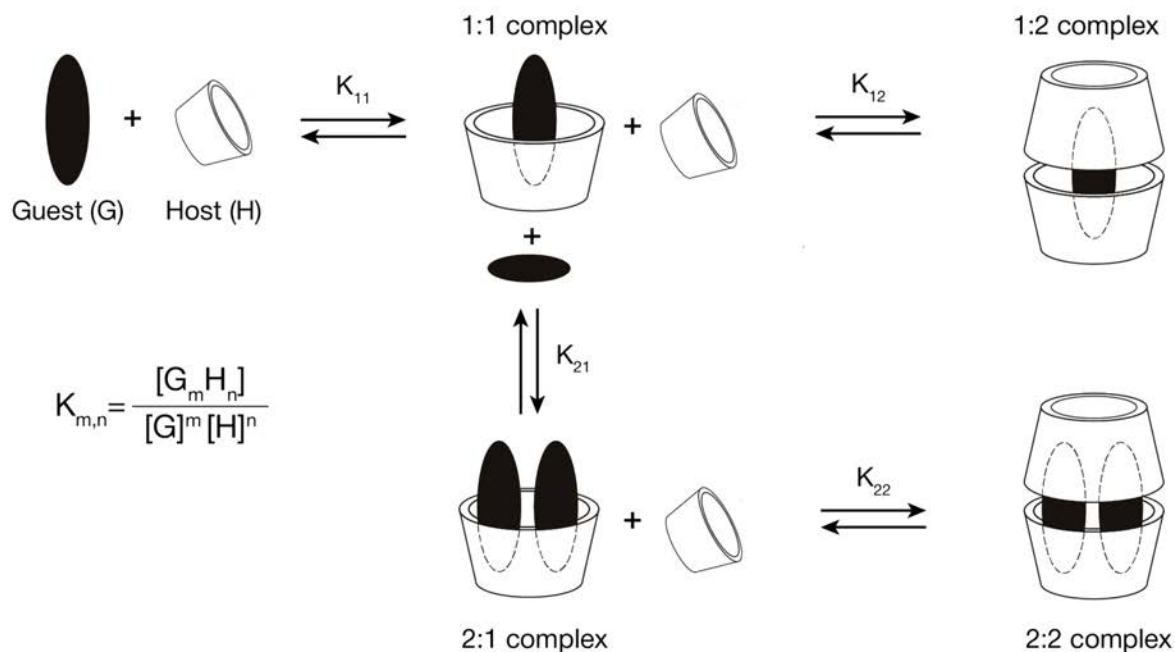


Figure 3.2 Typical supramolecular equilibria of inclusion complexes with 1:1, 1:2, 2:1 and 2:2 stoichiometries.

$K_{m,n}$ - association constant (K) of the guest-host complex with $m:n$ stoichiometry, $[G]$ – concentration of free guest molecules, $[H]$ – concentration of free host molecules, $[G_m H_n]$ – concentration of $m:n$ complexes.

Concerning the thermodynamic of complexation, the formation of inclusion complex is accomplished by the intermolecular interaction between CDs (host molecule) and guest molecule, which is driven by non-covalent interactions, including van der Waals, hydrophobic, electrostatic and charge transfer interactions, metal coordination, hydrogen bonding and steric effects (Rekharsky and Inoue, 1998). It is crucial that no covalent bonds are broken or formed during the formation of the inclusion complex (Schneiderman and Stalcup, 2000). In aqueous solutions, the inclusion of the (dehydrated) guest into the non-polar cavity of the CD is accompanied by the water release from the CD cavity and subsequent penetration of the guest molecule wholly or partly into the central cavity of the CDs (Song et al., 2009). Moreover, the conformational changes or strain release of the cyclodextrin molecule upon complexation also contributes in the formation of inclusion complex (Saenger, 1980). It is worth noting that the efficiency of the formation of inclusion complexes is determined by many factors, including temperature, solvents composition, amount of water (the degree of complexes dilution), complexation techniques. Ionization of the guest, salt formation, formation of metal complexes, application of supercritical fluids and addition of organic co-solvents to the drug/CDs aqueous solution will, if the conditions are

correct, lead to enhanced complexation efficiency (e.g., enhanced solubility) (Arun R. et al., 2008; Loftsson and Duchene, 2007; Van Hees et al., 1999). In addition, CDs are able to form non-inclusion complexes and complex aggregates (Loftsson et al., 2004)

In fine, the quantitative analysis of the intermolecular interactions of interest is one of the fundamental issues in supramolecular chemistry. To measure the efficiency of binding, supramolecular titration experiments were performed, providing the data for the estimation of the binding (association) constant values (Thordarson, 2011). The thermodynamic association (binding) constant (K) is related to the kinetics of the particular system, hence $K = k_1/k_{-1}$, with the k_1 and k_{-1} as forward (on) and backward (off) rate constants for the complex equilibria.

Traditionally, there are different methods of drug/CD complex preparation such as co-precipitation, kneading, spray drying, freeze-drying, solvent evaporation, or saturated aqueous solution methods (Gharib et al., 2015):

- *Complex preparation in the aqueous phase (co-precipitation)*: CD is dissolved in an aqueous phase and the drug is then added. Water-soluble inclusion complexes are formed after stirring the mixture for a specific period of time at a specific temperature.
- *Kneading*: CD and aqueous solution are mixed in a mortar to make a homogenous paste; the drug is then added slowly, while grinding, to dissolve the drug. Then, the mixture was ground with an appropriate quantity of water added to maintain a suitable consistency.
- *Co-evaporation (solvent evaporation method)*: mixing of the organic phase containing drug and an aqueous solution of CD by stirring to achieve molecular dispersion. The resulting suspension is followed by evaporation of the solvent under vacuum until dried mass obtained.
- *Spray drying*: mixing of the drug in an organic solution (ethanol) with an aqueous solution of CD at 1:1 molar ratio. The resulting mixture is then stirred at room temperature to attain equilibrium followed by removing the solvent using spray drying.
- *Freeze-drying (lyophilization)*: the drug and CD at 1:1 molar ratio are either dissolved in ethanol or water respectively or both in the aqueous phase. The resulted solution is stirred for a specific time at a certain temperature and then filtered, frozen and lyophilized under reduced pressure.

The fate of inclusion complexes in vivo

The inclusion complexes can be administered through different routes such as transdermal, ophthalmic, nasal, oral, intravenous, etc. (Shimpi et al., 2005). Pharmacokinetics of CDs and their excretion from the body will be defined *inter alia* by route

of administration. Concerning parenteral route of CD's administration, CDs are quickly eliminated from systemic circulation and more than 90% of the administrated CD are renally excreted intact (Stella and He, 2008). In addition, CDs exhibit a small volume of distribution in animal models or humans, indicating the preferable CD distribution in the extracellular compartments without involving deep compartments or storage pools (Stella and He, 2008). Although cyclodextrin complexes enable lipophilic drugs to be administered in much greater concentrations than in their free form, on injection, these complexes will rapidly dissociate depending to some extent on their affinity constants (McCormack and Gregoriadis, 1994). Dissociation occurs on dilution by the plasma and extracellular fluids (Stella et al., 1999). In addition to dilution, drug release mechanisms involve: (i) drug-protein binding causing a decrease in free drug concentration, (ii) competitive displacement by endogenous and exogenous molecules (i.e. cholesterol), (iii) and accumulation of the drug into tissues, which are not accessible by CDs (Stella et al., 1999). According to that, the behavior of the drug co-administrated with CDs is determined by the CD affinity to the drug molecule. Thus, the pharmacokinetics of the drugs, which exhibit binding constant values $K > 10^5 \text{ M}^{-1}$, can be altered by CDs (Stella and He, 2008). Thus, the dissociated drug will be eliminated from blood and tissues irrespective of its carrier and any remaining complexed drug will reach the kidneys only. Nevertheless, the methylation of the β -CD core increases CD's affinity for certain drugs as well as for the components of cellular membranes, resulting to a larger volume of distribution ($VD \approx 2.5 \text{ L/kg}$) and longer plasma half-life ($t_{1/2} \approx 7\text{h}$) in animal models compared to native β -CD ($VD \approx 0.2 \text{ L/kg}$; $t_{1/2} \approx 0.3\text{h}$) (Thompson, 1997). Moreover, the enhanced "CD-to-drug" affinity decreases the probability of the drug release upon the dilution providing stronger alteration of drug biodistribution and pharmacokinetics.

Biodistribution of CDs includes the following tissues: bladder, adrenal glands and liver with the highest concentration in the kidneys, while CD concentration in lungs and muscles is almost undetectable (Antlsperger and Schmid, 1996; De Bie et al., 1998; Gerloczy, A. et al., 1990; Kubota et al., 1996; Van Ommen et al., 2004). Concerning tumor-bearing animal models, the accumulation of CD in tumor tissue was observed in primary effusion non-Hodgkin lymphoma (Gotoh et al., 2014) and various carcinoma in xenograft tumor-bearing mice (Grosse et al., 1998; Onodera et al., 2013a).

To date, there are a considerable number of publications, including a detailed review of the toxicological status of CDs and their biological activity (Antlsperger and Schmid, 1996; Arima et al., 2011; Gould and Scott, 2005; Irie and Uekama, 1997; Loftsson and Brewster, 2010; Mosher and Thompson, 2007; Thompson, 1997; Zidovetzki and Levitan, 2007). Generally, CD toxicity is related to the ability of CD to interact with membrane components such as cholesterol and lipids (Kilsdonk et al., 1995; Mohammad et al., 2014; Zidovetzki and

Levitan, 2007), resulting in the increase of membrane fluidity and induction of membrane invagination through a loss of bending resistance and as such causing cell lysis (Challa et al., 2005). Since kidneys are the main absorption site of CDs in the body, the renal toxicity was demonstrated, especially for β -CD and its methylated derivatives (Frank et al., 1976; Irie and Uekama, 1997; Thompson, 1997). Nevertheless, it worth noting that the co-administration of CDs with drugs decreases toxicological effects of both substances (Arima et al., 2011; Mosher and Thompson, 2007).

In conclusion, CDs represent the example of nanocages imparting useful features to particles drug delivery system. Due to the ability to encapsulate hydrophobic drugs, i.e., the formation of CD-drug inclusion complexes, CDs are widely used in the medicinal and pharmaceutical applications, including the delivery of PSs in PDT (Ben Mihoub et al., 2018). Generally, complexation with CDs leads to an improvement of the water solubility, stability, bioavailability, release and under certain conditions, the permeability of the encapsulated drug. In the case of PS, CDs could particularly improve the photophysical characteristics of PSs (Lang et al., 2004), including the generation of ROS and even altering PS delivery to targets cells/tissues (Yankovsky et al., 2016). However, the application of CDs *in vivo* is limited due to the dilution effects and rapid renal excretion of CD from the blood. To overcome these limitations, drug/CD inclusion complexes could be encapsulated in liposomal vesicles in the DCL system.

3.3. DCL

DCL is an example of hybrid nanoplatform combining the advantages offered by CDs and liposomes (Chen et al., 2014). Traditionally, pre-formed drug/CD complexes are encapsulated into liposomal inner aqueous phase by different methods to obtain DCLs. DCLs are commonly prepared by means of thin-film hydration (Maestrelli et al., 2005; Piel et al., 2006), reverse-phase evaporation (Maestrelli et al., 2006), freeze and thaw (Ascenso et al., 2013), ethanol injection (Chen et al., 2007; Fatouros et al., 2001) and freeze-drying (Škalko et al., 1996) techniques (Figure 3.3). Generally, DCL could be classified according to drug loading. Single loaded DCLs encapsulate the drug in the inner aqueous core of liposomes only in the form of CD inclusion complexes, while double-loaded DCLs are vesicles loaded with lipophilic drug both in its free form (in the lipophilic bilayer) and in CD-complexed form (in the aqueous phase) (Gharib et al., 2015).

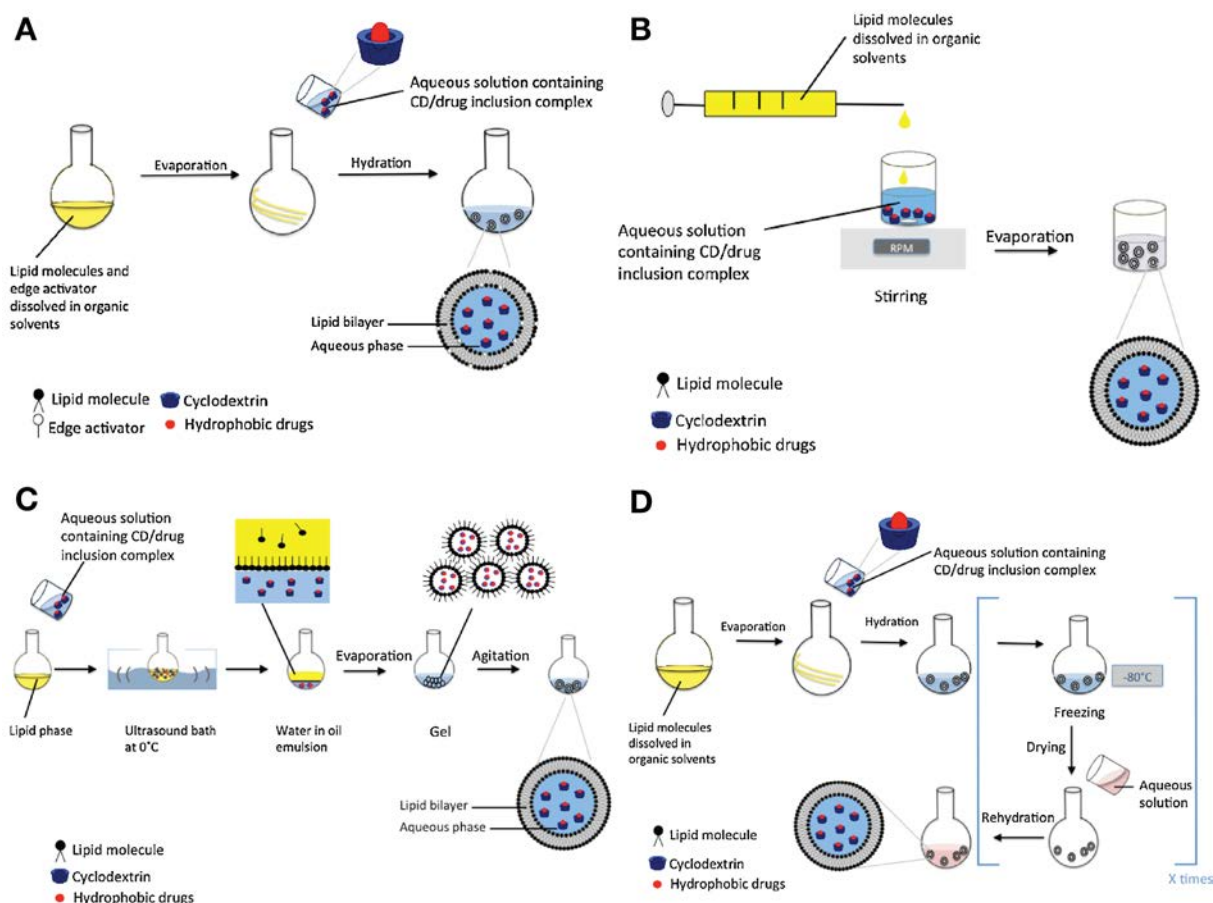


Figure 3.3 Preparation of DCL by (A) thin-film hydration, (B) ethanol injection, (C) reverse-phase evaporation and (D) dehydration-rehydration methods (Gharib et al., 2015)

Since many of the hydrophobic drugs are not lipophilic enough to be efficiently entrapped into the lipid bilayer without destabilization of the structural integrity of liposome, DCL was proposed as a strategy to increase encapsulation efficiency (EE) of hydrophobic drugs into liposomes (McCormack and Gregoriadis, 1994). The amount of hydrophobic drug incorporated into lipid bilayer is often limited in terms of drug to lipid ratio for small unilamellar vesicles. On the other hand, EE in the aqueous phase is limited by water-solubility of drug/CDs, preparation technique of DLCs and type of the used CD. It is well known that EE values of soluble drugs incorporated into the inner aqueous liposomal core are strongly limited by drug solubilization and are much lower than that of lipophilic molecules encapsulated into the lipid bilayer. Thus, for DCL, EE also depended on both the liposome preparation method and complex concentration in the aqueous phase and was ranged in the order MLV > LUV > SUV (Maestrelli et al., 2006). In the case of SUV, double-loaded DCL (DL-DCL) is supposed to be efficient for drug encapsulation, but drugs incorporated in the lipid bilayers rather than in the aqueous core of the liposomes are prone to more rapid release. It worth noting that EE could be also improved by the increase in CD concentration.

However, one should be careful, because CDs exhibit the destabilizing effect towards the liposomal membrane at high concentrations (Fatouros et al., 2001).

The presence of CDs affects liposome characteristics and membrane integrity depending on CD functionalization and liposome composition (Angelini et al., 2017; Hatzi et al., 2007; Maestrelli et al., 2010; Zappacosta et al., 2019). Generally, the addition of inclusion complexes increases the size of large liposomal vesicles (Jain et al., 2007; Maestrelli et al., 2006), while for small unilamellar vesicles the difference in size is negligible (Dhule et al., 2012; Maestrelli et al., 2006; Mendonça et al., 2012; Zappacosta et al., 2019). However, sometimes, the enhancement of the vesicle size during storage was observed (Lapenda et al., 2013; Rahman et al., 2012). A hypothesis could be that the high local CD concentration in the aqueous compartment of liposomes makes probable the replacing of drug molecule in CD cavity by lipids as a result of this reducing the stability of vesicles. In turn, the destabilization of the bilayer causes the changes in vesicles size and enables partial or complete leakage of drug content from DCL. The destructive effect of drug CD complexes on liposomes might be significantly different, depending on the affinity between CDs and drug molecules (Zappacosta et al., 2019). Thus, the extent of membrane destabilization due to CD is closely related to the amount of the free CD molecules which could interact with the membrane lipids (Puskás and Csempesz, 2007). To obtain stable DCL, the CDs should have a higher affinity for drug molecules compared with liposomal membrane lipids.

Compared to drug CD complexes, administration of DCLs could serve as a better way to control the action of a wide range of therapeutic agents. DCLs presented more prolonged release profiles compared with both liposomes and CDs. The encapsulation of drug CD complexes into the inner aqueous core of liposomes could result in a modulation of the *in vitro* kinetics of release of drug molecules due to the additional barriers to the diffusion of a drug (Jain et al., 2007). Since CD was found to be membrane impermeable (Joguparthi and Anderson, 2008; Zappacosta et al., 2019), the release of the drug should include the crossing of the lipid bilayer barrier (Chen et al., 2007). Thus, the rate of drug release is depending on various factors such as CD type (Fatouros et al., 2001; Piel et al., 2006), size and lamellarity of liposomes (Maestrelli et al., 2006) and lipid content (i.e. deformable liposomes) (Gillet et al., 2009; Jain et al., 2007).

At the same time, intravenously administrated DCLs will interact with plasma proteins and blood cells, resulting in the destabilization of liposomes and release of the drug in the form of CD inclusion complexes. In this case, the drug released not in a free form but in the CD inclusion complex which is ready to transport it to the target site. According to the literature data, encapsulation of drug CD complexes into liposomes results in a slow release profile *in vitro*, therefore, the systematic circulation time of the drug is prolonged (Arima et al.,

2011; Chen et al., 2007; Wang et al., 2011). Moreover, compared to drug CD complexes, administration of DCLs could be a more suitable way to control the biodistribution and excretion routes of various therapeutic agents (Agashe et al., 2011; McCormack and Gregoriadis, 1998). *In fine*, the application of DCLs provides the benefits in the delivery of anticancer drugs resulting in (i) better antiproliferative activity than free anticancer drugs (EF24 and LPSF/AC04) *in vitro* (Agashe et al., 2011; Mendonça et al., 2012); (ii) increase in DOX plasma-half time *in vivo* (Maestrelli et al., 2005); (iii) decrease in systemic toxicity *in vivo* of trans dehydrocrotonin (Lapenda et al., 2013) and vincristine (Cui et al., 2011).

To date, the DCL system has been applied to encapsulate a variety of lipophilic drugs including anti-inflammatory drugs such as ketoprofen (Maestrelli et al., 2005, 2006), celecoxib (Jain et al., 2007), prednisolone (Fatouros et al., 2001), indomethacin (Chen et al., 2007), betamethasone (Gillet et al., 2009; Piel et al., 2006), oxaprozin (Mennini et al., 2016) and ibuprofen (Angelini et al., 2017); anesthetic drugs as benzocaine, butamben (Maestrelli et al., 2010) and prilocaine (Bragagni et al., 2010); Ca²⁺channel blocker drugs as nifedipine (Škalko et al., 1996); immunosuppressive drugs, e.g. tacrolimus (Zhu et al., 2013); antimicrobial agents as trans-anethole (Gharib et al., 2016); and anti-cancer drugs such as β -lapachone (Cavalcanti et al., 2011), tretinoin (Ascenso et al., 2013), doxorubicin (Arima et al., 2006), curcumin (Dhule et al., 2012), vincristine (Cui et al., 2011), paclitaxel (Bhatt et al., 2018), including PDT agent hypericin tetraether (Plenagl et al., 2019). This demonstrates the interest of this nanoformulation as an advanced strategy in the delivery of poorly soluble drugs.

OBJECTIVES

OBJECTIVES

The general objective of this study is an improvement of mTHPC delivery to the target tumor tissue with mTHPC-loaded cyclodextrin-based liposomal nanoparticles. The development of drug-in-cyclodextrin-in-liposome nanoparticles also includes the investigation of complexation processes of drug with CDs, development of detection methods for monitoring and control of these processes in complex systems and study of the inclusion complexes behavior in tumor tissues.

The objective of this work was to explore the cyclodextrin-based liposomal nanoparticles for effective delivery of mTHPC to target tumor tissue. For this purpose, the following studies were carried out:

- Study of inclusion complex formation between mTHPC and β -CD derivatives.
- Development of experimental techniques to control the distribution of mTHPC between β -CDs and lipid membranes
- Investigation of the behavior of mTHPC loaded inclusion complexes in 3D *in vitro* tumor tissue model

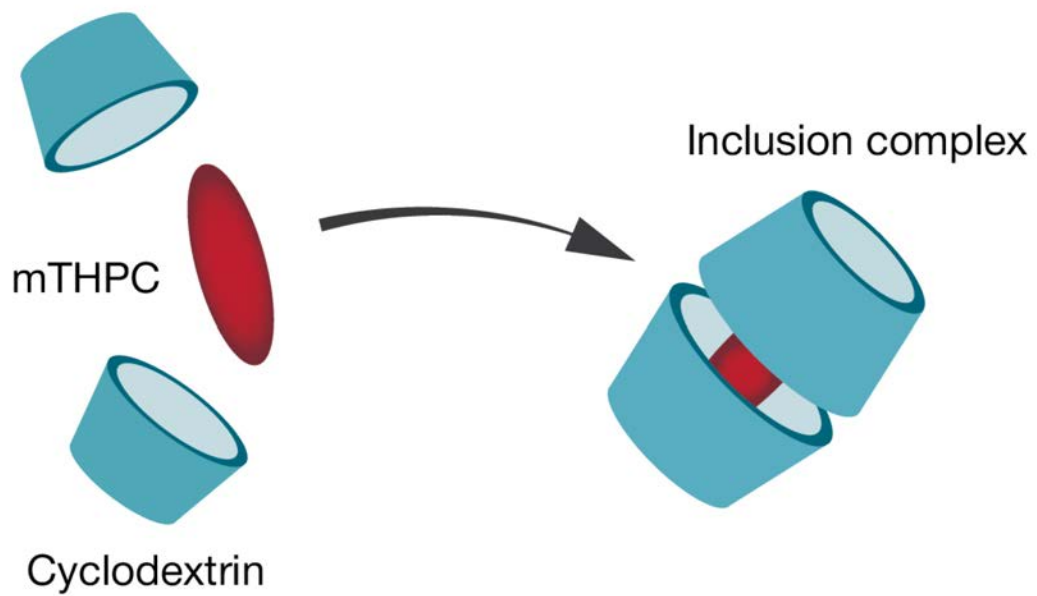
These tasks are addressed in the first research section (Chapter II).

- Optimization of cyclodextrin-based liposomal nanoparticles loaded with mTHPC
- Physical-chemical and photophysical characterization of drug-in-cyclodextrin-in-liposome formulation of mTHPC
- Study of the behavior of drug-in-cyclodextrin-in-liposome formulation of mTHPC in 2D and 3D *in vitro* tumor cell cultures
- Study of the mechanisms of mTHPC-CL photoinduced cell death in cultured cells *in vitro*
- Study of PDT efficiency of mTHPC-CL in pre-clinical xenografted mice *in vivo* model.

These points are addressed in the second research section (Chapter III).

CHAPTER II.

CD INCLUSION COMPLEXES



4. Characterization of inclusion complex formation

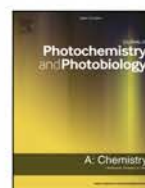
The first part of the results on the interaction of mTHPC with β -CDs is described in the article "Evaluation of temoporfin affinity to β -cyclodextrins assuming self-aggregation".

According to the literature data (Stella and He, 2008; Stella et al., 1999), the biological behavior of drug/ β -CDs complexes strongly depends on the binding affinity of the drug to β -CDs. Thus, we analyzed the processes of inclusion complex formation between mTHPC and three β -CD derivatives (hydroxypropyl-, methyl- and trimethyl- β -CD). Using several spectroscopic techniques and molecular dynamics simulations we experimentally assessed the binding affinity of β -CD derivatives to mTHPC and refined the value of the binding constant. Parameters of binding isotherms revealed that mTHPC strongly interacts with β -CD derivatives, forming 1:2 inclusion complexes in aqueous solution. We demonstrated that apparent binding constants strongly depend on mTHPC concentration due to the porphyrin self-aggregation. The accurate assumption of mTHPC self-aggregation effects in our model resulted in significantly higher values than those previously reported.



Contents lists available at ScienceDirect

Journal of Photochemistry & Photobiology A: Chemistry

journal homepage: www.elsevier.com/locate/jphotochem

Evaluation of temoporfin affinity to β -cyclodextrins assuming self-aggregation

I. Yakavets^{a,b,c}, H.-P. Lassalle^{b,c}, I. Yankovsky^a, F. Ingrosso^d, A. Monari^d, L. Bezdetnaya^{b,c}, V. Zorin^{a,c,*}

^a Laboratory of Biophysics and Biotechnology, Physics Faculty, Belarusian State University, Minsk, Belarus

^b Université de Lorraine, CNRS, CRAN, UMR 7039, F-54000 Nancy, France

^c Université de Lorraine, Institut de Cancérologie de Lorraine, F-54000, France

^d Université de Lorraine, CNRS, LPCT, UMR 7019, F-54000 Nancy, France

^e International Sakharov Environmental Institute, Minsk, Belarus



ARTICLE INFO

Keywords:

Supramolecular chemistry
 β -Cyclodextrins
 mTHPC
 Binding constants
 Aggregation
 Circular dichroism

ABSTRACT

The interaction between the potent photosensitizer *meta*-tetrakis(3-hydroxyphenyl)chlorin (temoporfin, mTHPC) and a series of β -cyclodextrins (β -CDs) was investigated using spectroscopic analysis and molecular dynamics simulations. The possibility of improving its poor aqueous solubility with β -CDs was estimated by measuring both equilibrium solubility and association constants. Parameters of binding isotherms revealed that mTHPC strongly interacts with β -CD derivatives, forming 1:2 inclusion complexes in aqueous solution. We demonstrated that apparent binding constants strongly depend on mTHPC concentration due to the porphyrin self-aggregation. The estimated "correct" binding constants demonstrated that completely methylated β -CD exhibits the highest affinity ($K = 1.1 \times 10^7 \text{ M}^{-1}$) as compared to randomly methylated β -CD ($K = 7.1 \times 10^5 \text{ M}^{-1}$) and 2-hydroxypropyl substituted β -CD ($K = 1.7 \times 10^5 \text{ M}^{-1}$). *In fine*, our results indicate that TM- β -CD should be considered as a potent vector for mTHPC targeted delivery.

1. Introduction

Meta-tetrakis(3-hydroxyphenyl)chlorin (mTHPC, temoporfin) is one of the most potent clinically approved photosensitizer (PS) for the photodynamic therapy (PDT) of head and neck cancers [1,2]. mTHPC molecules are highly hydrophobic and are prone to aggregation in biological media, resulting in decreased photodynamic efficacy, moderate selectivity and prolonged skin photosensitivity [1,3]. Various attempts are being made to use special drug delivery and formulations of mTHPC in order to prevent aggregation and improve its pharmacokinetic properties. The use of several nanosized systems for mTHPC delivery (liposomes, polymeric vesicles, dendrimers etc.) demonstrated a significant improvement in its bioavailability, biodistribution and photosensitizing activity.

Cyclic oligosaccharides such as β -cyclodextrins (β -CDs) are promising delivery systems for different nonpolar drugs including aryl-substituted porphyrin PSs [4–7]. It was reported, that β -CDs readily interact with mTHPC incorporating drug molecule or its part in the

inner hydrophobic cavity [8]. The formation of inclusion complexes increases mTHPC solubilization and recovers its photophysical properties. According to our recent study, β -CDs significantly modify *in vitro* and *in vivo* biodistribution of mTHPC, in particular inhibiting mTHPC aggregation and hence accelerating PS transportation by serum proteins, ultimately increasing PS accumulation at the target sites [7,9]. However, despite the growing amount of information on the interaction of porphyrins and other dyes with β -CDs, a detailed study unravelling the molecular bases of the host-guest complex formation in the context of PS pharmacokinetics alteration is still missing. It is obvious that the ability of cyclodextrins to favorably alter PS biodistribution is mainly determined by the values of their association constants [7,10,11].

The complex formation of mTHPC with 2-hydroxypropyl- β -cyclodextrin (HP- β -CD) and random methyl- β -cyclodextrin (Me- β -CD) was reported earlier [8,12,13], however the results were rather contradictory. The interaction of heptakis(2,3,6-tri-*O*-methyl)- β -cyclodextrin (TM- β -CD) with mTHPC was not studied yet, still it would be of big interest since as was pointed out by Kano et al. [14], a highly

* Corresponding author at: Laboratory of Biophysics and Biotechnology, Physics Faculty, Belarusian State University, 4 Nezavisimosti Ave, 220030, Minsk, Belarus.

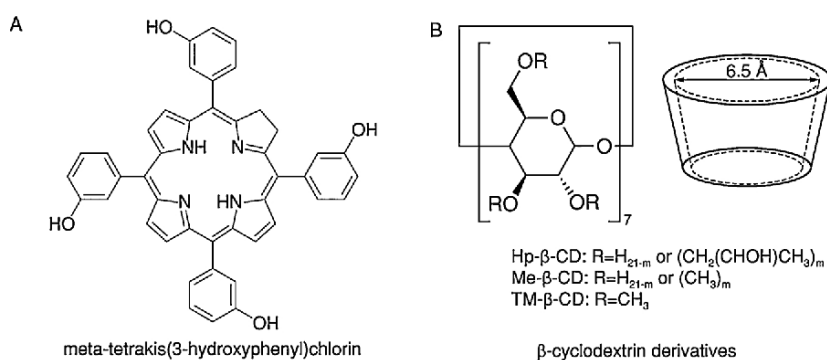
E-mail addresses: yakavetsiv@bsu.by, ilya.yakavets@univ-lorraine.fr, i.yakavets@nancy.unicancer.fr (I. Yakavets), henri-pierre.lassalle@univ-lorraine.fr, h.lassalle@nancy.unicancer.fr (H.-P. Lassalle), yankovsky@bsu.by (I. Yankovsky), francesca.ingrosso@univ-lorraine.fr (F. Ingrosso), antonio.monari@univ-lorraine.fr (A. Monari), lina.bolotina@univ-lorraine.fr, l.bolotina@nancy.unicancer.fr (L. Bezdetnaya), zorin@bsu.by (V. Zorin).

<https://doi.org/10.1016/j.jphotochem.2018.07.046>

Received 14 May 2018; Received in revised form 13 July 2018; Accepted 31 July 2018

Available online 01 August 2018

1010-6030/ © 2018 Elsevier B.V. All rights reserved.



Scheme 1. Molecular structures of (A) mTHPC and (B) β-CD derivatives. The degree of substitution (DS) is given by the *m* values, reported in the experimental section.

hydrophobic cavity of complete methylated β-CD could enhance the affinity to aryl-porphyrins. In this respect, the determination of exact binding constants is of fundamental value allowing the rationalization and prediction of β-CDs effects on drug distribution in complex biological systems.

The present work aims to estimate the association constants between mTHPC and several β-CD derivatives (Scheme 1) taking into account the impact of physical-chemical factors including porphyrins aggregation. We used Induced Circular Dichroism (ICD) and fluorescence techniques to assess the formation of the complexes between mTHPC and β-CDs, with the successive analysis of the results by a rather complex nonlinear mathematical model.

2. Material and methods

2.1. Materials

The photosensitizer mTHPC was kindly provided by biolitec research GmbH (Jena, Germany) with the purity > 99%. The cyclodextrins Me-β-CD (purity > 98%, DS = 11–14, average M.W. 1310 Da), TM-β-CD (purity > 98%, M.W. 1430 Da) and Hp-β-CD (purity > 98%, DS = 3.5–5.5, average M.W. 1380 Da) were purchased from AraChem (Tilburg, the Netherlands). β-CDs in powder were weighted and then dissolved in Dulbecco's phosphate-buffered saline (DPBS) (pH 7.4) at 4 °C at the final concentration of 20 mM using molar weight provided by the supplier. mTHPC stock solution (1 mM) was prepared in absolute ethanol (99.6%) and was kept at 4 °C in the dark. mTHPC concentration in the solution and the extinction coefficients were estimated by means of a spectrophotometric method using molar extinction coefficient of 30,000 M⁻¹ cm⁻¹ at 650 nm in ethanol [15].

Inclusion complexes between β-CDs and mTHPC were formed using the co-precipitation method reported in details in [16]. Briefly, stock ethanol solution of mTHPC (1 mM) was added to β-CDs dissolved in DPBS (pH 7.4) at the required concentrations. The final content of ethanol in the mTHPC/β-CD solutions did not exceed 0.5%. The solution was thoroughly mixed for 15 min under magnetic stirring and was recorded after at least 2 h of incubation.

2.2. Spectroscopic measurements

The absorption spectra were measured on Solar PV1251 (Solar, Belarus) spectrophotometer using 1 cm optical path quartz cuvettes. Fluorescent measurements were performed on Solar CM 2303 (Solar, Belarus) fluorescence spectrometer equipped with thermostat cuvette compartment and magnetic stirring. ICD spectra were recorded on a Chirascan-plus qCD (Applied Photophysics Limited, Surrey, United Kingdom) also equipped with thermostat cuvette compartment and magnetic stirring. The error in the wavelength measurements was estimated as ± 1 nm. All spectroscopic measurements were carried out

in triplicate at room temperature (23–25 °C). Optical density of all samples did not exceed 0.4 a.u.

The fluorescence quantum yields of mTHPC in complexes were determined using mTHPC solution in methanol, regarded as standard (fluorescence quantum yield is equal to 0.089 [15]). The fluorescence was excited at 416 nm. The absolute error in quantum yields values was estimated as ± 0.01.

2.3. Mathematical fitting

The binding isotherms were fitted with a MATLAB software (The Math Works, USA), using mathematical binding models (Eqs. (1)–(4)), which was previously described by Thordarson [17]. For optimization of the fit conditions, iterations were carried out until the difference in the value of chi-square for successive iterations did not exceed 5% of the previous value. To estimate the values beyond the original observation range, the mathematical extrapolation was used. The curves were mathematically extrapolated on the basis of experimental data in the range of mTHPC concentration 10 nM–3 μM using cubic spline algorithm (spline) as a basic function of Origin software (OriginLab, USA). The “correct” values of *K*₁₁ binding constants were calculated at 0.1 nM.

$$\Delta Y = (Y_{\Delta 0} + Y_{\Delta 1:1} K_{11} [\text{CD}]) / (1 + K_{11} [\text{CD}]) \quad (1)$$

Mathematical model for one-step 1:1 binding

$$\Delta Y = (Y_{\Delta 0} + Y_{\Delta 1:2} K_{12} [\text{CD}]^2) / (1 + K_{12} [\text{CD}]^2) \quad (2)$$

Mathematical model for one-step 1:2 binding

$$\Delta Y = (Y_{\Delta 0} + Y_{\Delta 1:1} K_{11} [\text{CD}] + Y_{\Delta 1:2} K_{12} [\text{CD}]^2) / (1 + K_{11} [\text{CD}] + K_{12} [\text{CD}]^2) \quad (3)$$

Mathematical model for two-step 1:2 binding

$$[\text{CD}]^2 (A) + [\text{CD}]^2 (B) + [\text{CD}] (C) + [\text{CD}]_0 = 0$$

With: $A = K_{11} K_{12}$
 $B = K_{11} (2K_{12} [\text{mTHPC}]_0 - K_{12} [\text{CD}]_0) + 1$
 $C = K_{11} ([\text{mTHPC}]_0 - [\text{CD}]_0) + 1 \quad (4)$

Expression for free guest concentration

Where Δ*Y* – measured signal; *Y*_{Δ0} – signal from mTHPC molecule; *Y*_{Δ1:1} – signal from 1:1 mTHPC/CD complex; *Y*_{Δ1:2} – signal from 1:2 mTHPC/CD complex; *K*₁₁ – binding constant of 1:1 mTHPC:CD complex; *K*₁₂ – binding constant of 1:2 mTHPC:CD complex; [CD] – concentration of free CD; [CD]₀ – total CD concentration; [mTHPC]₀ – total mTHPC concentration.

2.4. Molecular modeling

Molecular dynamics simulations were conducted using the sander

module of Amber14 [18]. mTHPC force field was specifically parameterized starting from the Generalized Amber Force Field (GAFF) approach, electrostatic point charges were obtained using the standard RESP procedure [19]. The q4md-CD force field developed by Cézard et al. was used for heptakis(2,3,6-tri-*O*-methyl)- β -cyclodextrin [20]. This potential was developed based on the GLYCAM04 parameters [21–23], modified in a consistent way to take into account substitution at the –OH groups of a native cyclodextrin.

Classical molecular dynamic simulations were performed at the constant pressure and temperature (NPT) ensemble ($T = 300$ K, $P = 1$ atm) for a 1:2 mTHPC:CD complex immersed in TIP3P water (about 18,000 molecules) [24]. The Amber14 default parameters were used for Andersen's temperature coupling scheme and Berendsen's barostat [25,26]. Periodic boundary conditions were used throughout the simulation, with long range electrostatics treated by means of the Particle Mesh Ewald (PME) expansion [27].

An equilibration along 500 ps in the NPT ensemble was performed, until reaching a box volume fluctuating around a value corresponding to a cubic box length of 80 \AA ($\pm 8 \text{ \AA}$) and constant energy. We then carried out a simulation run for a total time of 10 ns using a time step of 1 fs. Coordinates were saved every ps for data analysis.

Absorption spectrum was obtained as the convolution of 100 snapshots randomly taken from the MD trajectory. A hybrid QM/MM approach was used with the QM partition constituted by the mTHPC chromophore while CD and water were represented at MM level. Excited state energies were calculated at Time Dependent Density Functional Theory (TD-DFT) level using B3LYP as exchange-correlation functional and 6-31+G* basis set, a total of 20 excited states was calculated for each snapshot. QM/MM calculations have been performed by Terachem software interfaced with Amber [28].

3. Results

3.1. Spectral characteristics of mTHPC/ β -CD complexes

The absorption and fluorescence spectra of mTHPC in buffer solution alone and in the presence of β -CDs (Hp-, Me-, TM- β -CD) are shown in Figs. 1 and 2. The significant spectral changes upon the addition of β -CDs may be ascribed to mTHPC monomerization due to the formation of the inclusion complex. The modification of mTHPC spectral properties appeared to be β -CD concentration-dependent. At the highest β -CD concentration (2 mM), no more modifications of mTHPC spectra

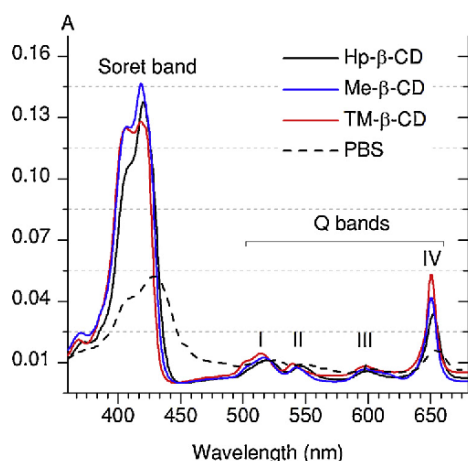


Fig. 1. Absorption spectra of mTHPC (1 μ M) in DPBS containing β -CD derivatives (2 mM): Hp- β -CD (black), Me- β -CD (blue) and TM- β -CD (red). The dotted line indicates mTHPC spectra in DPBS without β -CDs. (For interpretation of the references to colour in this figure legend, the reader is referred to the web version of this article.)

were observed, indicating the complete binding of mTHPC to β -CDs (100% mTHPC loading) (data not shown). Thus, mTHPC spectral characteristics at this concentration of β -CD could be directly related to the inherent features of inclusion complexes.

The main spectral variations of mTHPC observed due to the formation of the mTHPC/ β -CDs inclusion complexes include:

- slight changes in the position of Q_4 band maximums (shifts about 1–2 nm). The extinction coefficient of the Q_4 band significantly increases in the following order: Hp- β -CD ($34,700 \text{ M}^{-1} \text{ cm}^{-1}$) < Me- β -CD ($42,700 \text{ M}^{-1} \text{ cm}^{-1}$) < TM- β -CD ($54,200 \text{ M}^{-1} \text{ cm}^{-1}$);
- alterations in the shape of Soret band and the corresponding B bands in the fluorescence excitation spectra. The ratio between B_x and B_y shoulders increases from 0.78 for Hp- β -CD to 0.97 for TM- β -CD. A slight bathochromic shift (2 nm) of the Soret band was observed for mTHPC/Hp- β -CD complexes as compared with other β -CDs inclusion complexes;
- significant increase of the relative fluorescence quantum yield of mTHPC in TM- β -CD and Me- β -CD complexes, exceeding respectively 0.142 and 0.125 as compared with Hp- β -CD (0.095).

ICD is a widely used technique, complementary to absorption and emission spectroscopy, to characterize of the inclusion complexes formed by β -CDs. As shown in Fig. 3, the interaction of non-absorbing, chiral β -CDs, with the optically inactive mTHPC results in the occurrence of ICD signal in mTHPC visible spectral regions. This effect may hence be seen as the direct evidence of the formation of inclusion complexes between mTHPC and β -CDs. Further, as follows from Fig. 3, ICD spectra strongly depend on the type of the host β -CD moiety. In the case of Me- β -CD and Hp- β -CD inclusion complexes, the ICD spectrum of mTHPC consists of two positive maxima that correspond to B_x and Q_2 bands, respectively, and two negative bands assigned to B_y and Q_4 mTHPC electronic transitions. At the same time, mTHPC binding with TM- β -CD results in the occurrence of a strong negative ICD signal at B_y band position, while other ICD signals are globally much less intense. It should be noted that Q_1 and Q_3 mTHPC absorption bands do not exhibit ICD activity, probably due to their vibronic nature.

3.2. Inclusion complexes binding parameters

3.2.1. Stoichiometry

In order to provide a reasonable mathematical model describing the complex formation from a thermodynamic and kinetic point of view, and in particular to provide the binding constants, it is essential to know the inclusion complex stoichiometry. To determine the stoichiometry of the inclusion complexes, we applied Job's method of continuous variations [29]. In this case, the normalized mTHPC fluorescence intensity, which is directly related to the concentration of the complex, was measured and then plotted as a function of mTHPC molar fraction (Fig. 4). For all studied β -CDs, the maximum fluorescence intensity is detected at the mTHPC molar fraction of 0.30–0.35 indicating that the most probable mTHPC: β -CD stoichiometric ratio would be 1:2.

We performed classic molecular dynamics (MD) simulations of the 1:2 mTHPC:TM- β -CD complex to assess its persistence and evaluate the steric aspects related to its conformation (Fig. 5). Indeed, the 1:2 complex was stable all along the MD simulation experiencing very limited variation in the root mean square deviation compared to the starting structure. In addition, the distance between the centers of mass of TM- β -CD molecules stays close to 11.3 \AA during the MD simulation (Fig. 5D). As shown in Fig. 5(A–C) a tri-molecular 1:2 complex is needed to perfectly accommodate the hydrophobic mTHPC porphyrin moiety inside the TM- β -CD's core. Note also that this arrangement presents no particular steric clashes, while probably constraining the peripheral mTHPC phenyl groups rotation. In addition, the calculated hybrid quantum mechanics/molecular mechanics (QM/MM) absorption spectrum of the mTHPC/ β -CD complex also matches the

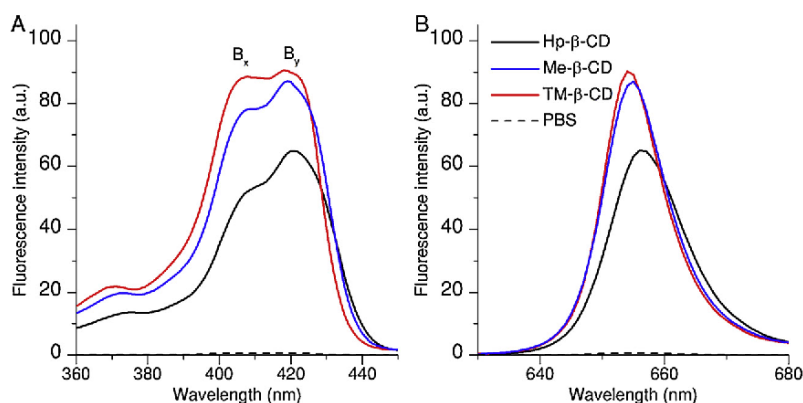


Fig. 2. Fluorescence excitation (A) and emission (B) spectra of mTHPC (1 μ M) in DPBS with β -CDs (2 mM): Hp- β -CD (black), Me- β -CD (blue) and TM- β -CD (red). The dotted lines indicate mTHPC spectra in DPBS without β -CDs. (For interpretation of the references to colour in this figure legend, the reader is referred to the web version of this article.)

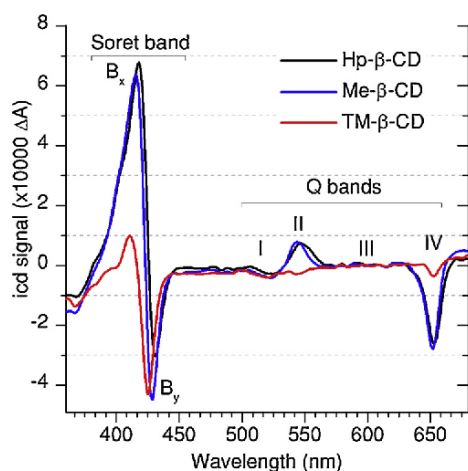


Fig. 3. Induced circular dichroism spectra of mTHPC (1 μ M) in DPBS containing β -CD derivatives (2 mM): Hp- β -CD (black), Me- β -CD (blue) and TM- β -CD (red). (For interpretation of the references to colour in this figure legend, the reader is referred to the web version of this article.)

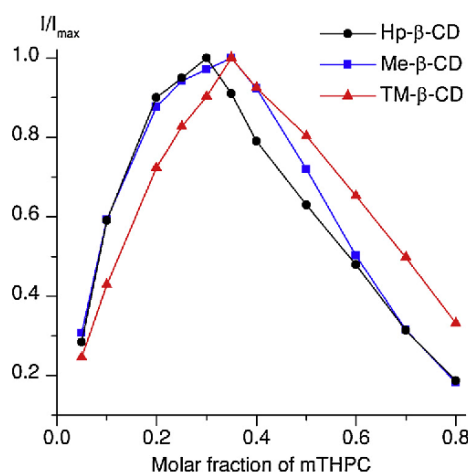


Fig. 4. Job's plots of mTHPC/ β -CD complexes in DPBS at fluorescence excitation 420 nm. mTHPC fluorescence were measured at 652 nm. The total ($C_{\beta\text{-CD}} + C_{\text{mTHPC}}$) concentration was 3 μ M. Molar mTHPC fraction is given by $X_{\text{mTHPC}} = C_{\text{mTHPC}} / (C_{\text{mTHPC}} + C_{\beta\text{-CD}})$.

experimental results with a reasonable accuracy, further confirming the nature of the complex (Fig. 5E).

3.2.2. Binding constants

Among numerous experimental techniques for the determination of binding constants, fluorescence or ICD, possess a high sensitivity to quantify the inclusion complex formation and hence allowing the determination of binding constant value with high accuracy. As an example, the variations of mTHPC fluorescence spectra in water solution upon the increase of β -CD concentration are presented in Fig. 6A. As was mentioned above, mTHPC fluorescence intensity is β -CD concentration-dependent and reaches its maximal values for Me- β -CD concentrations bigger than 0.1 mM. Titration curves, obtained for all studied β -CDs with mTHPC fluorescence at 652 nm ($\lambda_{\text{exc.}}$ at 420 nm), are presented in Fig. 6C. The comparison of the binding isotherms for different β -CD derivatives demonstrates that in order to achieve the same fraction of mTHPC/ β -CD complexes, one need to add 10 times less TM- β -CD than Hp- β -CD and 3 times less than Me- β -CD. This fact can obviously be related to the higher affinity of TM- β -CD to mTHPC compared with other β -CDs.

Similar results were obtained by means of ICD approach (Fig. 6B&D). To plot titration curves for ICD data, we determined the full amplitude of ICD signal as the ratio $\delta A = \Delta A_{\lambda_1} - \Delta A_{\lambda_2}$ to δA_{max} , where λ_1 and λ_2 were the wavelengths of ICD spectrum maxima for each mTHPC/ β -CDs sample. The comparison with fluorescence data showed that the shape and the position of binding isotherms are subjected to changes depending on the experimental technique. However, the affinity in the order TM- β -CD > Me- β -CD > Hp- β -CD persists for both experimental techniques.

To quantify the difference of β -CDs affinity to mTHPC, we performed a non-linear mathematical fitting analysis of the experimental isotherms using different models: one-step 1:1 and 1:2 models, two-step 1:2 model (Eqs. (1)–(3)). For calculations we used the assumptions that mTHPC in buffer solution is optically inactive and does not fluoresce ($Y_{\Delta 0} = 0$). For two-step 1:2 model, we suggested that the binding of the second β -CD molecule to mTHPC does not change the mTHPC fluorescence quantum yield and thus $Y_{\Delta 1:1} = 1$, $Y_{\Delta 1:2} = 1$, while binding of each β -CD molecule results in an equal effect on the ICD spectrum ($Y_{\Delta 1:1} = 0.5$, $Y_{\Delta 1:2} = 1$). Moreover, we considered the dependence of free β -CD on the concentration of “guest” (mTHPC) molecules (see experimental section; Eq. (4)), according to a previously described protocol [17]. To assess the appropriateness and robustness of our fitting, we considered the adjusted coefficient of determination (r^2).

According to our calculations, the best agreement is achieved when complex formation is considered as proceeding by a two-step association mechanism ($r^2 \geq 0.98$), compared with one-step 1:1 ($r^2 \leq 0.92$) and 1:2 ($r^2 \leq 0.96$) models. Indeed, such model accounts for the simultaneous presence of sufficient amount of both 1:1 as well as 1:2 complexes and hence allow better reproducing of experimental results

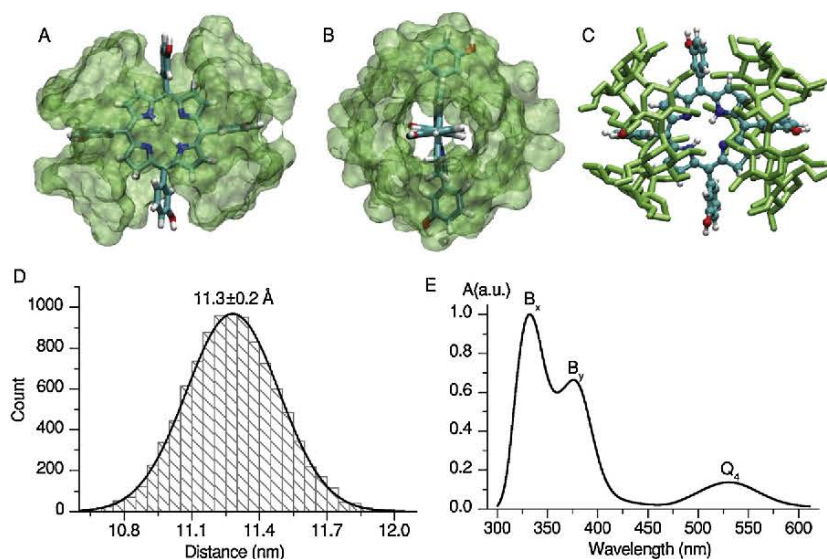


Fig. 5. Front (A) and side (B) views of representative snapshot of the mTHPC/TM- β -CD complex extracted from the MD simulation. mTHPC is represented in ball and sticks (A–C), while CD occupation is represented with its van der Waals surface (A, B). Panel (C) provides licorice representation of the complex. (D) Distribution of the distance between the centres of mass of two cyclodextrins in the complex with mTHPC as computed from molecular dynamics simulations. Panel (E) displays the calculated absorption spectrum of the inclusion complex.

(Scheme 2). The calculated association constants K_{11} correspond to the association with one β -CD and K_{12} represents the association with the second β -CD. For a quantitative comparison of β -CD affinity in the case of such stepwise association, the geometrical mean of K_{11} and K_{12} constants, $K = (K_{11} \times K_{12})^{1/2}$ was used. According to the fluorescence data, the obtained K values were $4.5 \times 10^4 \text{ M}^{-1}$, $3.0 \times 10^5 \text{ M}^{-1}$ and $5.6 \times 10^6 \text{ M}^{-1}$ for Hp-, Me- and TM- β -CD, respectively. On the contrary, when taking into account the apparent shift of ICD binding isotherms we obtain lower calculated K values ($2.8 \times 10^4 \text{ M}^{-1}$, $2.1 \times 10^5 \text{ M}^{-1}$ and $1.8 \times 10^6 \text{ M}^{-1}$ for Hp-, Me- and TM- β -CD,

respectively) as compared to the those obtained from fluorescence curves.

3.3. Influence of mTHPC aggregation on apparent binding constants

It is worth noting that mTHPC is a highly hydrophobic compound and that self-aggregation of mTHPC molecules (“guest” molecules) should be taken into account since it can affect the inclusion complexes association by decreasing the values of the apparent binding constants [30]. The impact of the aggregation on the estimation of mTHPC/ β -CDs

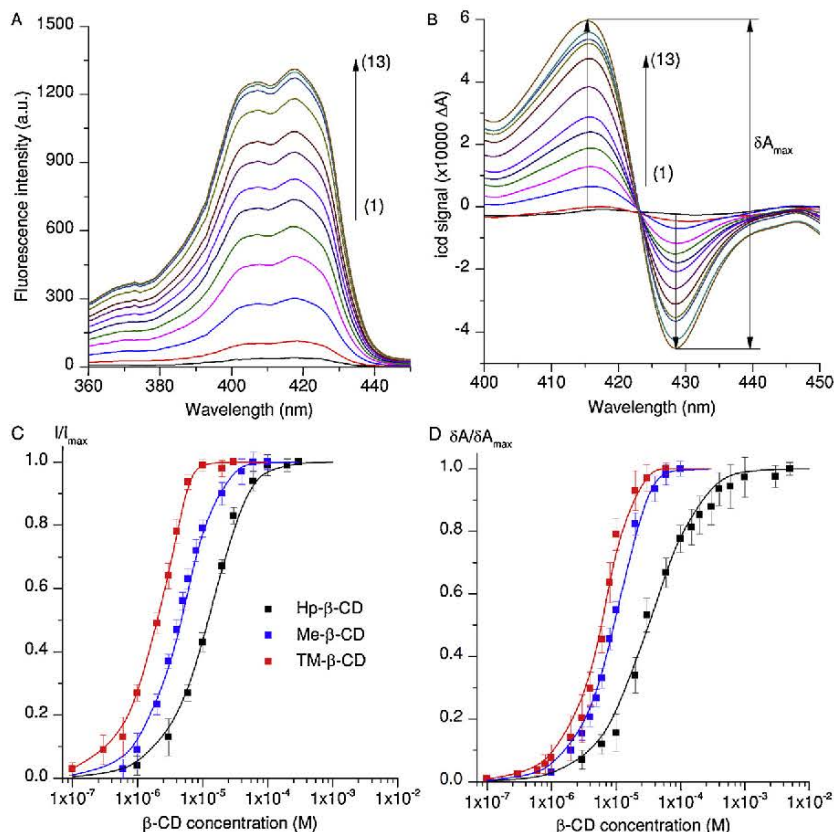
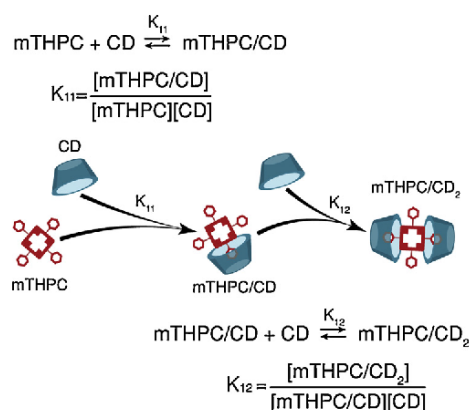


Fig. 6. (A) Fluorescence excitation and (B) ICD spectra of mTHPC ($3 \mu\text{M}$) in DPBS containing various amounts of Me- β -CD. Me- β -CD concentrations were: 1 – 0.6; 2 – 1; 3 – 2; 4 – 3; 5 – 4; 6 – 5; 7 – 6; 8 – 8; 9 – 10; 10 – 15; 11 – 20; 12 – 40; 13 – 100 μM . Arrows designate increasing concentration of Me- β -CD. mTHPC fluorescence was measured at 652 nm. Binding isotherms of $3 \mu\text{M}$ mTHPC upon titration by various β -CD derivatives in DPBS were obtained by (C) fluorescence and (D) ICD techniques. Black (Hp- β -CD), blue (Me- β -CD) and red (TM- β -CD) dots represent the experimental data, while the solid lines are the best fit to an equation for two-step 1:2 model. (For interpretation of the references to colour in this figure legend, the reader is referred to the web version of this article.)



Scheme 2. Schematic representation of the stepwise complex formation between mTHPC and β -CDs. The association constant K_{11} corresponds to 1:1 complex formation, while K_{12} is attributed to the association of 1:1 complex with the second β -CD molecule.

binding constants is feasible by comparison of the binding isotherms obtained at different mTHPC concentrations. Fig. 7A exhibits the dependence of the binding isotherms on mTHPC concentration for the Me- β -CD. Decreasing the mTHPC concentration shifts the titration curves towards left, i.e. towards the region of lower Me- β -CD concentrations, hence indicating an apparent increase of the β -CD's affinity to mTHPC. Similar results were also obtained for TM- and Hp- β -CD, or when using ICD titrations. However, the application of ICD technique is limited by mTHPC concentration of 1 μM , while fluorescence technique allows analysing of binding isotherms at much lower “guest” concentrations thus reducing the impact of mTHPC aggregation.

The quantification of the impact of mTHPC aggregation on the apparent binding constants indeed shows that K_{11} value significantly depends on mTHPC concentration, while the changes of K_{12} were random and not significant (data not shown). Therefore, for further calculations we used an average value of K_{12} as a “correct” binding constant to re-estimate K_{11} values for various mTHPC concentrations (Table 1). According to our fitting data, K_{11} value increases with decreasing mTHPC concentration and plateaued at mTHPC concentration less than 10 nM mTHPC (Fig. 7B).

The “correct” K_{11} values (Table 1) were estimated by extrapolation of the curves presented in Fig. 7B, while “correct” K_{12} values were taken as the average of the values obtained for all the mTHPC concentrations. The extrapolation of K_{11} vs mTHPC concentration curve was performed in the range of mTHPC concentrations 0.1 nM–3 μM , reaching a region where experimental techniques cannot be used due to their sensitivity limits. Moreover, the generalized constants (K) were calculated as a

Table 1

“Correct” binding constants of mTHPC and β -CDs.

	K_{11}, M^{-1}	K_{12}, M^{-1}	K, M^{-1}	α
Hp- β -CD	6.6×10^5	4.3×10^4	1.7×10^5	0.52
Me- β -CD	1.1×10^6	4.6×10^5	7.1×10^5	3.35
TM- β -CD	3.8×10^7	3.1×10^6	1.1×10^7	0.65

geometrical average of the “correct” K_{11} and K_{12} values simplifying the comparison of β -CD affinity for mTHPC. According to the obtained data, TM- β -CD exhibits extremely high affinity ($K = 1.1 \times 10^7 \text{M}^{-1}$), while Me- and Hp- β -CD are at least 10 times less prone to bind mTHPC ($7.1 \times 10^5 \text{M}^{-1}$ and $1.7 \times 10^5 \text{M}^{-1}$, respectively). Finally, to emphasize the relationship between 1:1 and 1:2 binding constants, cooperativity of binding (α) was estimated as $\alpha = b \times K_{12}/K_{11}$, where b is the statistical coefficient taken equal to 8 considering that it is impossible to distinguish between any of the four 1:1 complexes and two 1:2 complexes [17]. If $\alpha > 1$ the system is considered as positive cooperativity; $\alpha < 1$ presents negative cooperativity and finally if $\alpha = 1$, we conclude on the non-cooperative binding. As such, only Me- β -CD possesses positive binding cooperativity ($\alpha = 3.36$) and stands out from other β -CD derivatives presenting a slight negative cooperativity ($\alpha = 0.56$).

4. Discussion

In the present study we compared the mechanisms of interaction of mTHPC with three β -CD derivatives: Hp-, Me- and TM- β -CD. The focus of present study was the formation of mTHPC/ β -CDs complexes and quantitative estimation of different β -CDs affinity for mTHPC, taking into account self-aggregation of mTHPC.

According to the described spectral data (Figs. 1–3), all studied cyclodextrins readily interact with mTHPC. The most dramatic mTHPC spectral changes induced by β -CDs were observed for the relative quantum yield of fluorescence (Fig. 2). A similar effect was also observed for other aryl-porphyrins and was related to the chromophore monomerization due to the binding with the β -CDs competing with self-aggregation [31]. For *meta*-tetraphenyl substituted porphyrins and β -CD derivatives the typical binding mode can be described as a deep penetration of the porphyrin phenyl rings into the secondary face of the β -CD, so that a part of the porphyrin moiety in its bound state is located in the β -CD cavity and is separated from the external solution [8,14,32]. Due to the shielding action of β -CD molecule, the bound porphyrins are not able to form aggregates and hence are stable in monomeric state [31]. Similarly, as shown by our data the addition of β -CDs to the aqueous mTHPC solution prevents PS aggregation, as confirmed by the corresponding changes of mTHPC spectral characteristics. Our proposed mechanism for the formation of inclusion complex is also

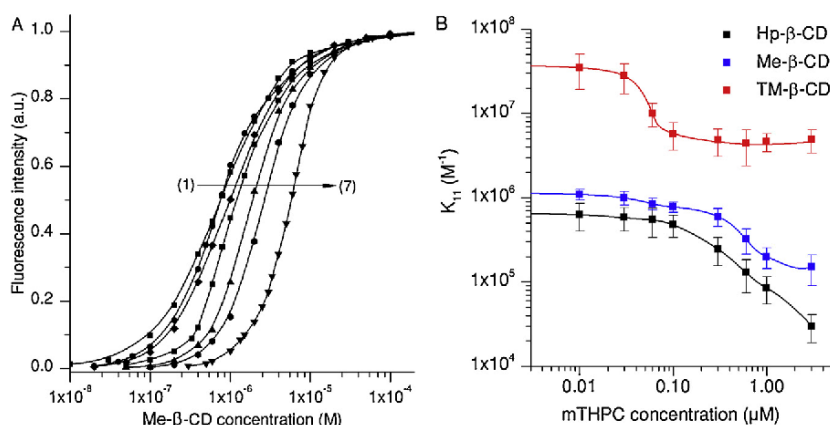


Fig. 7. (A) Titration curves by Me- β -CD of mTHPC in different concentrations. mTHPC concentration was: 1–3; 2–1; 3–0.6; 4–0.3; 5–0.1; 6–0.03; 7–0.01 μM . Arrow designates increasing concentration of mTHPC. (B) Dependence of K_{11} values on mTHPC concentration. The solid line indicates cubic-spline extrapolation curves.

fully consistent with the appearance of strong ICD effect as a result of the interaction of the optically inactive porphyrin with the chiral CD structure [4,12,33,34].

The alteration of the porphyrin microenvironment upon the complexation affects the photophysical properties of the PS, with the extent of spectroscopic response that depends on the type of lateral substituents [10,14,32]. Indeed, β -CD interaction with anionic and cationic aryl-porphyrins results in significant shifts of the Soret band as well as in a strong change of the fluorescence emission band [14,32,33]. On the contrary, when neutral mTHPC is bound to the β -CD cavity, only minor changes in the spectral signature are observed (Figs. 1 and 2), most probably due to a less pronounced polarization of the electronic density. Thus, according to our studies, the amplitudes of both ICD and fluorescence emission appear to provide the most reliable tools to analyze the interaction of mTHPC with different β -CDs (Fig. 2 and 3).

The main quantitative parameters describing the mechanism of formation of the porphyrins/ β -CD complexes are the stoichiometry and binding constants. The stoichiometry displays the number of molecules involved in the formation of the complex and determines the binding model, while binding constants reflect the affinity between the complexants [17]. As was mentioned above, the association process involves two β -CDs for one porphyrin due to steric restrictions. We confirmed the 1:2 stoichiometric ratio for all studied β -CDs by means of Job's plot (Fig. 4). This is also in agreement with the results provided earlier and demonstrating that 1:2 is the most probable stoichiometry of Me- and Hp- β -CD complexes with mTHPC [8]. The 1:2 stoichiometric ratio was also confirmed by MD simulation of the mTHPC/TM- β -CD complex (Fig. 5). It was shown, that TM- β -CDs molecules tightly interact with mTHPC influencing its conformation and hiding porphyrin molecule from polar solvent. The 1:2 complex was shown to be stable and persistent all along the MD trajectory, and the distances of the center of mass of the β -CDs moiety were also characterized as extremely stable. QM/MM calculations of the electronic spectra of mTHPC encapsulated in the β -CDs inclusion complex also supposed the changes in the Soret band shape, observed in the experimental absorption spectra upon complexation with TM- β -CD (Fig. 5E).

Taking into account the 1:2 stoichiometric ratio model, a two-step mechanism of complexation was postulated, and the corresponding binding constants have been estimated (Scheme 2). It is obvious, that the 1:2 stoichiometry should not be considered as absolute, and indeed the existence of a 1:1 complex should be taken into account as an intermediate species produced in the complex formation [14,17]. The fitting of experimental data by the corresponding mathematical model, which was described in details by Thordarson [17], allows us to quantify the difference in β -CDs affinity to mTHPC (Fig. 6). Both experimental techniques (ICD and fluorescence) demonstrated that TM- β -CD possesses higher affinity as compared to Me- and Hp- β -CD. The moderate deviations in the estimated values of the binding constants obtained from the analysis of ICD or fluorescence spectra may be attributed to the peculiarities of these two techniques. Indeed, while ICD responds to the structural changes induced by the inclusion of mTHPC molecule into the β -CD cavity, the increase of fluorescence quantum yield is due to the inhibition of mTHPC self-aggregation induced by the complexation with β -CDs.

Our numerical estimation of the binding constants for studied β -CDs without assuming mTHPC aggregation correlates well with similar data previously obtained for various cyclodextrins and meso-tetraphenyl substituted porphyrins [13,14,32,33]. Concerning mTHPC, there are several studies of Kasselouri and Prognon group on the binding constant values between β -CD and mTHPC [8,12,13]. In the earliest paper Me- β -CD affinity to mTHPC was lower than that for Hp- β -CD [8]. However, in further reports, they clarified the results using various experimental techniques and association models. In the latest study on this subject, the authors reported binding constants values of $4.8 \times 10^4 \text{ M}^{-1}$ and $1.2 \times 10^5 \text{ M}^{-1}$ for Hp- and Me- β -CD to mTHPC (3 μM) respectively [13]. Our estimations of K correlated well with these data and

demonstrated the values of $4.5 \times 10^4 \text{ M}^{-1}$, $3.0 \times 10^5 \text{ M}^{-1}$ and $5.6 \times 10^6 \text{ M}^{-1}$ for Hp-, Me- and TM- β -CD, respectively at mTHPC concentration of 3 μM .

Even though such data correlate well with the literature, in our opinion they are not sufficient to clearly and fully model the formation of the inclusion complex and to provide the affinity of β -CDs to mTHPC and related compounds. Indeed, when the guest molecules tend to form aggregates, as it is the case for mTHPC, the competition between aggregation and the formation of the inclusion complexes should lead to changes in the binding isotherms and, as a consequence, to different apparent binding constants. Such effect for a one-step model complexation was theoretically analyzed by Hammelin and Jullien [30]. Following their considerations, a decrease in the guest concentration is accompanied by a shift in the equilibrium processes towards the formation of the inclusion complexes hence reducing the impact of the guest aggregation on the measured apparent binding constants. In our experiments, the decrease in the porphyrin concentration was accompanied by a growth of the apparent binding constants values with respect to all the studied β -CDs (Fig. 7). It should be noted that the enhanced apparent binding efficiency of β -CDs for diluted mTHPC solutions is mainly associated with an increase of the apparent binding constant value for the first β -CD unit (K_{11}), whereas the value of the binding constant of the second β -CD molecule (K_{12}) remains almost unchanged. Such a difference in the behavior of the K_{11} and K_{12} apparent constants can be attributed to the changes in the guest solubility as a result of its interaction with β -CDs. Indeed, the binding of even a single β -CD molecule should significantly reduce mTHPC aggregation potential, hence reducing the influence of aggregation processes on the formation of inclusion complexes.

Extrapolation of the dependence of the K_{11} and K_{12} binding constants in the range of the smallest mTHPC concentrations allowed us to compare correct affinities of the studied β -CDs to the PS. TM- β -CD is characterized by the greatest affinity to mTHPC, the corrected K value for this cyclodextrin exceeds 10^7 M^{-1} . For Hp- and Me- β -CD the binding constants are equal to $1.1 \times 10^5 \text{ M}^{-1}$ and $7.1 \times 10^5 \text{ M}^{-1}$ respectively. It should be noted that such significant difference in the binding constants cannot be attributed to physical-chemical peculiarities such as solubility or aggregation of the cyclodextrins themselves. According to the work of Hammelin and Jullien [30], a change in the properties of the host molecules should not modify the isotherms of the inclusion complexes formation.

Our data demonstrate that complete methylated derivative (TM- β -CD) possesses the highest affinity to mTHPC among all studied β -CDs. According to the previous reports, the strong affinity of TM- β -CD to aryl-porphyrins is anticipated [14,35,36]. The formation of inclusion complex deals with the conformation changes of both TM- β -CD and porphyrin molecules due to the optimization of intermolecular interactions [14]. The complete methylation of β -CD contributes to the increase of flexibility of CD's core due to the absence of intramolecular hydrogen bonds between the secondary OH groups of β -CD glucopyranose units [37,38]. The complete methylated β -CDs exhibit highly hydrophobic cavity leading to the deeper encapsulation of mTHPC as well as stronger interaction with mTHPC phenol substitutes limiting the peripheral mTHPC phenyl groups rotation [14,36]. Similar features of inclusion association were demonstrated during the MD calculation of mTHPC/TM- β -CD complex. In the case of Hp- β -CD, long hydroxypropyl chains prevent rapprochement of mTHPC and Hp- β -CD molecules, significantly decreasing affinity compared with methylated β -CD derivatives.

Beside the quantitative characterization of β -CD and mTHPC inclusion complex formation, our results provide strong evidence suggesting the applicability of β -CDs as vectors for mTHPC-based PDT. The value of β -CD binding constant to mTHPC plays a key role in the case of co-administration of mTHPC with β -CDs. Depending on the type of β -CDs, we observed a different extent of the influence β -CDs on various stages of mTHPC biodistribution in tumor-bearing mice [7].

Methylation of β -CDs increases their affinity to mTHPC providing significant acceleration of PS transport to the target tissues and alterations in the biodistribution of mTHPC among different organs and tissues. In the present work, TM- β -CD was introduced as a new component possessing much higher affinity to mTHPC compared with previously studied compounds (Me- and Hp- β -CD). Thus, according to our calculations, we can suppose that TM- β -CD could be a potent vector for the alteration of the biodistribution profile of mTHPC-based PDT.

5. Conclusions

In the present work, we experimentally assessed the binding affinity of three β -CD derivatives to mTHPC. The results obtained are in a good agreement with the previous reports on the interaction of β -CD with aryl-porphyrins and complete the data array about the inclusion complex formation mechanisms. The estimated binding constant values confirmed a high affinity of β -CD to mTHPC. Moreover, the accurate assumption of mTHPC self-aggregation effects in our model resulted in significantly higher values than previously reported. As a corollary of our results concerning the high binding affinity and efficient solubilization of mTHPC by β -CD, one can assume the application of β -CDs as mTHPC nanovectors. Thus, the knowledge of correct values of binding constants could be helpful for the selection of optimal composition of β -CD-based delivery system for mTHPC-mediated PDT.

Acknowledgments

This work was supported by the Institut de Cancérologie de Lorraine; French “Ligue Nationale Contre le Cancer (CCIR-GE)”; Belarusian Republican Foundation for Fundamental Research (BRFFR) [grant numbers M17MC-028; M18MB-002; B17-106]; the Ministry of Education of the Republic. The authors thank biolitec research GmbH (Jena, Germany) for providing with mTHPC and Alexandre Kriznik (Platform of Biophysics and Structural Biology of UMS 2008 IBSLor, UL-CNRS-INSERM) for circular dichroism facilities access.

References

- M.O. Senge, mTHPC—a drug on its way from second to third generation photosensitizer? *Photodiagn. Photodyn. Ther.* 9 (2012) 170–179, <https://doi.org/10.1016/j.pdpdt.2011.10.001>.
- M.O. Senge, J.C. Brandt, Temoporfin (Foscan[®], 5,10,15,20-tetra(m-hydroxyphenyl)chlorin)—a second-generation photosensitizer, *Photochem. Photobiol.* 87 (2011) 1240–1296, <https://doi.org/10.1111/j.1751-1097.2011.00986.x>.
- D. Kachatkou, S. Sasnoski, V. Zorin, T. Zorina, M.-A. D'Hallewin, F. Guillemain, L. Bezdetsnaya, Unusual photoinduced response of mTHPC liposomal formulation (Foslip), *Photochem. Photobiol.* 85 (2009) 719–724, <https://doi.org/10.1111/j.1751-1097.2008.00466.x>.
- J. Mosinger, L. Slavětínská, K. Lang, P. Kouřal, P. Kubát, Cyclodextrin carriers of positively charged porphyrin sensitizers, *Org. Biomol. Chem.* 7 (2009) 3797, <https://doi.org/10.1039/b908772a>.
- H. Kolářová, M. Huf, J. Macedek, P. Nevrellová, M. Tomecka, R. Bajgar, J. Mosinger, M. Strnad, The cellular uptake of sensitizers bound to cyclodextrin carriers, *Acta Med. (Hradec Kralove)* 47 (2004) 313–315.
- K.T. Arun, D.T. Jayaram, R.R. Avirah, D. Ramaiah, β -Cyclodextrin as a photosensitizer carrier: effect on photophysical properties and chemical reactivity of squaraine dyes, *J. Phys. Chem. B* 115 (2011) 7122–7128, <https://doi.org/10.1021/jp201784b>.
- I. Yankovsky, E. Bastien, I. Yakavets, I. Khludeyev, H.-P. Lassalle, S. Gräfe, L. Bezdetsnaya, V. Zorin, Inclusion complexation with β -cyclodextrin derivatives alters photodynamic activity and biodistribution of meta-tetra(hydroxyphenyl)chlorin, *Eur. J. Pharm. Sci.* 91 (2016) 172–182, <https://doi.org/10.1016/j.ejps.2016.06.012>.
- D. Demore, A. Kasselouri, O. Bourdon, J. Blais, G. Mahuzier, P. Prognon, Enhancement of 5,10,15,20-tetra(m-hydroxyphenyl)chlorin fluorescence emission by inclusion in natural and modified cyclodextrins, *Appl. Spectrosc.* 53 (1999) 523–527.
- I. Yakavets, I. Yankovsky, M. Millard, L. Lamy, H.-P. Lassalle, A. Wiehe, V. Zorin, L. Bezdetsnaya, The alteration of temoporfin distribution in multicellular tumor spheroids by β -cyclodextrins, *Int. J. Pharm.* 529 (2017) 568–575, <https://doi.org/10.1016/j.ijpharm.2017.07.037>.
- I. Yakavets, I. Yankovsky, L. Bezdetsnaya, V. Zorin, Soret band shape indicates mTHPC distribution between β -cyclodextrins and serum proteins, *Dye Pigm.* 137 (2017) 299–306, <https://doi.org/10.1016/j.dyepig.2016.11.007>.

- V.J. Stella, Q. He, Cyclodextrins, *Toxicol. Pathol.* 36 (2008) 30–42, <https://doi.org/10.1177/0192623307310945>.
- M.-C. Desroches, A. Kasselouri, O. Bourdon, P. Chaminade, J. Blais, P. Prognon, A direct sensitized fluorimetric determination of 5,10,15,20-tetra(m-hydroxyphenyl)chlorin [m-THPC(Foscan[®])] in human plasma using a cyclodextrin inclusion complex, *Analyst* 126 (2001) 923–927, <https://doi.org/10.1039/B100808K>.
- A. Bautista-Sanchez, A. Kasselouri, M.-C. Desroches, J. Blais, P. Maillard, D.M. de Oliveira, A.C. Tedesco, P. Prognon, J. Delaire, Photophysical properties of glucoconjugated chlorins and porphyrins and their associations with cyclodextrins, *J. Photochem. Photobiol. B* 81 (2005) 154–162, <https://doi.org/10.1016/j.jphotochem.2005.05.013>.
- K. Kano, R. Nishiyabu, T. Asada, Y. Kuroda, Static and dynamic behavior of 2:1 inclusion complexes of cyclodextrins and charged porphyrins in aqueous organic media, *J. Am. Chem. Soc.* 124 (2002) 9937–9944, <https://doi.org/10.1021/ja020253n>.
- R. Bonnett, P. Charlesworth, B.D. Djelal, S. Foley, D.J. McGarvey, T.G. Truscott, Photophysical properties of 5,10,15,20-tetrakis(m-hydroxyphenyl)porphyrin (m-THPP), 5,10,15,20-tetrakis(m-hydroxyphenyl)chlorin (m-THPC) and 5,10,15,20-tetrakis(m-hydroxyphenyl)bacteriochlorin (m-THPBC): a comparative study, *J. Chem. Soc. Perkin Trans. 1* 2 (1999) 325–328, <https://doi.org/10.1039/A805328F>.
- E.M.M. Del Valle, Cyclodextrins and their uses: a review, *Process Biochem.* 39 (2004) 1033–1046, [https://doi.org/10.1016/S0032-9592\(03\)00258-9](https://doi.org/10.1016/S0032-9592(03)00258-9).
- P. Thordarson, Determining association constants from titration experiments in supramolecular chemistry, *Chem. Soc. Rev.* 40 (2011) 1305–1323, <https://doi.org/10.1039/C0CS00062K>.
- D.A. Case, V. Babin, J. Berryman, R.M. Betz, Q. Cai, D.S. Cerutti, T.E. Cheatham III, T.A. Darden, R.E. Duke, H. Gohlke, A.W. Goetz, N. Gusarov, N. Homeyer, P. Janowski, J. Kaus, I. Kolossváry, A. Kovalenko, T.S. Lee, S. LeGrand, T. Luchko, R. Luo, B. Madej, K.M. Merz, F. Paesani, D.R. Roe, A. Roitberg, C. Sagui, R. Salomon-Ferrer, G. Seabra, C.L. Simmerling, W. Smith, J. Swails, R.C. Walker, J. Wang, R.M. Wolf, X. Wu, P.A. Kollman, Amber 14, (2014) (Accessed 15 February 2018), <http://orbilu.uni.lu/handle/10993/16614>.
- Wang Junmei, Cieplak Piotr, A. Kollman Peter, How well does a restrained electrostatic potential (RESP) model perform in calculating conformational energies of organic and biological molecules? *J. Comput. Chem.* 21 (2000) 1049–1074, [https://doi.org/10.1002/1096-987X\(200009\)21:12<1049::AID-JCC3>3.0.CO;2-F](https://doi.org/10.1002/1096-987X(200009)21:12<1049::AID-JCC3>3.0.CO;2-F).
- C. Cézard, X. Trivelli, F. Aubry, F. Djedjini-Pilard, F.-Y. Dupradeau, Molecular dynamics studies of native and substituted cyclodextrins in different media: 1. Charge derivation and force field performances, *Phys. Chem. Chem. Phys.* 13 (2011) 15103–15121, <https://doi.org/10.1039/C1CP20854C>.
- K.N. Kirschner, R.J. Woods, Solvent interactions determine carbohydrate conformation, *Proc. Natl. Acad. Sci. U. S. A.* 98 (2001) 10541–10545, <https://doi.org/10.1073/pnas.191362798>.
- M. Basma, S. Sundara, D. Çalgan, T. Vernali, R.J. Woods, Solvated ensemble averaging in the calculation of partial atomic charges, *J. Comput. Chem.* 22 (2001) 1125–1137, <https://doi.org/10.1002/jcc.1072>.
- K.N. Kirschner, R.J. Woods, Quantum mechanical study of the nonbonded forces in water–methanol complexes, *J. Phys. Chem. A* 105 (2001) 4150–4155, <https://doi.org/10.1021/jp004413y>.
- W.L. Jorgensen, J. Chandrasekhar, J.D. Madura, R.W. Impey, M.L. Klein, Comparison of simple potential functions for simulating liquid water, *J. Chem. Phys.* 79 (1983) 926–935, <https://doi.org/10.1063/1.445869>.
- T.A. Andrea, W.C. Swope, H.C. Andersen, The role of long ranged forces in determining the structure and properties of liquid water, *J. Chem. Phys.* 79 (1983) 4576–4584, <https://doi.org/10.1063/1.446373>.
- H.J.C. Berendsen, J.P.M. Postma, W.F. van Gunsteren, A. DiNola, J.R. Haak, Molecular dynamics with coupling to an external bath, *J. Chem. Phys.* 81 (1984) 3684–3690, <https://doi.org/10.1063/1.448118>.
- U. Essmann, L. Perera, M.L. Berkowitz, T. Darden, H. Lee, L.G. Pedersen, A smooth particle mesh Ewald method, *J. Chem. Phys.* 103 (1995) 8577–8593, <https://doi.org/10.1063/1.470117>.
- D.A. Case, J.T. Berryman, R.M. Betz, D.S. Cerutti, T.E. Cheatham, T.A. Darden, R.E. Duke, T.J. Glese, H. Gohlke, A.W. Goetz, N. Homeyer, S. Izadi, P. Janowski, J. Kaus, A. Kovalenko, T.S. Lee, S. LeGrand, P. Li, T. Luchko, R. Luo, B. Madej, G. Monard, K.M. Merz, F. Paesani, D.R. Roe, A. Roitberg, C. Sagui, R. Salomon-Ferrer, G. Seabra, C.L. Simmerling, W. Smith, J. Swails, R.C. Walker, J. Wang, X. Wu, R.M. Wolf, P.A. Kollman, Amber 15, Univ. Calif. San Franc. (2015).
- W. Likussar, D.F. Boltz, Theory of continuous variations plots and a new method for spectrophotometric determination of extraction and formation constants, *Anal. Chem.* 43 (1971) 1265–1272, <https://doi.org/10.1021/ac60304a006>.
- B. Hamelin, L. Jullien, Does aggregation modulate the apparent association constant of host-guest complexes and related species? *J. Chem. Soc. Faraday Trans. 93* (1997) 2153–2160, <https://doi.org/10.1039/A700730B>.
- J.-J. Wu, H.-L. Ma, H.-S. Mao, Y. Wang, W.-J. Jin, Investigation on disassociation of porphyrin J-aggregates induced by β -cyclodextrins using absorption and fluorescence spectroscopy, *J. Photochem. Photobiol. Chem.* 173 (2005) 296–300, <https://doi.org/10.1016/j.jphotochem.2005.04.008>.
- J. Mosinger, V. Kliment, J. Sejbal, P. Kubát, K. Lang, Host-guest complexes of anionic porphyrin sensitizers with cyclodextrins, *J. Porphy. Phthalocya.* 06 (2002) 514–526, <https://doi.org/10.1142/S1088424602000646>.
- S. Hamai, T. Koshiyama, Electronic absorption, fluorescence, and circular dichroism spectroscopic studies on the inclusion complexes of tetrakis(4-sulfonatophenyl)porphyrin with cyclodextrins in basic aqueous solutions, *J. Photochem. Photobiol. Chem.* 127 (1999) 135–141, [https://doi.org/10.1016/S1010-6030\(99\)00144-6](https://doi.org/10.1016/S1010-6030(99)00144-6).
- I.V. Yakavets, I.V. Yankovsky, I.I. Khludeyev, H.P. Lassalle, L.N. Bezdetsnaya, V.P. Zorin, Optical methods for the analysis of the temoporfin photosensitizer

- distribution between serum proteins and methyl- β -cyclodextrin nanocarriers in blood serum, *J. Appl. Spectrosc.* 84 (2018) 1030–1036, <https://doi.org/10.1007/s10812-018-0582-z>.
- [35] K. Kano, R. Nishiyabu, T. Yamazaki, I. Yamazaki, Convenient scaffold for forming heteroporphyrin arrays in aqueous media, *J. Am. Chem. Soc.* 125 (2003) 10625–10634, <https://doi.org/10.1021/ja035055q>.
- [36] T. Carofiglio, R. Fornasier, V. Lucchini, C. Rosso, U. Tonellato, Very strong binding and mode of complexation of water-soluble porphyrins with a permethylated β -cyclodextrin, *Tetrahedron Lett.* 37 (1996) 8019–8022, [https://doi.org/10.1016/0040-4039\(96\)01814-X](https://doi.org/10.1016/0040-4039(96)01814-X).
- [37] W. Saenger, Cyclodextrin inclusion compounds in research and industry, *Angew. Chem. Int. Ed. Engl.* 19 (1980) 344–362, <https://doi.org/10.1002/anie.198003441>.
- [38] K. Harata, K. Uekama, M. Otagiri, F. Hirayama, Crystal structures of cyclodextrin complexes with chiral molecules, *J. Incl. Phenom.* 2 (1984) 583–594, <https://doi.org/10.1007/BF00662224>.

5. Development of spectral techniques for monitoring the distribution of inclusion complexes

The second part of the results on mTHPC/ β -CDs complexes is described in the article “Soret band shape indicates mTHPC distribution between β -cyclodextrins and serum proteins”.

In order to analyze PS microenvironment, the technique for recognition of molecules bound to mTHPC is required. With this aim, we analyzed fluorescence and absorbance characteristics of mTHPC in several organic solutions and complexes with various biological structures. Comparative data analysis showed that the shape of the Soret band was strongly dependent on the kind of biological structure bound with the PS. The well-detected difference in the ratio of two Soret band peaks is observed for mTHPC molecules bound to β -CD on the one hand and to serum proteins/lipid membranes on the other. Taking into account the possible mechanism of incorporation of mTHPC molecule into the β -CD cavities or lipid membranes, we suggested that the variability of Soret band shape is associated with the changes of mTHPC conformation, caused by the forced rotation of the aryl-substitutes. Using this spectral feature, we could control mTHPC distribution processes between β -CDs and biomembranes and assessed the fraction of inclusion of mTHPC/CD complexes inside DCLs. Moreover, this technique could be useful in analyzing both equilibrium and kinetic processes of PS distribution in the blood (Yakavets et al., 2018c).



Contents lists available at ScienceDirect

Dyes and Pigments

journal homepage: www.elsevier.com/locate/dyepigSoret band shape indicates mTHPC distribution between β -cyclodextrins and serum proteinsIlya Yakavets^{a, b, c, 1}, Igor Yankovsky^{a, b, c, 1}, Lina Bezdetnaya^{b, c}, Vladimir Zorin^{a, d, *}^a Laboratory of Biophysics and Biotechnology, Physics Faculty, Belarusian State University, 4 Nezavisimosti Avenue, 220030, Minsk, Belarus^b Centre de Recherche en Automatique de Nancy (CRAN), CNRS UMR 7039 (Centre National de la Recherche Scientifique), Université de Lorraine, Campus Sciences, Vandœuvre-lès-Nancy, France^c Institut de Cancérologie de Lorraine, Research Department, 6 Avenue de Bourgogne, 54519, Vandœuvre-lès-Nancy, France^d International Sakharov Environmental Institute, Dauhabrodskaja 23, 220070, Minsk, Belarus

ARTICLE INFO

Article history:

Received 29 September 2016

Received in revised form

4 November 2016

Accepted 5 November 2016

Available online 8 November 2016

Keywords:

Soret band

mTHPC

 β -Cyclodextrins

Serum proteins

Liposomes

ABSTRACT

Fluorescence and absorbance characteristics of 5,10,15,20-tetra(*m*-hydroxyphenyl)chlorin (mTHPC) in several organic solutions and in complexes with various biological structures have been analyzed. A comparison of data showed that the most variable mTHPC spectral characteristic is the Soret band shape. The ratio of two Soret band peaks are strongly dependent on the kind of biological structure bound with the pigment molecule. It has been suggested, that the observed variations of Soret band shape are associated with conformational changes of mTHPC molecule, caused by the forced rotation of the aryl-substitutes. On the basis of Soret band shape variations, the spectral technique for noninvasive monitoring of mTHPC release from inclusion complex with β -cyclodextrin carriers in blood serum was developed.

© 2016 Elsevier Ltd. All rights reserved.

1. Introduction

The expanding application of tetrapyrroles in photomedicine techniques (photoimaging, photodynamic diagnosis and therapy (PDT)) increases interest in the study of the porphyrin spectral characteristics in biological systems [1–4]. The spectral properties of porphyrins are often highly informative in analysis of the porphyrin interaction with biological structures, for instance in study of photosensitizer (PS) distribution in cellular and tissue systems.

5,10,15,20-Tetra(*m*-hydroxyphenyl)chlorin (mTHPC) (Scheme 1), the potent second-generation PS, which is currently under

clinical trial for the palliative treatment of head and neck cancer, appears as a promising PS exhibiting a high therapeutic ratio [5–7]. mTHPC possesses optimal photophysical characteristics for PDT [8], selectively accumulates in the tumor tissue and sensitizes its photodamage [7]. However, this drug is hydrophobic and is prone to aggregation in biological media, resulting in a decreased photodynamic efficacy, moderate selectivity and prolonged skin photosensitivity [6,9]. To abolish these problems, special pharmacological forms such as liposomes [10,11], polymeric nanoparticles [12] and bioconjugates [13] are proposed to use for mTHPC administration.

β -Cyclodextrin (β -CD) derivatives can be successfully used for nonpolar porphyrin administration [14–16]. Introduction of β -CDs into aqueous solutions of porphyrins causes PS disaggregation by forming the inclusion complexes [17]. It is also reported that porphyrins in combination with β -CDs efficiently accumulate in tumor cells *in vitro* [18–20]. In our recent study we have proposed to use β -CDs as a delivery system in mTHPC-PDT [20]. It was demonstrated that the β -CDs have a concentration-dependent effect on the process of mTHPC distribution in blood serum and significantly alter the selectivity of mTHPC accumulation in the tumor tissue. It was suggested, that β -CDs concentration dependent effect strongly depends on mTHPC distribution between inclusion complexes and

Abbreviations: PDT, photodynamic therapy; PS, photosensitizer; mTHPC, 5,10,15,20-Tetra(*m*-hydroxyphenyl)chlorin; β -CD, β -cyclodextrin; DPPC, dipalmitoyl phosphatidyl choline; DPPG, dipalmitoylphosphatidylglycerol; Me- β -CD, methyl- β -cyclodextrin; TM- β -CD, trimethyl- β -cyclodextrin; DPBS, dulbecco's phosphate-buffered saline; TGF, tetrahydrofuran; ϕ_f , fluorescence quantum yields; P , fluorescence polarization degree; r^2 , adjusted coefficient of determination; N , the fraction of mTHPC molecules bound to Me- β -CD.

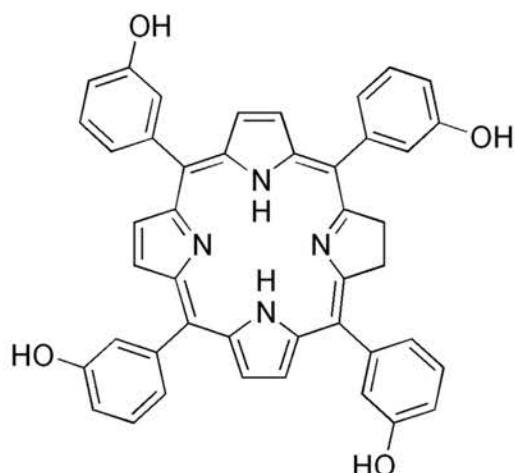
* Corresponding author. Laboratory of Biophysics and Biotechnology, Physics Faculty, Belarusian State University, 4 Nezavisimosti Ave, 220030, Minsk, Belarus.

E-mail address: vpzorin@mail.ru (V. Zorin).

¹ These authors have contributed equally to this work.

<http://dx.doi.org/10.1016/j.dyepig.2016.11.007>

0143-7208/© 2016 Elsevier Ltd. All rights reserved.



Scheme 1. Representation of the molecular structure of the 5,10,15,20-tetra(*m*-hydroxyphenyl)chlorin (mTHPC).

biological structures in the blood stream or interstitial media (serum proteins and cellular membranes). From this point of view, the rate and the extent of mTHPC transfer from the inclusion complex is an important determinant of this PS pharmacokinetics. In the present work we describe a new fluorescent spectral technique for noninvasive control of mTHPC distribution between β -CD nanocarriers and various biological structures.

2. Materials and methods

2.1. Chemicals and reagent preparation

The photosensitizer mTHPC was kindly provided by Biolitec Research GmbH (Jena, Germany) with the purity > 99%. Neutral detergent Triton[®] X-100 was purchased from Sigma Aldrich (France). Embryonal calf serum, dipalmitoylphosphatidyl choline (DPPC) and dipalmitoylphosphatidylglycerol (DPPG) were purchased from Sigma Chemical Co. (USA). The cyclodextrins methyl- β -cyclodextrin (Me- β -CD) and trimethyl- β -cyclodextrin (TM- β -CD) were purchased from AraChem (Tilburg, NL).

mTHPC stock solution (1 mM) was prepared in absolute ethanol (99.6%) and was kept at 4 °C in the dark. The concentration of mTHPC in the solution was estimated by a spectrophotometric method using molar extinction coefficient of 30 000 M⁻¹ cm⁻¹ at 650 nm in ethanol.

All aqueous solutions were prepared in Dulbecco's phosphate-buffered saline (DPBS) (pH 7.4) at 25 °C. To prepare mTHPC solution in organic solvents, mTHPC stock solution was dissolved 100 times. To prepare the solution with serum proteins, mTHPC was incubated for 3 h with 2% serum at 37 °C under light protection.

Me- β -CD and TM- β -CD complexes with mTHPC were formed using the co-precipitation method [21]. Briefly, β -CDs were dissolved in DPBS at the required concentrations with subsequent addition of the stock solution of mTHPC. The final content of ethanol in the mTHPC/ β -CD solutions did not exceed 0.5%. The solution was thoroughly mixed for 15 min under magnetic stirring.

All other chemicals and solvents (ethanol, methanol, tetrahydrofuran (THF), acetone) used in our experiments were commercial products of the highest grade of purity and its manufacturers will be specified below.

2.2. Preparation of liposomes

Unilamellar liposomes containing mTHPC were made by filter

extrusion technique as described in Ref. [22]. Briefly, 18 mg mL⁻¹ of DPPC (Avanti, USA) and 2 mg mL⁻¹ of DPPG (Avanti) were dissolved in 1 mL of 99.6% ethanol. A thin film was obtained by removal of the solvent by rotary evaporation at 60 °C. The film was hydrated in 1 mL of DPBS and underwent three freeze-thaw cycles. The suspension was extruded 21 times through 100 nm polycarbonate Nuclepore[®] membranes using Avanti Mini-Extruder (Avanti) at 50 °C. After extrusion liposomes were stored at 4 °C. mTHPC was added to the lipid vesicles on the stage of receiving of the lipid film to obtain dye: lipid ratio of 1: 100.

2.3. Spectroscopic measurements

The absorption spectra were measured on Solar PV1251 (Solar, Belarus) spectrophotometer using 1 cm optical path quartz cuvettes. Fluorescent measurements were performed on Solar CM 2303 (Solar, Belarus) fluorescence spectrometer equipped with thermostat cuvette compartment and magnetic stirring. The error in the wavelength measurements was estimated as ± 1 nm.

The concentration of mTHPC in all samples was 0.5 μ M. The spectroscopic measurements were carried out at room temperature 22–24 °C. Optical density at all measurements did not exceed 0.15 a.u. The concentrations of serum and Triton[®] X-100 were 5% (vol/vol) and 0.2% (vol/vol) respectively. The concentration of β -CDs was 0.1 mM.

2.4. Quantum yield measurements

The fluorescence quantum yields (ϕ_f) were determined using mTHPC in methanol ($\phi_f = 0.089$) [8] as the standard, and an excitation wavelength of 416 nm. The absolute error in quantum yields values was estimated as ± 0.01 .

2.5. Fluorescence polarization measurements

Measurements of mTHPC fluorescence polarization degree (P) were performed on Solar CM 2303 equipped with polarizers. In this case, samples were excited at 430 nm and fluorescence was registered at 652 nm as published before [20]. The polarization degree was calculated using a mean values of fluorescence intensities with the polarizers in parallel and perpendicular positions. The absolute error value for all measurements was less than 0.02.

2.6. Deconvolution of curve into component Gaussians

The experimental spectra were obtained and then were deconvoluted using a MATLAB software (The Math Works, USA). Using this program for an experimental curve, a multiple Gaussian fit can be done. With the approximate input parameters as above for each of the Gaussian curves an iterative nonlinear least square fit method was used. For optimization of the fit conditions, iterations were carried out until the difference in the value of chi-square for successive iterations was less than 5% of the previous value. The adjusted coefficient of determination (r^2) was more than 0.995 for all calculations.

2.7. Statistical analysis

Each experiment was repeated at least three times. Data are presented as mean \pm SD. The data were evaluated using Student's *t*-test. The difference was considered significant at $p < 0.05$. Data analysis was carried out with the STATISTICA 10 (StatSoft, Inc., USA).

3. Results and discussion

3.1. Absorption and fluorescence characteristics of mTHPC in solvents and solutions with different biological structures

The results obtained from spectral studies of mTHPC in neat solvents and different biological solutions are summarized in Table 1. The spectral characteristics of mTHPC are generally defined by PS belonging to chlorin-type compounds. Absorption spectra of mTHPC reveal most prominent peaks in the region of 420 nm (B-band or Soret band) and 651 nm (Q-band). In organic solvents mTHPC intensively fluoresces at 652 nm with a quantum yield (φ_f) around 0.09 [8] and the fluorescence lifetime of 10 ns [23]. In different organic solvents we detected only minor spectral changes: shifts of 1–2 nm in the peaks and the relative fluorescence quantum yield varying within 10% compared to ethanol solution.

Like many hydrophobic tetrapyrroles, mTHPC molecules in aqueous solutions tend to aggregate. The formation of large J-aggregates leads to a significant change in the absorption and mTHPC fluorescence properties [24,25]. The aggregated species are characterized by the decreased extinction coefficients for all bands and exhibit bathochromic shifts of the peaks (Table 1). According to the data obtained, the fluorescence quantum yield of mTHPC in DPBS decreases hundreds times.

The aggregation of mTHPC in aqueous media is completely prevented via interaction and binding with different biological structures *i.e.* liposomes, proteins, cyclodextrins [17,26–28]. Depending on the type of biological structure several features of mTHPC spectral properties are observed (Table 1):

- i) the positions of all spectral bands (except Soret band) remain practically unchanged;
- ii) an enhanced quantum yield of mTHPC fluorescence in solutions with β -CDs and liposomes, while in Triton® X-100 and serum solution this parameter is decreased;
- iii) the presence of mTHPC polarized fluorescence (in liposomes, neutral detergent micelles and serum proteins P up to 0.30, in inclusion complexes with β -CDs P up to 0.05 only), while in organic solutions fluorescence is totally depolarized (P less than 0.02). The fluorescence decay time varies slightly in studied samples [20], that allow us to use the detection of polarized fluorescence to confirm mTHPC binding to studied biological structures.

An analysis of the collected data allows the conclusion that the Soret band is the most variable characteristic, when we compared spectra of mTHPC bound to the studied biological structures (Fig. 1). This statement concerns both the position and the shape of the band.

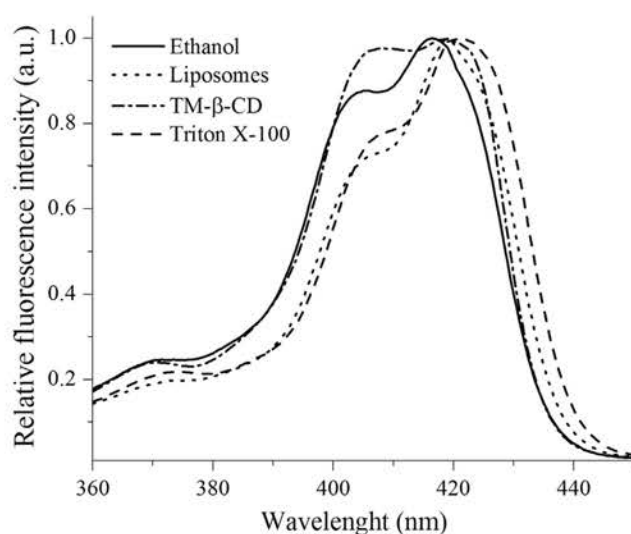


Fig. 1. Normalized fluorescence excitation spectra of mTHPC in various biological media. The solid black line is the mTHPC Soret band spectrum in ethanol, the dots are in liposomes, the dash dots are spectrum of mTHPC in complexes with TM- β -CD and the dash line is Soret band spectral region of mTHPC in micelles of Triton® X-100. The concentration of mTHPC was 0.5 μ M, the concentrations of serum and Triton® X-100 were 5% (vol/vol) and 0.2% (vol/vol) respectively. The concentration of TM- β -CD was 0.1 mM.

Soret band has a semi-resolved structure with two distinct peaks. In organic solvents the maxima of these peaks are located at 410 nm and 417 nm respectively with the intensity ratio 0.85. The binding of mTHPC to liposomes, neutral detergent micelles and serum proteins leads to 3–4 nm bathochromic shift of Soret band and the peaks intensity ratio decreasing by 15–20% compared to ethanol solution. In β -CDs solutions similar spectral shift (2–3 nm) is accompanied by the opposite changes of its shape (intensity of shortwave shoulder almost reaches the value of main peak).

3.2. Formalization of mTHPC Soret band

To formalize the description of mTHPC Soret band shape variations in different solutions we used the deconvolution technique. According to Palummo et al. [29], the absorption spectrum of free-base porphyrins and their derivatives over the range 350–450 nm may be approximated using five Gaussian components: B_x , B_y and N_x , N_y , L_x (Fig. 2). The components of this system are labeled according to the directions of polarization in the (x,y) planes of a macrocyclic system. B-band also known as the Soret band is located within the range 370–450 nm and is associated with the high-

Table 1
Spectral-fluorescent characteristics of mTHPC.

Surrounding	Absorbance		Fluorescence		
	λ_{\max} , nm (the Soret band)	λ_{\max} , nm (Q(0,0)-band)	λ_{\max} , nm	φ_f	P , a.u
Ethanol	417	651	652	0.092	0.02 \pm 0.01
Methanol	416	650	652	0.089	0.01 \pm 0.01
Acetone	417	651	653	0.085	0.01 \pm 0.01
TGF	418	653	654	0.083	0.01 \pm 0.01
DPBS	430–438	654	654	<0.001	–
Triton X-100®	421	653	654	0.074	0.23 \pm 0.02
Liposomes	420	651	652	0.132	0.30 \pm 0.01
Serum proteins	421	653	654	0.063	0.26 \pm 0.02
Me- β -CD	420	650	652	0.125	0.04 \pm 0.01
TM- β -CD	419	650	652	0.142	0.05 \pm 0.01

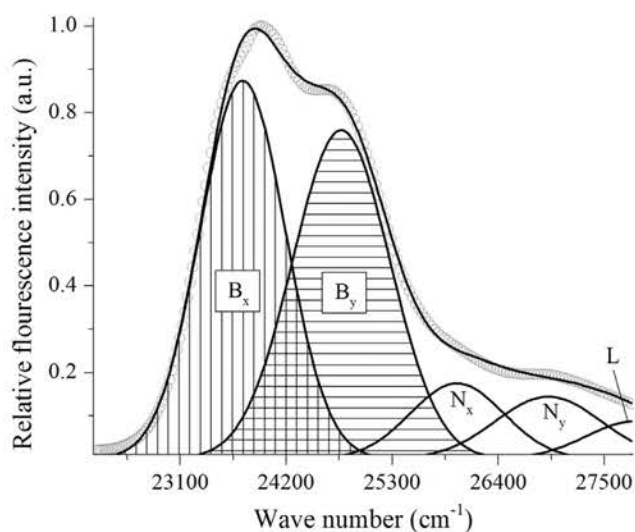


Fig. 2. Gaussian deconvolution for mTHPC in ethanol for the Soret band region. The open circles are the experimental data, the solid black lines are the theoretical curves obtained from Gaussian deconvolution.

energy $\pi-\pi^*$ transition to the 2nd degenerate excited state, ($S_0 \rightarrow S_2$) [29–31]. The B-band degenerates for the D_{4h} high symmetry porphyrins and splits in the case of lower symmetry derivatives such as mTHPC [31,32]. In the near UV region from 360 to 400 nm the higher-energy transitions known as the N-, L-bands are also found. These bands are associated with the allowed $\pi-\pi^*$ (N-band) and $n-\pi^*$ (L-band) electronic transitions to the high-energy states ($S_0 \rightarrow S_n$) [33,34].

The applied model may be used for the description and quantitative analysis of the observed spectral variations by Gaussian function expansion of the electronic spectra using the wave-numbers as coordinates [35,36]. The applicability of model proposed was checked by adjusted coefficient of determination (r^2) for each sample.

To compare the contribution of each component to the changes in the shape of the Soret band the relative weights of sub-bands were calculated (Table 2). A comparison of the numerical results for mTHPC absorption and excitation spectra deconvolution shows that the main factor determining observed mTHPC spectral features in the 360–450 nm region is a variation of ratio B_y/B_x . For monomeric unbound mTHPC molecules in organic solvents, the ratio B_y/B_x is within the range 0.73–0.93, whereas for mTHPC/ β -CD complexes its values are 1.03–1.42. For mTHPC bound to lipid vesicles and serum proteins, the value of B_y/B_x is less than 0.7.

Table 2

Results for deconvolution of the mTHPC Soret band in various solvents and solutions with different biological structures.

Medium	B_x	B_y	N_x, N_y, L_x	B_y/B_x	r^2
TM- β -CD	0.31	0.44	0.25	1.42	0.995
Me- β -CD	0.38	0.39	0.23	1.03	0.997
Ethanol	0.44	0.33	0.23	0.74	0.999
Methanol	0.45	0.33	0.22	0.73	0.998
Aceton	0.42	0.36	0.22	0.86	0.998
TGF	0.40	0.37	0.23	0.93	0.997
Triton X-100	0.45	0.35	0.20	0.78	0.998
Serum proteins	0.48	0.32	0.20	0.67	0.999
Liposomes	0.49	0.31	0.20	0.63	0.998

3.3. The analysis of Soret band shape of mTHPC in solvents and solutions with different biological structures

It is recognized, that the solvent impacts the spectral characteristics of free base porphyrins and chlorins [3]. Quantum calculations suggest that the main mechanism of this effect deals with the slight change of natural porphyrin ring conformation due to the interactions of solvent molecules with the lateral substituents. Based on mTHPC crystallographic data [37], we can suggest that in solvents the planar chlorin ring of free mTHPC molecule is surrounded by pairs of face-to-face positioned phenyl groups, with two of them related to the macrocycle meanplane dihedral angles (Fig. 3a). Organic solvents can have a minor impact on the rotation of phenyl groups of mTHPC and only slightly change the mTHPC Soret band shape. More significant changes of mTHPC conformation related to the phenyl groups are supposed to occur in organized biological structures as liposomes, serum proteins and inclusion complexes.

An incorporation in lipid membrane suggests strong interaction between mTHPC and lipid molecules [38]. Data concerning the mTHPC fluorescence quenching by membrane impermeable quenchers, mTHPC molecules penetrate into the lipid bilayer [39]. The inclusion of the mTHPC molecule into biological membranes in intact conformation should lead to a significant disordering of lipid bilayer and as the consequence to the modification of structural characteristics and stability of lipid vesicles. In fact, mTHPC loading into liposomes has practically no effect on the stability of the vesicles. Even at high dye: lipid ratio of 1: 12 the size of DPPC liposomes changes by only a few nanometers while the liposomal membrane retains the ability to change phase state when heated [40].

Absorption and fluorescence wavelengths provide valuable information of the microenvironment experienced by mTHPC in lipid membranes. It is proposed that the influence of the lipid bilayer on mTHPC spectral characteristics can occur through the effect of apolar environment or as a result of steric interactions in the bulk of the lipid bilayer. In accordance with our results an alteration of solvent polarity keeps the parameters of the Soret band unchanged (Table 1). At the same time for mTHPC molecules incorporated into lipid vesicles the membrane lateral pressure should change the orientation of two or more phenyl meso-substituents and arrange them in parallel relatively tetrapyrrolic cycle (Fig. 3b). This conformation of mTHPC molecule provides a minimal effect on the lipid bilayer structure. Discussed structural modification of mTHPC molecule in lipid membrane is associated with a significant increase of overlapping of the phenyl rings and chlorin core π -systems, and consequently with changes in the energy states and electronic spectra.

In accordance with our assumption, modifications of the mTHPC molecule conformation should depend on the rigidity of lipid bilayer. In this connection it is interesting to compare the temperature-dependent variations of the ratio B_y/B_x and polarization degree of fluorescence of mTHPC incorporated into DPPC lipid vesicles (Fig. 4).

Highly polarized fluorescence ($P = 33\%$) of mTHPC in liposomes in a quasi-crystal state (at the temperature less than 35 °C) indicates a significant restriction of fluorophore rotation in the lipid matrix [42]. The heating above 40 °C leads to the DPPC lipid bilayer phase transition, accompanied with the changing of lipid packing type [39]. The noted structural changes result in the increased mobility of mTHPC molecules as evidenced by the lowering of the fluorescence polarization degree by up to 24%. The decreased packing density of lipid molecules and lateral pressure in a bilayer [43], high conformational mobility of fatty-acid chains at temperatures above the phase-transition temperature should provide

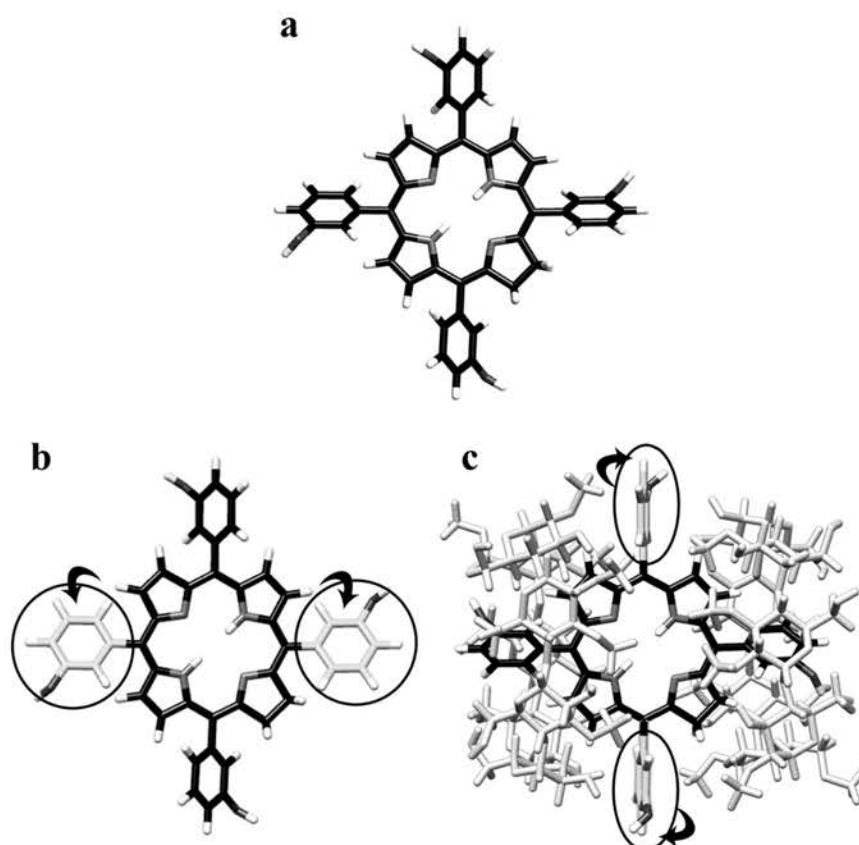


Fig. 3. Possible steric structures of mTHPC molecules: a – in organic solvent (natural conformation: phenyl groups are related to the macrocycle meanplane with dihedral angles of 61° and 76°), b – in lipid bilayer or serum lipoproteins (phenyl groups (grey coloured) tends to turn parallel to the macrocycle), c – in inclusion complex with β -CDs tends to turn perpendicular to the macrocycle). The structures were modeled in UCSF Chimera [41].

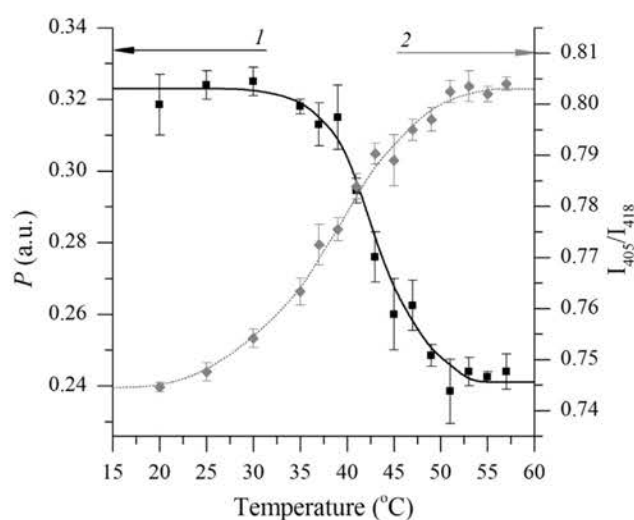


Fig. 4. The dependence of polarization degree of mTHPC fluorescence (1) and I_{405}/I_{418} value (2) from temperature for mTHPC in lipid bilayer. mTHPC concentration was $0.5 \mu\text{M}$. The liposome ratio dye: lipid = 1: 100. The results of three independent experiments are expressed as the mean with the vertical bar showing S.D.

enhanced freedom of mTHPC aryl substituents rotation. As a result, for mTHPC in liposomes at high temperatures the B_y/B_x ratio is growing.

It is recognized, that serum lipoproteins are the main binding sites for mTHPC (95% of mTHPC in serum plasma are bound to high and low density lipoproteins) [26]. This type of protein consists of a core of hydrophobic lipids surrounded by a shell of proteins and phosphatidyl glycerols and has quite similar structure as lipid micelles. As in the liposomes, a high value of the fluorescence polarization degree of mTHPC in serum indicates an extremely strong fixation of PS molecules. Thus, based on studies of mTHPC spectral characteristics in solutions of serum proteins, we can conclude that the interaction of the PS molecule with lipoproteins leads to the same conformational modifications as were observed in a lipid bilayer.

mTHPC effectively forms inclusion complexes with β -CDs [15,17]. β -CD/mTHPC complexes are reported to have a 1: 2 stoichiometry [17] and are characterized by a high values of binding constants ($1.2 \cdot 10^5 \text{ M}^{-1}$ for Me- β -CD) [15]. Molecular modeling and NMR spectroscopy of β -CD/aryl-porphyrins complexes structure indicate that two opposite porphyrin aryl-groups would be totally located in the hydrophobic β -CD cavity from the secondary hydroxyl-groups side (Fig. 3c) [17,44,45]. The proximity of β -CD's face groups has to limit the rotation of two hydroxyphenyl-groups, which are not involved into the formation of host-guest complex. On the contrary to mTHPC in lipid bilayer, mTHPC binding to β -CD induces steric restrictions leading to the increase of the average value of dihedral angles between macrocycle and phenyl

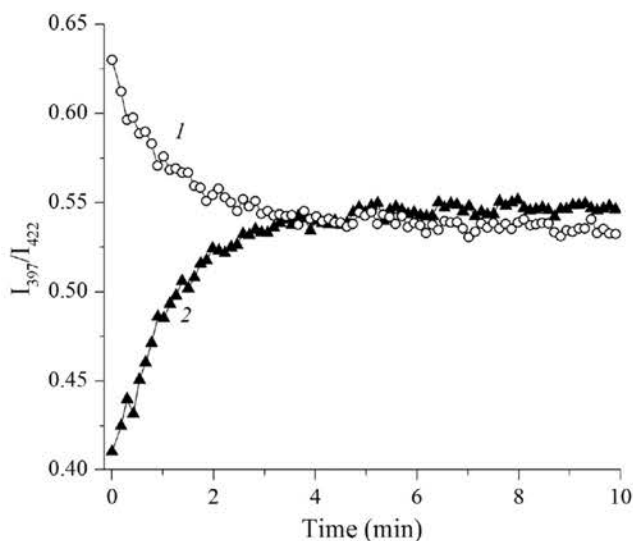


Fig. 5. Kinetics of I_{397}/I_{422} value changes after mixing of serum with mTHPC/Me- β -CD solution (curve 1) and after mixing of Me- β -CD solution with mTHPC/serum solution (curve 2). The concentration of mTHPC was 0.5 μ M, concentration of serum was 5% (vol/vol). The concentration of Me- β -CD was 60 μ M.

substituents (Fig. 3c). A similar conclusion on conformational changes of aryl-substituted porphyrins in complexes with β -CD has been obtained by computational studies [17,44]. The conformation changes of mTHPC molecule result in decreasing conjugation degree between hydroxyphenyl-group and chlorin-ring systems. Alteration of mTHPC electronic system is manifest as the decrease of B_y and B_x relative weight disbalancing, which corresponds to increasing of mTHPC B_y/B_x value in the complexes with β -CD.

It is obvious, that the role of discussed conformation-linked mechanism of mTHPC spectral alterations depends on characteristics of biological structures. Values of dihedral angles determine the degree of orbital-overlapping π -conjugated electron systems of aryl-groups and chlorin ring that affects the energy spectrum of mTHPC in complexes with biological structures [44,45]. It has been shown that increasing the degree of etherification of the hydroxyl groups of the β -CD leads to the enhancement of affinity between β -

CD and mTHPC [17]. According to the obtained data, the etherification of hydroxyl-groups results in increasing of binding constants as well as increasing of the penetration depth of mTHPC's aryl-groups in the β -CD's molecule.

3.4. Application of mTHPC spectral features for the control its redistribution in serum

Our results show that Soret band shape is dependent on mTHPC binding to the different biological structures (β -CDs and serum proteins/lipid membranes). We suggest that this feature allow one to control whether mTHPC molecules are in inclusion complex with β -CDs or they are bound to the serum protein/membrane.

Fig. 5 shows the kinetics of $I_{\lambda_1}/I_{\lambda_2}$ value changes when mTHPC/Me- β -CD complexes are mixed to the 5% serum solution (curve 1) and when Me- β -CD is added to the 5% serum solution preincubated with mTHPC (curve 2). We analyzed mTHPC excitation spectrum at 652 nm using $\lambda_1 = 397$ nm and $\lambda_2 = 422$ nm excitation wavelengths, providing the greatest difference in mTHPC emission intensities ratio. The I_{397}/I_{422} value of mTHPC complexed with Me- β -CD molecules is equal to 0.63, while the fluorescence spectrum of PS associated with serum proteins is characterized by $I_{397}/I_{422} = 0.41$. A competition between Me- β -CD and the serum proteins leads to redistribution of mTHPC molecules from inclusion complexes to serum proteins, which results in the drop of I_{397}/I_{422} value. The equilibrium value corresponding to used Me- β -CD and serum concentrations is equal to 0.55. Return transfer of mTHPC molecules from serum proteins to Me- β -CDs is controlled in a similar way (Fig. 5, curve 2). The application of this technique allows the estimation of the fraction of mTHPC molecules bound to serum proteins/Me- β -CD at each time point and the kinetic characteristics of mTHPC transfer.

Fig. 6a illustrates the kinetics of mTHPC redistribution from serum proteins to Me- β -CD depending on β -CD concentration. When Me- β -CD concentration is low (less than 20 μ M) the Soret band shape changes not significantly indicating that almost all mTHPC molecules remained bound to serum proteins (Fig. 6a, curves 1, 2, 3). In the samples containing moderate concentration of Me- β -CD, the I_{397}/I_{422} ratio value reaches 0.52 in 10 min of incubation meaning the transport of only limited amount of mTHPC molecules from the serum proteins to Me- β -CD (Fig. 6a, curve 4). Finally, after adding an excess amount of Me- β -CD (200 μ M) to the

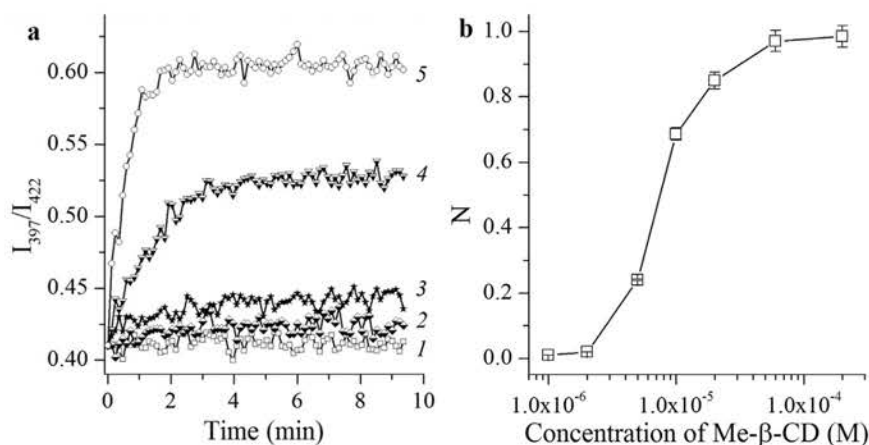


Fig. 6. A – The kinetics of I_{397}/I_{422} value changes after mixing of Me- β -CD solutions with mTHPC/serum solution. The concentration of Me- β -CD in the samples was (1) 5 μ M, (2) 10 μ M, (3) 20 μ M, (4) 50 μ M or (5) 200 μ M. B – Influence of Me- β -CD concentration on the equilibrium distribution of mTHPC in serum solution after 24 h of incubation at 37 $^{\circ}$ C. N – the fraction of mTHPC molecules bound to Me- β -CD. The concentration of mTHPC was 0.5 μ M, the concentration of serum was 5% (vol/vol). mTHPC was preincubated with serum at 37 $^{\circ}$ C during 2 h until complete binding of photosensitizer.

serum solution, containing mTHPC, the I_{397}/I_{422} value grows from 0.41 to 0.62 in several minutes confirming complete PS redistribution to Me- β -CD (Fig. 6a, curve 5).

Taking into account spectral shifts and variations of quantum yield of mTHPC fluorescence, it is possible to convert the value of I_{41}/I_{42} ratio to the relative weights of fractions of mTHPC molecules bound to serum proteins or β -CD. The dependence of the fraction of mTHPC molecules bound to Me- β -CD (N) on the concentration of Me- β -CD is shown on Fig. 6b. The data obtained allow to estimate the interval of Me- β -CD concentrations in which mTHPC distribution pattern in serum has undergone changes.

Similar results of mTHPC distribution between β -CD and serum proteins were obtained recently by means of fluorescence polarization measurements [20]. In this connection it is worth noting, that the spectral technique described in this paper is less sensitive to the influence of various physical factors, such as light scattering, fluorescence quenching. And for this reason the technique based on spectral features of the Soret band shape is more reliable for the non-invasive studies of mTHPC distribution in blood serum.

4. Conclusion

Spectral characteristics of Soret band is considered to be uninformative for the analysis of peculiarities of aryl-porphyrin micro-environment. In the present study it was shown that the shapes of the Soret band of mTHPC absorbance spectrum and corresponding band of fluorescence excitation spectrum are strongly dependent on the kind of biological structure bound with the pigment molecule. The well-detected difference in ratio of two Soret band peaks is observed for mTHPC molecules bound to β -CD on the one hand and to serum proteins/lipid membranes on the other. Taking into account the possible mechanism of incorporation of mTHPC molecule into the β -CD cavities or lipid membranes, one can suggest that the variability of Soret band shape is associated with the changes of pigment molecule conformation. This finding is useful for the development of spectral technique for noninvasive continuous control of mTHPC distribution from β -CDs to biological structures.

Acknowledgments

This work was supported by the Institut de Cancérologie de Lorraine, French "Ligue Nationale contre le Cancer (CCIR-GE)", Belarusian Republican Foundation for Fundamental Research (BRFFR) (grant number M16M-049) and the Ministry of Education of Belarus (joint grant with BRFFR number Φ 16MB-006). I.Y. acknowledges the fellowship of the Ministry of Foreign and European affairs of France. We thank Biolitec research GmbH (Jena, Germany) for providing mTHPC. The authors thank Dr. N. Kruk (Minsk, Belarus) for precious and precise discussion of this work and Dominique Marius Le Prince (Nancy, France) for help with manuscript preparation.

References

- [1] Ion R-M. Derivative UV-vis spectrophotometry for porphyrins interactions in photodynamic therapy. *Anal Lett* 2010;43:1277–86. <http://dx.doi.org/10.1080/00032710903518690>.
- [2] Fujita AKL, Rodrigues PGS, Requena MB, Escobar A, da Rocha RW, de Nardi AB, et al. Fluorescence evaluations for porphyrin formation during topical PDT using ALA and methyl-ALA mixtures in pig skin models. *Photodiagnosis Photodyn Ther* 2016;15:236–44. <http://dx.doi.org/10.1016/j.pdpdt.2016.05.008>.
- [3] Sampaio RN, Machado AEH, Piovesan E, Gonçalves PJ, De Paula R, Cavaleiro JAS, et al. Influence of the solvent-porphyrin interaction on the UV-Vis absorption of free base imidazol cationic porphyrin. *Dye Pigment* 2014;100:73–8. <http://dx.doi.org/10.1016/j.dyepig.2013.07.023>.
- [4] Zorin VP, Michalovsky I, Zorina TE, Khludayev II. Distribution of chlorin-e6 derivatives in biological systems: investigation of pH-effect. In: Ehrenberg B, Jori G, Moan J, editors. *International society for optics and photonics*; 1996. p. 146–55. <http://dx.doi.org/10.1117/12.230981>.
- [5] Bonnett R, White RD, Winfield UJ, Berenbaum MC. *Hydroporphyrins of the meso-tetra(hydroxyphenyl)porphyrin series as tumour photosensitizers*. *Biochem J* 1989;261:277–80.
- [6] Senge MO. mTHPC – a drug on its way from second to third generation photosensitizer? *Photodiagnosis Photodyn Ther* 2012;9:170–9. <http://dx.doi.org/10.1016/j.pdpdt.2011.10.001>.
- [7] Senge MO, Brandt JC. Temoporfin (Foscan®), 5,10,15,20-tetra(m-hydroxyphenyl)chlorin – a second-generation photosensitizer. *Photochem Photobiol* 2011;87:1240–96. <http://dx.doi.org/10.1111/j.1751-1097.2011.00986.x>.
- [8] Bonnett R, Charlesworth P, Djelal BD, Foley S, McGarvey DJ, Truscott TG. Photophysical properties of 5,10,15,20-tetrakis(m-hydroxyphenyl)porphyrin (m-THPP), 5,10,15,20-tetrakis(m-hydroxyphenyl)chlorin (m-THPC) and 5,10,15,20-tetrakis(m-hydroxyphenyl)bacteriochlorin (m-THPBC): a comparative study. *J Chem Soc Perkin Trans* 1999;2:325–8. <http://dx.doi.org/10.1039/A805328F>.
- [9] Kachatkou D, Sasnouski S, Zorin V, Zorina T, D'Hallewin M-A, Guillemin F, et al. Unusual photoinduced response of mTHPC liposomal formulation (Foslip). *Photochem Photobiol* 2009;85:719–24. <http://dx.doi.org/10.1111/j.1751-1097.2008.00466.x>.
- [10] Reshetov V, Lassalle H-P, François A, Dumas D, Hupont S, Gräfe S, et al. Photodynamic therapy with conventional and PEGylated liposomal formulations of mTHPC (temoporfin): comparison of treatment efficacy and distribution characteristics *in vivo*. *Int J Nanomedicine* 2013;8:3817–31. <http://dx.doi.org/10.2147/IJN.S51002>.
- [11] Garrier J, Reshetov V, Gräfe S, Guillemin F, Zorin V, Bezdetnaya L. Factors affecting the selectivity of nanoparticle-based photoinduced damage in free and xenografted chorioallantoic membrane model. *J Drug Target* 2013. <http://dx.doi.org/10.3109/1061186X.2013.860981>.
- [12] Ogawara K, Shiraishi T, Araki T, Watanabe T, Ono T, Higaki K. Efficient anti-tumor effect of photodynamic treatment with polymeric nanoparticles composed of polyethylene glycol and polylactic acid block copolymer encapsulating hydrophobic porphyrin derivative. *Eur J Pharm Sci Off J Eur Fed Pharm Sci* 2016;82:154–60. <http://dx.doi.org/10.1016/j.ejps.2015.11.016>.
- [13] Rogers L, Sergeeva NN, Paszko E, Vaz GMF, Senge MO. Lead structures for applications in photodynamic therapy. 6. Temoporfin anti-inflammatory conjugates to target the tumor microenvironment in *in vitro* PDT. *PLoS One* 2015;10:e0125372. <http://dx.doi.org/10.1371/journal.pone.0125372>.
- [14] Vinodh M, Alipour FH, Mohamad AA, Al-Azemi TF. Molecular assemblies of porphyrins and macrocyclic receptors: recent developments in their synthesis and applications. *Molecules* 2012;17:11763–99. <http://dx.doi.org/10.3390/molecules171011763>.
- [15] Bautista-Sanchez A, Kasselouri A, Desroches M-C, Blais J, Maillard P, de Oliveira DM, et al. Photophysical properties of glucoconjugated chlorins and porphyrins and their associations with cyclodextrins. *J Photochem Photobiol B* 2005;81:154–62. <http://dx.doi.org/10.1016/j.jphotobiol.2005.05.013>.
- [16] Kryjewski M, Goslinski T, Mielcarek J. Functionality stored in the structures of cyclodextrin-porphyrinoid systems. *Coord Chem Rev* 2015;300:101–20. <http://dx.doi.org/10.1016/j.ccr.2015.04.009>.
- [17] Demore D, Kasselouri A, Bourdon O, Blais J, Mahuzier G, Prognon P. Enhancement of 5,10,15,20-Tetra(m-Hydroxyphenyl)chlorin fluorescence emission by inclusion in natural and modified cyclodextrins. *Appl Spectrosc* 1999;53:523–7.
- [18] Kralova J, Synytsya A, Pouckova P, Koc M, Dvorak M, Kral V. Novel porphyrin conjugates with a potent photodynamic antitumor effect: differential efficacy of mono- and bis-beta-cyclodextrin derivatives *in vitro* and *in vivo*. *Photochem Photobiol* 2006;82:432–8. <http://dx.doi.org/10.1562/2005-05-06-RA-516>.
- [19] Mazzaglia A. Photodynamic tumor therapy with cyclodextrin nanoassemblies. In: Bilensky E, editor. *Cyclodextrins pharm. Cosmet. Biomed.* John Wiley & Sons, Inc; 2011. p. 343–61.
- [20] Yankovsky I, Bastien E, Yakavets I, Khludayev I, Lassalle H-P, Gräfe S, et al. Inclusion complexation with β -cyclodextrin derivatives alters photodynamic activity and biodistribution of meta-tetra(hydroxyphenyl)chlorin. *Eur J Pharm Sci* 2016;91:172–82. <http://dx.doi.org/10.1016/j.ejps.2016.06.012>.
- [21] Del Valle EMM. Cyclodextrins and their uses: a review. *Process Biochem* 2004;39:1033–46. [http://dx.doi.org/10.1016/S0032-9592\(03\)00258-9](http://dx.doi.org/10.1016/S0032-9592(03)00258-9).
- [22] Batzri S, Korn ED. Single bilayer liposomes prepared without sonication. *Biochim Biophys Acta* 1973;298:1015–9.
- [23] Howe L, Sucheta A, Einarsdóttir O, Zhang JZ. Time-resolved studies of the excited-state dynamics of meso-tetra(hydroxyphenyl)chlorin in solution. *Photochem Photobiol* 1999;69:617–23.
- [24] Desroches M-C, Kasselouri A, Bourdon O, Chaminade P, Blais J, Prognon P. A direct sensitized fluorimetric determination of 5,10,15,20-tetra(m-hydroxyphenyl)chlorin [m-THPC(Foscan®)] in human plasma using a cyclodextrin inclusion complex. *Analyst* 2001;126:923–7. <http://dx.doi.org/10.1039/B100808K>.
- [25] Kascáková S, Krujti B, de Bruijn HS, van der Ploeg-van den Heuvel A, Robinson DJ, Sterenberg HJCM, et al. Ex vivo quantification of mTHPC concentration in tissue: influence of chemical extraction on the optical properties. *J Photochem Photobiol B* 2008;91:99–107. <http://dx.doi.org/10.1016/j.jphotobiol.2008.02.003>.
- [26] Reshetov V, Zorin V, Siupa A, D'Hallewin M-A, Guillemin F, Bezdetnaya L.

- Interaction of liposomal formulations of meta-tetra(hydroxyphenyl)chlorin (temoporfin) with serum proteins: protein binding and liposome destruction. *Photochem Photobiol* 2012;88:1256–64. <http://dx.doi.org/10.1111/j.1751-1097.2012.01176.x>.
- [27] Belitchenko I, Melnikova V, Bezdetnaya L, Rezzoug H, Merlin JL, Potapenko a, et al. Characterization of photodegradation of meta-tetra(hydroxyphenyl)chlorin (mTHPC) in solution: biological consequences in human tumor cells. *Photochem Photobiol* 1998;67:584–90.
- [28] Compagnin C, Moret F, Celotti L, Miotto G, Woodhams JH, MacRobert AJ, et al. Meta-tetra(hydroxyphenyl)chlorin-loaded liposomes sterically stabilised with poly(ethylene glycol) of different length and density: characterisation, in vitro cellular uptake and phototoxicity. *Photochem Photobiol Sci* 2011;10:1751–9. <http://dx.doi.org/10.1039/c1pp05163f>.
- [29] Palumbo M, Hogan C, Sottile F, Bagalá P, Rubio A. Ab initio electronic and optical spectra of free-base porphyrins: the role of electronic correlation. *J Chem Phys* 2009;131:84102. <http://dx.doi.org/10.1063/1.3204938>.
- [30] Serrano-Andrés L, Merchán M, Rubio M, Roos BO. Interpretation of the electronic absorption spectrum of free base porphyrin by using multiconfigurational second-order perturbation theory. *Chem Phys Lett* 1998;295:195–203. [http://dx.doi.org/10.1016/S0009-2614\(98\)00934-8](http://dx.doi.org/10.1016/S0009-2614(98)00934-8).
- [31] Steiner E, Fowler PW. Mapping the global ring currents in porphyrins and chlorins. In: Grimm B, Porra RJ, Rüdiger W, Scheer H, editors. *Chlorophylls and bacteriochlorophylls*. Netherlands: Springer; 2006. p. 337–47.
- [32] Shkirman SF, Solov'ev KN, Kachura TF, Arabei SA, Skakovskii ED. Interpretation of the Soret band of porphyrins based on the polarization spectrum of N-methyltetraphenylporphyrin fluorescence. *J Appl Spectrosc* 2001;66:68–75. <http://dx.doi.org/10.1007/BF02679221>.
- [33] Tokita Y, Hasegawa J, Nakatsuji H. SAC-CI study on the excited and ionized states of free-base porphyrin: rydberg excited states and effect of polarization and rydberg functions. *J Phys Chem A* 1998;102:1843–9. <http://dx.doi.org/10.1021/jp9731361>.
- [34] Nguyen KA, Pachter R. Ground state electronic structures and spectra of zinc complexes of porphyrin, tetraazaporphyrin, tetrabenzoporphyrin, and phthalocyanine: a density functional theory study. *J Chem Phys* 2001;114:10757–67. <http://dx.doi.org/10.1063/1.1370064>.
- [35] Nemykin VN, Hadt RG, Belosludov RV, Mizuseki H, Kawazoe Y. Influence of molecular geometry, exchange-correlation functional, and solvent effects in the modeling of vertical excitation energies in phthalocyanines using time-dependent density functional theory (TDDFT) and polarized continuum model TDDFT methods: ca. *J Phys Chem A* 2007;111:12901–13. <http://dx.doi.org/10.1021/jp0759731>.
- [36] Tian F, Johnson EM, Zamarripa M, Sansone S, Brancalion L. Binding of porphyrins to tubulin heterodimers. *Biomacromolecules* 2007;8:3767–78. <http://dx.doi.org/10.1021/bm700687x>.
- [37] Krupitsky H, Stein Z, Goldberg I. Molecular structure and intermolecular organization in the crystalline 1:2 complex of Zn(II)-tetra(3-hydroxyphenyl)porphyrin with dimethylsulphoxide. *Z Für Krist - Cryst Mater* 2010;210:665–8. <http://dx.doi.org/10.1524/zkri.1995.210.9.665>.
- [38] Gravier J, Korchowicz B, Schneider R, Rogalska E. Interaction of amphiphilic chlorin-based photosensitizers with 1,2-dipalmitoyl-sn-glycero-3-phosphocholine monolayers. *Chem Phys Lipids* 2009;158:102–9. <http://dx.doi.org/10.1016/j.chemphyslip.2009.01.004>.
- [39] Reshetov V, Kachatkov D, Shmigol T, Zorin V, D'Hallewin M-A, Guillemin F, et al. Redistribution of meta-tetra(hydroxyphenyl)chlorin (m-THPC) from conventional and PEGylated liposomes to biological substrates. *Photochem Photobiol Sci* 2011;10:911–9. <http://dx.doi.org/10.1039/C0PP00303D>.
- [40] Reshetov VA, Zorina TE, D'Hallewin M-A, Bolotina LN, Zorin VP. Fluorescence methods for detecting the kinetics of photosensitizer release from nanosized carriers. *J Appl Spectrosc* 2011;78:103–9. <http://dx.doi.org/10.1007/s10812-011-9431-z>.
- [41] Pettersen EF, Goddard TD, Huang CC, Couch GS, Greenblatt DM, Meng EC, et al. UCSF Chimera – a visualization system for exploratory research and analysis. *J Comput Chem* 2004;25:1605–12. <http://dx.doi.org/10.1002/jcc.20084>.
- [42] Antonenko YN, Kotova EA, Omarova EO, Rokitskaya TI, Ol'shevskaya VA, Kalinin VN, et al. Photodynamic activity of the boronated chlorin e6 amide in artificial and cellular membranes. *Biochim Biophys Acta - Biomembr* 2014;1838:793–801. <http://dx.doi.org/10.1016/j.bbame.2013.11.012>.
- [43] Konttila R, Salonen I, Virtanen JA, Kinnunen PKJ. Estimation of the equilibrium lateral pressure in liposomes of 1-palmitoyl-2-[10-(pyren-1-yl)-10-ketodecanoyl]-sn-glycero-3-phosphocholine and the effect of phospholipid phase transition. *Biochemistry* 1988;27:7443–6. <http://dx.doi.org/10.1021/bi00419a040>.
- [44] Noss I, Liddell PA, Moore AL, Moore TA, Gust D. Aryl ring rotation in porphyrins. A carbon-13 NMR spin – lattice relaxation time study. *J Phys Chem B* 1997;101:458–65. <http://dx.doi.org/10.1021/jp962209y>.
- [45] Rosa A, Ricciardi G, Baerends EJ. Synergism of porphyrin-core saddling and twisting of meso-aryl substituents. *J Phys Chem A* 2006;110:5180–90. <http://dx.doi.org/10.1021/jp060931i>.

6. Nanoshuttle mechanism of mTHPC delivery

The third part of the results has published the article “The alteration of temoporfin distribution in multicellular tumor spheroids by β -cyclodextrins” and reveals the features of mTHPC/ β -CDs complexes behavior in tumor tissue.

We studied the ability of Me- β -CD and Hp- β -CD to alter the penetration and diffusion of mTHPC in HT29 multicellular tumor spheroid model. It was demonstrated that the presence of β -CDs significantly changed the distribution of mTHPC consisting in the increase of both the depth of PS penetration and accumulation in HT29 spheroids. Depending on the type and concentration of β -CD, mTHPC accumulation in spheroids could be increased up to 3 times for Hp- β -CD, while deeper penetration in the tumor tissue was observed for Me- β -CD-based complexes. Based on the obtained data, we suggested that β -CDs facilitate mTHPC transportation to the cells in the inner layers of spheroids *via* nanoshuttle mechanism. This study demonstrated the added value of β -CD to liposomes inducing improved accumulation, diffusion and penetration of the photosensitizer mTHPC in tumor tissue.



Contents lists available at ScienceDirect

International Journal of Pharmaceutics

journal homepage: www.elsevier.com/locate/ijpharm

Research Paper

The alteration of temoporfin distribution in multicellular tumor spheroids by β -cyclodextrinsIlya Yakavets^{a,b,c}, Igor Yankovsky^c, Marie Millard^{a,b}, Laureline Lamy^b, Henri-Pierre Lassalle^{a,b}, Arno Wiehe^d, Vladimir Zorin^{c,e}, Lina Bezdetnaya^{a,b,*}^a Centre de Recherche en Automatique de Nancy (CRAN), CNRS UMR 7039 (Centre National de la Recherche Scientifique), Université de Lorraine, Campus Sciences, 54500, Vandœuvre-lès-Nancy, France^b Institut de Cancérologie de Lorraine, Research Department, Avenue de Bourgogne, 54519, Vandœuvre-lès-Nancy, France^c Laboratory of Biophysics and Biotechnology, Physics Faculty, Belarusian State University, 4 Nezavisimosti Av., 220030, Minsk, Belarus^d Biolitec Research GmbH, Otto-Schott-Str. 15, 07745 Jena, Germany^e Belarusian State University, ISEI BSU, Dauhabrodskaja 23, 220070 Minsk, Belarus

ARTICLE INFO

Article history:

Received 11 April 2017

Accepted 11 July 2017

Available online 12 July 2017

Chemical compounds studied in this article:

meta-Tetrakis(3-hydroxyphenyl)chlorin

(PubChem CID: 60751)

Methyl- β -cyclodextrin (PubChem CID:

51051622)

2-Hydroxypropyl- β -cyclodextrin

(PubChem CID: 44134771)

Keywords:

Cyclodextrins

mTHPC

Inclusion complexes

Photodynamic therapy

Spheroid

Penetration

ABSTRACT

To be effective anticancer drugs must penetrate tissue efficiently, reaching all target population of cancer cells in a concentration sufficient to exert a therapeutic effect. This study aimed to investigate the ability of methyl- β -cyclodextrin (Me- β -CD) and 2-hydroxypropyl- β -cyclodextrin (Hp- β -CD) to alter the penetration and diffusion of temoporfin (mTHPC) in HT29 multicellular tumor spheroids. mTHPC had a nonhomogenous distribution only on the periphery of spheroids. The presence of β -CDs significantly altered the distribution of mTHPC consisting in the increase of both the depth of photosensitizer penetration and accumulation in HT29 spheroids. We suggest that this improvement is related to the nanoshuttle mechanism of β -CD action, when β -CDs facilitate mTHPC transportation to the cells in the inner layers of spheroids. As a result of mTHPC distribution improvement, β -CDs enhance mTHPC photosensitizing activity towards HT29 multicellular tumor spheroids. The observed effects strongly depend on the type of β -CD. Thus, varying the type of β -CD we can finely tune the possibility of using mTHPC for diagnostic (delimitation of tumor margins) or therapeutic purposes.

© 2017 Elsevier B.V. All rights reserved.

1. Introduction

Photodynamic therapy (PDT) is a promising approach for cancer treatment, which involves the photonic excitation of a photosensitizer (PS) in the presence of ambient oxygen, forming reactive oxygen species (Agostinis et al., 2011; Castano et al., 2004). These activated oxygen toxic species diffuse for a few tens of nanometers from PS binding site and therefore the PDT-induced phototoxic effect is limited to PS distribution volume and the compartments of PS intracellular localization (Josefsen and Boyle, 2012; Moan, 1990; Zorin et al., 1996). To be most effective anticancer drugs must penetrate tissue efficiently, reaching target population of cancer

cells in a concentration sufficient to exert a therapeutic effect. Since a while, nanoscale materials were extensively considered in PDT since they can overcome critical limitations of conventional PSs related to unfavorable PS distribution and incomplete tumor elimination (Duchêne and Bochet, 2016; Lim et al., 2013; Marchal et al., 2015; St Denis and Hamblin, 2015).

Temoporfin (*meta*-tetrakis(3-hydroxyphenyl)chlorin, mTHPC) is a highly efficient clinically approved photosensitizer, used as an ethanol/propylene glycol-based formulation (Foscan[®]; biolitec Pharma Ltd., Jena, Germany) for the treatment of head and neck cancers (Senge, 2012; Senge and Brandt, 2011). Actual studies, focused on nanoparticle-based mTHPC formulations, including

Abbreviations: PDT, photodynamic therapy; PS, photosensitizer; mTHPC, *meta*-tetrakis(3-hydroxyphenyl)chlorin; β -CD, β -cyclodextrin; 3D, three-dimensional; MTS, multicellular tumor spheroid; Me- β -CD, methyl- β -cyclodextrin; Hp- β -CD, 2-hydroxypropyl- β -cyclodextrin; PBS, phosphate buffered saline.

* Corresponding author at: Institut de Cancérologie de Lorraine, 6 Avenue de Bourgogne, CS 30519, 54519 Vandoeuvre-lès-Nancy, Cedex, France.

E-mail address: l.bolotina@nancy.unicancer.fr (L. Bezdetnaya).

<http://dx.doi.org/10.1016/j.ijpharm.2017.07.037>

0378-5173/© 2017 Elsevier B.V. All rights reserved.

liposomes, demonstrated numerous advantages (solubility, delivery and photodynamic action) of these formulations over free mTHPC. However, a fragile mTHPC liposomal integrity in the circulation along with a limited penetration of mTHPC liposomal formulations in tumor tissue may restrain mTHPC-based liposomal applications (Gaio et al., 2016; Mitra et al., 2005; Reshetov et al., 2012).

Recently, we have demonstrated the perspectives of using cyclic oligosaccharides, β -cyclodextrin (β -CD) derivatives, as nanoscale delivery system for mTHPC. According to our data, β -CDs increase diffusion movement of mTHPC molecules between serum proteins, significantly accelerating the delivery of PS to targets cells and tissues (Yakavets et al., 2017; Yankovsky et al., 2016). We suggested that β -CDs extract mTHPC molecule from lipoprotein carrier and form inclusion complexes. The small size of inclusion complexes makes possible faster diffusion of PS molecule in blood and interstitial medium. This mechanism, termed “nanoshuttle” could be used to improve both limited penetration and spatial distribution of mTHPC throughout a solid tumor in the presence of CDs.

The three-dimensional (3D) spheroid cancer cells closely resemble small avascular *in vivo* tumors representing a reliable model for investigating the ability of anticancer drugs to penetrate and diffuse into the tumor. Spheroids were also suggested to be a good predictive platform for studying the drug delivery systems, including mTHPC-loaded solid lipid nanoparticles and liposomal formulations (Gaio et al., 2016; Hinger et al., 2016; Patel et al., 2015).

The aim of present work was to explore the possibility afforded by β -CDs to exert a nanoshuttle action on mTHPC delivery, distribution and diffusion in multicellular tumor spheroids (MTSs). The photoinduced toxicity of mTHPC/ β -CDs complexes in spheroids was an end-point of the present research.

2. Material and methods

2.1. Chemicals and reagent preparation

mTHPC was kindly provided by biolitec research GmbH (Jena, Germany). mTHPC stock solution (1 mM) was prepared in absolute

ethanol (99.6%) and kept at 4 °C in the dark. The concentration of mTHPC in the solution was estimated by a spectroscopy using molar extinction coefficient of $30,000\text{ M}^{-1}\text{ cm}^{-1}$ at 650 nm in ethanol. For *in vitro* cell culture experiments mTHPC stock solution was diluted in phenol red-free Roswell Park Memorial Institute 1640 medium (RPMI-1640, Invitrogen™, Carlsbad, California, USA), supplemented with 2% fetal calf serum (Life Technologies, Carlsbad, California, USA) to reach, unless otherwise indicated the final mTHPC concentration of 4.5 μM .

Methyl- β -cyclodextrin (Me- β -CD) and 2-hydroxypropyl- β -cyclodextrin (Hp- β -CD) were purchased from AraChem (Tilburg, the Netherlands). Inclusion complexes between β -CDs and mTHPC (Scheme 1) were formed using co-precipitation method (Del Valle, 2004). Briefly, β -CDs were dissolved in phosphate buffered saline (PBS, GIBCO™, Thermo Fisher Scientific, Waltham, Massachusetts, USA) at the required concentrations with the subsequent addition of mTHPC stock solution. The final content of ethanol in the mTHPC/ β -CD solutions did not exceed 0.5%. Solution was thoroughly mixed over 15 min under magnetic stirring.

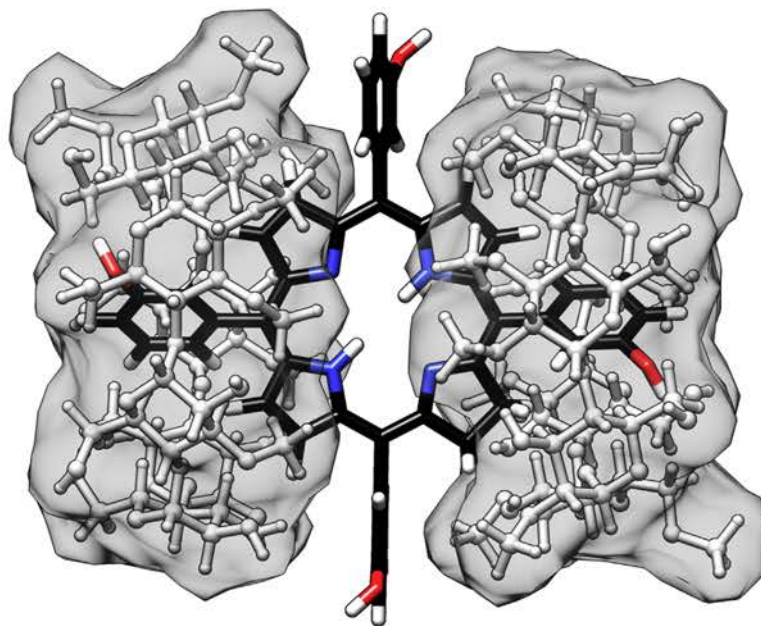
2.2. Monolayer and spheroid cell cultures

2.2.1. Culture conditions

HT29 human adenocarcinoma cells were obtained from the ATCC® (LGC Promochem, Molsheim, France) and regularly controlled for mycoplasma contamination. HT29 cells were maintained in RPMI-1640 medium supplemented with 9% (vol/vol) heat-inactivated fetal calf serum, penicillin (10,000 IU), streptomycin (10,000 $\mu\text{g}/\text{mL}$), and 1% (vol/vol) 0.1 M glutamine (Life Technologies, Carlsbad, CA, USA). Cells were kept as a monolayer culture in a humidified incubator (5% CO_2) at 37 °C. Cell culture was reseeded every week to ensure exponential growth.

2.2.2. Generation of spheroids

Multicellular spheroids were initiated by seeding 5×10^4 HT29 cells into 75 cm^2 flasks (Costar Corning, NY, USA) previously coated with 1% L-agarose. After 3 days, aggregates were transferred to 250 mL spinner flasks (Integra Biosciences, Zizers, Switzerland) containing 150 mL of culture medium. The flasks were then placed



Scheme 1. Possible structure of 1:2 inclusion complex of mTHPC/2 β -CDs.

on magnetic plates (Integra Biosciences, Zizers, Switzerland) at 75 rpm in 5% CO₂ and 37 °C humidified atmosphere. Five days after seeding, aggregates were filtered through 100 and 150 μm sterile nylon screen (VWR International, Radnor, Pennsylvania, USA) in order to obtain a homogeneous population of 100–150 μm in diameter. Spheroid culture medium was changed every 2–3 days. When spheroids reached 500 μm in diameter after 15 days, they were used for experiments.

For dissociation, spheroids were transferred into a 15 mL flask, washed twice with PBS and incubated with 0.05% trypsin (GIBCO™, Thermo Fisher Scientific, Waltham, Massachusetts, USA) – 0.02% ethylenediaminetetraacetic acid (EDTA, GIBCO™, Thermo Fisher Scientific, Waltham, Massachusetts, USA). After dissociation, trypsin action was inhibited by addition of culture medium, cell suspension was centrifuged to a pellet and further resuspended in fresh medium.

2.2.3. Uptake of mTHPC in spheroids

mTHPC was added to a set of 50 spheroids at the concentration 4.5 μM. Photosensitizer incubation was performed in the dark at 37 °C in a humidified 5% CO₂ air atmosphere for 24 h. After that, spheroids were dissociated and individual cells were subjected to the extraction of mTHPC with ethanol (99.6%). The mTHPC fluorescence intensity was measured by spectrofluorometer (PerkinElmer, Waltham, MA, USA) (λ_{ex} = 416 nm; λ_{em} = 652 nm) and was related to fluorescence calibration curves of mTHPC standard solution in ethanol. The obtained mTHPC concentration was normalized to the number of spheroids.

2.2.4. Flow cytometry experiments

Flow cytometry analysis was performed using FACSCalibur (BD, Franklin Lakes, USA), equipped with laser emitting at 488 nm. The mTHPC fluorescence was detected in fluorescence channel FL4 with a 661 ± 16 nm filter. HT29 cell suspension was obtained after spheroids dissociation. Data analysis was carried out with the trial version of Kaluza® Flow Analysis Software (Beckman Coulter, Inc., Brea, USA).

2.2.5. Imaging of mTHPC distribution

mTHPC was added to a set of 50 spheroids at the concentration 4.5 μM. Photosensitizer incubation was performed in the dark at 37 °C in a humidified 5% CO₂ air atmosphere for 24 h. After that spheroids have been transferred 35 mm Petri dishes, washed twice with PBS and directly observed on an upright epifluorescence microscope (AX-70 Provis, Olympus, Tokyo, Japan) equipped with a

100 W mercury vapor lamp and a Peltier cooled CCD camera (DP70, Olympus, Tokyo, Japan). The filter was set at 400–440 nm band pass excitation associated with a 570 nm dichroic mirror and a 590 nm long pass emission filter for mTHPC fluorescence measurements. Fluorescence images were recorded using 4× objective from the spheroid surface. The line profiles were calculated from 15 radial lines, which were randomly drawn at the images of spheroid equatorial planes with the ImageJ software.

2.2.6. Photodynamic treatment

Fifty HT29 spheroids were transferred from the spinner flask to 35 mm Petri dishes. Incubation with 3 mL of complete medium containing 4.5 μM of mTHPC was performed at 37 °C in the dark for 24 h. After three washes with PBS, spheroids were transferred into 35 mm Petri dishes containing 3 mL culture medium and subjected to irradiation. Irradiations were performed at 652 nm with a Ceralas PDT diode laser (CeramOptec GmbH, Bonn, Germany) at various fluences administered at the fluence rate of 30 mW cm⁻². The irradiation times were adapted for each irradiation so that equivalent fluences of 10, 20, 30 and 40 J cm⁻² were delivered. Control spheroids were exposed to mTHPC only (drug, no light).

2.2.7. Photocytotoxicity experiments

Cells were collected from spheroids with trypsin immediately after PDT. They were counted with a Thoma hemocytometer by using trypan blue exclusion assay in order to determine cell yield following PDT treatment. Intact cells were seeded in triplicate into 6-well plates for plating efficiency according to a clonogenic cell survival assay previously described (Franken et al., 2006). Over this bottom layer, 500 cells were plated in 1 mL culture medium. Cultures were incubated at 37 °C with 5% CO₂ in air for 14 days. Colonies composed of more than 50 cells were counted manually.

2.2.8. Statistics

All the experimental data were presented as mean values ± standard error of mean. The data were evaluated using Student's *t*-test. The difference was considered significant at *P* < 0.05.

3. Results

3.1. mTHPC uptake in MTSs

mTHPC uptake in MTSs was evaluated at different β-CDs concentrations after 24 h incubation. Spheroids treated with mTHPC only (4.5 μM) were taken as a control sample (100% of

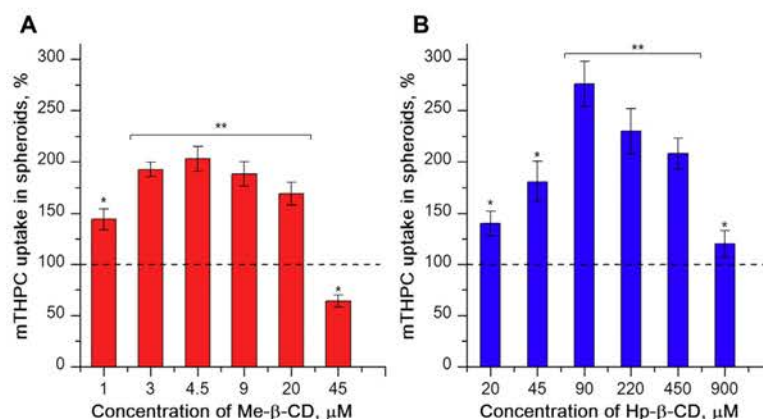


Fig 1. Effect of β-CDs on the relative level of mTHPC uptake in HT29 spheroids. mTHPC uptake in HT29 spheroids after 24 h incubation in the presence of (A) Me-β-CD and (B) Hp-β-CD. mTHPC uptake with β-CDs was normalized to control sample (mTHPC in β-CD free medium) taken as 100% (dashed line). *statistically different from control sample, *P* < 0.05; **statistically different from control, *P* < 0.01.

mTHPC uptake). According to Fig. 1(A&B), the β -CDs alter the mTHPC accumulation in MTSs. This effect critically depends on the concentration and on the type of β -CD derivatives. In a certain range of β -CDs concentrations, its increase leads to the enhancement of mTHPC uptake. Twice higher accumulation of mTHPC was observed at 4.5 μ M Me- β -CD (Fig. 1A) while nearly a three times higher mTHPC uptake was registered in the presence of 90 μ M Hp- β -CD (Fig. 1B). Further increase in concentrations of both β -CDs was accompanied by a gradual decrease of mTHPC uptake in MTSs.

In the next step we compared the rates of mTHPC accumulation in the presence of β -CDs. To observe the maximal effect, the optimal concentrations of β -CDs were taken as 4.5 μ M and 90 μ M for Me- β -CD and of Hp- β -CD respectively. HT29 spheroids incubated in the cyclodextrin-free medium accumulate mTHPC very slowly with a high initial uptake rate (0.75 ng spheroid⁻¹ h⁻¹ at 3 h of incubation) (Fig. 2). The addition of β -CDs significantly accelerates mTHPC accumulation. The highest effect was observed with Hp- β -CD (the initial uptake rate was up to 3.03 ng spheroid⁻¹ h⁻¹) (Fig. 2), while in the presence of Me- β -CD we noted an increase of initial uptake rate up to 1.55 ng spheroid⁻¹ h⁻¹ (Fig. 2). The uptake rate at 24 h was 0.37 ng spheroid⁻¹ h⁻¹ for both Hp- β -CD and Me- β -CD inclusion complexes, compared to 0.17 ng spheroid⁻¹ h⁻¹ for mTHPC without β -CDs.

3.2. mTHPC distribution in HT29 spheroids

Epifluorescent microscopy technique was used to obtain the distribution patterns of either mTHPC alone or mTHPC/ β -CD formulations in MTSs after 24 h incubation (Fig. 3). In this 3D tumor model, mTHPC without β -CDs was mainly accumulated on the MTS periphery (Fig. 3A). The analysis of linear profiles demonstrated a strong pattern of mTHPC fluorescence in the outer rim of the spheroid with the intensity 30 a.u. that falls off twice in the center (Fig. 3D). The addition of β -CDs significantly increased the overall mTHPC fluorescence intensity (Figures 3 B&C). The most interesting features were observed in the case of Me- β -CD. This compound completely modified mTHPC fluorescence distribution pattern (Fig. 3C). The fluorescence profiles were characterized by a smooth mTHPC distribution across the spheroid

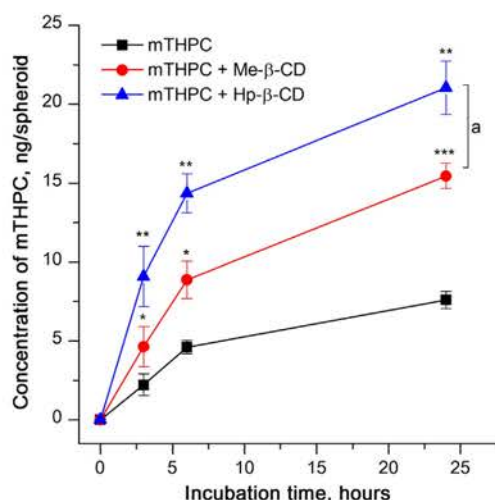


Fig. 2. Kinetics of mTHPC uptake in HT29 spheroids. Concentration of mTHPC was evaluated after the different times of spheroids incubation with mTHPC alone, mTHPC/Me- β -CD and mTHPC/Hp- β -CD. CDs concentrations were 4.5 μ M for Me- β -CD and 90 μ M for Hp- β -CD. mTHPC concentration was 4.5 μ M. *statistically different from control (mTHPC alone) sample $P < 0.05$; **statistically different from control sample, $P < 0.01$; ***statistically different from control sample, $P < 0.001$; ^astatistically different between the samples with Me- β -CD and Hp- β -CD, $P < 0.05$.

with the mean fluorescence intensity 35 a.u. (Fig. 3E). At the same time, Hp- β -CD demonstrated the increase of the fluorescence intensity on the periphery of MTSs up to 47 a.u. while in the central area it was comparable with that of Me- β -CD/mTHPC (30 a.u.) (Fig. 3F).

The fluorescence microscopy study was further refined by evaluating the heterogeneity of mTHPC distribution in spheroid cells by flow cytometry technique (Fig. 4). The level of cellular autofluorescence in spheroid cells was very low (0.21 a.u.) (Fig. 4A). Typical fluorescence profiles of dissociated spheroids exposed to 4.5 μ M mTHPC alone or to mTHPC/ β -CDs are displayed on the Fig. 4(B–D). We discriminate two subpopulations of spheroid cells based on mTHPC fluorescence intensity: dimmest and brightest. In the case of mTHPC only, the brightest subpopulation (B+) counts for only 10.6% (Fig. 4B), while the addition of β -CDs leads to the increase of this fraction up to ca 32% and 51% for Hp- β -CD (Fig. 4C) and Me- β -CD (Fig. 4D) respectively. The degree of heterogeneity of mTHPC distribution was assessed through the ratio of mean fluorescence intensity of single cells (x-median value) in subpopulation (B+) to that of (B–). Without β -CDs, (B+) subpopulation was more than 50 times brighter as compared to the dimmest one. The presence of Hp- β -CD increased the heterogeneity of mTHPC distribution and the ratio reached 130. At the same time, the addition of Me- β -CD leads to a more homogeneous mTHPC distribution throughout spheroid. In this case, the intensity ratio (B+/B–) was only about 19. Taken as a whole, the flow cytometry results were consistent with fluorescent microscopy data and indicated the heterogeneity of mTHPC distribution in spheroid cells for all PS formulations decreasing in a range Hp- β -CD > mTHPC > Me- β -CD.

3.3. mTHPC photocytotoxicity in MTSs

Considering that the better mTHPC homogeneity in spheroids was achieved with Me- β -CD/mTHPC formulations, we further assessed the clonogenic ability of spheroids loaded with Me- β -CD/mTHPC and subjected to different fluences of red light irradiation (Fig. 5). The data were compared with photokilling activity of mTHPC only. For both formulations cellular viability strongly depended on the applied fluence with a higher photocytotoxicity observed for Me- β -CD/mTHPC formulations. At the light dose as low as 20 J cm⁻² the Me- β -CD/mTHPC photocytotoxicity was 25% higher than that of mTHPC-PDT only ($P < 0.05$). This difference decreased at higher light fluences.

4. Discussion

High accumulation and penetration of anticancer drugs have always been primary factors responsible for optimal antitumor efficiency. These parameters must be carefully considered when evaluating photosensitizing agents, since their non-homogeneous distribution into the tumor mass may lead to incomplete tumor eradication (West and Moore, 1992). The distribution processes in tissues is especially important in the case of non-polar compounds, such as mTHPC (Senge, 2012), which possesses a complex time-dependent distribution in tumor tissues (Mitra et al., 2005). Multicellular spheroids allow to simulate the penetration and intratumor transport of anticancer nanomedicines, including photoactive nanoparticles (Evans, 2015; Khanna et al., 2014; Waite and Roth, 2012).

To date, numerous nano-platforms using a variety of organic and inorganic nanomaterials have been studied for efficient and targeted mTHPC delivery (Chen et al., 2010; Hinger et al., 2016; Hofman et al., 2008; Löw et al., 2011; Reshetov et al., 2013; Yankovsky et al., 2016). However, current mTHPC nanocarriers sometimes are not able to overcome the complications of mTHPC

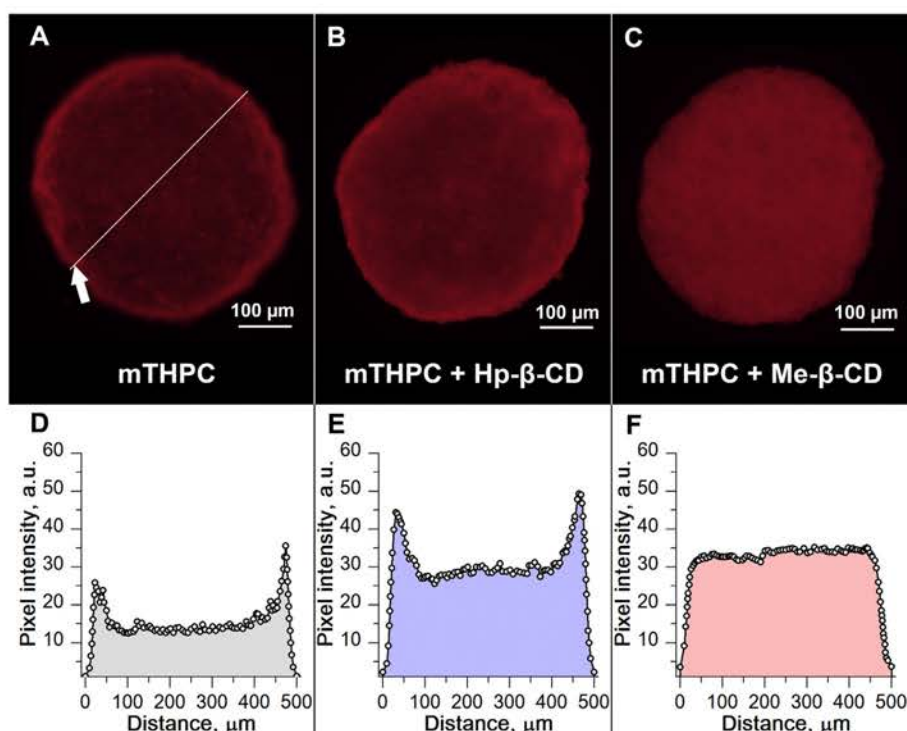


Fig. 3. Fluorescence patterns of spheroids after 24 h incubation with mTHPC, mTHPC/Me- β -CD and mTHPC/Hp- β -CD β -CDs. Fluorescence image (A) and fluorescence intensity profile (D) of mTHPC in HT29 spheroids. Fluorescence image (B) and fluorescence intensity profile (E) of mTHPC in spheroids in the presence of Hp- β -CD. Fluorescence image (C) and fluorescence intensity profile (F) of mTHPC in spheroids in the presence of Me- β -CD. Concentrations of Me- β -CD and Hp- β -CD were 4.5 μ M and 90 μ M respectively. mTHPC concentration was 4.5 μ M.

distribution. For example, non-PEGylated (Foslip[®]) and PEGylated (Fospeg[®]) liposomal mTHPC formulations were unable to improve mTHPC distribution in HeLa spheroids (Gaio et al., 2016), perhaps due to limited penetration of liposomal carriers. Similar results were observed for nanostructured mTHPC lipid carriers (Lipidots) and mTHPC-loaded PLGA nanoparticles (Hinger et al., 2016; Löw et al., 2011). Authors suggested that the size of nanoparticles matters significantly (Hinger et al., 2016). However, even the smallest (50 nm) Lipidots demonstrated less penetration depth and uptake than mTHPC alone in 3D tumor model.

Recently, we proposed a new type of mTHPC formulations based on the inclusion complexation with cyclic oligosaccharides as β -CDs (Yakavets et al., 2017; Yankovsky et al., 2016). β -CD is a common drug delivery system and finds numerous applications in nanomedicine due to the unique ability to form noncovalent inclusion complexes with a variety of drugs (Bautista-Sanchez et al., 2005; Duchêne, 2011; Stella et al., 1999). The complexation of mTHPC with β -CDs results in a complete abolishment of mTHPC aggregation in aqueous solutions and significantly alters mTHPC distribution *in vitro* and *in vivo* through nanoshuttle mechanism. In the present study we addressed the mechanisms of β -CDs alteration of mTHPC distribution in multicellular tumor spheroids.

Figs. 1 and 2 illustrate the influence of β -CDs on mTHPC accumulation in HT29 spheroids. mTHPC uptake critically depends on concentration and type of β -CDs. Recently, we reported the similar concentration dependence pattern of mTHPC uptake in HT29 monolayer cells (Yankovsky et al., 2016). We demonstrated that at moderate concentrations β -CDs accelerated mTHPC transportation between serum proteins and cells, while excess of β -CDs led to the high probability of inclusion complex formation, hampering mTHPC availability for biological targets. An optimal mTHPC accumulation was obtained at the concentration of Me- β -CD 15–20 times less as compared to Hp- β -CD, being

apparently the result of different mTHPC affinity to β -CDs. Indeed, according to Bautista-Sanchez et al. (Bautista-Sanchez et al., 2005), the Hp- β -CD binding constant is at least 5 times lower than that for Me- β -CD.

We further assessed an impact of β -CDs on mTHPC distribution in spheroid bulk. According to our results, the most intensive mTHPC fluorescence was observed on the periphery of MTSs (Fig. 3A&D). The application of a more sensitive laser confocal scanning microscopy technique suggested the heterogeneous fluorescence pattern of MTSs and showed that practically all mTHPC fluorescence concentrated in 2530 μ m of HeLa and EMT6 spheroids outer layer (Coutier et al., 2001; Gaio et al., 2016). The presence of Hp- β -CD increases the overall fluorescence level, however mTHPC fluorescence pattern with the peripheral intensities peaks remains almost unchanged (Fig. 3B&E). A quite different mTHPC fluorescence distribution was observed in the case of another β -CD (Fig. 3C). In the presence of Me- β -CD mTHPC penetrated deeper in MTS and a more homogeneous mTHPC distribution was achieved (Fig. 3F).

Flow cytometry analysis confirmed the alteration of mTHPC distribution in HT29 spheroids in the presence of β -CDs (Fig. 4). According to our data, only 10% of cells incubated with mTHPC alone were characterized by an enhanced mTHPC fluorescence (Fig. 4B), suggesting a limited penetration depth of mTHPC through tumor tissue. This pattern could be attributed to the unique binding and retention mTHPC properties in cells (Ball et al., 1999; Mitra and Foster, 2005), conditioning an increased sequestration ability of mTHPC in cells and as such limiting the PS penetration in tissue. In the case of Hp- β -CD we observed 30% of bright cells, with the ratio between brightness and dimmest cell population intensities as 130 (Fig. 4C). The addition of Me- β -CD increased the number of cells with high mTHPC fluorescence intensity B+ (up to 50%) (Fig. 4D). In addition, Me- β -CD treatment leads to the

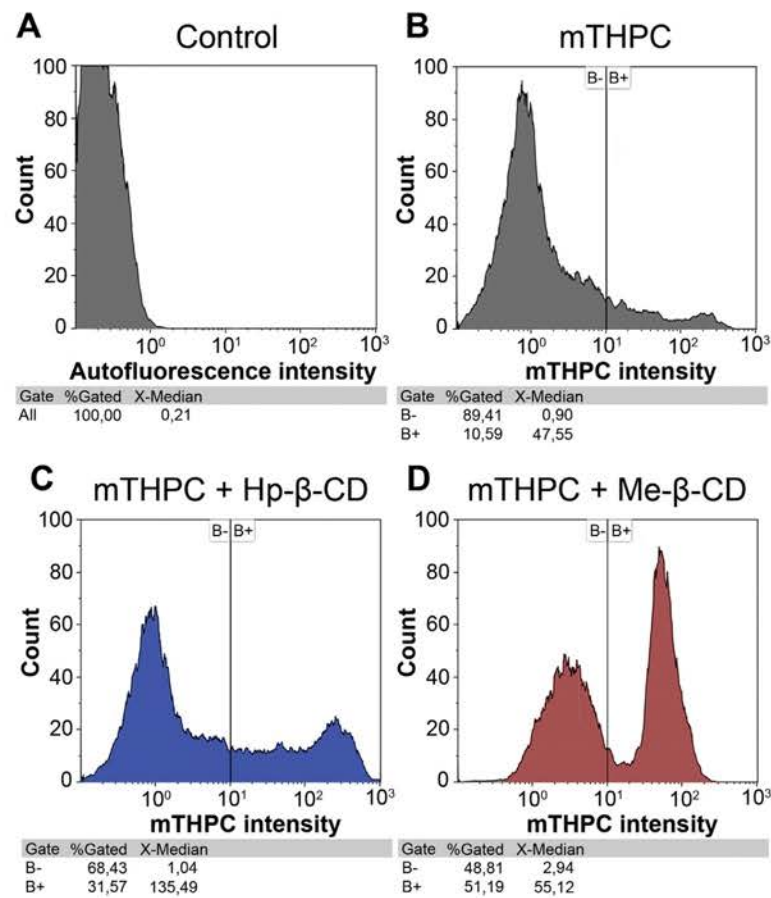


Fig. 4. Histogram of cellular autofluorescence and mTHPC fluorescence in function of cell counts in HT29 spheroids after 24 h incubation with different mTHPC formulations. (A) Spheroids cells autofluorescence. Spheroids treated with (B) mTHPC alone (4.5 μM), (C) mTHPC (4.5 μM) with 90 μM Hp- β -CD and (D) mTHPC (4.5 μM) with 4.5 μM Me- β -CD. Log scale fluorescence is shown on the x-axis. The brightest subpopulation (mTHPC intensity >10) was gated as (B+); (B-) stands for the dimmest cell subpopulation (mTHPC intensity <10).

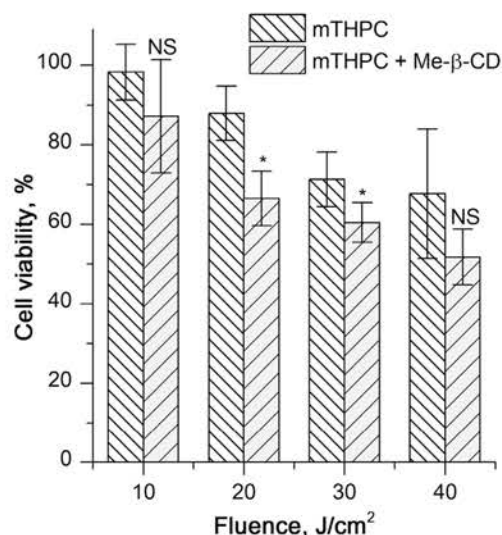
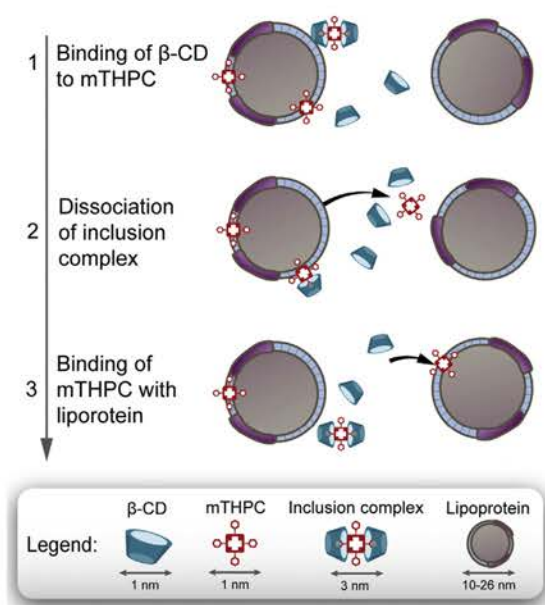


Fig. 5. Cell viability of spheroids incubated 24h with different mTHPC formulations. The percentage of cell survival was counted by means of clonogenic assay 15 days after PDT. mTHPC concentration was 4.5 μM . *statistically different from mTHPC alone treatment at the given fluence, $P < 0.05$; NS – no significant differences from mTHPC alone treatment at the given fluence, $P > 0.05$.

increase of mTHPC fluorescence intensity of cells from internal spheroid volume. As a result, the ratio of mean cellular intensities (B+/B-) decreased from 53 (mTHPC alone) to 19. Therefore, Me- β -CD delivers mTHPC more efficiently to inaccessible inner cell layers of spheroid improving the mTHPC penetration. Varying the different types of β -CDs, an optimal balance could be achieved between efficient diffusion and cellular affinity.

According to the recent study (Yankovsky et al., 2016), nanoshuttle mechanism of β -CDs action consists in three main stages (Scheme 2): i) the extraction of mTHPC by β -CDs from lipoprotein carrier; ii) the diffusion of inclusion complex until its dissociation; iii) the binding of mTHPC molecule to the nearest target. While the first two stages are strongly dependent on the properties of β -CDs. The higher Me- β -CD affinity to mTHPC, as compared to Hp- β -CD (Bautista-Sanchez et al., 2005), determines longer lifetime of inclusion complexes (Stella et al., 1999), thus rendering possible a deeper mTHPC penetration through spheroid, while inclusion complexes with Hp- β -CD are subjected to quick dissociation.

The additional factor, which facilitates PS penetration is a small size of β -CD inclusion complexes. According to numerous studies, the size of nanoparticles has a significant impact on their penetration rate into the tissues (Dreher et al., 2006). Inclusion complexes between mTHPC and β -CDs have a size about 3 nm (Glisoni et al., 2011). This value is much smaller as compared to the main natural transporter of mTHPC in plasma, lipoproteins (Sasnouski et al., 2005), with the size ca. 10–26 nm (Dobiášová



Scheme 2. Schematic representation of nanoshuttle mechanism exerted by β -cyclodextrins.

et al., 2005). Therefore, β -CD nanoshuttles can provide both the increase in intracellular mTHPC concentration and the improvement of mTHPC penetration across the spheroid. Similar mechanism may be involved in β -CD dependent alteration of mTHPC accumulation in the tumor tissues *in vivo* (Yankovsky et al., 2016).

Finally, we demonstrated that β -CDs impact the mTHPC-based PDT efficiency in HT29 spheroids. It is obvious, that enhanced mTHPC distribution should lead to the increased PDT efficacy. Me- β -CD induced 2 times higher mTHPC accumulation after 24 h incubation, compared to mTHPC only, while mTHPC-PDT cell viability decreased by only 25% in the presence of Me- β -CD/mTHPC complexes (Fig. 5). This could be related to the heterogeneous structure of spheroid with different properties of cell proliferation and with the various accessibility of deep layers to irradiation light (Patel et al., 2015).

5. Conclusions

Our study clearly demonstrated an advantage of using β -cyclodextrins as nanoshuttle systems inducing improved accumulation, diffusion and penetration of the photosensitizer mTHPC in spheroids. mTHPC formulations with Me- β -CD and Hp- β -CD showed 2 and 3 times higher mTHPC accumulation in spheroids. Microscopy and flow cytometry techniques demonstrated that besides higher mTHPC accumulation, different patterns of mTHPC distribution were inherent to both formulations. Hp- β -CD increases the mTHPC accumulation at the tumor periphery while in the presence of Me- β -CD intratumoral penetration of mTHPC is deeper and its distribution is much more homogeneous. Thus, varying the type of β -CD we can finely tune the possibility of using mTHPC for diagnostic (delimitation of tumor margins) or therapeutic purposes.

Acknowledgements

This work was supported by the Institut de Cancérologie de Lorraine, French "Ligue Nationale contre le Cancer (CCIR-GE)", Belarusian Republican Foundation for Fundamental Research (BRFFR) [grant number M16M-049 and grant number M17MC-

028]. Ilya Yakavets acknowledges the fellowship of the Ministry of Education of Belarus.

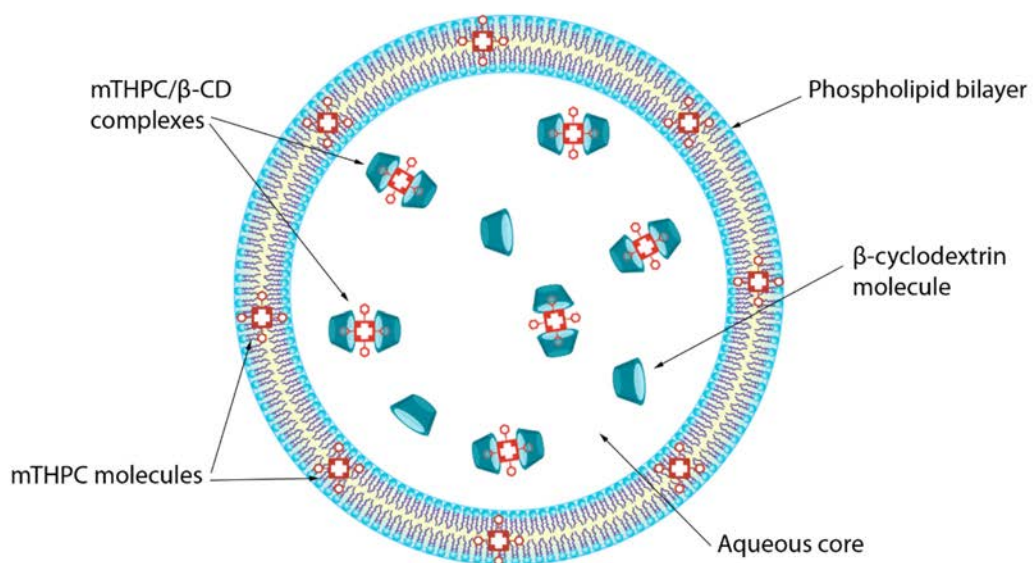
References

- Agostinis, P., Berg, K., Cengel, K.A., Foster, T.H., Girotti, A.W., Gollnick, S.O., Hahn, S. M., Hamblin, M.R., Juzeniene, A., Kessel, D., Korbelik, M., Moan, J., Mroz, P., Nowis, D., Piette, J., Wilson, B.C., Golab, J., 2011. Photodynamic therapy of cancer: an update. *CA Cancer J. Clin.* 61, 250–281. doi:http://dx.doi.org/10.3322/caac.20114.
- Ball, D.J., Vernon, D.I., Brown, S.B., 1999. The high photoactivity of m-THPC in photodynamic therapy. Unusually strong retention of m-THPC by RIF-1 cells in culture. *Photochem. Photobiol.* 69, 360–363. doi:http://dx.doi.org/10.1111/j.1751-1097.1999.tb03299.x.
- Bautista-Sanchez, A., Kasselouri, A., Desroches, M.-C., Blais, J., Maillard, P., de Oliveira, D.M., Tedesco, A.C., Prognon, P., Delaire, J., 2005. Photophysical properties of glucoconjugated chlorins and porphyrins and their associations with cyclodextrins. *J. Photochem. Photobiol. B* 81, 154–162. doi:http://dx.doi.org/10.1016/j.jphotobiol.2005.05.013.
- Castano, A.P., Demidova, T.N., Hamblin, M.R., 2004. Mechanisms in photodynamic therapy: part one-photosensitizers, photochemistry and cellular localization. *Photodiagn. Photodyn. Ther.* 1, 279–293. doi:http://dx.doi.org/10.1016/S1572-1000(05)00007-4.
- Chen, K., Wacker, M., Hackbarth, S., Ludwig, C., Langer, K., Röder, B., 2010. Photophysical evaluation of mTHPC-loaded HSA nanoparticles as novel PDT delivery systems. *J. Photochem. Photobiol. B* 101, 340–347. doi:http://dx.doi.org/10.1016/j.jphotobiol.2010.08.006.
- Coutier, S., Mitra, S., Bezdetsnaya, L.N., Parache, R.M., Georgakoudi, I., Foster, T.H., Guillemin, F., 2001. Effects of fluence rate on cell survival and photobleaching in meta-tetra-(hydroxyphenyl)chlorin-photosensitized colo 26 multicell tumor spheroids. *Photochem. Photobiol.* 73, 297–303. doi:http://dx.doi.org/10.1562/0031-8655(2001)073<0297:EOFROC>2.0.CO;2.
- Del Valle, E.M.M., 2004. Cyclodextrins and their uses: a review. *Process Biochem.* 39, 1033–1046. doi:http://dx.doi.org/10.1016/S0032-9592(03)00258-9.
- Dobiášová, M., Urbanová, Z., Samánek, M., 2005. Relations between particle size of HDL and LDL lipoproteins and cholesterol esterification rate. *Physiol. Res. Acad. Sci. Bohemoslov.* 54, 159–165.
- Dreher, M.R., Liu, W., Michelfich, C.R., Dewhirst, M.W., Yuan, F., Chilkoti, A., 2006. Tumor vascular permeability, accumulation, and penetration of macromolecular drug carriers. *J. Natl. Cancer Inst.* 98, 335–344. doi:http://dx.doi.org/10.1093/jnci/djj070.
- Duchêne, D., Bochet, A., 2016. Thirty years with cyclodextrins. *Int. J. Pharm.* 514, 58–72. doi:http://dx.doi.org/10.1016/j.ijpharm.2016.07.030.
- Duchêne, D., 2011. Cyclodextrins and their inclusion complexes. In: Bilensoy, E. (Ed.), *Cyclodextrins in Pharmaceuticals, Cosmetics, and Biomedicine*. John Wiley & Sons, Inc, Hoboken, NJ USA, pp. 1–18.
- Evans, C.L., 2015. Three-dimensional *in vitro* cancer spheroid models for photodynamic therapy: strengths and opportunities. *Front. Phys.* 3. doi:http://dx.doi.org/10.3389/fphy.2015.00015.
- Franken, N.A.P., Rodermond, H.M., Stap, J., Haveman, J., van Bree, C., 2006. Clonogenic assay of cells *in vitro*. *Nat. Protoc.* 1, 2315–2319. doi:http://dx.doi.org/10.1038/nprot.2006.339.
- Gaio, E., Scheglmann, D., Reddi, E., Moret, F., 2016. Uptake and photo-toxicity of Foscan[®], Foslip[®] and Fospeg[®] in multicellular tumor spheroids. *J. Photochem. Photobiol. B* 161, 244–252. doi:http://dx.doi.org/10.1016/j.jphotobiol.2016.05.011.
- Glisoni, R.J., Chiappetta, D.A., Moglioni, A.G., Sosnik, A., 2011. Novel 1-indanone thiosemicarbazone antiviral candidates: aqueous solubilization and physical stabilization by means of cyclodextrins. *Pharm. Res.* 29, 739–755. doi:http://dx.doi.org/10.1007/s11095-011-0599-y.
- Hinger, D., Navarro, F., Käch, A., Thomann, J.-S., Mittler, F., Couffin, A.-C., Maake, C., 2016. Photoinduced effects of m-tetrahydroxyphenylchlorin loaded lipid nanoemulsions on multicellular tumor spheroids. *J. Nanobiotechnol.* 14. doi:http://dx.doi.org/10.1186/s12951-016-0221-x.
- Hofman, J.-W., Carstens, M.G., van Zeeland, F., Helwig, C., Flesch, F.M., Hennink, W.E., van Nostrum, C.F., 2008. Photocytotoxicity of mTHPC (Temoporfin) loaded polymeric micelles mediated by lipase catalyzed degradation. *Pharm. Res.* 25, 2065–2073. doi:http://dx.doi.org/10.1007/s11095-008-9590-7.
- Josefsen, L.B., Boyle, R.W., 2012. Unique diagnostic and therapeutic roles of porphyrins and phthalocyanines in photodynamic therapy, imaging and theranostics. *Theranostics* 2, 916–966. doi:http://dx.doi.org/10.7150/thno.4571.
- Khanna, S., Bhatt, A.N., Dwarakanath, B.S., 2014. Chapter 11 – multicellular spheroid: 3-D tissue culture model for cancer research A2. In: Verma, Ashish S., Singh, A. (Eds.), *Animal Biotechnology*. Academic Press, San Diego, pp. 195–210.
- Löw, K., Knobloch, T., Wagner, S., Wiehe, A., Engel, A., Langer, K., von Briesen, H., 2011. Comparison of intracellular accumulation and cytotoxicity of free mTHPC and mTHPC-loaded PLGA nanoparticles in human colon carcinoma cells. *Nanotechnology* 22, 245102. doi:http://dx.doi.org/10.1088/0957-4484/22/24/245102.
- Lim, S.P., Kumar, R., Akkamsetty, Y., Wang, W., Ho, K., Neilsen, P.M., Walther, D.J., Suetani, R.J., Prestidge, C., Callen, D.F., 2013. Development of a novel cell-based assay system EPISSAY for screening epigenetic drugs and liposome formulated decitabine. *BMC Cancer* 13, 113. doi:http://dx.doi.org/10.1186/1471-2407-13-113.

- Marchal, S., Dolivet, G., Lassalle, H.-P., Guillemin, F., Bezdetnaya, L., 2015. Targeted photodynamic therapy in head and neck squamous cell carcinoma: heading into the future. *Lasers Med. Sci.* 30, 2381–2387. doi:<http://dx.doi.org/10.1007/s10103-014-1703-4>.
- Mitra, S., Foster, T.H., 2005. Photophysical parameters, photosensitizer retention and tissue optical properties completely account for the higher photodynamic efficacy of meso-tetra-hydroxyphenyl-chlorin vs photofrin. *Photochem. Photobiol.* 81, 849–859. doi:<http://dx.doi.org/10.1111/j.1751-1097.2005.tb01453.x>.
- Mitra, S., Maugain, E., Bolotine, L., Guillemin, F., Foster, T.H., 2005. Temporally and spatially heterogeneous distribution of mTHPC in a murine tumor observed by two-color confocal fluorescence imaging and spectroscopy in a whole-mount model. *Photochem. Photobiol.* 81, 1123–1130. doi:<http://dx.doi.org/10.1562/2005-03-24-RA-471>.
- Moan, J., 1990. On the diffusion length of singlet oxygen in cells and tissues. *J. Photochem. Photobiol. B* 6, 343–344. doi:[http://dx.doi.org/10.1016/1011-1344\(90\)85104-5](http://dx.doi.org/10.1016/1011-1344(90)85104-5).
- Patel, N.R., Aryasomayajula, B., Abouzeid, A.H., Torchilin, V.P., 2015. Cancer cell spheroids for screening of chemotherapeutics and drug-delivery systems. *Ther. Deliv.* 6, 509–520. doi:<http://dx.doi.org/10.4155/tde.15.1>.
- Reshetov, V., Zorin, V., Siupa, A., D'Hallewin, M.-A., Guillemin, F., Bezdetnaya, L., 2012. Interaction of liposomal formulations of meta-tetra(hydroxyphenyl)chlorin (temoporfin) with serum proteins: protein binding and liposome destruction. *Photochem. Photobiol.* 88, 1256–1264. doi:<http://dx.doi.org/10.1111/j.1751-1097.2012.01176.x>.
- Reshetov, V., Lassalle, H.-P., François, A., Dumas, D., Hupont, S., Gräfe, S., Filipe, V., Jiskoot, W., Guillemin, F., Zorin, V., Bezdetnaya, L., 2013. Photodynamic therapy with conventional and PEGylated liposomal formulations of mTHPC (temoporfin): comparison of treatment efficacy and distribution characteristics in vivo. *Int. J. Nanomed.* 8, 3817–3831. doi:<http://dx.doi.org/10.2147/IJN.S51002>.
- Sasnouski, S., Zorin, V., Khludeyev, I., D'Hallewin, M.-A., Guillemin, F., Bezdetnaya, L., 2005. Investigation of Foscan interactions with plasma proteins. *Biochim. Biophys. Acta* 1725, 394–402. doi:<http://dx.doi.org/10.1016/j.bbagen.2005.06.014>.
- Senge, M.O., Brandt, J.C., 2011. Temoporfin (Foscan[®], 5,10,15,20-tetra(m-hydroxyphenyl)chlorin) – a second-generation photosensitizer. *Photochem. Photobiol.* 87, 1240–1296. doi:<http://dx.doi.org/10.1111/j.1751-1097.2011.00986.x>.
- Senge, M.O., 2012. mTHPC – a drug on its way from second to third generation photosensitizer? *Photodiagnosis Photodyn. Ther.* 9, 170–179. doi:<http://dx.doi.org/10.1016/j.pdpdt.2011.10.001>.
- St Denis, T.G., Hamblin, M.R., 2015. 22 – Supramolecular drug delivery platforms in photodynamic therapy. *Applications of Nanoscience in Photomedicine*. Chandos Publishing, Oxford, pp. 465–485.
- Stella, V.J., Rao, V.M., Zannou, E.A., Zia, V., 1999. Mechanisms of drug release from cyclodextrin complexes. *Adv. Drug Deliv. Rev.* 36, 3–16. doi:[http://dx.doi.org/10.1016/S0169-409X\(98\)00052-0](http://dx.doi.org/10.1016/S0169-409X(98)00052-0).
- Waite, C.L., Roth, C.M., 2012. Nanoscale drug delivery systems for enhanced drug penetration into solid tumors: current progress and opportunities. *Crit. Rev. Biomed. Eng.* 40, 21–41. doi:<http://dx.doi.org/10.1615/CritRevBiomedEng.v40.i1.20>.
- West, C.M., Moore, J.V., 1992. Mechanisms behind the resistance of spheroids to photodynamic treatment: a flow cytometry study. *Photochem. Photobiol.* 55, 425–430. doi:<http://dx.doi.org/10.1111/j.1751-1097.1992.tb04257.x>.
- Yakavets, I., Yankovsky, I., Bezdetnaya, L., Zorin, V., 2017. Soret band shape indicates mTHPC distribution between β -cyclodextrins and serum proteins. *Dyes Pigm.* 137, 299–306. doi:<http://dx.doi.org/10.1016/j.dyepig.2016.11.007>.
- Yankovsky, I., Bastien, E., Yakavets, I., Khludeyev, I., Lassalle, H.-P., Gräfe, S., Bezdetnaya, L., Zorin, V., 2016. Inclusion complexation with β -cyclodextrin derivatives alters photodynamic activity and biodistribution of meta-tetra(hydroxyphenyl)chlorin. *Eur. J. Pharm. Sci. Off. J. Eur. Fed. Pharm. Sci.* 91, 172–182. doi:<http://dx.doi.org/10.1016/j.ejps.2016.06.012>.
- Zorin, V.P., Michalovsky, I., Zorina, T.E., Khludeyev, I.I., 1996. Distribution of chlorin-e6 derivatives in biological systems: investigation of pH-effect. *Proc. SPIE* 146–155. doi:<http://dx.doi.org/10.1117/12.230981>.

CHAPTER III.

mTHPC-IN-CYCLODEXTRINS-IN-LIPOSOME



7. Development and optimization of mTHPC-DCL


This chapter will be devoted to the development, optimization and screening aspects of hybrid liposomes loaded with mTHPC/ β -CD inclusion complexes. Firstly, we optimized and characterized liposomes encapsulated mTHPC/ β -CD complexes. This part of the results is described in the article “Temoporfin-in-Cyclodextrin-in-Liposome - A New Approach for Anticancer Drug Delivery: The Optimization of Composition”.

We have synthesized 9 various DCL compositions encapsulated inclusion complexes of mTHPC with three different β -CD derivatives (HP-, Me- and TM- β -CD) containing three various mTHPC concentrations. The obtained DCLs were characterized using dynamic light scattering, atomic force microscopy and spectroscopic techniques. It was demonstrated that > 85% of mTHPC is bound to β -CD inclusion complexes in the inner aqueous core of liposomes. The study of colloidal stability showed that DCLs with methylated β -CDs and the highest mTHPC loading remained stable more than 3 months. Intracellular uptake, penetration and distribution of mTHPC delivered by DCLs were studied in HT29 monolayer cells and multicellular tumor spheroids *in vitro*. Among all tested DCLs, TM- β -CD-based mTHPC-DCL with the demonstrated a homogenous accumulation of mTHPC across tumor spheroid volume supposing better PS distribution in tumor tissue.



Article

Temoporfin-in-Cyclodextrin-in-Liposome—A New Approach for Anticancer Drug Delivery: The Optimization of Composition

Ilya Yakavets ^{1,2,3} , Henri-Pierre Lassalle ^{1,2}, Dietrich Scheglmann ⁴, Arno Wiehe ⁴, Vladimir Zorin ^{3,5} and Lina Bezdetnaya ^{1,2,*}

¹ Centre de Recherche en Automatique de Nancy, Centre National de la Recherche Scientifique UMR 7039, Université de Lorraine, Campus Sciences, Boulevard des Aiguillettes, 54506 Vandoeuvre-lès-Nancy, France; i.yakovets@nancy.unicancer.fr (I.Y.); h.lassalle@nancy.unicancer.fr (H.-P.L.)

² Research Department, Institut de Cancérologie de Lorraine, 6 Avenue de Bourgogne, 54519 Vandoeuvre-lès-Nancy, France

³ Laboratory of Biophysics and Biotechnology, Belarusian State University, 4 Nezavisimosti Avenue, 220030 Minsk, Belarus; vpzorin@mail.ru

⁴ Biolitec Research GmbH, Otto-Schott-Strasse 15, 07745 Jena, Germany; dietrich.scheglmann@biolitec.com (D.S.); arno.wiehe@biolitec.com (A.W.)

⁵ International Sakharov Environmental Institute, Belarusian State University, Dauhabrodskaja 23, 220030 Minsk, Belarus

* Correspondence: l.bolotina@nancy.unicancer.fr; Tel.: +33-(0)3-08-59-83-53

Received: 12 September 2018; Accepted: 16 October 2018; Published: 18 October 2018



Abstract: The main goal of this study was to use hybrid delivery system for effective transportation of temoporfin (*meta*-tetrakis(3-hydroxyphenyl)chlorin, mTHPC) to target tissue. We suggested to couple two independent delivery systems (liposomes and inclusion complexes) to achieve drug-in-cyclodextrin-in-liposome (DCL) nanoconstructs. We further optimized the composition of DCLs, aiming to alter in a more favorable way a distribution of temoporfin in tumor tissue. We have prepared DCLs with different compositions varying the concentration of mTHPC and the type of β -cyclodextrin (β -CD) derivatives (Hydroxypropyl-, Methyl- and Trimethyl- β -CD). DCLs were prepared by thin-hydration technique and mTHPC/ β -CD complexes were added at hydration step. The size was about 135 nm with the surface charge of (−38 mV). We have demonstrated that DCLs are stable and almost all mTHPC is bound to β -CDs in the inner aqueous liposome core. Among all tested DCLs, trimethyl- β -CD-based DCL demonstrated a homogenous accumulation of mTHPC across tumor spheroid volume, thus supposing optimal mTHPC distribution.

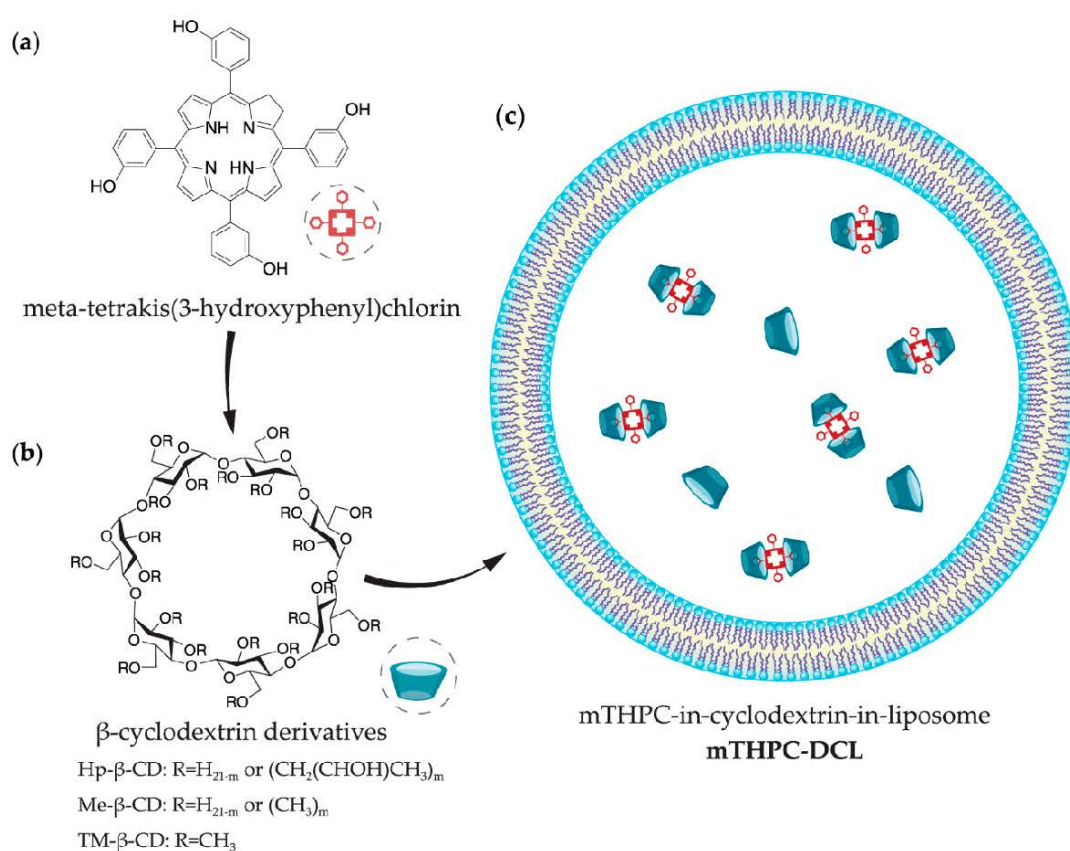
Keywords: temoporfin; drug-in-cyclodextrin-in-liposome; nanoparticles; multicellular tumor spheroids; flow cytometry; photodynamic therapy

1. Introduction

Application of nanomaterials in drug delivery of anticancer therapeutics has become one of the greatest challenges in cancer therapy, including photodynamic therapy (PDT) [1]. PDT is based on the combined action of photosensitizer (PS), light, and molecular oxygen, leading to the generation of toxic reactive oxygen species, which in turn can damage tumor tissue [2,3]. High accumulation and penetration of PS are primary factors that are responsible for PDT efficiency due to the high selectivity of its treatment. The main cytotoxic species, the singlet oxygen ($^1\text{O}_2$), has only a short lifetime in biological media and consequently limited action distance, therefore non-homogeneous distribution of PS into the tumor mass may lead to incomplete tumor eradication [4]. In turn, nanotechnology-based

drug delivery systems could significantly improve the transportation of poorly soluble PS providing the opportunities for active targeting, controlled release, and multimodality. Nonetheless, all developed nanomaterials are not without drawbacks, such as quick uncontrolled release of the drug, rapid clearance, limited penetration in tissues, etc. [5]. Therefore, hybrid systems as a combination of several nanomaterials have been recently suggested as an alternative approach. The present work deals with the application of hybrid delivery system based on the combination of liposomes and cyclodextrins for the clinically approved PS temoporfin.

Temoporfin (*meta*-tetrakis(3-hydroxyphenyl)chlorin, mTHPC) is a highly potent second-generation photosensitizer (Scheme 1a). The commercial medicinal product that is based on mTHPC (Foscan[®]) requires low light doses and concentrations to be photoactive and has already been approved by the European Medicines Agency (EMA) for the palliative treatment of advanced head and neck squamous cell carcinoma since 2001 [6,7]. Recently, we demonstrated a unique possibility to alter the biodistribution of mTHPC using β -cyclodextrin (β -CD) derivatives (Scheme 1b) [8,9]. The binding constants of mTHPC with β -CD derivatives vary from 10^5 to 10^7 M⁻¹ [10], providing the unique “nanoshuttle” transportation mechanism of mTHPC in biological media. Depending on the concentration of β -CD derivatives, they could either accelerate mTHPC distribution from serum proteins to tumor targets increasing cellular uptake and providing a deeper mTHPC penetration in three-dimensional (3D) tumor models or “isolate” drug molecules hampering PS delivery [9]. Such remarkable results in vitro strongly depend on the local concentration of β -CD, and as such, in vivo application of β -CD formulations is complicated due to the quick β -CD removal from the circulating system after intravenous injection [8]. The control release of inclusion complexes in target tissue may be better achieved in the case of hybrid drug-in-cyclodextrin-in-liposome (DCL) formulation (Scheme 1c).



Scheme 1. Representative scheme of (a) *meta*-tetrakis(3-hydroxyphenyl)chlorin (mTHPC), (b) β -cyclodextrin (β -CD) derivatives, and (c) drug-in-cyclodextrin-in-liposome (DCL) nanoconstruct.

DCL nanoconstruct, which was firstly proposed by McCormack and Gregoriadis (1994) [11], was already used for the delivery of a number of lipophilic bioactive molecules, including anti-inflammatory, anesthetic, immunosuppressive, and anti-cancer drugs [12,13]. Based on that, we suppose that the encapsulation of β -CD-complexed mTHPC into liposomes increases the drug loading capacity, entrapment efficiency, avoids burst release of the drug, and prolongs its systemic circulation. The resultant DCL could restrain the dissociation of drug-mTHPC complexes, avoid rapid drug release, and contribute to the altering PSs pharmacokinetics in vivo. To the best of our knowledge, such nanoconstruct, associating PS/ β -CD complexes and liposomes has never been proposed before. Thus, the comprehensive optimization of DCL composition is needed to achieve appropriate mTHPC intra-tissue distribution.

The present work is focused on the optimization of DCL composition. With this aim, we varied mTHPC concentration and the type of β -CD to achieve the most appropriate penetration of PS into the multicellular tumor spheroids. Additionally, we characterized DCLs spectroscopically and studied their colloidal stability.

2. Materials and Methods

2.1. Materials

Liposomal mTHPC formulation, Foslip[®], was kindly provided by biolitec research GmbH (Jena, Germany). mTHPC stock solution was prepared in methanol and kept at 4 °C in the dark. The concentration of mTHPC in the solution was estimated spectroscopically using molar extinction coefficient of 30,000 M⁻¹ cm⁻¹ at 650 nm in ethanol [14]. Foslip[®] is based on L- α -dipalmitoylphosphatidyl-choline (DPPC), dipalmitoylphosphatidylglycerol (DPPG), and mTHPC, with a drug:lipid ratio of 1:12 (mol/mol) and a DPPC:DPPG ratio of 9:1 (*w/w*). Foslip[®] was reconstituted from lyophilized powder in distilled water as per the manufacturer's instructions.

DPPC and DPPG were purchased from (Sigma-Aldrich, St. Louis, MO, USA). 2-hydroxypropyl- β -cyclodextrin (Hp- β -CD; product code CY-2005.2,27; substitution degree of 4.5, average molecular weight 1135 Da), random methyl- β -cyclodextrin (Me- β -CD; product code CY-2004.1,29; substitution degree of 12, average molecular weight 1135 Da), and heptakis(2,3,6-tri-*O*-methyl)- β -cyclodextrin (TM- β -CD; product code CY-2003,34; molecular weight 1429.6 Da) were purchased from CYCLOLAB R&D. Ltd., (Budapest, Hungary). For in vitro cell culture experiments, we used phenol red-free Roswell Park Memorial Institute 1640 medium (RPMI-1640, Invitrogen[™], Carlsbad, CA, USA), supplemented with 2% fetal bovine serum (FBS) (Life Technologies, Carlsbad, CA, USA). Ultrapure water (RiOs[™] 8, Millipore, Milli-Q[®] Advantage A10[®] System, Millipore, Eschborn, Germany) was used for sample preparation.

2.2. Drug-in-Cyclodextrin-in-Liposome Vesicles Preparation

2.2.1. Preparation of Inclusion Complexes

Inclusion complexes between β -CDs and mTHPC were formed using co-evaporation method [15]. Briefly, β -CDs were dissolved in ultrapure water (UPW) at the required concentrations. mTHPC stock solution (10 mM) was prepared in methanol. mTHPC was afterwards added to β -CDs solution (1:2 *w/w*) and solvent was removed by rotary evaporation (Rotavapor R-100, Büchi Labortechnik AG, Flawil, Switzerland) at 65 °C. mTHPC/ β -CDs complexes were dissolved in UPW at the required concentrations and were kept at 4 °C in the dark.

2.2.2. Thin Film Hydration

The composition of the prepared different liposomal formulations is provided in Table 1. Unilamellar liposomes were made by filter extrusion technique. All liposomal vesicles contained a combination DPPC and DPPG at a molar ratio 9:1. The total amount of lipids was 20 mg/mL

(26 mM) for all formulations. Empty liposomes were prepared by thin lipid film hydration followed by extrusion, as was described previously [16]. Briefly, 18 mg/mL of DPPC and 2 mg/mL of DPPG were dissolved in 0.6 mL of 99.6% ethanol. A thin film was obtained by the removal of the solvent by rotary evaporation at 65 °C. The film was hydrated in 0.3 mL of UPW and underwent three freeze-thaw cycles. The suspension was extruded 21 times through 100 nm polycarbonate Nuclepore® membranes using Avanti Mini-Extruder (Avanti, Alabaster, AL, USA) at 60 °C. After extrusion liposomes were stored at 4 °C. Liposomes containing mTHPC/ β -CDs complexes (DCLs) were prepared in the same manner. The mTHPC/ β -CDs complexes were added at the lipid film hydration step, as was previously reported [17].

Table 1. Composition of the different mTHPC-DCL formulations.

Formulation	CD	CD (mM)	mTHPC (mM)	Lipid (mM)
Empty liposomes	-	-	-	26
DCLs with Hp-β-CD¹				
HDCL 1	Hp- β -CD	200	5	26
HDCL 2			1.7	
HDCL 3			0.5	
DCLs with Me-β-CD²				
MDCL 1	Me- β -CD	20	5	26
MDCL 2			1.7	
MDCL 3			0.5	
DCLs with TM-β-CD³				
TDCL 1	TM- β -CD	10	5	26
TDCL 2			1.7	
TDCL 3			0.5	

¹ Lipid vesicles with mTHPC/Hp- β -CD complexes encapsulated into the inner core. ² Lipid vesicles with mTHPC/Me- β -CD complexes encapsulated into the inner core. ³ Lipid vesicles with mTHPC/TM- β -CD complexes encapsulated into the inner core.

Throughout the paper, abbreviations HDCL, MDCL, and TDCL stand for DCL encapsulated mTHPC complexes with various β -CD derivatives (Hydroxypropyl-, Methyl-, and Trimethyl- β -CD), with each of them containing three different mTHPC concentrations (5 mM, 1.7 mM, and 0.5 mM, denoted as 1–3, respectively) (Table 1).

2.2.3. Purification of DCLs

To purify DCL samples from not encapsulated mTHPC/ β -CDs, a minicolumn chromatography technique was used [18]. Briefly, minicolumns from 2.5 mL syringes pre-filled with Sephadex G-50 superfine (GE Healthcare Life Sciences, Buckinghamshire, UK) were dried by centrifugation for 3 min at 2000 g. Then, the DCL samples were placed into the minicolumns and were collected after centrifugation at the same conditions.

2.3. Characterization of Liposomes

2.3.1. Determination of Encapsulation Efficiency (EE)

Encapsulation efficiency of mTHPC in DCLs was calculated as the ratio ($A_{\text{final}}/A_{\text{total}} \times 100\%$), where (A_{total}) is mTHPC optical density measured immediately after extrusion and A_{final} is the mTHPC optical density measured after purification. The optical density was measured at 652 nm for the samples that were diluted 1500 times in 0.2% Triton® X-100 solution.

2.3.2. Photon Correlation Spectroscopy (PCS)

Particle size (hydrodynamic diameter) and polydispersity index (PDI) were determined by PCS (Zetasizer Nano ZS, Malvern Instruments, Worcestershire, UK). The samples were diluted 1000 times in ultrapure water at 25 °C. The measurements were performed at the angle of 173°. The calculations

of particle size were done assuming a spherical particle shape, a medium viscosity of 0.89 mPas, and a refractive index of 1.33. The results were presented as the mean of three consecutive measurements.

2.3.3. Atomic Force Microscopy (AFM)

Imaging was performed using an atomic force microscope Solver P47PRO (NT-MDT, Moscow, Russia). Images were done in semi-contact scanning mode at the frequency 150 kHz using NSG 11 cantilever. The ROTH slides (Carl Roth GmbH, Karlsruhe, Germany) with the films of DCLs samples being diluted 10 times were dried on the air for 10–12 h before the experiment. Processing and analysis of images were carried out using the offline portion of NT-MDT Image Analysis software (software version 2.2).

2.3.4. Spectroscopic Measurements

Absorption measurements were recorded with a Lambda 35 spectrometer (PerkinElmer, Waltham, MA, USA) using 1 cm optical path quartz cuvettes. Fluorescence measurements were conducted with LS55B spectrofluorometer (PerkinElmer, Waltham, MA, USA) equipped with polarizers, thermostated cuvette compartments, and magnetic stirring. Induced circular dichroism spectra were registered by Chirascan-plus qCD (Applied Photophysics Limited, Surrey, UK), which was equipped with thermostat. All spectroscopic measurements were carried out at a room temperature (23–25 °C). Optical density of all samples did not exceed 0.4 a.u. All of the measurements were performed in triplicate.

2.4. Monolayer and Spheroid Cell Cultures

2.4.1. Culture Conditions

Human colon adenocarcinoma cells HT29 were obtained from the ATCC® (LGC Promochem, Molsheim, France) and controlled for mycoplasma contamination. Cells were maintained in RPMI-1640 medium (Thermo Fisher Scientific, Waltham, MA, USA) supplemented with 9% (*v/v*) heat-inactivated fetal calf serum, antibiotics (penicillin 10,000 IU and streptomycin 10,000 µg/mL), and 1% (*v/v*) 0.1 M glutamine (Life Technologies, Carlsbad, CA, USA). Cells were kept as a monolayer culture in a humidified incubator (5% CO₂) at 37 °C.

2.4.2. Generation of Spheroids

The procedure of initiation of multicellular tumor spheroids (MCTS) by spinner technique was described previously [9,19]. Cell aggregates were transferred to 250 mL spinner flasks (Integra Biosciences, Zizers, Switzerland) containing 150 mL of culture medium. The spinner flasks were then placed on magnetic plates (Integra Biosciences) at 75 rpm in 5% CO₂ and 37 °C humidified atmosphere. The culture medium was changed every 2–3 days. MCTSs were used for experiments, once they reached 500 µm in diameter (after 15 days).

In order to dissociate MCTSs, they were transferred into a flask (15 mL), then washed twice with PBS, and further incubated with 0.05% trypsin (GIBCO™, Thermo Fisher Scientific, Waltham, MA, USA), 0.02% ethylenediaminetetraacetic acid (EDTA, GIBCO™, Thermo Fisher Scientific). Afterwards, the complete culture medium was added to inhibit trypsination. Finally, cell suspension was centrifuged to a pellet and resuspended in fresh culture medium.

2.4.3. Imaging of mTHPC Distribution

HT29 cells (3×10^4 cells/mL) were plated into Lab-Tek II chamber Slide (Roskilde, Denmark), incubated in the dark at 37 °C with 4.5 µM of mTHPC in different formulations for 3 h, and then rinsed with PBS. The experiments on MCTSs with mTHPC formulations were performed in accordance with the previously published protocol [9]. Briefly, DLCs and mTHPC liposomes were added to the samples for 24 h. The concentration of mTHPC was 4.5 µM. The incubation of samples was

performed in the dark conditions in a humidified incubator (5% CO₂) at 37 °C. Afterwards, MCTSs have been transferred to Petri dishes, then washed twice with PBS, and finally directly observed by epifluorescence microscope.

mTHPC fluorescence was observed under an upright epifluorescence microscope (AX-70 Provis, Olympus, France). The filter was set at 400–440 nm band pass excitation associated with a 570 nm dichroic mirror and a 590 nm long pass emission filter for mTHPC fluorescence measurements. Fluorescence images were recorded using an oil immersion ×40 objective in the case of cellular monolayer and ×4 objective for spheroid cell culture. The line profiles of mTHPC fluorescence across spheroids were calculated using ImageJ software from 10 radial lines, which were randomly drawn at the spheroid images.

2.5. Statistical Analysis

Student's *t*-test was used for the statistical analysis. Statistical significance was established at $P < 0.05$. All experiments were repeated at least three times and the results were expressed as mean values ± S.D.

3. Results and Discussion

3.1. Characterization of mTHPC-DCLs

3.1.1. Preparation of mTHPC-DCLs

mTHPC-loaded DCLs were prepared by thin hydration method with various β-CD derivatives containing different amounts of mTHPC. In practice, the soluble mTHPC/β-CD inclusion complexes were encapsulated in an aqueous core of conventional liposomes at the step of lipid film hydration, thus forming DCLs. Such methodology is considered as the most widely used method for DCLs preparation [17,20–22]. After the reduction of the size of lipid vesicles by extrusion, mTHPC/β-CD loaded liposomes were purified by means of minicolumn chromatography technique to eliminate external PS/cyclodextrin inclusion complexes [18]. This minicolumn chromatography allows for easy separation of small inclusion complexes from bulk liposomes with minor dilution in a short time (about 5 min). Other purification techniques like ultracentrifugation can damage the liposomes and stimulate their aggregation, while the dialysis technique is very slow (about 24 h) and unexpected mTHPC redistribution from liposomes to β-CD in medium can happen.

To optimize DCL composition, we varied mTHPC concentration as well as the type of β-CDs. To prepare the solutions of inclusion complexes we used mTHPC concentrations as 0.5, 1.7, and 5 mM. DCLs, prepared with these solutions, were named as DCL3, DCL2, and DCL1, respectively (Table 1). The concentration of β-CD was chosen in a way to completely prevent mTHPC aggregation at 5 mM (data not shown). The concentrations for Hp-, M-, and TM-β-CD were 200, 20, and 10 mM, respectively (HDCL, MDCL, and TDCL). The total lipid concentration was 26 mM for all DCLs in order to achieve high concentration of lipid vesicles and higher amount of encapsulated inclusion complexes in them.

According to the data obtained, EE of mTHPC in DCLs depends on mTHPC concentration added during DCL preparation (Table 2). The highest amount of mTHPC encapsulated in DCLs was observed for solution of inclusion complexes with 0.5 mM of mTHPC (DCL3) as compared to DCL2 and DCL1. However, EE did not exceed 20%, irrespective of mTHPC-DCL formulations. In contrast, the encapsulation of hydrophobic mTHPC molecules in lipid bilayer is characterized by the EE more than 85%, according to the literature data [16]. It is well known that EE values of soluble drugs incorporated into the inner aqueous liposomal core are strongly limited by drug solubilization and are much lower than the EE of hydrophobic molecules encapsulated into lipid bilayer. Evidently, low EE is a limiting factor for the potential commercial application of DCLs. However, this could be improved by the additional encapsulation of hydrophobic drugs into the lipid membrane of liposomes (double loaded DCL) [23].

Table 2. Characterization parameters of different liposomal formulations of mTHPC.

Formulation	EE (%)	Size (nm)	Polydispersity Index	Zeta-Potential (mV)
Foslip [®]	>85 [16]	113.6 ± 0.7	0.110 ± 0.015	−34.4 ± 4.3
DCLs with Hp-β-CD				
HDCL 1	7	137.7 ± 3.3	0.067 ± 0.030	−38.1 ± 1.9
HDCL 2	13	128.5 ± 0.3	0.037 ± 0.015	−36.7 ± 0.8
HDCL 3	17	125.7 ± 0.9	0.050 ± 0.004	−37.3 ± 1.6
DCLs with Me-β-CD				
MDCL 1	5	132.7 ± 0.8	0.045 ± 0.012	−37.8 ± 1.8
MDCL 2	7	141.0 ± 2.2	0.101 ± 0.019	−39.0 ± 2.6
MDCL 3	9	142.2 ± 0.8	0.073 ± 0.022	−36.4 ± 0.9
DCLs with TM-β-CD				
TDCL 1	7	135.9 ± 1.4	0.101 ± 0.034	−38.1 ± 1.2
TDCL 2	9	139.2 ± 0.9	0.065 ± 0.017	−36.9 ± 1.5
TDCL 3	14	130.6 ± 1.3	0.078 ± 0.026	−37.3 ± 2.1

3.1.2. Size and Zeta Potential

Morphology and size of DCLs and Foslip[®] were analyzed by means of atomic force microscopy and PCS. The physical characteristics of DCLs are summarized in Table 2. As shown in Figure 1a, the AFM images of DCLs illustrate a spherical morphology. The representative topography and three-dimensional (3D) reconstruction of AFM image is presented in Figure 1b. The analysis of the line profiles demonstrates the presence of spherical vesicles ≈110 nm with appropriate homogeneity. The hydrodynamic size and zeta-potential of the nanoparticles (NPs) were precisely analyzed by PCS (Table 2). In accordance with the previously reported data [24,25], Foslip[®] solution exhibits homogenous distribution in lipid vesicles with the diameter of 113.6 ± 0.7 nm (PDI = 0.110 ± 0.015). Mean hydrodynamic diameter of DCLs varied between 125.7 ± 0.9 and 142.2 ± 0.8 nm. DCL populations were homogeneous in size (PDI varied between 0.037 ± 0.015 and 0.146 ± 0.040). Additionally, no obvious differences were detected in the mTHPC-DCLs particle sizes in function of the types of β-CDs.

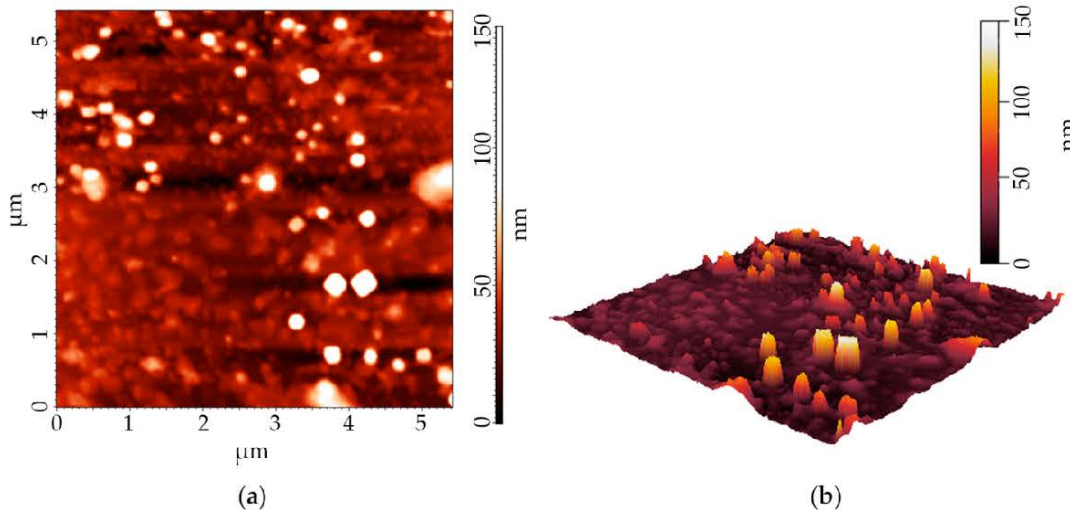


Figure 1. (a) Typical height image of DCL by means of atomic force microscopy. (b) Three-dimensional (3D) reconstruction of DCL height image. The presented image corresponds to the MDCL1.

Zeta-potential of NPs was also measured to characterize their surface charge. The lipid membrane of Foslip[®] consists of negatively charged lipid in the membrane (DPPG) with a ratio 1:9 DPPG/DPPC. Thus, zeta-potential of Foslip[®] is (−34.4 ± 4.3) mV. Similar composition of lipid membrane was used for DCL formulations; therefore all the studied DCLs had strong negative surface charge from (−36.7 mV) to (−39.0 mV). Obviously, negative charge of vesicles (<−30.0 mV) could prevent its

aggregation in solution and determines their high colloidal stability [26,27]. Moreover, it should be taken into account that negative surface charge is also important in terms of NPs interactions with cells and could determine their efficacy in vivo [28,29].

3.1.3. mTHPC Localization in DCLs

The localization of mTHPC in DCLs plays an important role in terms of understanding the delivery mechanism of mTHPC by hybrid nanoconstructs. It is acknowledged that mTHPC exhibits high affinity to the lipid environment [30]. Therefore, it would be hardly possible that mTHPC is completely bound with β -CDs in the inner aqueous core of DCLs. In all probability, mTHPC molecules partially redistribute between inclusion complexes and a liposomal bilayer. Actually, the localization of mTHPC in DCLs may be analyzed by spectroscopic techniques as a special case of equilibrium competitive binding [31,32].

The spectral data related to Foslip[®], DCLs loaded with mTHPC/Me- β -CD inclusion complexes (MDCLs) and mTHPC/Me- β -CD inclusion complexes are presented in Figure 2. Spectral characteristics of mTHPC/Me- β -CD inclusion complexes and Foslip[®] were previously described and were used here only for comparative analysis [16,32]. To estimate the fraction of mTHPC bound to β -CDs, we used two different spectral techniques: conventional circular dichroism and spectroscopic based approach related to the shape of Soret band (Figure 2) [31,32].

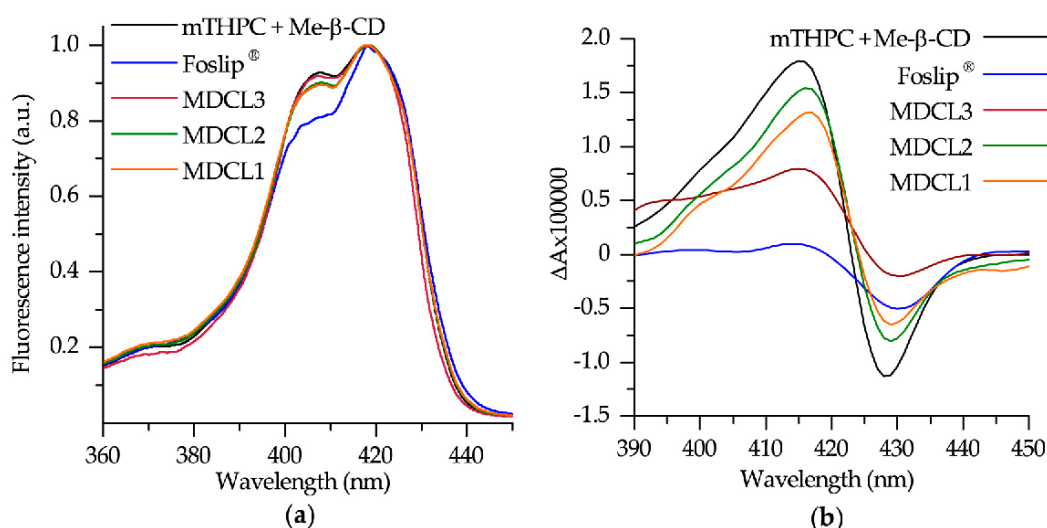
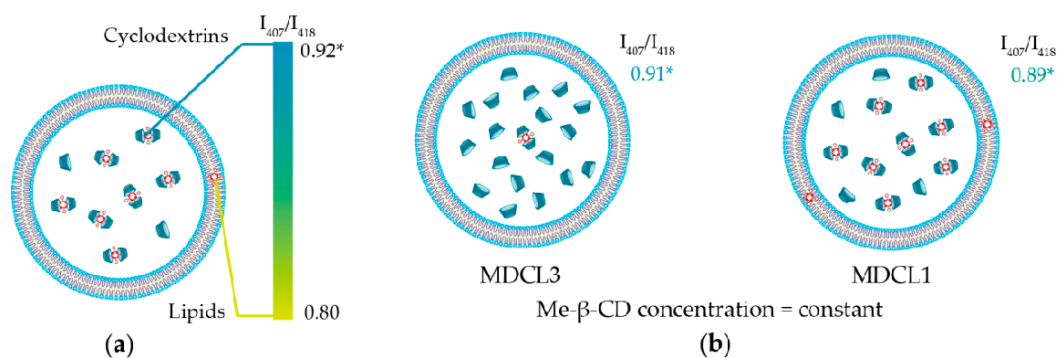


Figure 2. (a) Normalized fluorescence excitation spectra of 1 μ M mTHPC in different formulations. Fluorescence signal was measured at 652 nm. (b) Induced circular dichroism spectra of 1 μ M mTHPC in different formulations. Concentration of Me- β -CD was 0.2 mM.

As seen in Figure 2a, the shape of mTHPC Soret band in DCLs is similar to that of mTHPC/Me- β -CD. According to our recent study [32], the shape of Soret band of mTHPC fluorescence excitation spectra is sensitive to the changes of mTHPC microenvironment and B_x/B_y ratio could be used for the quantitative analysis. The mTHPC/Me- β -CD inclusion complexes are characterized by $I_{407}/I_{418} = 0.92$ ratio (where I_{407} and I_{418} stand for the fluorescence intensities at 407 nm and 418 nm excitation respectively), while liposomes (Foslip[®]) exhibits $I_{407}/I_{418} = 0.80$ (Scheme 2a). The calculated B_x/B_y ratios for mTHPC in MDCLs are equal to 0.89, 0.90, and 0.91 for MDCL1, MDCL2, and MDCL3 respectively. It corresponds to the mTHPC fraction of 75%, 83% and 92% bound to Me- β -CD in the inner aqueous core (Scheme 2b). Similar tendency was observed for other types of β -CDs (data not shown). We obtained that for TM- β -CD the fraction of mTHPC in inclusion complexes for all TDCLs exceeds 90%. At the same time, the percentage of mTHPC bound to Hp- β -CD was 70%, 80%, and 90% for HDCL1, HDCL2, and HDCL3, respectively. The preferable localization of mTHPC in inclusion

complexes was further confirmed by circular dichroism technique (Figure 2b). However, circular dichroism is an absorbance-based technique, therefore medium turbidity could also complicate the quantitative analysis, as was described already for absorbance spectra.



Scheme 2. (a) Schematic representation of possible localization of mTHPC in MDCL. Color bar displays the range of I_{407}/I_{418} ratios. Maximal value (0.92) corresponds to complete binding of mTHPC to Me- β -CD, while minimal ratio (0.80) displays the location of all mTHPC molecules in lipid bilayer. (b) Schematic representation of mTHPC localization in MDCLs depending on the initial mTHPC concentration. *—all values correspond to mTHPC/Me- β -CD inclusion complexes.

Summarizing this spectroscopic part, we can conclude that mTHPC molecules are mainly located in the inclusion complexes with β -CDs in the inner aqueous core of DCLs. We demonstrated that the localization of mTHPC strongly depends on the β -CDs' affinity to mTHPC and concentration of β -CD what is in a good agreement with the competitive mechanism of mTHPC binding. For instance, binding constant of TM- β -CD with mTHPC is $>10^7 \text{ M}^{-1}$ [10], which is at least ten times higher than these for other β -CDs. Such tight binding of PS in the inclusion complexes allows TDCLs encapsulate almost all mTHPC (>90%) in the inner aqueous core. On the contrary, decreasing of mTHPC concentration upon complex preparation leads to the increase of concentration of free β -CDs in the cavity (Scheme 2b). Therefore, in the case of DCL3, the amount of mTHPC bound in inclusion complexes is higher than for DCL1.

3.1.4. Storage Stability

It is acknowledged that β -CDs remove lipid components from liposomes, thus destabilizing them [33,34]. The stability of different liposome dispersions was investigated by means of PCS analysis during their storage at 4 °C in the dark (Figure 3). Foslip[®] was used as a reference sample since according to the manufacturer it is stable during more than six months after dissolution. No marked variations in the size were observed for DCL1 (HDCL1, MDCL1 and TDCL1) after 1 month of storage (Figure 3a). The size of DCLs with low initial mTHPC loading (DCL2 and DCL3) was slightly increased, especially for HDCLs (Figure 3a). At the same time, the measurements of PDI clearly demonstrated that PDI for HDCL1, MDCL1, and TDCL1 were in the range of acceptable homogeneity (PDI < 0.2), while DCL2 and DCL3 for all β -CDs were characterized by PDI > 0.2 (Figure 3b). Meanwhile, the PDI of HDCL1 was significantly increased after 1 month and tended to degrade after 1.5 month (Figure 3c,d). Similarly to Foslip[®], MDCL1 and TDCL1 exhibit the colloidal stability during more than three months.

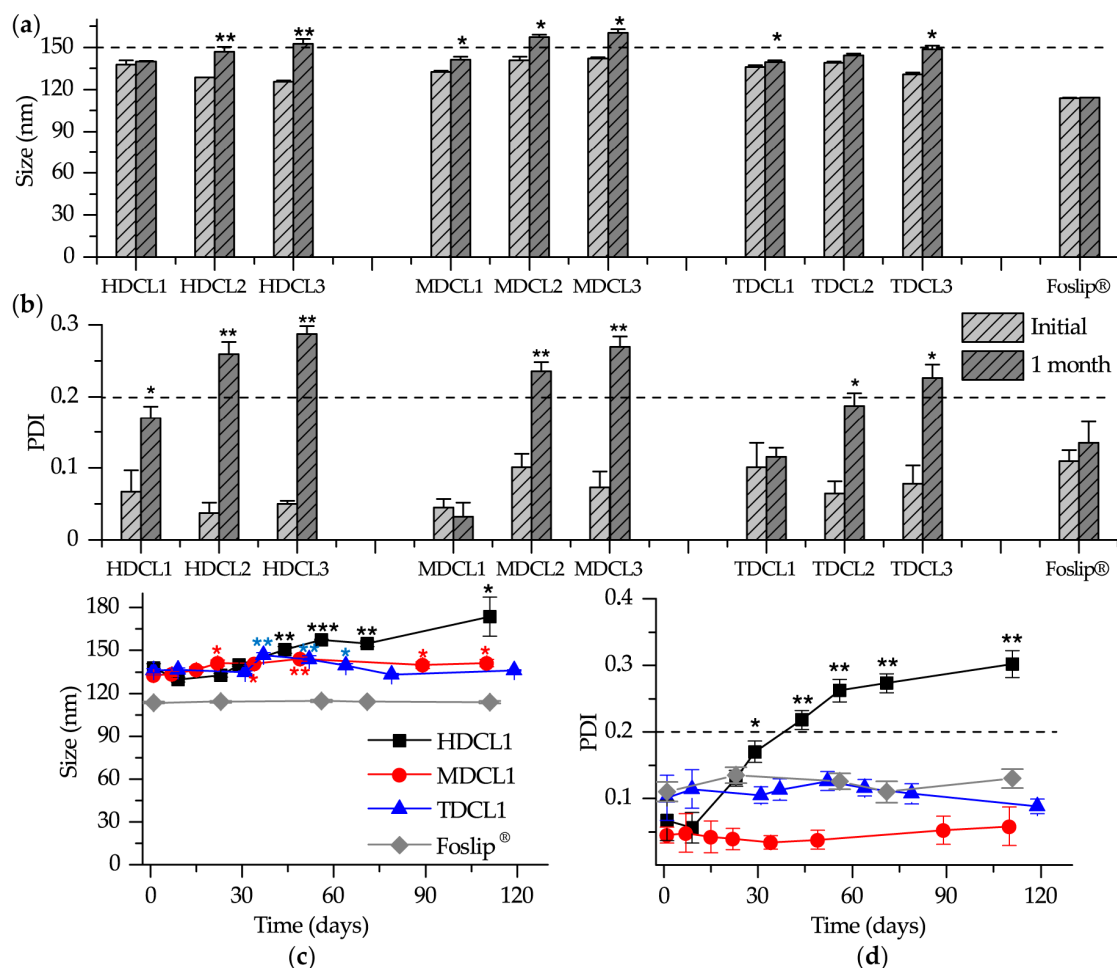


Figure 3. (a) Size and (b) polydispersity index (PDI) of mTHPC formulations after one month of the storage. Kinetics of (c) size and (d) PDI of HDCL1, MDCL1, TDCL1 and Foslip® during three months of storage. The samples were stored at 4 °C in the dark. The samples were diluted 1000 times in ultrapure water (UPW). *—statistically different from initial sample, $P < 0.05$; **—statistically different from initial sample, $P < 0.01$; ***—statistically different from initial sample, $P < 0.001$.

Obviously, the observed heterogeneity of DCLs with low initial mTHPC loading (DCL2 and DCL3) could be due to β -CD-induced liposomes' destabilization. Cyclodextrins are known to interact with lipid components removing them from membrane by forming inclusion complexes with lipids [30,35]. The intensity of such process is mainly determined by the relative concentration of free β -CD molecules [36]. According to that, when we decrease initial mTHPC concentration used for DCL preparation, the number of free β -CD molecules in the aqueous core increases accelerating destabilization of lipid bilayer. Moreover, we used 10 and 20 times lower concentrations of Me- β -CD and TM- β -CD as compared with Hp- β -CD to achieve complete mTHPC solubilization during DCL preparation. Therefore, in the case of Hp- β -CD we have the large extent of free β -CD molecules, leading to the quick HDCL1 destabilization compared to MDCL1 and TDCL1.

In fine, DCL is rather stable nanoconstruct, which contains mTHPC mainly in inclusion complexes in the inner aqueous core of liposomes. It means that mTHPC delivery by DCLs should be quite different from conventional liposomes (Foslip®) and it may lead to the significant enhancement of mTHPC penetration in tumor tissue in vitro.

3.2. mTHPC Delivery to the Tumor Cells In Vitro

As stated above, the main purpose for encapsulating of mTHPC in the form of inclusion complexes in liposomes is to control PS release by β -CDs after liposome destruction in the medium. In order to investigate the validity of this hypothesis, we analyzed intracellular localization of mTHPC in HT29 human colon adenocarcinoma monolayer cells and PS distribution in HT29 MCTSs after pre-treatment with DCLs (Figure 4). Preliminary studies have shown that cellular uptake strongly depends on the absolute mTHPC concentration loaded in DCLs (data not shown). We demonstrated that DCLs containing less mTHPC (DCL2 and DCL3) exhibited lower accumulation in HT29 cells when compared with DCL1. Therefore, for our further in vitro studies we selected only HDCL1, MDCL1 and TDCL1.

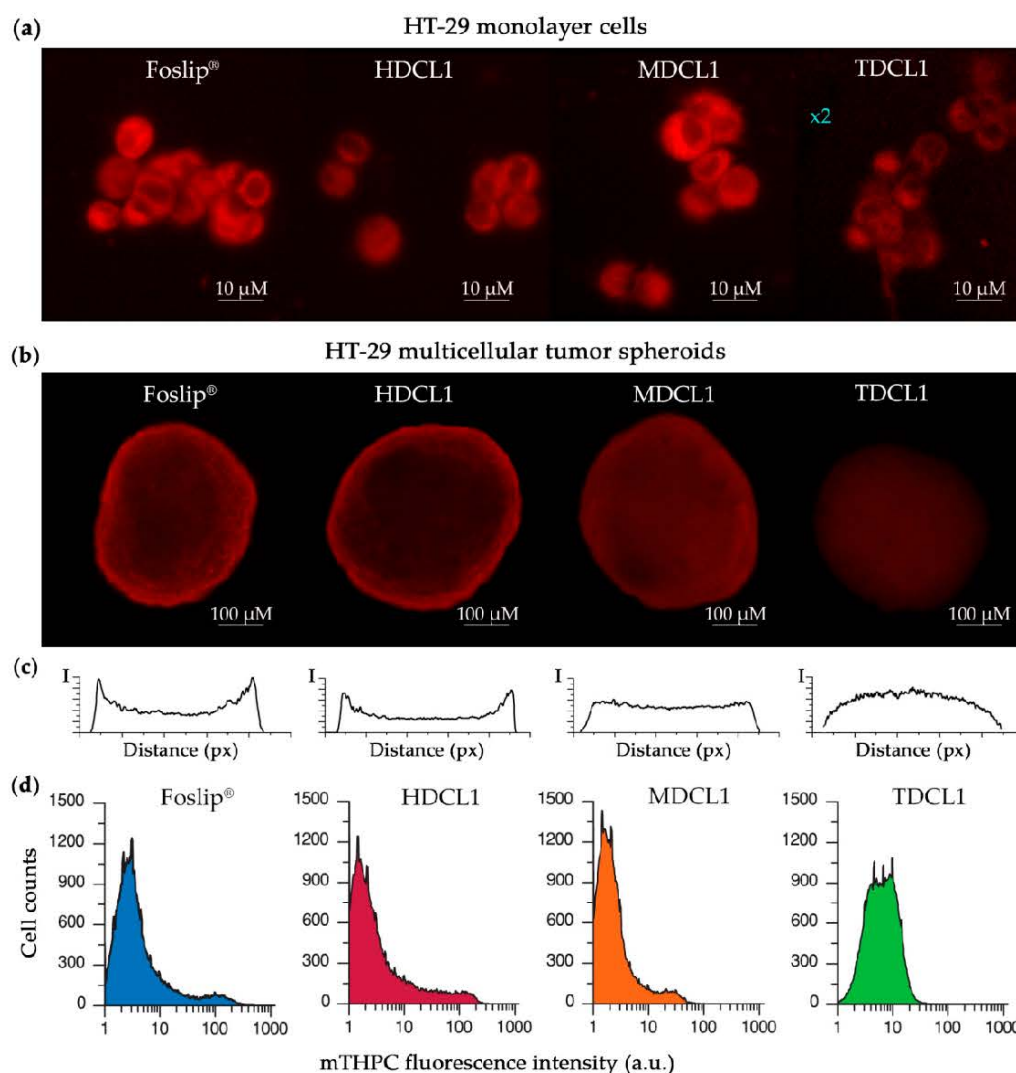


Figure 4. (a) Fluorescence images of mTHPC in different formulations in HT-29 monolayer cells 3 h post-incubation. (b) Fluorescence patterns of mTHPC in different formulations in HT-29 MCTSs 24 h post-incubation. (c) Linear profiles of mTHPC fluorescence intensity in HT-29 MCTSs treated by different mTHPC liposomal formulations for 24 h. (d) Histograms of mTHPC fluorescence in function of cell counts in HT29 spheroids after 24 h incubation with different mTHPC formulations. Log scale mTHPC fluorescence is shown on the x-axis. mTHPC concentration for all samples was 4.5 μ M.

Figure 4a displays the fluorescence images of HT29 cells treated with mTHPC and Foslip[®] for 3 h. All formulations deliver mTHPC into the cells and we did not observe an obvious difference

in intracellular localization between Foslip[®] and DCLs. mTHPC is predominantly localized in the perinuclear region with diffuse fluorescence in the cytoplasm, as consistent with literature data related to Foslip[®] [37]. It is worth to note that fluorescence intensity of TDCL1 in HT29 cells is significantly lower compared with other mTHPC formulations, perhaps because of the tight binding of mTHPC in TM- β -CD complexes.

Understanding the PS distribution processes in target tissues is a primary factor that is responsible for prediction of antitumor efficiency of photodynamic agents. MCTSs represent avascular regions found in many solid tumor tissues and allow for simulating the penetration and intratumor transport of anticancer nanomedicines, including photoactive NPs [38,39]. In the present work, HT-29 MCTSs were generated by spinner technique and filtered by the size from 380 to 520 μ M for further experiments. Figure 4b displays epifluorescence imaging of the intact spheroids treated by Foslip[®] and mTHPC-DCLs for 24 h. As seen on these images, the red fluorescence pattern of mTHPC was mainly localized on the periphery of Foslip[®]-treated spheroids, consistent with the literature data [40]. It is worth noting that HT-29 MCTSs that were treated with free mTHPC demonstrated similar peripheral profiles of fluorescence distribution [9]. The corresponding linear profile of mTHPC fluorescence across MCTSs, as presented in Figure 4c, demonstrates the presence of intensity peaks in the outer rim of spheroids that were treated with Foslip[®]. MCTSs exposed to HDCL1 also display high fluorescence in the outer rim of spheroids. The significant changes of mTHPC distribution in HT-29 MCTSs were observed for DCLs that contained mTHPC inclusion complexes with methylated β -CDs (MDCL1 and TDCL1). In the case of MDCL1, the intensity peaks on the periphery were smoothed, displaying an increase in the penetration depth of mTHPC. Similar changes of mTHPC distribution in spheroids were reported for free mTHPC/CD complexes in our recent paper [9]. However, the strongest changes of the mTHPC fluorescence pattern in MCTSs were observed for TDCL1. Linear profiles obtained after incubation of MCTSs with TDCL1 display spherical pattern with the maximal fluorescence intensity in the center. Taking into the account distortions due to the limited penetration of excitation light and spherical geometry of spheroids one can conclude that such fluorescence pattern corresponds to the almost complete penetration of mTHPC in spheroid depth and probably homogeneous PS distribution between cells of spheroids.

To confirm the DCLs-induced alterations of mTHPC distribution in spheroids we used a flow cytometry technique (Figure 4d). The spheroids treated with various mTHPC formulations were trypsinized after 24 h incubation and analyzed by flow cytometry to assess the heterogeneity of mTHPC distribution between spheroid cells. Foslip[®]-treated spheroids exhibited a strong heterogeneity of mTHPC distribution between the cells. The distribution is broad and consists of several peaks. Obviously, mTHPC accumulates insufficiently in the deep layers of spheroids. Application of HDCL1 for mTHPC delivery in MCTSs does not significantly affect its distribution. Meanwhile, in the case of MDCL1, the distribution histogram slightly changes, still conserving strong heterogeneity similarly to Foslip[®] and HDCL1. Finally, the incubation of MCTSs with TDCL1 results in an almost homogeneous distribution of mTHPC, supposing similar PS bioavailability for peripheral cells as well as for cells in the core of spheroid.

Thus, our data clearly demonstrate that DCLs significantly alter mTHPC distribution in spheroids. The alteration strength strongly depends on the type of used β -CD and increases in function of the affinity of β -CD to mTHPC in the following order (HDCL1 < MDCL1 < TDCL1). Taking into the account the influence of free CDs on mTHPC distribution in spheroids [9], one can suppose that the higher affinity of β -CD to mTHPC leads to the longer life-time of complex and as a matter of fact to the deeper delivery of mTHPC in the tumor tissue after the destruction of liposomes. In turn, deeper PS penetration results in its more homogeneous distribution of between cells [9]. Thus, in the case of TM- β -CD, the affinity is so high ($>10^7$ M⁻¹) [10] that mTHPC remains in the complex, even in the deep cell layers, resulting in almost homogeneous PS distribution in spheroid.

4. Conclusions

Our study clearly demonstrated the potential use of drug-in-cyclodextrin-in-liposome formulation as a nanosized delivery system for mTHPC. The novel drug-loading procedure ensures the stable and efficient encapsulation of mTHPC bound to β -CDs into conventional liposomes. DCLs with various compositions were prepared in order to select the optimal nanoconstruct for mTHPC delivery in the target tissues. This study shows that liposomes may be effectively used as a reservoir for mTHPC/ β -CDs complexes. It was demonstrated that TM- β -CD-based DCL retains almost all mTHPC in inclusion complexes and it remains stable for more than three months. Moreover, TDCL-treated tumor spheroids homogeneously accumulated mTHPC across spheroid volume supposing optimal PS distribution in tumor tissue.

In long term perspectives, the limited accumulation of mTHPC delivered by DCLs should be optimized additionally. We suppose that double loading of drug could be applied to increase the total amount of mTHPC in DCLs and, perhaps, improving cellular uptake of TDCL. Currently, we are investigating biopharmaceutical properties of double loaded mTHPC-TDCL using in vitro 3D tumor models.

Author Contributions: I.Y. performed and designed the experiments and drafted the manuscript, H.-P.L. contributed to manuscript editing, D.S. and A.W. validated the manuscript; V.Z. and L.B. participated to the conceptualization and supervision of the work. All authors read and approved the final manuscript.

Funding: This work was supported by the Institut de Cancérologie de Lorraine, French “Ligue Nationale contre le Cancer (CCIR-GE)”, Belarusian Republican Foundation for Fundamental Research (BRFFR) [grant numbers: M17MC-028, M18MB002-002. B17-106] and the Ministry of Education of the Republic.

Acknowledgments: The authors thank Dr. Tatiana Zorina for the atomic forces microscopy measurements and Alexandre Kriznik (Platform of Biophysics and Structural Biology of UMS 2008 IBSLor, UL-CNRS-INSERM) for the access to circular dichroism facilities. We also acknowledge Mrs. Dominique Le Prince for careful English editing.

Conflicts of Interest: The authors declare no conflict of interest.

References

1. Marchal, S.; Hor, A.E.; Millard, M.; Gillon, V.; Bezdetsnaya, L. Anticancer Drug Delivery: An Update on Clinically Applied Nanotherapeutics. *Drugs* **2015**, *75*, 1601–1611. [[CrossRef](#)] [[PubMed](#)]
2. Bhuvaneswari, R.; Gan, Y.Y.; Soo, K.C.; Olivo, M. The effect of photodynamic therapy on tumor angiogenesis. *Cell. Mol. Life Sci.* **2009**, *66*, 2275–2283. [[CrossRef](#)] [[PubMed](#)]
3. Castano, A.P.; Mroz, P.; Hamblin, M.R. Photodynamic therapy and anti-tumour immunity. *Nat. Rev. Cancer* **2006**, *6*, 535–545. [[CrossRef](#)]
4. West, C.M.; Moore, J.V. Mechanisms behind the resistance of spheroids to photodynamic treatment: A flow cytometry study. *Photochem. Photobiol.* **1992**, *55*, 425–430. [[CrossRef](#)] [[PubMed](#)]
5. Peer, D.; Karp, J.M.; Hong, S.; Farokhzad, O.C.; Margalit, R.; Langer, R. Nanocarriers as an emerging platform for cancer therapy. *Nat. Nanotechnol.* **2007**, *2*, 751–760. [[CrossRef](#)] [[PubMed](#)]
6. Senge, M.O.; Brandt, J.C. Temoporfin (Foscan[®], 5,10,15,20-tetra(m-hydroxyphenyl)chlorin)—A second-generation photosensitizer. *Photochem. Photobiol.* **2011**, *87*, 1240–1296. [[CrossRef](#)] [[PubMed](#)]
7. Senge, M.O. Mthpc—A drug on its way from second to third generation photosensitizer? *Photodiagnosis Photodyn. Ther.* **2012**, *9*, 170–179. [[CrossRef](#)] [[PubMed](#)]
8. Yankovsky, I.; Bastien, E.; Yakavets, I.; Khludayev, I.; Lassalle, H.-P.; Gräfe, S.; Bezdetsnaya, L.; Zorin, V. Inclusion complexation with β -cyclodextrin derivatives alters photodynamic activity and biodistribution of meta-tetra(hydroxyphenyl)chlorin. *Eur. J. Pharm. Sci.* **2016**, *91*, 172–182. [[CrossRef](#)] [[PubMed](#)]
9. Yakavets, I.; Yankovsky, I.; Millard, M.; Lamy, L.; Lassalle, H.-P.; Wiehe, A.; Zorin, V.; Bezdetsnaya, L. The alteration of temoporfin distribution in multicellular tumor spheroids by β -cyclodextrins. *Int. J. Pharm.* **2017**, *529*, 568–575. [[CrossRef](#)] [[PubMed](#)]
10. Yakavets, I.; Lassalle, H.-P.; Yankovsky, I.; Ingrosso, F.; Monari, A.; Bezdetsnaya, L.; Zorin, V. Evaluation of temoporfin affinity to β -cyclodextrins assuming self-aggregation. *J. Photochem. Photobiol. Chem.* **2018**, *367*, 13–21. [[CrossRef](#)]

11. McCormack, B.; Gregoriadis, G. Entrapment of cyclodextrin-drug complexes into liposomes: Potential advantages in drug delivery. *J. Drug Target.* **1994**, *2*, 449–454. [[CrossRef](#)] [[PubMed](#)]
12. Gharib, R.; Greige-Gerges, H.; Jraij, A.; Auezova, L.; Charcosset, C. Preparation of drug-in-cyclodextrin liposomes at a large scale using a membrane contactor: Application to trans-anethole. *Carbohydr. Polym.* **2016**, *154*, 276–286. [[CrossRef](#)] [[PubMed](#)]
13. Dhule, S.S.; Penfornis, P.; Frazier, T.; Walker, R.; Feldman, J.; Tan, G.; He, J.; Alb, A.; John, V.; Pochampally, R. Curcumin-loaded γ -cyclodextrin liposomal nanoparticles as delivery vehicles for osteosarcoma. *Nanomed. Nanotechnol. Biol. Med.* **2012**, *8*, 440–451. [[CrossRef](#)] [[PubMed](#)]
14. Bonnett, R.; Charlesworth, P.; Djelal, B.D.; Foley, S.; McGarvey, D.J.; Truscott, T.G. Photophysical properties of 5,10,15,20-tetrakis(m-hydroxyphenyl)porphyrin (m-THPP), 5,10,15,20-tetrakis(m-hydroxyphenyl)chlorin (m-THPC) and 5,10,15,20-tetrakis(m-hydroxyphenyl)bacteriochlorin (m-THPBC): A comparative study. *J. Chem. Soc. Perkin Trans. 2* **1999**, 325–328. [[CrossRef](#)]
15. Maestrelli, F.; González-Rodríguez, M.L.; Rabasco, A.M.; Mura, P. Preparation and characterisation of liposomes encapsulating ketoprofen–cyclodextrin complexes for transdermal drug delivery. *Int. J. Pharm.* **2005**, *298*, 55–67. [[CrossRef](#)] [[PubMed](#)]
16. Reshetov, V.; Kachatkou, D.; Shmigol, T.; Zorin, V.; D'Hallewin, M.-A.; Guillemin, F.; Bezdetnaya, L. Redistribution of meta-tetra(hydroxyphenyl)chlorin (m-THPC) from conventional and PEGylated liposomes to biological substrates. *Photochem. Photobiol. Sci.* **2011**, *10*, 911–919. [[CrossRef](#)] [[PubMed](#)]
17. Gharib, R.; Greige-Gerges, H.; Fourmentin, S.; Charcosset, C.; Auezova, L. Liposomes incorporating cyclodextrin-drug inclusion complexes: Current state of knowledge. *Carbohydr. Polym.* **2015**, *129*, 175–186. [[CrossRef](#)] [[PubMed](#)]
18. Lasch, J.; Weissig, V.; Brandl, M. *Liposomes: A Practical Approach*, 2nd ed.; Torchilin, V., Weissig, V., Eds.; Oxford University Press: Oxford, UK, 2003.
19. Marchal, S.; Fadloun, A.; Maugain, E.; D'Hallewin, M.-A.; Guillemin, F.; Bezdetnaya, L. Necrotic and apoptotic features of cell death in response to Foscan photosensitization of HT29 monolayer and multicell spheroids. *Biochem. Pharmacol.* **2005**, *69*, 1167–1176. [[CrossRef](#)] [[PubMed](#)]
20. Wang, W.-X.; Feng, S.-S.; Zheng, C.-H. A comparison between conventional liposome and drug-cyclodextrin complex in liposome system. *Int. J. Pharm.* **2016**, *513*, 387–392. [[CrossRef](#)] [[PubMed](#)]
21. Zhang, L.; Zhang, Q.; Wang, X.; Zhang, W.; Lin, C.; Chen, F.; Yang, X.; Pan, W. Drug-in-cyclodextrin-in-liposomes: A novel drug delivery system for flurbiprofen. *Int. J. Pharm.* **2015**, *492*, 40–45. [[CrossRef](#)] [[PubMed](#)]
22. Arima, H.; Hagiwara, Y.; Hirayama, F.; Uekama, K. Enhancement of antitumor effect of doxorubicin by its complexation with gamma-cyclodextrin in pegylated liposomes. *J. Drug Target.* **2006**, *14*, 225–232. [[CrossRef](#)] [[PubMed](#)]
23. Chen, J.; Lu, W.-L.; Gu, W.; Lu, S.-S.; Chen, Z.-P.; Cai, B.-C.; Yang, X.-X. Drug-in-cyclodextrin-in-liposomes: A promising delivery system for hydrophobic drugs. *Expert Opin. Drug Deliv.* **2014**, *11*, 565–577. [[CrossRef](#)] [[PubMed](#)]
24. Reshetov, V.; Lassalle, H.-P.; François, A.; Dumas, D.; Hupont, S.; Gräfe, S.; Filipe, V.; Jiskoot, W.; Guillemin, F.; Zorin, V.; et al. Photodynamic therapy with conventional and PEGylated liposomal formulations of mTHPC (temoporfin): Comparison of treatment efficacy and distribution characteristics in vivo. *Int. J. Nanomed.* **2013**, *8*, 3817–3831. [[CrossRef](#)] [[PubMed](#)]
25. Reshetov, V.; Zorin, V.; Siupa, A.; D'Hallewin, M.-A.; Guillemin, F.; Bezdetnaya, L. Interaction of liposomal formulations of meta-tetra(hydroxyphenyl)chlorin (temoporfin) with serum proteins: Protein binding and liposome destruction. *Photochem. Photobiol.* **2012**, *88*, 1256–1264. [[CrossRef](#)] [[PubMed](#)]
26. Lyklema, J.; Fleer, G.J. Electrical contributions to the effect of macromolecules on colloid stability. *Colloids Surf.* **1987**, *25*, 357–368. [[CrossRef](#)]
27. Hunter, R.J.; Midmore, B.R.; Zhang, H. Zeta Potential of Highly Charged Thin Double-Layer Systems. *J. Colloid Interface Sci.* **2001**, *237*, 147–149. [[CrossRef](#)] [[PubMed](#)]
28. Lee, K.D.; Nir, S.; Papahadjopoulos, D. Quantitative analysis of liposome-cell interactions in vitro: Rate constants of binding and endocytosis with suspension and adherent J774 cells and human monocytes. *Biochemistry* **1993**, *32*, 889–899. [[CrossRef](#)] [[PubMed](#)]
29. Chonn, A.; Semple, S.C.; Cullis, P.R. Association of blood proteins with large unilamellar liposomes in vivo. Relation to circulation lifetimes. *J. Biol. Chem.* **1992**, *267*, 18759–18765. [[PubMed](#)]

30. Szente, L.; Fenyvesi, É. Cyclodextrin-Lipid Complexes: Cavity Size Matters. *Struct. Chem.* **2017**, *28*, 479–492. [[CrossRef](#)]
31. Yakavets, I.V.; Yankovsky, I.V.; Khludeyev, I.I.; Lassalle, H.P.; Bezdetnaya, L.N.; Zorin, V.P. Optical Methods for the Analysis of the Temoprolin Photosensitizer Distribution Between Serum Proteins and Methyl- β -Cyclodextrin Nanocarriers in Blood Serum. *J. Appl. Spectrosc.* **2018**, *84*, 1030–1036. [[CrossRef](#)]
32. Yakavets, I.; Yankovsky, I.; Bezdetnaya, L.; Zorin, V. Soret band shape indicates mTHPC distribution between β -cyclodextrins and serum proteins. *Dyes Pigments* **2017**, *137*, 299–306. [[CrossRef](#)]
33. Piel, G.; Piette, M.; Barillaro, V.; Castagne, D.; Evrard, B.; Delattre, L. Betamethasone-in-cyclodextrin-in-liposome: The effect of cyclodextrins on encapsulation efficiency and release kinetics. *Int. J. Pharm.* **2006**, *312*, 75–82. [[CrossRef](#)] [[PubMed](#)]
34. Puskás, I.; Barcza, L.; Szente, L.; Csémpesz, F. Features of the Interaction between Cyclodextrins and Colloidal Liposomes. *J. Incl. Phenom. Macrocycl. Chem.* **2006**, *54*, 89–93. [[CrossRef](#)]
35. Uekama, K.; Otagiri, M. Cyclodextrins in drug carrier systems. *Crit. Rev. Ther. Drug Carr. Syst.* **1987**, *3*, 1–40. [[CrossRef](#)]
36. Fatouros, D.G.; Hatzidimitriou, K.; Antimisiaris, S.G. Liposomes encapsulating prednisolone and prednisolone-cyclodextrin complexes: Comparison of membrane integrity and drug release. *Eur. J. Pharm. Sci.* **2001**, *13*, 287–296. [[CrossRef](#)]
37. Kiesslich, T.; Berlanda, J.; Plaetzer, K.; Krammer, B.; Berr, F. Comparative characterization of the efficiency and cellular pharmacokinetics of Foscan- and Foslip-based photodynamic treatment in human biliary tract cancer cell lines. *Photochem. Photobiol. Sci.* **2007**, *6*, 619–627. [[CrossRef](#)] [[PubMed](#)]
38. Zanoni, M.; Piccinini, F.; Arienti, C.; Zamagni, A.; Santi, S.; Polico, R.; Bevilacqua, A.; Tesi, A. 3D tumor spheroid models for in vitro therapeutic screening: A systematic approach to enhance the biological relevance of data obtained. *Sci. Rep.* **2016**, *6*, 19103. [[CrossRef](#)] [[PubMed](#)]
39. Millard, M.; Yakavets, I.; Zorin, V.; Kulmukhamedova, A.; Marchal, S.; Bezdetnaya, L. Drug Delivery to Solid Tumors: The Predictive Value of the Multicellular Tumor Spheroid Model for Nanomedicine Screening. Available online: <https://www.dovepress.com/drug-delivery-to-solid-tumors-the-predictive-value-of-the-multicellul-peer-reviewed-article-IJN> (accessed on 19 February 2018).
40. Gaio, E.; Scheglmann, D.; Reddi, E.; Moret, F. Uptake and photo-toxicity of Foscan[®], Foslip[®] and Fospeg[®] in multicellular tumor spheroids. *J. Photochem. Photobiol. B* **2016**, *161*, 244–252. [[CrossRef](#)] [[PubMed](#)]



© 2018 by the authors. Licensee MDPI, Basel, Switzerland. This article is an open access article distributed under the terms and conditions of the Creative Commons Attribution (CC BY) license (<http://creativecommons.org/licenses/by/4.0/>).

8. Double loaded mTHPC-DCL

In the second part, we upgraded mTHPC-DCLs by additional loading of mTHPC in the lipid bilayer of liposomes. These results were reported in the article “Matryoshka-type liposomes offer the synergistic delivery of temoporfin to tumor spheroids”.

Double-loaded mTHPC-DCLs encapsulated inclusion complexes of mTHPC with Me- β -CD (MD) and mTHPC-TM- β -CD (TD) were prepared, characterized and tested in 2D and 3D *in vitro* models of HT29 human adenocarcinoma cells and tumor xenografted mice *in vivo*. The physico-chemical properties of double-loaded mTHPC-DCLs were comparable with single-loaded ones (Yakavets et al., 2018a). Based on the spectral characteristics, we assessed that almost 30% of mTHPC in DL-DCLs is bound to β -CDs in the inner aqueous core, while 70% of PS is localized in the lipid bilayer. In 2D monolayer cell culture, DL-DCLs behavior was similar to Foslip[®]. At the same time, the distribution of mTHPC in 3D multicellular tumor spheroids was significantly changed. The kinetics of mTHPC distribution were studied by flow cytometry and confirmed using laser scanning confocal microscopy of spheroids' cryosections at 24h. Moreover, we analyzed the content of mTHPC in the medium supplemented with different serum concentrations by means of gel-chromatography. Our studies indicated that TM- β -CD-based DL-DCL provides deep penetration of mTHPC into the multicellular tumor spheroids via TM- β -CD nanoshuttles upon the liposomes destabilization by serum proteins. Finally, we assessed PDT efficiency of DL-DCLs in multicellular spheroids *in vitro* and xenografted mice *in vivo* demonstrating similar photokilling ability of hybrid liposomes and Foslip[®] in both preclinical models.



Article

Matryoshka-Type Liposomes Offer the Improved Delivery of Temoporfin to Tumor Spheroids

Ilya Yakavets ^{1,2,3}, Marie Millard ^{1,2}, Laureline Lamy ^{1,2}, Aurelie Francois ^{1,2}, Dietrich Scheglmann ⁴, Arno Wiehe ⁴, Henri-Pierre Lassalle ^{1,2}, Vladimir Zorin ^{3,5} and Lina Bezdetnaya ^{1,2,*}

¹ Centre de Recherche en Automatique de Nancy, Centre National de la Recherche Scientifique UMR 7039, Université de Lorraine, Campus Sciences, Boulevard des Aiguillettes, 54506 Vandoeuvre-lès-Nancy, France

² Research Department, Institut de Cancérologie de Lorraine, 6 avenue de Bourgogne, 54519 Vandoeuvre-lès-Nancy, France

³ Laboratory of Biophysics and Biotechnology, Belarusian State University, 4 Nezavisimosti Avenue, 220030 Minsk, Belarus

⁴ Biolitec research GmbH, Otto-Schott-Strasse 15, 07745 Jena, Germany

⁵ International Sakharov Environmental Institute, Belarusian State University, Dauhabrodskaja 23, 220030 Minsk, Belarus

* Correspondence: l.bolotina@nancy.unicancer.fr (L.B.); Tel.: +33-(0)3-08-59-83-53

Received: 23 August 2019; Accepted: 12 September 2019; Published: 13 September 2019

Abstract: The balance between the amount of drug delivered to tumor tissue and the homogeneity of its distribution is a challenge in the efficient delivery of photosensitizers (PSs) in photodynamic therapy (PDT) of cancer. To date, many efforts have been made using various nanomaterials to efficiently deliver temoporfin (mTHPC), one of the most potent photosensitizers. The present study aimed to develop double-loaded matryoshka-type hybrid nanoparticles encapsulating mTHPC/cyclodextrin inclusion complexes in mTHPC-loaded liposomes. This system was expected to improve the transport of mTHPC to target tissues and to strengthen its accumulation in the tumor tissue. Double-loaded hybrid nanoparticles (DL-DCL) were prepared, characterized, and tested in 2D and 3D *in vitro* models and in xenografted mice *in vivo*. Our studies indicated that DL-DCL provided deep penetration of mTHPC into the multicellular tumor spheroids via cyclodextrin nanoshuttles once the liposomes had been destabilized by serum proteins. Unexpectedly, we observed similar PDT efficiency in xenografted HT29 tumors for liposomal mTHPC formulation (Foslip®) and DL-DCL.

Keywords: temoporfin; drug-in-cyclodextrin-in-liposome; hybrid nanoparticles; multicellular tumor spheroids; cyclodextrins; photodynamic therapy article; yet reasonably common within the subject discipline.)

1. Introduction

Nanomaterials are the cornerstone in the rapidly advancing field of nanotechnology, playing a crucial role in successful drug delivery at diseased sites [1]. To date, many nanoplateforms have been applied for the delivery of temoporfin (5,10,15,20-tetra(m-hydroxyphenyl)chlorin, mTHPC), one of the most promising photosensitizers (PSs) used in the photodynamic therapy (PDT) of solid cancers. Temoporfin has been marketed in the European Union since 2001 under the trade name Foscan® (biolitec pharma Ltd., Jena, Germany), and is indicated for the palliative treatment of head and neck squamous cell carcinoma [2]. Nanodelivery systems were supposed to overcome or improve the major constraints of mTHPC, such as low solubility, unfavorable pharmacokinetic profiles, and side effects (pain upon injection, skin photosensitivity) [3]. However, due to the complexity of drug

distribution processes, the use of individual NPs offered neither optimal, leakage-free delivery of mTHPC to the tumor nor the local release of large amounts of mTHPC. At the same time, multifunctional nanomedicines featuring high drug loading capacity, controllable drug release, and real-time self-monitoring are attracting immense interest due to their potential to improve cancer therapy efficacy [4–6].

In the present study, we have suggested combining NPs into one nanoplatfrom as an advanced alternative strategy for mTHPC delivery. Recently, we reported the encapsulation of mTHPC-cyclodextrin (CD) supramolecular complex into liposomes, namely drug-in-cyclodextrin-in-liposome (DCL), as a prospective nanodelivery system for mTHPC [7]. The upgraded double-loaded mTHPC-DCLs (DL-DCL) contained mTHPC in both lipid and aqueous compartments of lipid vesicles. We hypothesized that such “matryoshka-type” hybrid liposomes would combine the advantages of each delivery system (Figure 1). Liposomes are effective containers for selective mTHPC delivery to target sites [8]. However, liposomes have limited penetration into deep tissue layers [9,10]. Alternatively, mTHPC/CDs inclusion complexes easily penetrate tumor tissue, thereby significantly increasing PS accumulation [11]. However, these supramolecular complexes are prone to dissociation in vivo, once diluted in the bloodstream [12]. Thus, we suggested that the coupling of both delivery systems into one DL-DCL could restrain the dissociation of drug–mTHPC complexes, avoid rapid drug release, and favorably alter PS-penetration into tumor tissues.

In the present work, we prepared and characterized DL-DCLs and tested these complexes in 2D and 3D tumor cell cultures. We focused on the study of double-loaded mTHPC-DCLs in 3D multicellular tumor spheroids in terms of PS penetration and accumulation. Finally, we conducted a preliminary study on double-loaded mTHPC-DCL efficacy in vivo in tumor-xenografted mice.

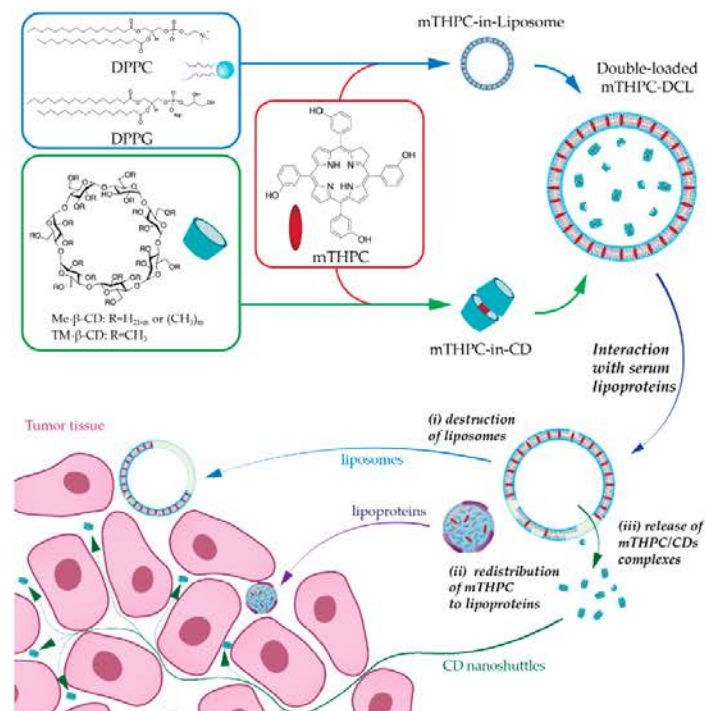


Figure 1. Double-loaded matryoshka-type mTHPC drug-in-cyclodextrin-in-liposomes (mTHPC-DCLs). Schematic illustration of the serum-mediated mTHPC release and penetration into the tumor tissue: (i) serum proteins disintegrate liposomal bilayer resulting in (ii) redistribution of lipid bilayer components (lipids and mTHPC) to serum lipoproteins (iii) as well as the release of water-soluble mTHPC/CD (cyclodextrin) inclusion complexes. Liposomes (blue arrow, Foslip®) and serum lipoproteins (purple arrow) interact only with outer layer cells, while CDs (green arrow) can penetrate the tumor tissue and deliver PS.

2. Results

2.1. Characterization

We prepared DL-DCLs with mTHPC encapsulated in the lipid membrane as well as in the aqueous core in the soluble form of inclusion complexes with β -CDs. Abbreviations MD and TD stand for DL-DCL with encapsulated mTHPC-Methyl- β -CD or mTHPC-Trimethyl- β -CD complexes, respectively. The hydrodynamic size, polydispersity index (PDI), and Zeta-potential of MD and TD were measured by dynamic light scattering. Both DL-DCLs had a narrow size distribution with a mean hydrodynamic diameter of 143.2 ± 1.5 nm for MD (PDI = 0.055 ± 0.033) and 122.9 ± 1.1 nm for TD (PDI = 0.040 ± 0.013) (Figure 2). The surface charge of MD and TD was negative, with Zeta potentials of -36.2 ± 4.3 mV and -37.5 ± 1.6 mV, respectively. It is worth noting that DL-DCLs have high colloidal stability (> 3 months) (data not shown). The encapsulation efficiencies (EE) of mTHPC in MD and TD were estimated as 11% and 16%. As control NPs, we used a conventional liposomal mTHPC formulation (Foslip[®]) with a hydrodynamic size of 114.2 ± 1.0 nm (PDI = 0.110 ± 0.015) and a Zeta potential of -34.4 ± 4.3 mV.

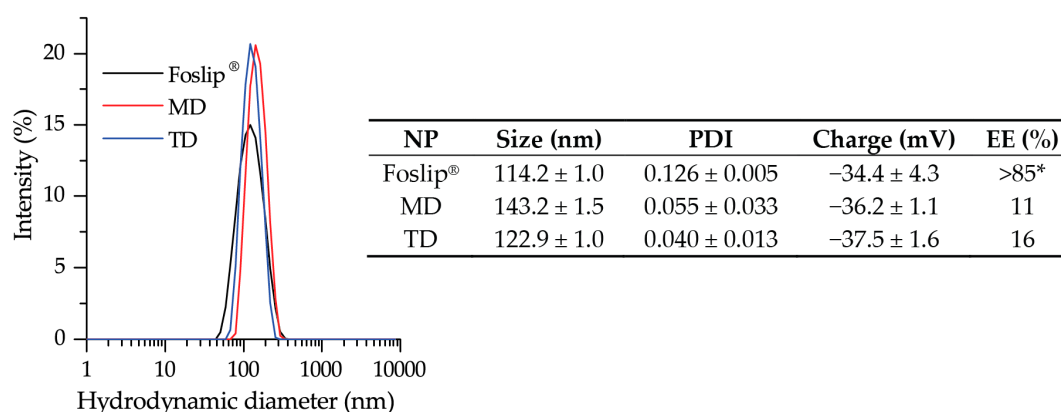


Figure 2. The hydrodynamic size of Foslip[®] (black) and DL-DCLs: MD (red) and TD (blue). Insert shows the physico-chemical characteristics of the NPs of hydrodynamic diameter (nm), polydispersity index (PDI), Z-potential (mV), and encapsulation efficiency (EE,%). *—taken from Reference [13]. Abbreviations MD and TD stand for DL-DCL with encapsulated mTHPC-Methyl- β -CD or mTHPC-Trimethyl- β -CD complexes, respectively.

Spectral characteristics of mTHPC-based nanoformulations in PBS are presented in Figure 3. All mTHPC formulations exhibited narrow spectral bands, indicating the monomeric state of mTHPC. The absorption spectra of Foslip[®], MD, and TD in PBS were characterized by a Soret band (maximum at 416 nm) and four Q-bands with prominent peaks at 650 nm (Figure 3a). The extinction coefficients of mTHPC in DL-DCLs were slightly higher ($35,400 \text{ M}^{-1}\text{cm}^{-1}$ and $37,200 \text{ M}^{-1}\text{cm}^{-1}$) than that of Foslip[®] ($31,100 \text{ M}^{-1}\text{cm}^{-1}$). The mTHPC fluorescence was emitted at 652 nm for all NPs. The relative fluorescence quantum yield (FY) of mTHPC encapsulated in DL-DCLs was comparable with Foslip[®] and was only 20% lower than a standard mTHPC ethanol solution. Figure 3b exhibits the excitation fluorescence spectra of mTHPC in various NPs in the Soret band region, which is considered to be sensitive to the binding of mTHPC with β -CDs [14]. The relative fluorescence in a short wavelength shoulder was significantly increased in DL-DCLs compared with Foslip[®] due to the formation of inclusion complexes between mTHPC and β -CD derivatives. To assess the changes in the shape of spectral band, we calculated I_1/I_2 , where I_1 and I_2 stand for the fluorescence intensities at 407 nm and 418 nm excitation, respectively. The calculated I_1/I_2 ratios for mTHPC in MD and TD were 0.88 and 1.00, while that of Foslip[®] was 0.80 (Figure 3b, insert). The microenvironment of mTHPC in NPs could also be characterized using fluorescence parameters such as fluorescence anisotropy and photoinduced fluorescence quenching (PIQ). Consistent with our previous report [13], the fluorescence anisotropy (r) of mTHPC in Foslip[®] was $6.2 \pm 0.4\%$, and the PIQ was $12 \pm 2\%$ (Figure 3b,

insert). In DL-DCL, both fluorescence anisotropy and PIQ values were increased, providing $r = 7.3 \pm 0.6\%$ and $PIQ = 21 \pm 5\%$ for MD, and $r = 9.9 \pm 0.7\%$ and $PIQ = 33 \pm 5\%$ for TD. Based on these values, we assessed that about 70% of mTHPC in the DL-DCLs was attached to the lipid bilayer, while 30% of PS was bound to CDs in the inner aqueous cores of the lipid vesicles.

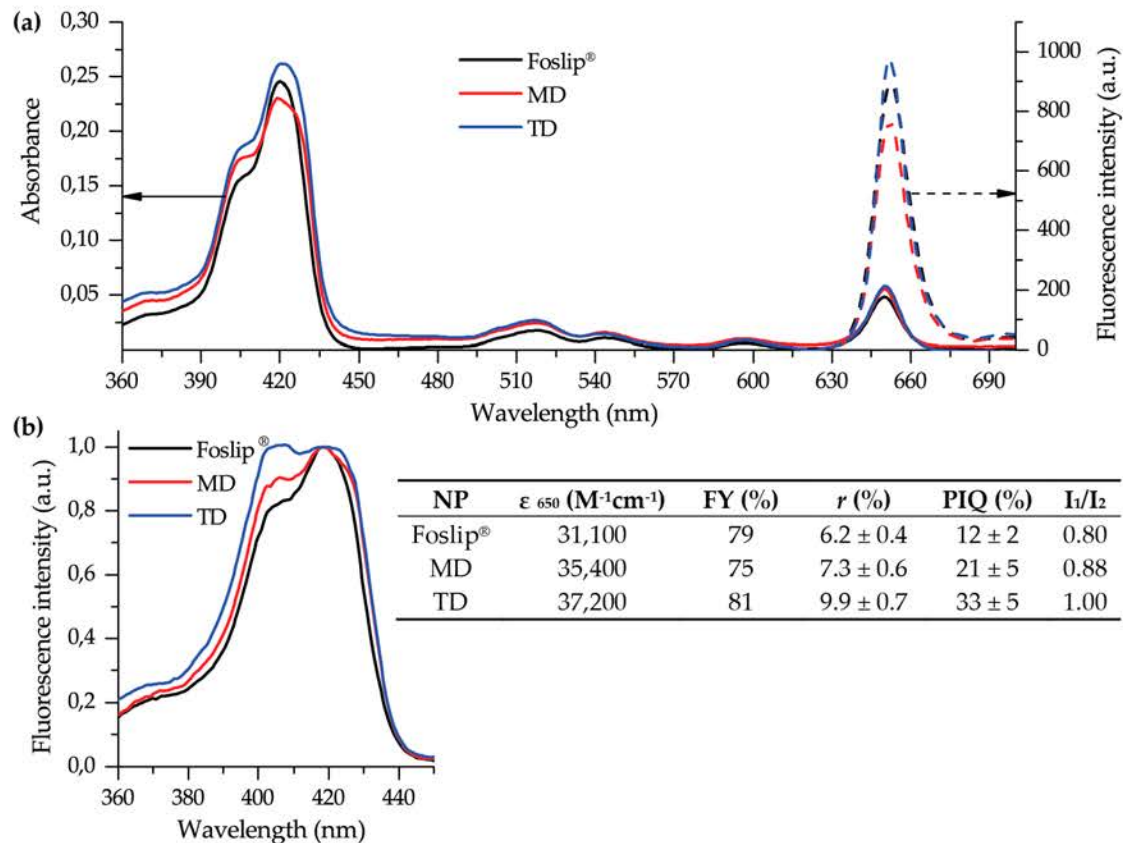


Figure 3. Spectral characteristics of Foslip® (black), MD (red), and TD (blue) in PBS. (a) Absorbance (solid line) and fluorescence emission (dotted line) spectra ($\lambda_{ex} = 420$ nm); (b) normalized fluorescence excitation spectra ($\lambda_{em} = 652$ nm). mTHPC concentration was $1.5 \mu M$. Insert shows the main spectral characteristics of NPs, such as extinction coefficient at 650 nm (ϵ_{650}); FY—fluorescence yield, relative to the fluorescence of mTHPC in ethanol; r —the degree of fluorescence anisotropy; PIQ—the degree of photoinduced quenching; I_1/I_2 —the ratio of Soret band components (I_1 and I_2 were measured under excitation at 407 nm and 418 nm, respectively, and emission at 652 nm).

2.2. Two-Dimensional (2D) Monolayer Cell Culture

The cellular uptake of mTHPC delivered by Foslip® or DL-DCLs was analyzed by flow cytometry. Flow cytometry histograms of HT29 human colon adenocarcinoma monolayer cells treated for 24 h with Foslip®, MD, and TD ($1.5 \mu M$) are presented in Figure 4a. All profiles had a narrow homogeneous distribution. The accumulation of mTHPC in HT29 monolayer was slightly lower for TD compared with MD and Foslip®. The estimated mean cellular fluorescent intensities for Foslip® and MD were 140 ± 14 a.u. and 149 ± 21 a.u. ($p > 0.05$), respectively, while that for TD was significantly lower (80 ± 9 a.u.; $p < 0.05$).

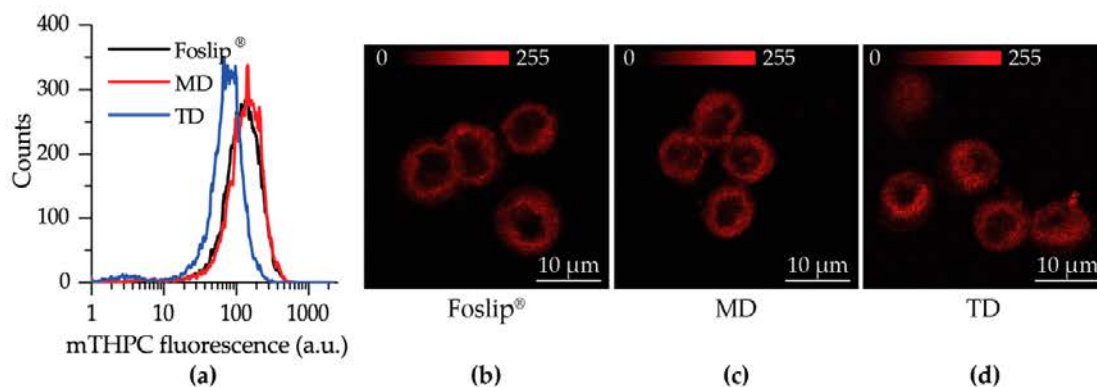


Figure 4. (a) Flow cytometry histograms of HT29 monolayer cells treated with Foslip® (black), MD, (red) and TD (blue) for 24 h; (b–d) Typical confocal images of mTHPC fluorescence in HT29 monolayer cells at 3 h post-incubation with (b) Foslip®, (c) MD, and (d) TD. Scale bar: 10 µm. The concentration of mTHPC was 1.5 µM. Serum concentration was 2%.

Intracellular localization of mTHPC in HT29 monolayer cells was evaluated using confocal microscopy after 3 h of incubation (Figure 4b–d). No remarkable difference in intracellular mTHPC localization between Foslip® and DL-DCLs was observed. All NPs exhibited a similar mTHPC fluorescence pattern in cells, characterized by diffuse fluorescence in the cytoplasm outside both the nucleus and outer plasma membrane. Similar localization patterns were observed in human pharynx squamous cell carcinoma (FaDu) (Figure S1).

2.3. Three-Dimensional (3D) Multicellular Tumor Spheroids

2.3.1. Accumulation and Distribution

We performed chemical extraction of mTHPC from HT29 spheroids after 3, 6, and 24 h incubation with Foslip® or DL-DCLs (4.5 µM) (Figure 5a). Accumulation of mTHPC in spheroids for all NPs increased continuously over 24 h. At short incubation times (3 and 6 h), mTHPC accumulation was slightly but significantly higher in TD-treated spheroids compared to those treated with Foslip® ($p > 0.05$). At 24 h incubation, the highest amount of mTHPC was observed in MD-treated spheroids (17.3 ± 2.9 ng/spheroid), although it was not significant compared with TD and Foslip® (14.6 ± 2.3 and 11.9 ± 2.6 ng/spheroid, respectively; $p > 0.05$).

Afterwards, we assessed the accumulation of mTHPC in individual cells in spheroids using flow cytometry analysis (Figure 5b–e and Figures S2, S3). Figure 5b–d displays the kinetics of mTHPC uptake in HT29 spheroids treated with various nanoformulations. We observed that Foslip® continuously accumulated from 3 h incubation, but only in a small fraction of cells, thus resulting in a strongly heterogeneous distribution of mTHPC across the spheroids. On the other hand, spheroids treated with MD demonstrated a more homogeneous distribution, especially visible after 24 h of incubation (Figure 5e). Figure 5e displays a typical distribution of mTHPC in HT29 spheroids treated with nanoformulations, while the histograms from independent experiments are presented in Figure S2. Finally, the fluorescence in TD treated spheroids represented one narrow peak in the histogram irrespective of incubation time, indicating an almost homogeneous mTHPC distribution across spheroids. FaDu spheroids were assessed after 24 h incubation with nanoformulations (Figure S3). Foslip® and TD provided distribution profiles in FaDu spheroids similar to those in HT29 spheroids, while the MD distribution was more heterogeneous compared with that in HT29.

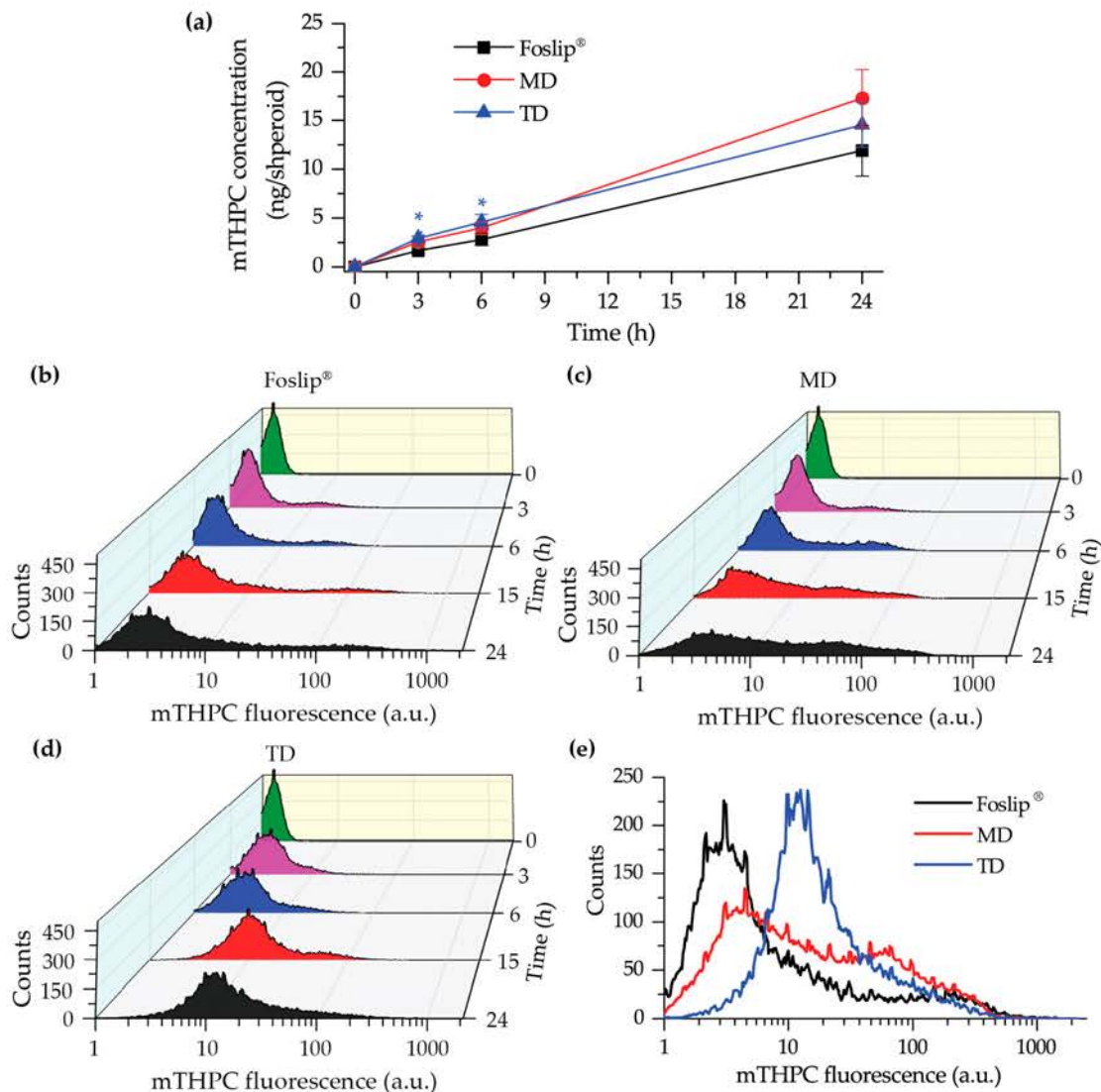


Figure 5. (a) Kinetics of mTHPC uptake in HT29 spheroids after incubation with Foslip® (black), MD (red), and TD (blue) using chemical extraction in absolute ethanol. The data are presented as mean \pm standard deviation. * $p < 0.05$ compared to Foslip®; (b–e) Typical flow cytometry histograms of trypsinized spheroids treated with (b) Foslip®, (c) MD, and (d) TD at 3, 6, 15, and 24 h post-incubation. (e) Typical flow cytometry histograms of HT29 spheroids treated with Foslip® (black), MD (red), and TD (blue) for 24 h. mTHPC concentration was 4.5 μ M. Serum concentration was 2%.

2.3.2. Penetration

To confirm the results of the flow cytometry-based distribution, we analyzed cryosections of spheroids treated with NPs for 24 h using laser scanning confocal microscopy (Figure 6a). For a better comparison of mTHPC distribution in spheroids, the images were completed with surface plots of fluorescence patterns (Figure 6b). As seen in Figure 6a,b, Foslip® and MD displayed strong mTHPC fluorescence only on the periphery of the spheroids, while for TD, mTHPC fluorescence was observed across the whole spheroid, demonstrating complete PS penetration. Similar patterns of mTHPC distribution were observed in FaDu spheroids treated with Foslip® and TD (Figure S4). The comparison of linear profiles demonstrated a slightly deeper penetration of MD in HT29 spheroids compared with Foslip®. However, the mTHPC fluorescence signal at 100 μ m from the periphery of the spheroids was undetectable for both formulations. At the same time, the fluorescence of mTHPC delivered by TD was almost constant throughout the whole spheroid depth.

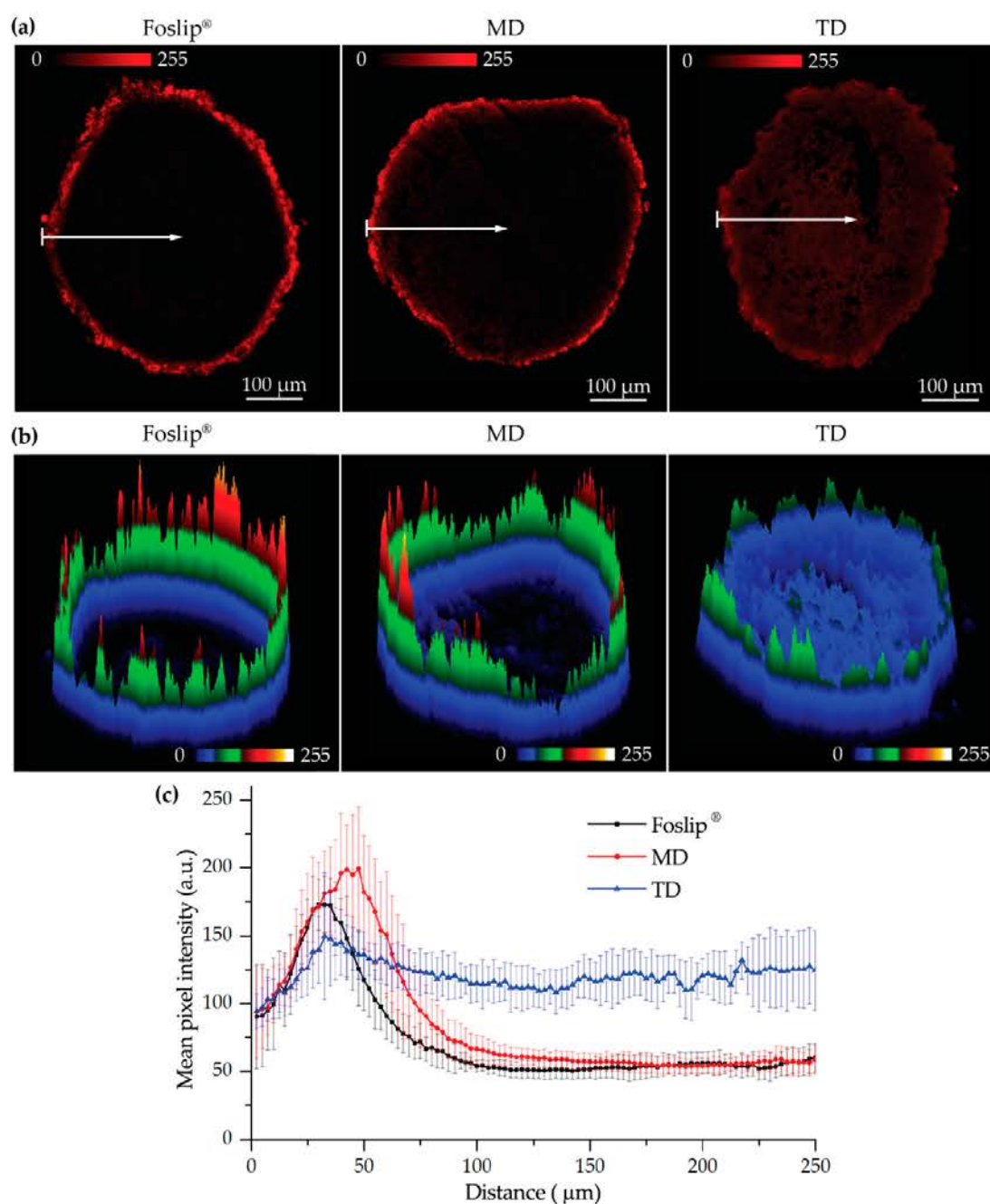


Figure 6. (a) Typical fluorescence images and corresponding (b) surface plots of mTHPC fluorescence in HT29 spheroids after 24 h incubation with various mTHPC formulations (Foslip®, MD, and TD); (c) penetration profiles of Foslip® (black), MD (red), and TD (blue) in HT29 spheroids after 24 h. The data are presented as mean \pm standard deviation obtained from $n = 7$ spheroids. mTHPC concentration was 4.5 μM . Serum concentration was 2%. mTHPC fluorescence is displayed in red color (2D images) and in pseudo-colors (3D surface plots).

2.3.3. Serum-Induced Release of CDs

In order to confirm the release of CDs upon serum-induced destabilization of the liposomal vesicles, we analyzed mTHPC fluorescence intensities in the medium supplemented with serum at different concentrations (Figure 7a). After 24 h incubation of spheroids with NPs, the collected supernatant was centrifugated, filtered, and analyzed by gel exclusion chromatography. Figure 7b,c represents the distribution of mTHPC between eluted fractions. Based on the calibration experiment

(data not shown), the elution range of liposomes and DL-DCLs was 30–45 mL, serum protein fractions were eluted at 50–90 mL, and mTHPC-CD complexes, as the smallest in size, were eluted only at 90–105 mL. The estimated percentage of mTHPC bound to each fraction is displayed in Figure 7d. According to these data, mTHPC was efficiently released from Foslip® and 50% of PS was bound to serum proteins in the medium enriched with 2% of serum. When the percentage of serum was increased up to 9%, only 15% of mTHPC was detected in liposomes. On the other hand, both DL-DCLs contained higher mTHPC concentrations after 24 h incubation with spheroids compared to Foslip®. The remaining fraction of mTHPC in MD and TD for 2% of serum was 79% and 76%, respectively, and 48% and 50% for 9% serum. Most importantly, we directly detected the presence of mTHPC-CD complexes in the medium after incubation of the spheroids with TD, and the fraction of mTHPC-CD complexes increased from 13% to 23% when the serum content in the medium increased from 2% to 9%. Alternatively, in the case of MD, the released mTHPC was bound to serum proteins only.

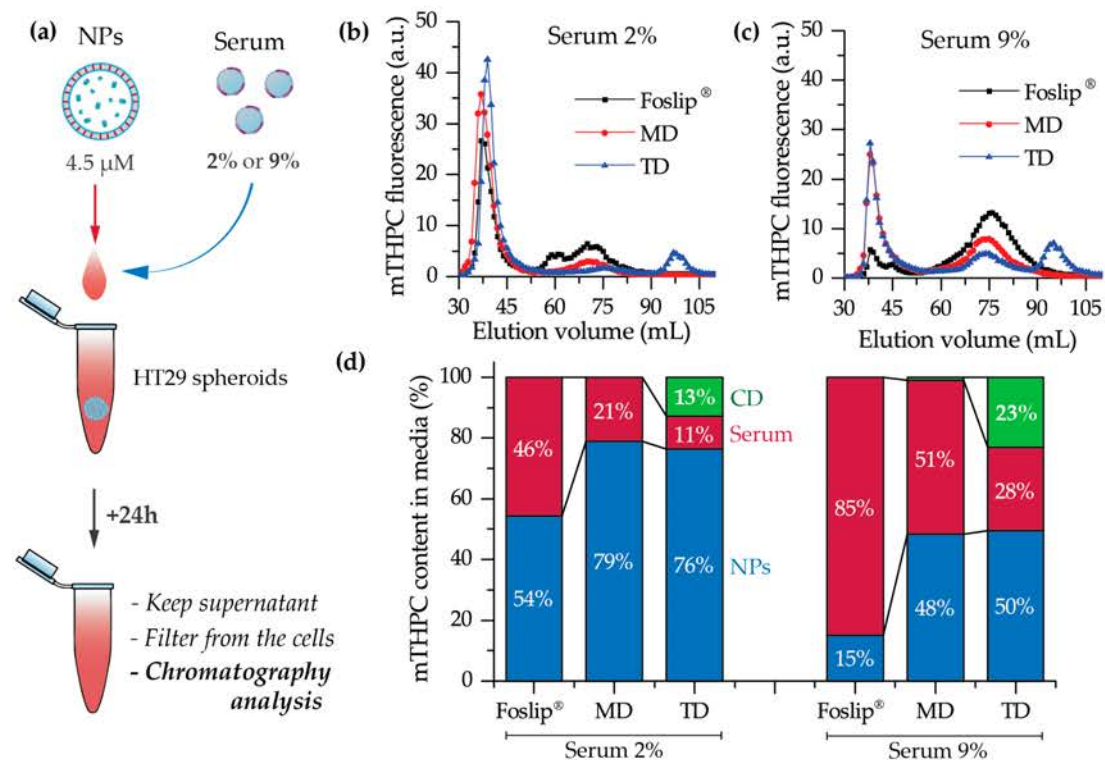


Figure 7. (a) Scheme of the experiment; (b,c) chromatography histograms of culture medium after 24 h incubation of HT29 spheroids with mTHPC (4.5 μM) in nanoformulations in the presence of (b) 2% and (c) 9% of serum; (d) the percentage of mTHPC bound with NPs (blue) or serum proteins (red) and in complexes with CDs (green).

2.4. PDT

Considering that better penetration and distribution of mTHPC delivered by DL-DCLs could improve PDT efficiency, we assessed the viability of HT29 spheroid cells using a propidium iodide fluorescent probe. Spheroids, treated with NPs for 24 h were irradiated at 40 J/cm² (90 mW/cm²), trypsinated 6 h later, and analyzed by flow cytometry. Cell viability in control (no-drug, no-light) and (no-light) groups was about 82% for all NPs. PDT resulted in a significant decrease in cell viability, yielding about 40% necrotic cells. Surprisingly, photoinduced necrosis was similar for all types of NPs (39 ± 2% vs. 40 ± 4% vs. 41 ± 2% for Foslip®, MD, and TD, respectively; *p* > 0.05).

We further studied PDT tumor response in vivo in a xenografted mice model. Kaplan–Meier plots of tumor response to Foslip®- and TD-PDT are presented in Figure 8. The tumor growth delay

was about 30.7 days for Foslip® and 26.6 days for TD ($p > 0.05$). For both NPs, the response was significantly different from the control no-light (n.l.) groups ($p < 0.05$).

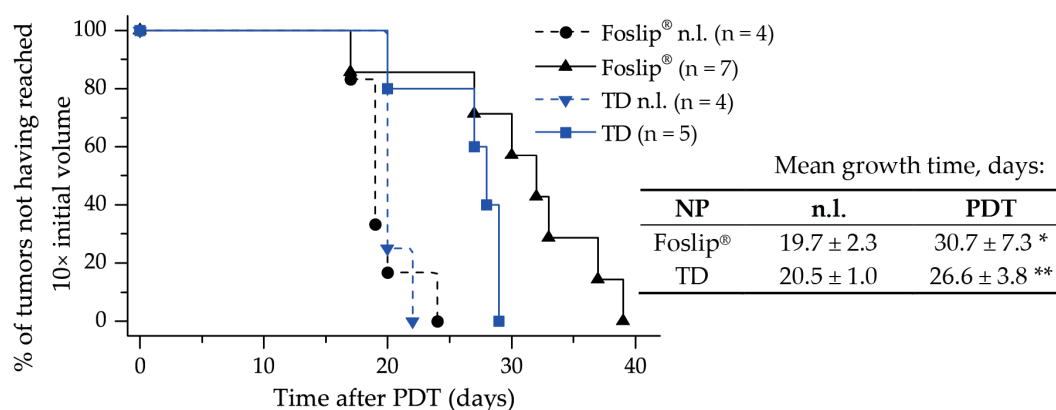


Figure 8. Kaplan–Meier plots of HT29 tumor growth delay and mean tumor growth time (time to reach 10× the initial tumor volume) of control no-light (n.l.) groups and mice after PDT with Foslip® and TD at 24 h of drug-light-interval. * statistically different from Foslip® n.l. control group, $p < 0.05$; ** statistically different from TD n.l. control group, $p < 0.05$.

3. Discussion

To date, hybrid NPs, combining several nanomaterials in one, have attracted increasing attention as anti-cancer delivery systems [15]. The careful selection of the combined nanomaterials could result in a considerable synergistic effect overcoming the individual nanostructures' limitations. In the case of mTHPC, a synergy could be achieved by a coupling of CD-based nanoshuttles and liposomes. mTHPC exhibits an extremely strong affinity to methylated β -CDs (10^6 – 10^7 M⁻¹ for Me- β -CD and TM- β -CD, respectively [16]) leading to the unique possibility of altering mTHPC biodistribution via a nanoshuttle mechanism [11,17]. At the same time, liposomal formulations of mTHPC display selective delivery of PS to tumor tissue [8]. CDs could be regarded as an added value to mTHPC-based liposomes, and as such, could increase drug loading capacity, entrapment efficiency, prolong the circulation time of the drug in the bloodstream, reduce toxicity, and finally provide controlled release [18,19]. Thus, we supposed that such a “matryoshka-doll” nanostructure could be a potent delivery system, providing both passive tumor targeting by liposomes and deep penetration of mTHPC/CD complexes into the tumor tissue (Figure 1).

Recently, we optimized the composition of mTHPC-DCLs, selecting two of the most potent DCLs based on methylated β -CDs [7]. In the present study, the lipid bilayers of selected DCLs were additionally loaded with lipophilic mTHPC, achieving DL-DCLs. Physico-chemical characteristics (size, PDI, charge, and colloidal stability) of DL-DCLs were similar to those of single-loaded DCLs [7], and comparable with liposomal mTHPC formulation Foslip® (Figure 2). According to the preparation technique, the ratio between aqueous volume of liposomes and void volume during the liposome preparation was low, explaining the low EE values of mTHPC in DL-DCLs [7,20]. The complete monomerization of mTHPC in all NPs was confirmed by absorption spectra (Figure 3a), and double encapsulation of mTHPC in DCLs was established using fluorescence spectroscopy (Figure 3b). The presence of mTHPC/CD complexes led to the increase of I_1/I_2 ratio [14], demonstrating $I_1/I_2 = 0.88$ and 1.00 for MD and TD, respectively, while in the case of Foslip®, I_1/I_2 was 0.8 (Figure 3b). At the same time, the high loading of mTHPC in the lipid bilayer resulted in fluorescence quenching [13,21], causing the decrease of FY, PIQ, and r values (Figure 3b, insert). Overall, 30% of mTHPC was encapsulated in CD complexes, while the fraction of PS in the lipid bilayer was 70%.

We further tested DL-DCLs in 2D and 3D in vitro tumor models. In 2D monolayer cell cultures, the behavior of both double-loaded mTHPC-DCLs was similar to that of Foslip® (Figure 4 and Figure

S1), while in 3D multicellular spheroids, we clearly demonstrated the benefits of matryoshka-type hybrid liposomes against conventional lipid vesicles. The 3D multicellular tumor spheroids more closely mimicked the native tumor environment, representing the tumor stroma tissue and offering better prediction potential when testing the penetration ability of nanomedicines [22]. The data of chemical extraction of mTHPC from spheroids demonstrated an almost similar amount of mTHPC at various incubation times (Figure 5a). However, detailed study using flow cytometry showed different profiles of mTHPC accumulation in the spheroid cells for DL-DCLs and Foslip®. The spheroids treated with TD displayed a homogeneous distribution between all cells at all time points for both HT29 (Figure 5d) and FaDu spheroids (Figure S2), while for MD and Foslip®, the accumulation of mTHPC was mainly associated with the PS uptake in a small fraction of cells (Figure 5b,c and Figure S2). At 24 h post-incubation, MD exhibited a slightly more homogeneous PS distribution in HT29 spheroids than Foslip® (Figure 6). The fluorescence imaging data of spheroid frozen-cut sections confirmed the almost homogeneous distribution of mTHPC delivered by TD in both types of spheroid cells (Figure 6 and Figure S3). In the case of TD, the mTHPC fluorescence signal was uniform for the whole spheroid, while for MD and Foslip®, a strong peripheral fluorescence signal dropped to background values at 50 and 100 μM from the spheroid periphery, respectively. In all probability, the observed effect was related to the presence of mTHPC/CDs in the media due to DL-DCL disintegration, as has been previously observed for Foslip® [10,23]. Indeed, in the case of TD, chromatography analysis of culture media after 24 h incubation of NPs with tumor spheroids demonstrated the presence of mTHPC/CD complexes. To confirm the serum-induced destruction of DL-DCLs, we demonstrated the increase of the mTHPC-TM- β -CD fraction in the medium supplemented with 9% of serum compared to 2% (Figure 7). It is worth noting that the MD-treated samples contained a similar amount of mTHPC in NPs, while all released mTHPC in the medium was localized only in serum proteins. Compared with TM- β -CD, Me- β -CDs possess less affinity to mTHPC [17]; thus, the equilibrium distribution of mTHPC is shifted to serum proteins [18]. Therefore, we suppose that the lifetime of mTHPC-Me- β -CDs was too short to penetrate the deep layers of spheroids, and mTHPC released from the MD was quickly redistributed to both serum proteins and the nearest tumor cells by Me- β -CDs, while long-living mTHPC-TM- β -CD complexes could easily penetrate to the deep tissue regions.

Finally, we assessed the PDT efficiency of TD and MD in 3D multicellular tumor spheroids *in vitro*, and of TD in xenografted mice *in vivo*. Despite the remarkable difference in penetration profiles, PDT-induced cell death in spheroids treated with TD and MD was similar to Foslip®. The same tendency was observed in the xenografted mice model: the difference in mean tumor growth delay for both TD and Foslip® was about 30 days (Figure 8). We likely did not achieve the desired balance between the accumulation and distribution of PS in the tumor. We suggest that increasing the TD concentration could be helpful in exceeding the threshold of intracellular PS accumulation needed for efficient DCL-PDT photokilling.

4. Materials and Methods

4.1. Materials

mTHPC and its liposomal formulation (Foslip®) were kindly provided by biolitec research GmbH (Jena, Germany). The stock solution of mTHPC (2 mM) was prepared in methanol and kept at 4 °C in the dark. Foslip®, based on dipalmitoylphosphatidylcholine (DPPC) and dipalmitoylphosphatidylglycerol (DPPG) liposomes with a mTHPC/lipid ratio of 1:12 (mol/mol), was prepared by solubilizing powder in ultrapure water (UPW, Milli-Q® Advantage A10® System, Millipore, Eschborn, Germany) to a final mTHPC concentration of 2 mM.

Random methyl- β -cyclodextrin (Me- β -CD; product code CY-2004.1,29; substitution degree of 12, average molecular weight 1135 Da) and heptakis(2,3,6-tri-O-methyl)- β -cyclodextrin (TM- β -CD; product code CY-2003,34; molecular weight 1429.6 Da) were purchased from CYCLOLAB R&D. Ltd., (Budapest, Hungary). DPPC and DPPG were purchased from Sigma (USA).

4.2. DL-DCL Preparation

DCLs were prepared by the thin lipid film hydration method, as described previously [7]. Briefly, inclusion complexes of mTHPC with β -CDs were formed using the solvent co-evaporation method in UPW. DPPC/DPPG liposomes loaded with mTHPC were prepared by membrane extrusion technique according to the previously published procedure, yielding unilamellar liposomes [24]. These liposomes contained DPPC and DPPG at a molar ratio of 9:1, with a final lipid concentration of 15 mg/mL. To obtain DL-DCLs, mTHPC was added at the step of the preparation of lipid mixture at a molar drug/lipid ratio of 1:15, and mTHPC/ β -CD inclusion complexes were encapsulated at the lipid film hydration step. The purification of DCLs from the non-encapsulated mTHPC/ β -CDs in the medium was performed using a minicolumn chromatography technique [25].

4.3. Cell Lines

HT29 human colon adenocarcinoma cell line was purchased from ATCC (LGC Promochem, Molsheim, France). FaDu (human pharynx squamous cell carcinoma) cell line was purchased from ATCC (Cat. No: ATCC1 HTB-43™). Cells were cultured in phenol red-free Roswell Park Memorial Institute 1640 medium (RPMI-1640, Invitrogen™, Carlsbad, California, USA), supplemented with 9% (vol/vol) heat-inactivated fetal bovine serum (Sigma-Aldrich, St. Louis, MO, USA), penicillin (10,000 IU) streptomycin (10,000 mg/mL) and 1% (vol/vol) 0.2 M glutamine (Invitrogen™, Carlsbad, California, USA). Cells were kept as a monolayer culture in a humidified incubator (5% CO₂) at 37 °C. Cell culture was reseeded every week to ensure exponential growth.

4.4. Multicellular Tumor Spheroid Model

HT29 MCTSs were initiated as previously described [26]. Briefly, flasks coated with 1% L-agarose were seeded with 5×10^4 HT29 cells/mL. After three days, cellular aggregates were transferred into spinner flasks (Integra Biosciences, Cergy Pontoise, France) containing 125 mL RPMI-1640 medium supplemented with 9% FBS. Spinner flasks were placed under constant agitation at 75 rpm at 37 °C (5% CO₂, humidified atmosphere) for 15 days. Spheroids were filtered to approximately 500 μ m in diameter before conducting experiments.

MCTSs were generated from FaDu cells using the liquid overlay technique (LOT), as described previously [27]. Briefly, 100 μ L of FaDu cells (5×10^4 cells/ml) and 100 μ L of full RPMI medium were added to each well of a 96-well plate previously coated with 1% agarose (w/v in water), and cultured at 37 °C, 5% CO₂ for 5 days before being taken into experiments.

For dissociation, spheroids were transferred into a 12-well plate, washed twice with PBS and further incubated with 0.025% trypsin (GIBCO™, ThermoFisher, Waltham, MA, USA) and 0.01% ethylenediaminetetraacetic acid (GIBCO™, ThermoFisher, Waltham, MA, USA). For complete trypsinization, the plate with spheroids was placed on a rotatory shaker (60 rpm) for 30 min in subdued light. After dissociation, trypsin action was inhibited by the addition of 3 mL complete culture medium (9% FBS), and the cell suspension was centrifuged to a pellet and further re-suspended in a fresh medium.

4.5. Fluorescence Staining

For in vitro cell experiments, stock NP solutions were diluted in RPMI-1640 supplemented with 2% heat-inactivated fetal bovine serum (FBS, Life Technologies, Carlsbad, California, USA) to obtain the final mTHPC concentration of 1.5 μ M for 2D monolayer cells and 4.5 μ M for 3D tumor spheroid experimentation.

For the 2D monolayer cell culture, cells (5×10^4 cells/mL) were seeded in 24-well plates for 72 h and then incubated with Foslip®, MD, or TD (1.5 μ M). In the case of 3D cell culture, before incubation with mTHPC NPs (4.5 μ M), spheroids were washed with serum-free RPMI-1640 medium. PS incubation was performed in the dark at 37 °C in a humidified 5% CO₂ air atmosphere.

4.6. Animal Model

All experiments were performed in accordance with animal care guidelines from the European Union and were approved by the appropriate authority. The animal project registered under the number (#2438) received a favorable assessment from the Ethics Committee and was approved by the French Higher Education and Research Minister. All procedures involving animals were performed under general anesthesia with inhaled isoflurane (Vetflurane; Virbac, France) using a Univentor 400 anesthesia unit (Genestil, Royaucourt, France). Mice were housed in filtered air cabinets with a 12 h light/dark cycle at 22–24 °C and 50% humidity, provided with food and water ad libitum, and manipulated following aseptic procedures. Female NMRInu/nu mice (Janvier, St Berthevin, France) aged 9–10 weeks were used, with a mean bodyweight of 30 ± 3 g. Mice were inoculated subcutaneously in the left flank with 8×10^6 exponentially growing HT29 cells and the experiments were initiated 5–7 days after inoculation when the tumors reached 50 mm³ in volume.

4.7. Analytical Techniques

4.7.1. Spectroscopy

Absorption measurements were recorded with a Lambda 35 spectrometer (Perkin Elmer, USA) and fluorescence measurements were conducted with a LS55B spectrofluorometer (PerkinElmer, USA) equipped with polarizers, thermostated cuvette compartments, and magnetic stirring for polarization experiments. The concentrations of mTHPC in DL-DCLs and Foslip® were estimated spectroscopically ($\lambda_{em} = 652$ nm) by dissolving nanoparticles in methanol. DL-DCLs were previously purified by minicolumn chromatography. Fluorescence quantum yield and photoinduced fluorescence quenching were measured as previously described (λ_{ex} : 416 nm; λ_{em} : 652 nm) [15]. The measurements of mTHPC fluorescence anisotropy were performed as described earlier (λ_{ex} : 430 nm; λ_{em} : 652 nm) [15]. EE of mTHPC in DCLs was measured spectroscopically (λ_{em} : 652 nm) immediately after extrusion and purification, as previously described [7].

The hydrodynamic diameter of NPs, polydispersity index, and Z-potential were determined using photon-correlated spectroscopy by a Zetasizer Nano ZS (Malvern Instruments, UK) as previously reported [7].

4.7.2. Flow Cytometry

Flow cytometry analysis was performed using a FACSCalibur (BD, Franklin Lakes, NJ, USA), equipped with lasers emitting at 488 nm and 633 nm. Flow cytometry histograms were obtained from the suspension of cells after dissociation of 50 NP-treated spheroids. The fluorescence of mTHPC was detected in the fluorescence channel FL4 with a 661 ± 16 nm filter under excitation at 633 nm. Propidium iodide (PI) fluorescence was detected in the FL2 channel with a 585 ± 42 nm filter (excitation at 488 nm). Data analysis was carried out using Flowing Software (Turku Centre for Biotechnology, Turku, Finland).

4.7.3. Fluorescence Microscopy

HT29 cells (3×10^4 cells/mL) were plated into Lab-Tek II chamber Slide (Roskilde, Denmark), incubated in the dark at 37 °C with 1.5 μ M of mTHPC in different formulations for 3 h and then rinsed with PBS. mTHPC fluorescence was observed with a confocal laser-scanning microscope (Leica SP5 X AOBs LCSM, Leica microsystem, Wetzlar, Germany). For the 2D monolayer cell culture, fluorescence images were recorded using an oil immersion $\times 40$ objective. The 3D tumor spheroids were embedded into a resin Shandon™ Cryomatrix™ (ThermoFisher, Waltham, MA, USA), frozen, cut, and 20 μ m thick cryosections were further analyzed by confocal microscopy ($\times 10$ objective). Fluorescence of mTHPC in FaDu 2D monolayer cells and frozen-cut cryosections of FaDu spheroids was analyzed using an upright epifluorescence microscope (AX-70 Provis, Olympus, France). The fluorescence images were obtained using a filter set at 405–445 nm excitation associated with a 570 nm dichroic mirror and a 590 nm long-pass emission filter for fluorescence measurements.

Analysis of the images was performed with ImageJ (NIH, USA) software. To estimate the penetration profile of dye in the spheroids, special macros were proposed. Briefly, the spheroid area was divided into 100 concentric rims, with the diameter decreasing in a linear way. After that we calculated the mean intensity of pixels in each rim. The final profiles were plotted as mean \pm standard deviation from different cryo-sections ($n = 7$).

4.7.4. Uptake in Spheroids

mTHPC uptake in spheroids was measured by chemical extraction of mTHPC. After 3, 6, and 24 h incubation with NPs (4.5 μ M), spheroids were dissociated and individual cells were subjected to the extraction of mTHPC with ethanol (99.6%) as previously described [11]. Briefly, after sonication (15 min) and centrifugation (5 min, 1500 rpm), mTHPC fluorescence in the supernatant was assessed (λ_{ex} : 420 nm; λ_{em} : 652 nm).

4.7.5. Chromatography

Chromatographic experiments were performed on a Sigma 1.5 \times 75 cm column filled with Sepharose CL-6B gel (GE Healthcare, USA) pre-equilibrated with PBS, with a total bed volume of 150 mL. HT29 tumor spheroids were incubated in RPMI-1640 media which was supplemented with 2% and 9% FBS. The NPs were added at final mTHPC concentration of 4.5 μ M. After 24 h incubation, the supernatant was centrifuged (5 min, 1500 rpm), filtered using a 450 μ m Millex[®] – HV syringe driven filter unit (Sigma-Aldrich, St. Louis, MO, USA), and injected into the column using a three-way connector. Fractions of 1 mL were collected by an automated fraction collector. The column was stored at room temperature and separation was carried out in a partially light-protected environment to avoid mTHPC photobleaching. Fractions with elution volumes from 25 to 120 mL were collected and analyzed for mTHPC content using a SAFAS Xenius XM (SAFAS, Monaco, France) spectrofluorometer, as previously reported [28]. The mTHPC content in the chromatographic fractions was estimated by measurements the fluorescence intensity after the addition of 0.2% Triton[®] X-100 to the samples. The analysis of chromatography histograms was performed using Origin software (OriginLab, Northampton, MA, USA).

4.8. Photoirradiation of Spheroids

HT29 spheroids were transferred from the spinner flask to 12-well plates and incubated with NPs for 24 h (4.5 μ M). Spheroids were then washed and subjected to irradiation. Irradiation was performed at 652 nm with a Ceralas PDT diode laser (CeramOptec GmbH, Bonn, Germany) at 40 J/cm² (fluence rate of 90 mW/cm²). Control spheroids were exposed to mTHPC only (drug, no light). The viability of the spheroid cells was assessed by propidium iodide probe. Spheroids were trypsinated 6 h post-PDT and the obtained cell suspension was stained with 1 μ g/mL PI (Biolegend, San Diego, CA, USA) for 15 min in the dark at 37 °C, rinsed, and analyzed by flow cytometry.

4.9. Animal Experiments

NPs were administered intravenously by a tail vein injection at a dose of 0.15 mg/kg of mTHPC. Following the injection, mice were kept in the dark, and experiments were undertaken with minimal ambient light. Tumor irradiation was performed at 652 nm with a Ceralas PDT diode laser. The mice were treated 24 h post-administration at a fluence of 10 J/cm² and the fluence rate of 100 mW/cm². Just after PDT and 24 h later, mice received analgesia by subcutaneous injection of a mixture of 0.08 mg/kg buprenorphine (Axiene, Pantin, France) and 1 mg/kg of the non-steroid anti-inflammatory Metacam (Boehringer Ingelheim, Ingelheim, Germany) Mice were kept in the dark for 7 days after PDT. Three times per week, the perpendicular diameters of the tumors were measured to document tumor growth. Tumor volume (V) was calculated using the equation: $V = W^2 \times Y/2$, where (W) and (Y) are the smaller and larger diameters. Mice were sacrificed when tumor volume reached the ethical size of 1000 mm³.

4.10. Statistics

The data from at least three independent experiments are presented as mean \pm standard deviation. The data were evaluated using nonparametric Mann–Whitney U test (StatView™ software) with a significance level of $p < 0.05$.

5. Conclusions

The complexity of drug distribution processes requires innovative approaches in designing drug delivery platforms. Hybrid delivery systems have proven to be a powerful tool capable of combining the benefits of individual NPs into one nanoplatform. Our study confirmed the advantage of double-loaded mTHPC-DCLs over a conventional mTHPC liposomal formulation (Foslip®) in terms of tumor tissue penetration. Altogether, the proposed matryoshka-type lipid vesicles releasing mTHPC/CD complexes illustrated an optimal PS distribution in in vitro 3D models of tumor tissue.

Unexpectedly, we did not find phototoxic benefits of matryoshka-type liposomes over Foslip® in multicellular spheroids in vitro or in an animal experiment in vivo, at least under our experimental conditions. Our ongoing studies address different experimental settings, aiming for matryoshka system optimization in preclinical models. One of the possible solutions is the incorporation of stimulus-response moieties in liposomes to promote the release of CD nanoshuttles at the target site.

Supplementary Materials: Figure S1: Typical epifluorescence images of mTHPC fluorescence in FaDu monolayer cells at 3 h post-incubation with Foslip®, MD, and TD; Figure S2: Flow cytometry histograms of HT29 spheroids treated with Foslip®, MD, and TD for 24 h. Figure S3: Typical flow cytometry histograms of FaDu spheroids treated with Foslip®, MD, and TD for 24 h; Figure S4: Typical brightfield/fluorescence overlay images of mTHPC in FaDu spheroid cryosections after 24 h incubation with various mTHPC formulations (Foslip®, MD, and TD).

Author Contributions: I.Y. designed and performed the experiments and drafted the manuscript, M.M., L.L. and A.F. performed the experiments; HP.L. contributed to manuscript editing, D.S. and A.W. contributed to manuscript editing and validated the manuscript; V.Z. and L.B. participated in the conceptualization and supervision of the work. All authors read and approved the final manuscript.

Funding: This work was supported by the Institut de Cancérologie de Lorraine, French “Ligue Nationale contre le Cancer (CCIR-GE)”, Belarusian Republican Foundation for Fundamental Research (BRFFR) [grant numbers: M17MC-028, M18MB-002] and the Ministry of Education of the Republic.

Acknowledgments: The authors are grateful to IBISA platform for the acquisition of confocal images and Platform of Biophysics and Structural Biology (UMS 2008 IBSLor, UL-CNRS-INSERM) for the access to photon correlation spectroscopy.

Conflicts of Interest: The authors declare no conflict of interest.

References

1. Patra, J.K.; Das, G.; Fraceto, L.F.; Campos, E.V.R.; del Pilar Rodriguez-Torres, M.; Acosta-Torres, L.S.; Diaz-Torres, L.A.; Grillo, R.; Swamy, M.K.; Sharma, S.; et al. Nano based drug delivery systems: Recent developments and future prospects. *J. Nanobiotechnol.* **2018**, *16*, 71.
2. Senge, M.O.; Brandt, J.C. Temoporfin (Foscan®), 5,10,15,20-tetra(m-hydroxyphenyl)chlorin—A second-generation photosensitizer. *Photochem. Photobiol.* **2011**, *87*, 1240–1296.
3. Yakavets, I.; Millard, M.; Zorin, V.; Lassalle, H.-P.; Bezdetnaya, L. Current state of the nanoscale delivery systems for temoporfin-based photodynamic therapy: Advanced delivery strategies. *J. Control. Release* **2019**, *304*, 268–287.
4. Genchi, G.G.; Marino, A.; Tapeinos, C.; Ciofani, G. Smart Materials Meet Multifunctional Biomedical Devices: Current and Prospective Implications for Nanomedicine. *Front. Bioeng. Biotechnol.* **2017**, *5*, 80.
5. Fortuni, B.; Inose, T.; Ricci, M.; Fujita, Y.; Zundert, I.V.; Masuhara, A.; Fron, E.; Mizuno, H.; Latterini, L.; Rocha, S.; et al. Polymeric Engineering of Nanoparticles for Highly Efficient Multifunctional Drug Delivery Systems. *Sci. Rep.* **2019**, *9*, 1–13.
6. Sarma, S.J.; Khan, A.A.; Goswami, L.N.; Jalisatgi, S.S.; Hawthorne, M.F. A Trimodal Closoamer Drug-Delivery System Tailored with Tracing and Targeting Capabilities. *Chem. A Eur. J.* **2016**, *22*, 12715–12723.

7. Yakavets, I.; Lassalle, H.-P.; Scheglmann, D.; Wiehe, A.; Zorin, V.; Bezdetnaya, L.; Yakavets, I.; Lassalle, H.-P.; Scheglmann, D.; Wiehe, A.; et al. Temoporfin-in-Cyclodextrin-in-Liposome—A New Approach for Anticancer Drug Delivery: The Optimization of Composition. *Nanomaterials* **2018**, *8*, 847.
8. Reshetov, V.; Lassalle, H.-P.; François, A.; Dumas, D.; Hupont, S.; Gräfe, S.; Filipe, V.; Jiskoot, W.; Guillemin, F.; Zorin, V.; et al. Photodynamic therapy with conventional and PEGylated liposomal formulations of mTHPC (temoporfin): Comparison of treatment efficacy and distribution characteristics in vivo. *Int. J. Nanomed.* **2013**, *8*, 3817–3831.
9. Gaio, E.; Scheglmann, D.; Reddi, E.; Moret, F. Uptake and photo-toxicity of Foscan®, Foslip® and Fospeg® in multicellular tumor spheroids. *J. Photochem. Photobiol. B* **2016**, *161*, 244–252.
10. Millard, M.; Yakavets, I.; Piffoux, M.; Brun, A.; Gazeau, F.; Guigner, J.-M.; Jasniewski, J.; Lassalle, H.-P.; Wilhelm, C.; Bezdetnaya, L. mTHPC-loaded extracellular vesicles outperform liposomal and free mTHPC formulations by an increased stability, drug delivery efficiency and cytotoxic effect in tridimensional model of tumors. *Drug Deliv.* **2018**, *25*, 1790–1801.
11. Yakavets, I.; Yankovsky, I.; Millard, M.; Lamy, L.; Lassalle, H.-P.; Wiehe, A.; Zorin, V.; Bezdetnaya, L. The alteration of temoporfin distribution in multicellular tumor spheroids by β -cyclodextrins. *Int. J. Pharm.* **2017**, *529*, 568–575.
12. Stella, V.J.; He, Q. Cyclodextrins. *Toxicol. Pathol.* **2008**, *36*, 30–42.
13. Reshetov, V.; Kachatkou, D.; Shmigol, T.; Zorin, V.; D’Hallewin, M.-A.; Guillemin, F.; Bezdetnaya, L. Redistribution of meta-tetra(hydroxyphenyl)chlorin (m-THPC) from conventional and PEGylated liposomes to biological substrates. *Photochem. Photobiol. Sci.* **2011**, *10*, 911–919.
14. Yakavets, I.; Yankovsky, I.; Bezdetnaya, L.; Zorin, V. Soret band shape indicates mTHPC distribution between β -cyclodextrins and serum proteins. *Dyes Pigment.* **2017**, *137*, 299–306.
15. Sailor, M.J.; Park, J.-H. Hybrid nanoparticles for detection and treatment of cancer. *Adv. Mater. Technol.* **2012**, *24*, 3779–3802.
16. Yakavets, I.; Lassalle, H.-P.; Yankovsky, I.; Ingrosso, F.; Monari, A.; Bezdetnaya, L.; Zorin, V. Evaluation of temoporfin affinity to β -cyclodextrins assuming self-aggregation. *J. Photochem. Photobiol. A* **2018**, *367*, 13–21.
17. Yankovsky, I.; Bastien, E.; Yakavets, I.; Khludeyev, I.; Lassalle, H.-P.; Gräfe, S.; Bezdetnaya, L.; Zorin, V. Inclusion complexation with β -cyclodextrin derivatives alters photodynamic activity and biodistribution of meta-tetra(hydroxyphenyl)chlorin. *Eur. J. Pharm. Sci.* **2016**, *91*, 172–182.
18. Gharib, R.; Greige-Gerges, H.; Fourmentin, S.; Charcosset, C.; Auezova, L. Liposomes incorporating cyclodextrin-drug inclusion complexes: Current state of knowledge. *Carbohydr. Polym.* **2015**, *129*, 175–186.
19. Chen, J.; Lu, W.-L.; Gu, W.; Lu, S.-S.; Chen, Z.-P.; Cai, B.-C.; Yang, X.-X. Drug-in-cyclodextrin-in-liposomes: A promising delivery system for hydrophobic drugs. *Expert Opin. Drug Deliv.* **2014**, *11*, 565–577.
20. Akbarzadeh, A.; Rezaei-Sadabady, R.; Davaran, S.; Joo, S.W.; Zarghami, N.; Hanifehpour, Y.; Samiei, M.; Kouhi, M.; Nejati-Koshki, K. Liposome: Classification, preparation, and applications. *Nanoscale Res. Lett* **2013**, *8*, 102.
21. Yakavets, I.V.; Yankovsky, I.V.; Khludeyev, I.I.; Lassalle, H.P.; Bezdetnaya, L.N.; Zorin, V.P. Optical Methods for the Analysis of the Temoporfin Photosensitizer Distribution Between Serum Proteins and Methyl- β -Cyclodextrin Nanocarriers in Blood Serum. *J. Appl. Spectrosc.* **2018**, *84*, 1030–1036.
22. Millard, M.; Yakavets, I.; Zorin, V.; Kulmukhamedova, A.; Marchal, S.; Bezdetnaya, L. Drug delivery to solid tumors: The predictive value of the multicellular tumor spheroid model for nanomedicine screening. *Int. J. Nanomed.* **2017**, *12*, 7993–8007.
23. Reshetov, V.; Zorin, V.; Siupa, A.; D’Hallewin, M.-A.; Guillemin, F.; Bezdetnaya, L. Interaction of liposomal formulations of meta-tetra(hydroxyphenyl)chlorin (temoporfin) with serum proteins: Protein binding and liposome destruction. *Photochem. Photobiol.* **2012**, *88*, 1256–1264.
24. Kuntsche, J.; Freisleben, I.; Steiniger, F.; Fahr, A. Temoporfin-loaded liposomes: Physicochemical characterization. *Eur. J. Pharm. Sci.* **2010**, *40*, 305–315.
25. Torchilin, V.; Weissig, V. *Liposomes: A Practical Approach*; Oxford University Press: Oxford, UK, 2003; ISBN 978-0-19-963654-9.
26. Marchal, S.; Fadloun, A.; Maugain, E.; D’Hallewin, M.-A.; Guillemin, F.; Bezdetnaya, L. Necrotic and apoptotic features of cell death in response to Foscan photosensitization of HT29 monolayer and multicell spheroids. *Biochem. Pharm.* **2005**, *69*, 1167–1176.

27. Colley, H.E.; Hearnden, V.; Jones, A.V.; Weinreb, P.H.; Violette, S.M.; Macneil, S.; Thornhill, M.H.; Murdoch, C. Development of tissue-engineered models of oral dysplasia and early invasive oral squamous cell carcinoma. *Br. J. Cancer* **2011**, *105*, 1582–1592.
28. Yakavets, I.; Lassalle, H.-P.; Zorin, V.; Bezdetnaya, L. Cyclodextrin-based photoactive liposomal nanoparticles for tumor targeting. In Proceedings of the 17th International Photodynamic Association World Congress SPIE, Boston, MA, USA, 28 June–4 July 2019; Volume 11070, p. 110701P.



© 2019 by the authors. Licensee MDPI, Basel, Switzerland. This article is an open access article distributed under the terms and conditions of the Creative Commons Attribution (CC BY) license (<http://creativecommons.org/licenses/by/4.0/>).

GENERAL DISCUSSION

GENERAL DISCUSSION

Nowadays, we observe certain saturation in the development of nanomaterials for drug delivery. The assembly of more than one type of nanomaterial in one hybrid nanoparticle could be considered as an advanced strategy in nanomedicine development (Deljoo et al., 2019; Sailor and Park, 2012; Yakavets et al., 2019). Hybrid nanoparticles that contain two or more distinct nanoparticles assembled in a functional nanostructure could provide synergistic medical effects when nanomaterials are carefully selected. In the case of mTHPC, we suggested that combination of liposomes and cyclodextrin in “drug-in-cyclodextrin-in-liposome” nanoassembly could restrain the dissociation of drug-mTHPC complexes, avoid rapid drug release and favorably alter PSs penetration into tumor tissues. Thus, we supposed that mTHPC-DCL could overcome the individual nanostructure limitations providing passive targeting of the tumor by liposomes and deep penetration of mTHPC/CD complexes in tumor tissue.

Liposomes represent bilayered phospholipid nanocapsules, which could be loaded with hydrophobic compounds in the lipid bilayer or hydrophilic drugs in the inner aqueous core (Torchilin, 2005). After almost two decades of investigation, mTHPC liposomal formulation (Foslip[®]) is one of the most successful and the most studied mTHPC-based NPs (Reshetov et al., 2013). Conventional liposomes encapsulate almost 8% (w/w) of mTHPC in lipid bilayer providing complete solubilization of a highly hydrophobic mTHPC molecule during its administration. Foslip[®] exhibits lower dark toxicity and potentially could passively target tumor by EPR effect, thus improving the mTHPC selectivity. Moreover, it has been demonstrated that Foslip[®]-PDT was more efficient at shorter DLIs of 6-15h compared with 24h DLI for Foscan[®] (Reshetov et al., 2013). Nevertheless, liposomes have limited penetration in the tumor tissue (Gaio et al., 2016; Millard et al., 2018) and rapidly release mTHPC in blood upon the interaction with serum components (Reshetov et al., 2013). In summary, liposomes were suggested as potent nanocages.

Cyclodextrins (CDs) have been widely investigated as a unique pharmaceutical excipient for the past few decades and are still explored for new applications. Recent reports demonstrated the potency of β -CDs as an individual nanocarrier of mTHPC in *in vitro* and *in vivo* preclinical tumor models (Yankovsky et al., 2016). Deep investigations of CDs as pharmaceutical agents demonstrated that CD effect strongly depends on CD affinity to the drug (Stella and He, 2008). When we refined the value of binding constants assuming self-aggregation of mTHPC molecules, we obtained much higher values that were already reported in the literature (Bautista-Sanchez et al., 2005; Desroches et al., 2001). According to our calculations (Yakavets et al., 2018b), completely methylated TM- β -CD exhibits the

highest affinity ($K = 1.1 \times 10^7 \text{ M}^{-1}$) as compared to randomly methylated Me- β -CD ($K = 7.1 \times 10^5 \text{ M}^{-1}$) and 2-hydroxypropyl substituted Hp- β -CD ($K = 1.7 \times 10^5 \text{ M}^{-1}$). One could suggest that β -CDs methylation increases their affinity to mTHPC, providing the opportunity to modulate PS behavior in biological media. Also, the detailed study of the photophysical properties of mTHPC/CD inclusion complexes revealed the changes of mTHPC Soret band shape upon the inclusion complex formation (Yakavets et al., 2017a). We suggested and further confirmed using molecular dynamics simulations (Yakavets et al., 2018b) that spectral changes were induced by the interaction of CDs with phenyl groups causing the rotation of phenyl substitutes (Yakavets et al., 2017a). It should be noted that the intercalation of mTHPC molecule in the lipid microenvironment is possible only in planar conformation, resulting in the opposite changes of mTHPC Soret band shape. Thus, the spectral technique based on the Soret band shape could be used for the monitoring of mTHPC microenvironment and could be applied for detection of mTHPC/CD complexes in the aqueous core of hybrid liposomes.

As was mentioned above, methylation of β -CDs increases their affinity to mTHPC, providing the opportunity to modulate PS behavior in biological media. To describe the mechanism of alteration, we studied mTHPC distribution in 3D multicellular tumor spheroids in the presence of different types of β -CDs (Yakavets et al., 2017b). We found that mTHPC accumulation in spheroids is strongly depended on the type and concentration of CDs, as was already reported for monolayer cells (Yankovsky et al., 2016). Varying the concentrations of β -CDs, we could increase PS uptake in 3D spheroids as well as inhibit it. We showed that β -CD with lower affinity to mTHPC (Hp- β -CD) provided a threefold increase in total PS concentration, while Me- β -CD could enhance mTHPC uptake maximum 2-times. However, higher affinity constant of Me- β -CD binding to mTHPC allows transporting the PS in the deeper cell layers than that of Me- β -CD. We suggested that the small size of inclusion complex (about 3 nm) along with its long life-time determine the transportation of PS in the tumor tissue depth *via* nanoshuttle mechanism. By this mechanism, mTHPC rapidly redistributes from serum proteins to cellular membranes (increased uptake) and easily diffuses into the interstitial medium in the host-guest complexes with β -CD (increased penetration). Thus, it was suggested that mTHPC/ β -CDs could considerably improve the properties of mTHPC-loaded liposomes overcoming the limited penetration of liposomes in tumor tissue.

After all preliminary studies on the inclusion complex formation, we started to construct hybrid liposomes. In order to find the most optimal DCL composition for mTHPC delivery, we synthesized 9 various compositions based on three types of β -CD (Hp-, Me- and TM- β -CD) and three PS loading concentrations (Yakavets et al., 2018a). Lipid composition of DCL

vesicles was similar to Foslip[®], thus physical-chemical characteristics (size and surface charge) of DCLs were that of Foslip[®]. Using developed spectral techniques we confirmed the possibility to encapsulate β -CD/mTHPC in the inner aqueous core of liposomes without destruction of liposomes and unexpected redistribution of mTHPC to the lipid bilayer. According to our data, more than 85% of mTHPC was bound with CDs inside of liposomes. We also addressed the issue of colloidal stability of mTHPC-DCL due to the reported destabilization of liposomes in the presence of β -CDs (Hammoud et al., 2019; Piel et al., 2006; Puskás et al., 2006). According to the dynamic light scattering data, the colloidal stability of DCLs depended on the mTHPC: β -CD loading ratio and the type of β -CD. So, DCLs with the highest mTHPC loading based on the methylated β -CD exhibit the colloidal stability during more than 3 months, similar to Foslip[®]. We supposed that the key factor of DCLs destabilization was the concentration of free β -CD molecules in the aqueous core, which remove lipid components forming inclusion complexes (Fatouros et al., 2001; Szente and Fenyvesi, 2017; Uekama and Otagiri, 1987).

Concerning the screening of mTHPC-DCLs in HT29 colon adenocarcinoma monolayer cell culture and 3D multicellular tumor spheroids, we revealed the crucial role of mTHPC loading concentration on the intracellular uptake. Single loaded mTHPC-DCLs demonstrated improved penetration and distribution in the tumor spheroids, however, the total accumulation was significantly lower than Foslip[®] due to the highly competitive mTHPC binding among CDs, liposomal membranes serum proteins and cells. Thus, we upgraded mTHPC-DCLs by mTHPC loading in the lipid bilayer wholly replicating Foslip[®]. The physico-chemical characteristics as well as colloidal stability of DL-DCLs were not changed compared to mTHPC-DCLs. The loading of high mTHPC concentrations in lipid bilayer resulted in the fluorescence quenching, confirmed spectroscopically. Overall, 70% of mTHPC was bound in the lipid bilayer and 30% of PS was encapsulated in the inner aqueous core with β -CDs that was very close for theoretical predictions. By this way, DL-DCLs provide an appropriate cellular accumulation of PS in both 2D and 3D cell cultures. However, since the main aim was to increase the penetration ability of mTHPC in tumor tissues, we mainly focused our studies on 3D multicellular spheroid model. We demonstrated significant improvement of mTHPC distribution upon utilization of TD nanoconstruct. TD-treated spheroids almost homogeneously accumulated mTHPC that was confirmed by flow cytometry and fluorescence microscopy, while MD provided mTHPC distribution mainly at the periphery of spheroids similar to Foslip[®]. We supposed that the extremely high mTHPC affinity to TM- β -CD leads to the formation of long-living inclusion complexes capable to transfer mTHPC to the depth of tumor tissue. Thus, we could detect mTHPC/TM- β -CDs inclusion complexes in the culture medium after 24h incubation with spheroids, while Me- β -

CD complexes possess a shorter complex lifetime resulting in partial penetration of mTHPC in spheroids.

However, the benefits of DL-DCLs as mTHPC delivery system were not enough to overcome PDT efficiency of Foslip[®] in multicellular tumor spheroid *in vitro* as well as tumor-xenografted mice *in vivo*. Despite the improved mTHPC distribution in spheroids, PDT-induced cell death in spheroids treated with TD and MD was similar to Foslip[®]. Similarly, PDT in tumor xenografted mice induced the mean tumor growth delay of 30 days for TD as well as Foslip[®]. Probably, the intracellular concentration of mTHPC delivered by DL-DCL is below the limit of necrosis induction and mTHPC dose could be increased. It should be noted, that the improved PDT response in the case of homogeneous PS distribution is obvious however should be additionally investigated.

Nevertheless, the concept of synergistic mTHPC delivery by DL-DCLs which was clearly proved in 3D multicellular tumor spheroids should be also confirmed *in vivo* as potent nanoconstruct for mTHPC-PDT. Overall, DL-DCL is a perspective prototypical hybrid nanosystem which could be a good example of combined drug delivery.

CONCLUSION AND

PERSPECTIVES

CONCLUSION

The present thesis covers the study of hybrid liposomes that encapsulate inclusion complexes of CDs and second-generation photosensitizer mTHPC. The main research results are summarized as follows:

- **The formation of mTHPC/CD inclusion complexes.** The complexes between mTHPC and β -CD derivatives possess mainly 1:2 stoichiometry and very high affinity constants (up to 10^7 M^{-1}) compared to other anticancer drugs. Strong binding of mTHPC between β -CD molecules results in the changes of PS molecule conformation, causing the changes of Soret band spectral band. Also, such high mTHPC affinity to β -CD provides the unique opportunity to alter PS biodistribution via CD nanoshuttle mechanism.
- **The drug-in-cyclodextrin-in-liposome formulations (DCL).** DCLs were successfully prepared and characterized. The prepared hybrid liposomes replicated lipid composition of Foslip[®]. mTHPC was localized in the aqueous core in the complexes with β -CDs. All prepared DCLs were colloiddally stable for > 3weeks. The particular DCLs encapsulated methylated β -CD derivatives were stable more than 3 months. The possible mechanisms of DCLs destabilization were proposed.
- **Double loaded drug-in-cyclodextrin-in-liposomes (DL-DCL): Proof of the concept.** DL-DCL were prepared and characterized. Double loading of DCLs significantly increased cellular uptake of mTHPC. The localization of mTHPC in DL-DCLs was analyzed spectroscopically (70% in lipid bilayer and 30% in CD complexes). The kinetic processes of DL-DCLs interaction with tumor cells were studied in 2D and 3D tumor culture models. Spheroids treated with TD displayed almost homogeneous mTHPC distribution between the cells. Hypothetically, TM- β -CD nanoshuttles are able to transport mTHPC in the tumor depth due to the high affinity to mTHPC compared to Me- β -CD. No difference in PDT efficiency was observed in 3D multicellular tumor spheroids *in vitro* as well as tumor xenografted mice *in vivo*.

The data obtained confirmed the advantage of double-loaded mTHPC-DCLs over conventional mTHPC liposomal formulation (Foslip[®]) in terms of tumor tissue penetration. Altogether, the proposed matryoshka-type lipid vesicles releasing mTHPC/CD complexes illustrate an optimal balance between plasma stability and efficient PS release.

PERSPECTIVES

Our ongoing studies are focused on the proof of the DCL concept on different cell cancer lines and 3D co-culture spheroid models. In fact, we investigate the influence of tumor microenvironment on distribution of mTHPC-DCLs in tumor tissue. With this aim, we analyzed the distribution profiles of mTHPC delivered by DL-DCL in co-culture stroma-rich spheroids.

Further continuation of research is related to the optimization of mTHPC-DCLs composition for *in vivo* application and PDT protocol. Optimization of PDT regimens necessarily requires knowledge of mTHPC/CD complexes pharmacokinetics and biodistribution, including the intratumoral spatial distribution of the PS. Also, the serum-induced destabilization of DL-DCLs in blood flow will be studied in detail. Based on these results, the optimal DLI for PDT treatment will be selected and PDT efficiency (necrotic/apoptotic response and tumor growth kinetics) will be analyzed. In addition, skin photosensitivity after DL-DCL administration studies should be performed.

Also, we suppose that the application of stimuli-response liposomes (e.g. light-responsive) could provide external control of mTHPC/CD complexes release at the target site. Thus, additional optimization of mTHPC-DCL composition is required including screening in the preclinical *in vitro* and *in vivo* tumor models.

The overall results of such work would be beneficial for understanding the synergistic behavior of hybrid liposomes.

REFERENCES

REFERENCES

- Abra, R.M., and Hunt, C.A. (1981). Liposome disposition in vivo. III. Dose and vesicle-size effects. *Biochim. Biophys. Acta* 666, 493–503.
- Abrahamse, H., and Hamblin, M.R. (2016). New photosensitizers for photodynamic therapy. *Biochem. J.* 473, 347–364.
- Agashe, H., Sahoo, K., Lagisetty, P., and Awasthi, V. (2011). Cyclodextrin-mediated entrapment of curcuminoid 4-[3,5-bis(2-chlorobenzylidene-4-oxo-piperidine-1-yl)-4-oxo-2-butenic acid] or CLEFMA in liposomes for treatment of xenograft lung tumor in rats. *Colloids Surf. B Biointerfaces* 84, 329–337.
- Agostinis, P., Buytaert, E., Breysens, H., and Hendrickx, N. (2004). Regulatory pathways in photodynamic therapy induced apoptosis. *Photochem. Photobiol. Sci. Off. J. Eur. Photochem. Assoc. Eur. Soc. Photobiol.* 3, 721–729.
- Agostinis, P., Berg, K., Cengel, K.A., Foster, T.H., Girotti, A.W., Gollnick, S.O., Hahn, S.M., Hamblin, M.R., Juzeniene, A., Kessel, D., et al. (2011). Photodynamic therapy of cancer: An update. *CA. Cancer J. Clin.* 61, 250–281.
- Akbarzadeh, A., Rezaei-Sadabady, R., Davaran, S., Joo, S.W., Zarghami, N., Hanifehpour, Y., Samiei, M., Kouhi, M., and Nejati-Koshki, K. (2013). Liposome: classification, preparation, and applications. *Nanoscale Res. Lett.* 8, 102.
- Allison, R.R., and Sibata, C.H. (2010). Oncologic photodynamic therapy photosensitizers: a clinical review. *Photodiagnosis Photodyn. Ther.* 7, 61–75.
- Almeida, R.D., Manadas, B.J., Carvalho, A.P., and Duarte, C.B. (2004). Intracellular signaling mechanisms in photodynamic therapy. *Biochim. Biophys. Acta* 1704, 59–86.
- Angelini, G., Campestre, C., Boncompagni, S., and Gasbarri, C. (2017). Liposomes entrapping β -cyclodextrin/ibuprofen inclusion complex: Role of the host and the guest on the bilayer integrity and microviscosity. *Chem. Phys. Lipids* 209, 61–65.
- Antlisperger, G., and Schmid, G. (1996). Toxicological Comparison of Cyclodextrins. In *Proceedings of the Eighth International Symposium on Cyclodextrins*, J. Szejtli, and L. Szenté, eds. (Springer Netherlands), pp. 149–155.
- Arima, H., Hagiwara, Y., Hirayama, F., and Uekama, K. (2006). Enhancement of antitumor effect of doxorubicin by its complexation with gamma-cyclodextrin in pegylated liposomes. *J. Drug Target.* 14, 225–232.
- Arima, H., Motoyama, K., and Irie, T. (2011). Recent Findings on Safety Profiles of Cyclodextrins, Cyclodextrin Conjugates, and Polypseudorotaxanes. In *Cyclodextrins in Pharmaceuticals, Cosmetics, and Biomedicine*, E. Bilensoy, ed. (Hoboken, NJ, USA: John Wiley & Sons, Inc.), pp. 91–122.
- Arun R., ASHOK K. C. K., and SRAVANTHI V. V. N. S. S. (2008). Cyclodextrins as Drug Carrier Molecule: A Review. *Sci. Pharm.* 76, 567–598.
- Ascenso, A., Cruz, M., Euletério, C., Carvalho, F.A., Santos, N.C., Marques, H.C., and Simões, S. (2013). Novel tretinoin formulations: a drug-in-cyclodextrin-in-liposome approach. *J. Liposome Res.* 23, 211–219.
- Awuah, S.G., and You, Y. (2012). Boron dipyrromethene (BODIPY)-based photosensitizers for photodynamic therapy. *RSC Adv.* 2, 11169–11183.

- Ball, D.J., Vernon, D.I., and Brown, S.B. (1999). The high photoactivity of m-THPC in photodynamic therapy. Unusually strong retention of m-THPC by RIF-1 cells in culture. *Photochem. Photobiol.* *69*, 360–363.
- Bangham, A.D., and Horne, R.W. (1964). Negative staining of phospholipids and their structural modification by surface-active agents as observed in the electron microscope. *J. Mol. Biol.* *8*, 660-IN10.
- Bangham, A.D., Standish, M.M., and Watkins, J.C. (1965). Diffusion of univalent ions across the lamellae of swollen phospholipids. *J. Mol. Biol.* *13*, 238-IN27.
- Barenholz, Y. (2012). Doxil®--the first FDA-approved nano-drug: lessons learned. *J. Control. Release Off. J. Control. Release Soc.* *160*, 117–134.
- Baskaran, R., Lee, J., and Yang, S.-G. (2018). Clinical development of photodynamic agents and therapeutic applications. *Biomater. Res.* *22*.
- Battaglia Parodi, M., La Spina, C., Berchicci, L., Petrucci, G., and Bandello, F. (2016). Photosensitizers and Photodynamic Therapy: Verteporfin. *Dev. Ophthalmol.* *55*, 330–336.
- Bautista-Sanchez, A., Kasselouri, A., Desroches, M.-C., Blais, J., Maillard, P., de Oliveira, D.M., Tedesco, A.C., Prognon, P., and Delaire, J. (2005). Photophysical properties of glucoconjugated chlorins and porphyrins and their associations with cyclodextrins. *J. Photochem. Photobiol. B* *81*, 154–162.
- Ben Mihoub, A., Larue, L., Moussaron, A., Youssef, Z., Colombeau, L., Baros, F., Frochot, C., Vanderesse, R., and Acherar, S. (2018). Use of Cyclodextrins in Anticancer Photodynamic Therapy Treatment. *Molecules* *23*, 1936.
- Berenbaum, M.C., Akande, S.L., Bonnett, R., Kaur, H., Ioannou, S., White, R.D., and Winfield, U.J. (1986). meso-Tetra(hydroxyphenyl)porphyrins, a new class of potent tumour photosensitisers with favourable selectivity. *Br. J. Cancer* *54*, 717–725.
- Berlanda, J., Kiesslich, T., Engelhardt, V., Krammer, B., and Plaetzer, K. (2010). Comparative in vitro study on the characteristics of different photosensitizers employed in PDT. *J. Photochem. Photobiol. B* *100*, 173–180.
- Betz, C.S., Rauschnig, W., Stranadko, E.P., Riabov, M.V., Volgin, V.N., Albrecht, V., Nifantiev, N.E., and Hopper, C. (2012). Long-term outcomes following Foscan®-PDT of basal cell carcinomas. *Lasers Surg. Med.* *44*, 533–540.
- Beyer, W. (1996). Systems for light application and dosimetry in photodynamic therapy. *J. Photochem. Photobiol. B* *36*, 153–156.
- Bhatt, P., Lalani, R., Vhora, I., Patil, S., Amrutiya, J., Misra, A., and Mashru, R. (2018). Liposomes encapsulating native and cyclodextrin enclosed paclitaxel: Enhanced loading efficiency and its pharmacokinetic evaluation. *Int. J. Pharm.* *536*, 95–107.
- Bizik, J., Kankuri, E., Ristimäki, A., Taïeb, A., Vapaatalo, H., Lubitz, W., and Vaheri, A. (2004). Cell-cell contacts trigger programmed necrosis and induce cyclooxygenase-2 expression. *Cell Death Differ.* *11*, 183–195.
- Blanchard, J., and Proniuk, S. (1999). Some important considerations in the use of cyclodextrins. *Pharm. Res.* *16*, 1796–1798.
- Bonnett, R., White, R.D., Winfield, U.J., and Berenbaum, M.C. (1989). Hydroporphyrins of the meso-tetra(hydroxyphenyl)porphyrin series as tumour photosensitizers. *Biochem. J.* *261*, 277–280.
- Bonnett, R., Charlesworth, P., Djelal, B.D., Foley, S., McGarvey, D.J., and Truscott, T.G. (1999). Photophysical properties of 5,10,15,20-tetrakis(m-hydroxyphenyl)porphyrin (m-THPP), 5,10,15,20-tetrakis(m-hydroxyphenyl)chlorin (m-THPC) and 5,10,15,20-tetrakis(m-

hydroxyphenyl)bacteriochlorin (m-THPBC): a comparative study. *J. Chem. Soc. Perkin Trans. 2* 325–328.

Bown, S.G., Rogowska, A.Z., Whitelaw, D.E., Lees, W.R., Lovat, L.B., Ripley, P., Jones, L., Wyld, P., Gillams, A., and Hatfield, A.W.R. (2002). Photodynamic therapy for cancer of the pancreas. *Gut* 50, 549–557.

Bragagni, M., Maestrelli, F., Mennini, N., Ghelardini, C., and Mura, P. (2010). Liposomal formulations of prilocaine: effect of complexation with hydroxypropyl- β -cyclodextrin on drug anesthetic efficacy. *J. Liposome Res.* 20, 315–322.

Cai, H., Wang, Q., Luo, J., and Lim, C.K. (1999a). In vitro and in vivo metabolism of 5,10,15,20-tetra (m-hydroxyphenyl)chlorin in rats and humans. *Biomed. Chromatogr.* 13, 184–186.

Cai, H., Wang, Q., Luo, J., and Lim, C.K. (1999b). Study of temoporfin metabolism by HPLC and electrospray mass spectrometry. *Biomed. Chromatogr. BMC* 13, 354–359.

Campbell, G.A., Bartels, K.E., Arnold, C., Healey, T., Cowell, R.L., Lucroy, M.D., and Ronn, A.M. (2002). Tissue levels, histologic changes and plasma pharmacokinetics of meta-Tetra (hydroxyphenyl) chlorin (mTHPC) in the cat. *Lasers Med. Sci.* 17, 79–85.

Carneiro, S.B., Duarte, F.Í.C., Heimfarth, L., Quintans, J. de S.S., Quintans-Júnior, L.J., Júnior, V.F. da V., and Lima, Á.A.N. de (2019). Cyclodextrin–Drug Inclusion Complexes: In Vivo and In Vitro Approaches. *Int. J. Mol. Sci.* 20.

Castano, A.P., Demidova, T.N., and Hamblin, M.R. (2004). Mechanisms in photodynamic therapy: part one-photosensitizers, photochemistry and cellular localization. *Photodiagnosis Photodyn. Ther.* 1, 279–293.

Castano, A.P., Demidova, T.N., and Hamblin, M.R. (2005). Mechanisms in photodynamic therapy: part two-cellular signaling, cell metabolism and modes of cell death. *Photodiagnosis Photodyn. Ther.* 2, 1–23.

Castano, A.P., Mroz, P., and Hamblin, M.R. (2006). Photodynamic therapy and anti-tumour immunity. *Nat. Rev. Cancer* 6, 535–545.

Castedo, M., Perfettini, J.-L., Roumier, T., Andreau, K., Medema, R., and Kroemer, G. (2004). Cell death by mitotic catastrophe: a molecular definition. *Oncogene* 23, 2825–2837.

Cavalcanti, I.M.F., Mendonça, E.A.M., Lira, M.C.B., Honrato, S.B., Camara, C.A., Amorim, R.V.S., Mendes Filho, J., Rabello, M.M., Hernandez, M.Z., Ayala, A.P., et al. (2011). The encapsulation of β -lapachone in 2-hydroxypropyl- β -cyclodextrin inclusion complex into liposomes: a physicochemical evaluation and molecular modeling approach. *Eur. J. Pharm. Sci. Off. J. Eur. Fed. Pharm. Sci.* 44, 332–340.

Challa, R., Ahuja, A., Ali, J., and Khar, R.K. (2005). Cyclodextrins in drug delivery: An updated review. *AAPS PharmSciTech* 6, E329–E357.

Chen, H., Gao, J., Wang, F., and Liang, W. (2007). Preparation, Characterization and Pharmacokinetics of Liposomes-Encapsulated Cyclodextrins Inclusion Complexes for Hydrophobic Drugs. *Drug Deliv.* 14, 201–208.

Chen, J., Lu, W.-L., Gu, W., Lu, S.-S., Chen, Z.-P., Cai, B.-C., and Yang, X.-X. (2014). Drug-in-cyclodextrin-in-liposomes: a promising delivery system for hydrophobic drugs. *Expert Opin. Drug Deliv.* 11, 565–577.

Connors, K.A. (1997). The Stability of Cyclodextrin Complexes in Solution. *Chem. Rev.* 97, 1325–1358.

Coutier, S., Bezdetnaya, L.N., Foster, T.H., Parache, R.-M., and Guillemin, F. (2002). Effect of irradiation fluence rate on the efficacy of photodynamic therapy and tumor

oxygenation in meta-tetra (hydroxyphenyl) chlorin (mTHPC)-sensitized HT29 xenografts in nude mice. *Radiat. Res.* 158, 339–345.

Craig, R.A., McCoy, C.P., Gorman, S.P., and Jones, D.S. (2015). Photosensitisers – the progression from photodynamic therapy to anti-infective surfaces. *Expert Opin. Drug Deliv.* 12, 85–101.

Crini, G. (2014). Review: A History of Cyclodextrins. *Chem. Rev.* 114, 10940–10975.

Cui, J., Li, C., Wang, C., Li, Y., Zhang, L., Zhang, L., Xiu, X., Li, Y., and Wei, N. (2011). Development of pegylated liposomal vincristine using novel sulfobutyl ether cyclodextrin gradient: is improved drug retention sufficient to surpass DSPE-PEG-induced drug leakage? *J. Pharm. Sci.* 100, 2835–2848.

Daniell, M.D., and Hill, J.S. (1991). A history of photodynamic therapy. *Aust. N. Z. J. Surg.* 61, 340–348.

Davis, M.E., and Brewster, M.E. (2004). Cyclodextrin-based pharmaceuticals: past, present and future. *Nat. Rev. Drug Discov.* 3, 1023–1035.

De Bie, A.T., Van Ommen, B., and Bär, A. (1998). Disposition of [¹⁴C]gamma-cyclodextrin in germ-free and conventional rats. *Regul. Toxicol. Pharmacol.* RTP 27, 150–158.

Del Valle, E.M.M. (2004). Cyclodextrins and their uses: a review. *Process Biochem.* 39, 1033–1046.

Delaey, E., van Laar, F., De Vos, D., Kamuhabwa, A., Jacobs, P., and de Witte, P. (2000). A comparative study of the photosensitizing characteristics of some cyanine dyes. *J. Photochem. Photobiol. B* 55, 27–36.

Deljoo, S., Rabiee, N., and Rabiee, M. (2019). Curcumin-hybrid Nanoparticles in Drug Delivery System (Review). *Asian J. Nanosci. Mater.* 2, 66–91.

Desroches, M.-C., Kasselouri, A., Bourdon, O., Chaminade, P., Blais, J., and Prognon, P. (2001). A direct sensitized fluorimetric determination of 5,10,15,20-tetra(m-hydroxyphenyl)chlorin [m-THPC(Foscan)®] in human plasma using a cyclodextrin inclusion complex. *Analyst* 126, 923–927.

Dewaele, M., Maes, H., and Agostinis, P. (2010). ROS-mediated mechanisms of autophagy stimulation and their relevance in cancer therapy. *Autophagy* 6, 838–854.

Dhule, S.S., Penfornis, P., Frazier, T., Walker, R., Feldman, J., Tan, G., He, J., Alb, A., John, V., and Pochampally, R. (2012). Curcumin-loaded γ -cyclodextrin liposomal nanoparticles as delivery vehicles for osteosarcoma. *Nanomedicine Nanotechnol. Biol. Med.* 8, 440–451.

Diamond, I., Mcdonagh, A., Wilson, C., Granelli, S., Nielsen, S., and Jaenicke, R. (1972). PHOTODYNAMIC THERAPY OF MALIGNANT TUMOURS. *The Lancet* 300, 1175–1177.

Dolmans, D.E.J.G.J., Fukumura, D., and Jain, R.K. (2003). Photodynamic therapy for cancer. *Nat. Rev. Cancer* 3, 380–387.

Dos Santos, A.F., De Almeida, D.R.Q., Terra, L.F., Baptista, M.S., and Labriola, L. (2019). Photodynamic therapy in cancer treatment - an update review. *J. Cancer Metastasis Treat.* 2019, 25.

Dougherty, T.J. (2002). An update on photodynamic therapy applications. *J. Clin. Laser Med. Surg.* 20, 3–7.

- Duchêne, D. (2011). Cyclodextrins and Their Inclusion Complexes. In *Cyclodextrins in Pharmaceutics, Cosmetics, and Biomedicine*, E. Bilensoy, ed. (Hoboken, NJ, USA: John Wiley & Sons, Inc.), pp. 1–18.
- Dysart, J.S., and Patterson, M.S. (2005). Characterization of Photofrin photobleaching for singlet oxygen dose estimation during photodynamic therapy of MLL cells *in vitro*. *Phys. Med. Biol.* *50*, 2597–2616.
- Eberhard, A., Kahlert, S., Goede, V., Hemmerlein, B., Plate, K.H., and Augustin, H.G. (2000). Heterogeneity of angiogenesis and blood vessel maturation in human tumors: implications for antiangiogenic tumor therapies. *Cancer Res.* *60*, 1388–1393.
- Ellerkamp, V., Bortel, N., Schmid, E., Kirchner, B., Armeanu-Ebinger, S., and Fuchs, J. (2016). Photodynamic Therapy Potentiates the Effects of Curcumin on Pediatric Epithelial Liver Tumor Cells. *Anticancer Res.* *36*, 3363–3372.
- Fatouros, D.G., Hatzidimitriou, K., and Antimisiaris, S.G. (2001). Liposomes encapsulating prednisolone and prednisolone–cyclodextrin complexes: comparison of membrane integrity and drug release. *Eur. J. Pharm. Sci.* *13*, 287–296.
- Fingar, V.H., Taber, S.W., Haydon, P.S., Harrison, L.T., Kempf, S.J., and Wieman, T.J. (2000). Vascular damage after photodynamic therapy of solid tumors: a view and comparison of effect in pre-clinical and clinical models at the University of Louisville. *Vivo Athens Greece* *14*, 93–100.
- Fitzmaurice, S., and Eisen, D.B. (2016). Daylight Photodynamic Therapy: What is Known and What is Yet to be Determined. *Dermatol. Surg. Off. Publ. Am. Soc. Dermatol. Surg. AI* *42*, 286–295.
- Forsyth, T.P., Nurco, D.J., Pandey, Ravindra K., and Smith, K.M. (1995). Synthesis and structure of a 5,15-bis(4-pyridyl)purpurin. *Tetrahedron Lett.* *36*, 9093–9096.
- Frank, D.W., Gray, J.E., and Weaver, R.N. (1976). Cyclodextrin nephrosis in the rat. *Am. J. Pathol.* *83*, 367–382.
- Franzè, S., Musazzi, U.M., Minghetti, P., and Cilurzo, F. (2019). Drug-in-micelles-in-liposomes (DiMiL) systems as a novel approach to prevent drug leakage from deformable liposomes. *Eur. J. Pharm. Sci. Off. J. Eur. Fed. Pharm. Sci.* *130*, 27–35.
- Frömming, K.-H., and Szejtli, J. (1994). *Cyclodextrins in Pharmacy* (Dordrecht: Springer Netherlands).
- Gaio, E., Scheglmann, D., Reddi, E., and Moret, F. (2016). Uptake and photo-toxicity of Foscan®, Foslip® and Fospeg® in multicellular tumor spheroids. *J. Photochem. Photobiol. B* *161*, 244–252.
- Garg, A.D., Krysko, D.V., Vandenabeele, P., and Agostinis, P. (2012). Hypericin-based photodynamic therapy induces surface exposure of damage-associated molecular patterns like HSP70 and calreticulin. *Cancer Immunol. Immunother.* *61*, 215–221.
- Garrier, J., Bressenot, A., Gräfe, S., Marchal, S., Mitra, S., Foster, T.H., Guillemin, F., and Bezdetnaya, L. (2010). Compartmental targeting for mTHPC-based photodynamic treatment *in vivo*: Correlation of efficiency, pharmacokinetics, and regional distribution of apoptosis. *Int. J. Radiat. Oncol. Biol. Phys.* *78*, 563–571.
- van Geel, I.P., Oppelaar, H., Oussoren, Y.G., van der Valk, M.A., and Stewart, F.A. (1995). Photosensitizing efficacy of MTHPC-PDT compared to photofrin-PDT in the RIF1 mouse tumour and normal skin. *Int. J. Cancer* *60*, 388–394.
- Gerloczy, A., Antal, S., Szathmari, I., Muller-Horvath, R., and Szejtli, J. (1990). Absorption, distribution and excretion of ¹⁴C-labelled hydroxypropyl β -cyclodextrin in rats

following oral administration. Minutes 5th Int. Symp. Cyclodextr. Paris March 1990 Duchéne Ed Pp 507-13 Sante Paris.

Gharib, R., Greige-Gerges, H., Fourmentin, S., Charcosset, C., and Auezova, L. (2015). Liposomes incorporating cyclodextrin-drug inclusion complexes: Current state of knowledge. *Carbohydr. Polym.* *129*, 175–186.

Gharib, R., Greige-Gerges, H., Jraij, A., Auezova, L., and Charcosset, C. (2016). Preparation of drug-in-cyclodextrin-in-liposomes at a large scale using a membrane contactor: Application to trans-anethole. *Carbohydr. Polym.* *154*, 276–286.

Gidwani, B., and Vyas, A. (2015). A Comprehensive Review on Cyclodextrin-Based Carriers for Delivery of Chemotherapeutic Cytotoxic Anticancer Drugs. *BioMed Res. Int.* *2015*, e198268.

Gillet, A., Grammenos, A., Compère, P., Evrard, B., and Piel, G. (2009). Development of a new topical system: Drug-in-cyclodextrin-in-deformable liposome. *Int. J. Pharm.* *380*, 174–180.

Glanzmann, T., Hadjur, C., Zellweger, M., Grosiean, P., Forrer, M., Ballini, J.P., Monnier, P., van den Bergh, H., Lim, C.K., and Wagnières, G. (1998). Pharmacokinetics of tetra(m-hydroxyphenyl)chlorin in human plasma and individualized light dosimetry in photodynamic therapy. *Photochem. Photobiol.* *67*, 596–602.

Gollnick, S.O., Vaughan, L., and Henderson, B.W. (2002). Generation of effective antitumor vaccines using photodynamic therapy. *Cancer Res.* *62*, 1604–1608.

Gotoh, K., Kariya, R., Alam, M.M., Matsuda, K., Hattori, S., Maeda, Y., Motoyama, K., Kojima, A., Arima, H., and Okada, S. (2014). The antitumor effects of methyl- β -cyclodextrin against primary effusion lymphoma via the depletion of cholesterol from lipid rafts. *Biochem. Biophys. Res. Commun.* *455*, 285–289.

Gould, S., and Scott, R.C. (2005). 2-Hydroxypropyl- β -cyclodextrin (HP- β -CD): A toxicology review. *Food Chem. Toxicol.* *43*, 1451–1459.

Gregoriadis, G., Wills, E.J., Swain, C.P., and Tavill, A.S. (1974). Drug-carrier potential of liposomes in cancer chemotherapy. *Lancet Lond. Engl.* *1*, 1313–1316.

Grosse, P.Y., Bressolle, F., and Pinguet, F. (1998). Antiproliferative effect of methyl-beta-cyclodextrin in vitro and in human tumour xenografted athymic nude mice. *Br. J. Cancer* *78*, 1165–1169.

Guardiano, M., Biolo, R., Jori, G., and Schaffner, K. (1989). Tetra-n-propylporphycene as a tumour localizer: pharmacokinetic and phototherapeutic studies in mice. *Cancer Lett.* *44*, 1–6.

Gulati, M., Grover, M., Singh, S., and Singh, M. (1998). Lipophilic drug derivatives in liposomes. *Int. J. Pharm.* *165*, 129–168.

Hammoud, Z., Khreich, N., Auezova, L., Fourmentin, S., Elaissari, A., and Greige-Gerges, H. (2019). Cyclodextrin-membrane interaction in drug delivery and membrane structure maintenance. *Int. J. Pharm.* *564*, 59–76.

Hansch, A., Frey, O., Gajda, M., Susanna, G., Boettcher, J., Bräuer, R., and Kaiser, W.A. (2008). Photodynamic treatment as a novel approach in the therapy of arthritic joints. *Lasers Surg. Med.* *40*, 265–272.

Hatzi, P., Mourtas, S., G. Klepetsanis, P., and Antimisariis, S.G. (2007). Integrity of liposomes in presence of cyclodextrins: Effect of liposome type and lipid composition. *Int. J. Pharm.* *333*, 167–176.

Henderson, B.W., and Dougherty, T.J. (1992). How does photodynamic therapy work? *Photochem. Photobiol.* *55*, 145–157.

Henderson, B.W., Waldow, S.M., Mang, T.S., Potter, W.R., Malone, P.B., and Dougherty, T.J. (1985). Tumor destruction and kinetics of tumor cell death in two experimental mouse tumors following photodynamic therapy. *Cancer Res.* *45*, 572–576.

Henderson, B.W., Gollnick, S.O., Snyder, J.W., Busch, T.M., Kousis, P.C., Cheney, R.T., and Morgan, J. (2004). Choice of oxygen-conserving treatment regimen determines the inflammatory response and outcome of photodynamic therapy of tumors. *Cancer Res.* *64*, 2120–2126.

Horlings, R.K., Terra, J.B., and Witjes, M.J.H. (2015). mTHPC mediated, systemic photodynamic therapy (PDT) for nonmelanoma skin cancers: Case and literature review. *Lasers Surg. Med.* *47*, 779–787.

Irie, T., and Uekama, K. (1997). Pharmaceutical applications of cyclodextrins. III. Toxicological issues and safety evaluation. *J. Pharm. Sci.* *86*, 147–162.

Ishida, T., Harada, M., Wang, X.Y., Ichihara, M., Irimura, K., and Kiwada, H. (2005). Accelerated blood clearance of PEGylated liposomes following preceding liposome injection: effects of lipid dose and PEG surface-density and chain length of the first-dose liposomes. *J. Control. Release Off. J. Control. Release Soc.* *105*, 305–317.

Jablonka, L., Ashtikar, M., Gao, G., Jung, F., Thurn, M., Preuß, A., Scheglmann, D., Albrecht, V., Röder, B., and Wacker, M.G. (2019). Advanced in silico modeling explains pharmacokinetics and biodistribution of temoporfin nanocrystals in humans. *J. Controlled Release* *308*, 57–70.

Jain, S., Hirst, D.G., and O'Sullivan, J.M. (2012). Gold nanoparticles as novel agents for cancer therapy. *Br. J. Radiol.* *85*, 101–113.

Jain, S.K., Gupta, Y., Jain, A., and Bhole, M. (2007). Multivesicular liposomes bearing celecoxib-beta-cyclodextrin complex for transdermal delivery. *Drug Deliv.* *14*, 327–335.

Jensen, T.J., Vicente, M.G.H., Luguaya, R., Norton, J., Fronczek, F.R., and Smith, K.M. (2010). Effect of overall charge and charge distribution on cellular uptake, distribution and phototoxicity of cationic porphyrins in HEp2 cells. *J. Photochem. Photobiol. B* *100*, 100–111.

Jerjes, W., Upile, T., Hamdoon, Z., Alexander Mosse, C., Morcos, M., and Hopper, C. (2011). Photodynamic therapy outcome for T1/T2 N0 oral squamous cell carcinoma. *Lasers Surg. Med.* *43*, 463–469.

Joguparthi, V., and Anderson, B.D. (2008). Effect of Cyclodextrin Complexation on the Liposome Permeability of a Model Hydrophobic Weak Acid. *Pharm. Res.* *25*, 2505.

Jones, H.J., Vernon, D.I., and Brown, S.B. (2003). Photodynamic therapy effect of m-THPC (Foscan) in vivo: correlation with pharmacokinetics. *Br. J. Cancer* *89*, 398–404.

Josefsen, L.B., and Boyle, R.W. (2012). Unique diagnostic and therapeutic roles of porphyrins and phthalocyanines in photodynamic therapy, imaging and theranostics. *Theranostics* *2*, 916–966.

Juzeniene, A., Nielsen, K.P., and Moan, J. (2006). Biophysical aspects of photodynamic therapy. *J. Environ. Pathol. Toxicol. Oncol. Off. Organ Int. Soc. Environ. Toxicol. Cancer* *25*, 7–28.

Kachatkou, D., Sasnouski, S., Zorin, V., Zorina, T., D'Hallewin, M.-A., Guillemin, F., and Bezdetnaya, L. (2009). Unusual photoinduced response of mTHPC liposomal formulation (Foslip). *Photochem. Photobiol.* *85*, 719–724.

- Kennedy, J.C., Pottier, R.H., and Pross, D.C. (1990). Photodynamic therapy with endogenous protoporphyrin: IX: Basic principles and present clinical experience. *J. Photochem. Photobiol. B* 6, 143–148.
- Kessel, D. (1999). Transport and localisation of m-THPC in vitro. *Int. J. Clin. Pract.* 53, 263–267.
- Kessel, D., and Luo, Y. (1999). Photodynamic therapy: a mitochondrial inducer of apoptosis. *Cell Death Differ.* 6, 28–35.
- Kessel, D., and Oleinick, N.L. (2009). Chapter 1 Initiation of Autophagy by Photodynamic Therapy. In *Methods in Enzymology*, (Academic Press), pp. 1–16.
- Kilsdonk, E.P., Yancey, P.G., Stoudt, G.W., Bangerter, F.W., Johnson, W.J., Phillips, M.C., and Rothblat, G.H. (1995). Cellular cholesterol efflux mediated by cyclodextrins. *J. Biol. Chem.* 270, 17250–17256.
- Kochneva, E.V., Filonenko, E.V., Vakulovskaya, E.G., Scherbakova, E.G., Seliverstov, O.V., Markichev, N.A., and Reshetnikov, A.V. (2010). Photosensitizer Radachlorin®: Skin cancer PDT phase II clinical trials. *Photodiagnosis Photodyn. Ther.* 7, 258–267.
- Korbelik, M. (1996). Induction of tumor immunity by photodynamic therapy. *J. Clin. Laser Med. Surg.* 14, 329–334.
- Korbelik, M., and Krosli, G. (1994). Cellular levels of photosensitizers in tumours: the role of proximity to the blood supply. *Br. J. Cancer* 70, 604–610.
- Koudinova, N.V., Pinthus, J.H., Brandis, A., Brenner, O., Bendel, P., Ramon, J., Eshhar, Z., Scherz, A., and Salomon, Y. (2003). Photodynamic therapy with Pd-bacteriopheophorbide (TOOKAD): Successful in vivo treatment of human prostatic small cell carcinoma xenografts. *Int. J. Cancer* 104, 782–789.
- Kousis, P.C., Henderson, B.W., Maier, P.G., and Gollnick, S.O. (2007). Photodynamic therapy enhancement of antitumor immunity is regulated by neutrophils. *Cancer Res.* 67, 10501–10510.
- Kruijt, B., van der Ploeg-van den Heuvel, A., de Bruijn, H.S., Sterenborg, H.J.C.M., Amelink, A., and Robinson, D.J. (2009). Monitoring interstitial m-THPC-PDT in vivo using fluorescence and reflectance spectroscopy. *Lasers Surg. Med.* 41, 653–664.
- Kryjewski, M., Goslinski, T., and Mielcarek, J. (2015). Functionality stored in the structures of cyclodextrin–porphyrinoid systems. *Coord. Chem. Rev.* 300, 101–120.
- Kübler, A.C. (2005). Photodynamic therapy. *Med. Laser Appl.* 20, 37–45.
- Kubota, Y., Fukuda, M., Muroguchi, M., and Koizumi, K. (1996). Absorption, distribution and excretion of beta-cyclodextrin and glucosyl-beta-cyclodextrin in rats. *Biol. Pharm. Bull.* 19, 1068–1072.
- Kuntsche, J., Freisleben, I., Steiniger, F., and Fahr, A. (2010). Temoporfin-loaded liposomes: Physicochemical characterization. *Eur. J. Pharm. Sci.* 40, 305–315.
- Lang, K., Mosinger, J., and Wagnerová, D.M. (2004). Photophysical properties of porphyrinoid sensitizers non-covalently bound to host molecules; models for photodynamic therapy. *Coord. Chem. Rev.* 248, 321–350.
- Lange, C., Lehmann, C., Mahler, M., and Bednarski, P.J. (2019). Comparison of Cellular Death Pathways after mTHPC-mediated Photodynamic Therapy (PDT) in Five Human Cancer Cell Lines. *Cancers* 11, 702.
- Lapenda, T.L.S., Morais, W.A., Almeida, F.J.F., Ferraz, M.S., Lira, M.C.B., Santos, N.P.S., Maciel, M. a. M., and Santos-Magalhães, N.S. (2013). Encapsulation of trans-

dehydrocrotonin in liposomes: an enhancement of the antitumor activity. *J. Biomed. Nanotechnol.* **9**, 499–510.

Lassalle, H.-P., Wagner, M., Bezdetnaya, L., Guillemin, F., and Schneckenburger, H. (2008). Fluorescence imaging of Foscan® and Foslip in the plasma membrane and in whole cells. *J. Photochem. Photobiol. B* **92**, 47–53.

Laza-Knoerr, A.L., Gref, R., and Couvreur, P. (2010). Cyclodextrins for drug delivery. *J. Drug Target.* **18**, 645–656.

Leist, M., and Jäättelä, M. (2001). Triggering of apoptosis by cathepsins. *Cell Death Differ.* **8**, 324–326.

Loftsson, T., and Brewster, M.E. (1996). Pharmaceutical applications of cyclodextrins. 1. Drug solubilization and stabilization. *J. Pharm. Sci.* **85**, 1017–1025.

Loftsson, T., and Brewster, M.E. (2010). Pharmaceutical applications of cyclodextrins: basic science and product development. *J. Pharm. Pharmacol.* **62**, 1607–1621.

Loftsson, T., and Brewster, M.E. (2013). Drug Solubilization and Stabilization by Cyclodextrin Drug Carriers. In *Drug Delivery Strategies for Poorly Water-Soluble Drugs*, D. Douroumis, and A. Fahr, eds. (John Wiley & Sons Ltd), pp. 67–101.

Loftsson, T., and Duchene, D. (2007). Cyclodextrins and their pharmaceutical applications. *Int. J. Pharm.* **329**, 1–11.

Loftsson, T., Másson, M., and Brewster, M.E. (2004). Self-association of cyclodextrins and cyclodextrin complexes. *J. Pharm. Sci.* **93**, 1091–1099.

López-Pinto, J.M., González-Rodríguez, M.L., and Rabasco, A.M. (2005). Effect of cholesterol and ethanol on dermal delivery from DPPC liposomes. *Int. J. Pharm.* **298**, 1–12.

Lucky, S.S., Soo, K.C., and Zhang, Y. (2015). Nanoparticles in Photodynamic Therapy. *Chem. Rev.* **115**, 1990–2042.

Lynch, D.H., Haddad, S., King, V.J., Ott, M.J., Straight, R.C., and Jolles, C.J. (1989). Systemic immunosuppression induced by photodynamic therapy (PDT) is adoptively transferred by macrophages. *Photochem. Photobiol.* **49**, 453–458.

Ma, L.W., Bjørklund, E., and Moan, J. (1999). Photochemotherapy of tumours with mesotetrahydroxyphenyl chlorin is pH dependent. *Cancer Lett.* **138**, 197–201.

Macdonald, I.J., and Dougherty, T.J. (2001). Basic principles of photodynamic therapy. *J. Porphyr. Phthalocyanines* **5**, 105–129.

Maeda, H. (2001). The enhanced permeability and retention (EPR) effect in tumor vasculature: the key role of tumor-selective macromolecular drug targeting. *Adv. Enzyme Regul.* **41**, 189–207.

Maestrelli, F., González-Rodríguez, M.L., Rabasco, A.M., and Mura, P. (2005). Preparation and characterisation of liposomes encapsulating ketoprofen–cyclodextrin complexes for transdermal drug delivery. *Int. J. Pharm.* **298**, 55–67.

Maestrelli, F., González-Rodríguez, M.L., Rabasco, A.M., and Mura, P. (2006). Effect of preparation technique on the properties of liposomes encapsulating ketoprofen–cyclodextrin complexes aimed for transdermal delivery. *Int. J. Pharm.* **312**, 53–60.

Maestrelli, F., González-Rodríguez, M.L., Rabasco, A.M., Ghelardini, C., and Mura, P. (2010). New “drug-in cyclodextrin-in deformable liposomes” formulations to improve the therapeutic efficacy of local anaesthetics. *Int. J. Pharm.* **395**, 222–231.

Magda, D., and Miller, R.A. (2006). Motexafin gadolinium: A novel redox active drug for cancer therapy. *Semin. Cancer Biol.* **16**, 466–476.

Marchal, S., Bezdetnaya, L., and Guillemin, F. (2004). Modality of cell death induced by Foscan-based photodynamic treatment in human colon adenocarcinoma cell line HT29. *Biochem. Biokhimiia* 69, 45–49.

Marchal, S., Fadloun, A., Maugain, E., D'Hallewin, M.-A., Guillemin, F., and Bezdetnaya, L. (2005). Necrotic and apoptotic features of cell death in response to Foscan photosensitization of HT29 monolayer and multicell spheroids. *Biochem. Pharmacol.* 69, 1167–1176.

Marchal, S., François, A., Dumas, D., Guillemin, F., and Bezdetnaya, L. (2007). Relationship between subcellular localisation of Foscan and caspase activation in photosensitised MCF-7 cells. *Br. J. Cancer* 96, 944–951.

Marchal, S., El Hor, A., Millard, M., Gillon, V., and Bezdetnaya, L. (2015). Anticancer Drug Delivery: An Update on Clinically Applied Nanotherapeutics. *Drugs* 75, 1601–1611.

Matoba, Y., Banno, K., Kisu, I., and Aoki, D. (2018). Clinical application of photodynamic diagnosis and photodynamic therapy for gynecologic malignant diseases: A review. *Photodiagnosis Photodyn. Ther.* 24, 52–57.

Matsumura, Y., and Maeda, H. (1986). A new concept for macromolecular therapeutics in cancer chemotherapy: mechanism of tumoritropic accumulation of proteins and the antitumor agent smancs. *Cancer Res.* 46, 6387–6392.

McCormack, B., and Gregoriadis, G. (1994). Entrapment of cyclodextrin-drug complexes into liposomes: potential advantages in drug delivery. *J. Drug Target.* 2, 449–454.

McCormack, B., and Gregoriadis, G. (1998). Drugs-in-cyclodextrins-in-liposomes: an approach to controlling the fate of water insoluble drugs in vivo. *Int. J. Pharm.* 162, 59–69.

Melnikova, V.O., Bezdetnaya, L.N., Bour, C., Festor, E., Gramain, M.P., Merlin, J.L., Potapenko AYa, null, and Guillemin, F. (1999). Subcellular localization of meta-tetra (hydroxyphenyl) chlorin in human tumor cells subjected to photodynamic treatment. *J. Photochem. Photobiol. B* 49, 96–103.

Mendonça, E.A.M., Lira, M.C.B., Rabello, M.M., Cavalcanti, I.M.F., Galdino, S.L., Pitta, I.R., Lima, M. do C.A., Pitta, M.G.R., Hernandez, M.Z., and Santos-Magalhães, N.S. (2012). Enhanced antiproliferative activity of the new anticancer candidate LPSF/AC04 in cyclodextrin inclusion complexes encapsulated into liposomes. *AAPS PharmSciTech* 13, 1355–1366.

Mennini, N., Cirri, M., Maestrelli, F., and Mura, P. (2016). Comparison of liposomal and NLC (nanostructured lipid carrier) formulations for improving the transdermal delivery of oxaprozin: Effect of cyclodextrin complexation. *Int. J. Pharm.* 515, 684–691.

Miki, Y., Akimoto, J., Hiranuma, M., and Fujiwara, Y. (2014). Effect of talaporfin sodium-mediated photodynamic therapy on cell death modalities in human glioblastoma T98G cells. *J. Toxicol. Sci.* 39, 821–827.

Millard, M., Yakavets, I., Piffoux, M., Brun, A., Gazeau, F., Guigner, J.-M., Jasniewski, J., Lassalle, H.-P., Wilhelm, C., and Bezdetnaya, L. (2018). mTHPC-loaded extracellular vesicles outperform liposomal and free mTHPC formulations by an increased stability, drug delivery efficiency and cytotoxic effect in tridimensional model of tumors. *Drug Deliv.* 25, 1790–1801.

Miller, J.D., Baron, E.D., Scull, H., Hsia, A., Berlin, J.C., McCormick, T., Colussi, V., Kenney, M.E., Cooper, K.D., and Oleinick, N.L. (2007). Photodynamic therapy with the phthalocyanine photosensitizer Pc 4: The case experience with preclinical mechanistic and early clinical–translational studies. *Toxicol. Appl. Pharmacol.* 224, 290–299.

Mitra, S., and Foster, T.H. (2005). Photophysical parameters, photosensitizer retention and tissue optical properties completely account for the higher photodynamic efficacy of meso-tetra-hydroxyphenyl-chlorin vs Photofrin. *Photochem. Photobiol.* *81*, 849–859.

Mitra, S., Maugain, E., Bolotine, L., Guillemin, F., and Foster, T.H. (2005). Temporally and spatially heterogeneous distribution of mTHPC in a murine tumor observed by two-color confocal fluorescence imaging and spectroscopy in a whole-mount model. *Photochem. Photobiol.* *81*, 1123–1130.

Moan, J., Berg, K., Kvam, E., Western, A., Malik, Z., Rück, A., and Schneckenburger, H. (1989). Intracellular localization of photosensitizers. *Ciba Found. Symp.* *146*, 95–107; discussion 107–111.

Mohammad, N., Malvi, P., Meena, A.S., Singh, S.V., Chaube, B., Vannuruswamy, G., Kulkarni, M.J., and Bhat, M.K. (2014). Cholesterol depletion by methyl- β -cyclodextrin augments tamoxifen induced cell death by enhancing its uptake in melanoma. *Mol. Cancer* *13*, 204.

Mosher, G., and Thompson, D.O. (2007). Complexation: Cyclodextrins. In *Encyclopedia of Pharmaceutical Technology*, Third Edition, (Taylor & Francis), pp. 671–696.

Muehlmann, L.A., Rodrigues, M.C., Longo, J.P.F., Garcia, M.P., Py-Daniel, K.R., Veloso, A.B., de Souza, P.E.N., da Silva, S.W., and Azevedo, R.B. (2015). Aluminium-phthalocyanine chloride nanoemulsions for anticancer photodynamic therapy: Development and in vitro activity against monolayers and spheroids of human mammary adenocarcinoma MCF-7 cells. *J. Nanobiotechnology* *13*, 36.

Nakamura, Y., Mochida, A., Choyke, P.L., and Kobayashi, H. (2016). Nanodrug Delivery: Is the Enhanced Permeability and Retention Effect Sufficient for Curing Cancer? *Bioconjug. Chem.* *27*, 2225–2238.

O'Connor, A.E., Gallagher, W.M., and Byrne, A.T. (2009). Porphyrin and Nonporphyrin Photosensitizers in Oncology: Preclinical and Clinical Advances in Photodynamic Therapy. *Photochem. Photobiol.* *85*, 1053–1074.

Oleinick, N.L., Morris, R.L., and Belichenko, I. (2002). The role of apoptosis in response to photodynamic therapy: what, where, why, and how. *Photochem. Photobiol. Sci. Off. J. Eur. Photochem. Assoc. Eur. Soc. Photobiol.* *1*, 1–21.

Olusanya, T.O.B., Haj Ahmad, R.R., Ibegbu, D.M., Smith, J.R., and Elkordy, A.A. (2018). Liposomal Drug Delivery Systems and Anticancer Drugs. *Molecules* *23*, 907.

Oniszczyk, A., Wojtunik-Kulesza, K.A., Oniszczyk, T., and Kasprzak, K. (2016). The potential of photodynamic therapy (PDT)—Experimental investigations and clinical use. *Biomed. Pharmacother.* *83*, 912–929.

Onodera, R., Motoyama, K., Okamatsu, A., Higashi, T., and Arima, H. (2013a). Potential use of Folate-appended Methyl- β -Cyclodextrin as an Anticancer Agent. *Sci. Rep.* *3*.

Ormond, A.B., and Freeman, H.S. (2013). Dye Sensitizers for Photodynamic Therapy. *Materials* *6*, 817–840.

Ossmann, A., Kranz, S., Andre, G., Völpel, A., Albrecht, V., Fahr, A., and Sigusch, B.W. (2015). Photodynamic killing of *Enterococcus faecalis* in dentinal tubules using mTHPC incorporated in liposomes and invasomes. *Clin. Oral Investig.* *19*, 373–384.

Panzarini, E., Inguscio, V., Fimia, G.M., and Dini, L. (2014). Rose Bengal Acetate PhotoDynamic Therapy (RBAC-PDT) Induces Exposure and Release of Damage-Associated Molecular Patterns (DAMPs) in Human HeLa Cells. *PLOS ONE* *9*, e105778.

- Piel, G., Piette, M., Barillaro, V., Castagne, D., Evrard, B., and Delattre, L. (2006). Betamethasone-in-cyclodextrin-in-liposome: The effect of cyclodextrins on encapsulation efficiency and release kinetics. *Int. J. Pharm.* 312, 75–82.
- Plenagl, N., Duse, L., Seitz, B.S., Goergen, N., Pinnapireddy, S.R., Jedelska, J., Brüssel, J., and Bakowsky, U. (2019). Photodynamic therapy – hypericin tetraether liposome conjugates and their antitumor and antiangiogenic activity. *Drug Deliv.* 26, 23–33.
- Pogue, B.W., Redmond, R.W., Trivedi, N., and Hasan, T. (1998). Photophysical Properties of Tin Ethyl Etiopurpurin I (SnET2) and Tin Octaethylbenzochlorin (SnOEBC) in Solution and Bound to Albumin. *Photochem. Photobiol.* 68, 809–815.
- PubChem Temoporfin.
- Pushpan, S.K., Venkatraman, S., Anand, V.G., Sankar, J., Parmeswaran, D., Ganesan, S., and Chandrashekar, T.K. (2002). Porphyrins in photodynamic therapy - a search for ideal photosensitizers. *Curr. Med. Chem. Anti-Cancer Agents* 2, 187–207.
- Puskás, I., and Csempeš, F. (2007). Influence of cyclodextrins on the physical stability of DPPC-liposomes. *Colloids Surf. B Biointerfaces* 58, 218–224.
- Puskás, I., Barcza, L., Szente, L., and Csempeš, F. (2006). Features of the Interaction between Cyclodextrins and Colloidal Liposomes. *J. Incl. Phenom. Macrocycl. Chem.* 54, 89–93.
- Rahman, S., Cao, S., Steadman, K.J., Wei, M., and Parekh, H.S. (2012). Native and β -cyclodextrin-enclosed curcumin: entrapment within liposomes and their in vitro cytotoxicity in lung and colon cancer. *Drug Deliv.* 19, 346–353.
- Rajewski, R.A., and Stella, V.J. (1996). Pharmaceutical applications of cyclodextrins. 2. In vivo drug delivery. *J. Pharm. Sci.* 85, 1142–1169.
- Reinhard, A., Sandborn, W.J., Melhem, H., Bolotine, L., Chamailard, M., and Peyrin-Biroulet, L. (2015). Photodynamic therapy as a new treatment modality for inflammatory and infectious conditions. *Expert Rev. Clin. Immunol.* 11, 637–657.
- Rekharsky, M.V., and Inoue, Y. (1998). Complexation Thermodynamics of Cyclodextrins. *Chem. Rev.* 98, 1875–1918.
- Reshetov, V., Zorin, V., Siupa, A., D'Hallewin, M.-A., Guillemin, F., and Bezdetnaya, L. (2012). Interaction of liposomal formulations of meta-tetra(hydroxyphenyl)chlorin (temoporfin) with serum proteins: protein binding and liposome destruction. *Photochem. Photobiol.* 88, 1256–1264.
- Reshetov, V., Lassalle, H.-P., François, A., Dumas, D., Hupont, S., Gräfe, S., Filipe, V., Jiskoot, W., Guillemin, F., Zorin, V., et al. (2013). Photodynamic therapy with conventional and PEGylated liposomal formulations of mTHPC (temoporfin): comparison of treatment efficacy and distribution characteristics in vivo. *Int. J. Nanomedicine* 8, 3817–3831.
- Rezzoug, H., Bezdetnaya, L., A'amar, O., Merlin, J.L., and Guillemin, F. (1998). Parameters Affecting Photodynamic Activity of Foscan® or Meta-tetra(hydroxyphenyl)chlorin (mTHPC) In Vitro and In Vivo. *Lasers Med. Sci.* 13, 119–125.
- Ris, H.B., Li, Q., Krueger, T., Lim, C.K., Reynolds, B., Althaus, U., and Altermatt, H.J. (1998). Photosensitizing effects of m-tetrahydroxyphenylchlorin on human tumor xenografts: correlation with sensitizer uptake, tumor doubling time and tumor histology. *Int. J. Cancer* 76, 872–874.
- Robertson, C.A., Evans, D.H., and Abrahamse, H. (2009). Photodynamic therapy (PDT): A short review on cellular mechanisms and cancer research applications for PDT. *J. Photochem. Photobiol. B* 96, 1–8.

Ronn, A.M., Nouri, M., Lofgren, L.A., Steinberg, B.M., Westerborn, A., Windahl, T., Shikowitz, M.J., and Abramson, A.L. (1996). Human tissue levels and plasma pharmacokinetics of temoporfin (Foscan®, mTHPC). *Lasers Med. Sci.* 11, 267–272.

Ronn, A.M., Batti, J., Lee, C.J., Yoo, D., Siegel, M.E., Nouri, M., Lofgren, L.A., and Steinberg, B.M. (1997). Comparative biodistribution of meta-Tetra(Hydroxyphenyl) chlorin in multiple species: clinical implications for photodynamic therapy. *Lasers Surg. Med.* 20, 437–442.

Sachar, M., Anderson, K.E., and Ma, X. (2016). Protoporphyrin IX: the Good, the Bad, and the Ugly. *J. Pharmacol. Exp. Ther.* 356, 267–275.

Saenger, W. (1980). Cyclodextrin Inclusion Compounds in Research and Industry. *Angew. Chem. Int. Ed. Engl.* 19, 344–362.

Sailor, M.J., and Park, J.-H. (2012). Hybrid nanoparticles for detection and treatment of cancer. *Adv. Mater. Deerfield Beach Fla* 24, 3779–3802.

Samad, A., Sultana, Y., and Aqil, M. (2007). Liposomal drug delivery systems: an update review. *Curr. Drug Deliv.* 4, 297–305.

Sasnouski, S., Zorin, V., Khludeyev, I., D'Hallewin, M.-A., Guillemin, F., and Bezdetsnaya, L. (2005). Investigation of Foscan interactions with plasma proteins. *Biochim. Biophys. Acta* 1725, 394–402.

Sasnouski, S., Kachatkou, D., Zorin, V., Guillemin, F., and Bezdetsnaya, L. (2006). Redistribution of Foscan® from plasma proteins to model membranes. *Photochem. Photobiol. Sci.* 5, 770–777.

Savary, J.F., Monnier, P., Fontollet, C., Mizeret, J., Wagnières, G., Braichotte, D., and van den Bergh, H. (1997). Photodynamic therapy for early squamous cell carcinomas of the esophagus, bronchi, and mouth with m-tetra (hydroxyphenyl) chlorin. *Arch. Otolaryngol. Head Neck Surg.* 123, 162–168.

Schneiderman, E., and Stalcup, A.M. (2000). Cyclodextrins: a versatile tool in separation science. *J. Chromatogr. B. Biomed. Sci. App.* 745, 83–102.

Senge, M.O. (2012). mTHPC – A drug on its way from second to third generation photosensitizer? *Photodiagnosis Photodyn. Ther.* 9, 170–179.

Senge, M.O., and Brandt, J.C. (2011). Temoporfin (Foscan®, 5,10,15,20-tetra(m-hydroxyphenyl)chlorin)--a second-generation photosensitizer. *Photochem. Photobiol.* 87, 1240–1296.

Senge, M.O., and Radomski, M.W. (2013). Platelets, photosensitizers, and PDT. *Photodiagnosis Photodyn. Ther.* 10, 1–16.

Shams, M., Owczarczak, B., Manderscheid-Kern, P., Bellnier, D.A., and Gollnick, S.O. (2015). Development of photodynamic therapy regimens that control primary tumor growth and inhibit secondary disease. *Cancer Immunol. Immunother. CII* 64, 287–297.

Shimpi, S., Chauhan, B., and Shimpi, P. (2005). Cyclodextrins: application in different routes of drug administration. *Acta Pharm. Zagreb Croat.* 55, 139–156.

Shirata, C., Kaneko, J., Inagaki, Y., Kokudo, T., Sato, M., Kiritani, S., Akamatsu, N., Arita, J., Sakamoto, Y., Hasegawa, K., et al. (2017). Near-infrared photothermal/photodynamic therapy with indocyanine green induces apoptosis of hepatocellular carcinoma cells through oxidative stress. *Sci. Rep.* 7, 13958.

Shliakhtsin, S.V., Trukhachova, T.V., Isakau, H.A., and Istomin, Y.P. (2009). Pharmacokinetics and biodistribution of Photolon® (Fotolon®) in intact and tumor-bearing rats. *Photodiagnosis Photodyn. Ther.* 6, 97–104.

- Siemann, D.W. (2011). The Unique Characteristics of Tumor Vasculature and Preclinical Evidence for its Selective Disruption by Tumor-Vascular Disrupting Agents. *Cancer Treat. Rev.* 37, 63–74.
- Škalko, N., Brandl, M., Bećirević-Laćan, M., Filipović-Grčić, J., and Jalšenjak, I. (1996). Liposomes with nifedipine and nifedipine-cyclodextrin complex: calorimetric and plasma stability comparison. *Eur. J. Pharm. Sci.* 4, 359–366.
- Slingerland, M., Guchelaar, H.-J., and Gelderblom, H. (2012). Liposomal drug formulations in cancer therapy: 15 years along the road. *Drug Discov. Today* 17, 160–166.
- Smith, G., McGimpsey, W.G., Lynch, M.C., Kochevar, I.E., and Redmond, R.W. (1994). An Efficient Oxygen Independent Two-Photon Photosensitization Mechanism. *Photochem. Photobiol.* 59, 135–139.
- Song, L.X., Bai, L., Xu, X.M., He, J., and Pan, S.Z. (2009). Inclusion complexation, encapsulation interaction and inclusion number in cyclodextrin chemistry. *Coord. Chem. Rev.* 253, 1276–1284.
- Stella, V.J., and He, Q. (2008). Cyclodextrins. *Toxicol. Pathol.* 36, 30–42.
- Stella, V.J., Rao, V.M., Zannou, E.A., and Zia, V. (1999). Mechanisms of drug release from cyclodextrin complexes. *Adv. Drug Deliv. Rev.* 36, 3–16.
- van Straten, D., Mashayekhi, V., de Bruijn, H.S., Oliveira, S., and Robinson, D.J. (2017). Oncologic Photodynamic Therapy: Basic Principles, Current Clinical Status and Future Directions. *Cancers* 9.
- Swartling, J., Axelsson, J., Ahlgren, G., Kälkner, K.M., Nilsson, S., Svanberg, S., Svanberg, K., and Andersson-Engels, S. (2010). System for interstitial photodynamic therapy with online dosimetry: first clinical experiences of prostate cancer. *J. Biomed. Opt.* 15, 058003.
- Swartling, J., Höglund, O.V., Hansson, K., Södersten, F., Axelsson, J., and Lagerstedt, A.-S. (2016). Online dosimetry for temoporfin-mediated interstitial photodynamic therapy using the canine prostate as model. *J. Biomed. Opt.* 21, 28002.
- Szeimies, R.M., Karrer, S., Abels, C., Steinbach, P., Fickweiler, S., Messmann, H., Bäuml, W., and Landthaler, M. (1996). 9-Acetoxy-2,7,12,17-tetrakis-(beta-methoxyethyl)-porphycene (ATMPn), a novel photosensitizer for photodynamic therapy: uptake kinetics and intracellular localization. *J. Photochem. Photobiol. B* 34, 67–72.
- Szejtli, J. (1998). Introduction and General Overview of Cyclodextrin Chemistry. *Chem. Rev.* 98, 1743–1754.
- Szente, L. (1999). Highly soluble cyclodextrin derivatives: chemistry, properties, and trends in development. *Adv. Drug Deliv. Rev.* 36, 17–28.
- Szente, L., and Fenyvesi, É. (2017). Cyclodextrin-Lipid Complexes: Cavity Size Matters. *Struct. Chem.* 28, 479–492.
- Taneja, S.S., Bennett, J., Coleman, J., Grubb, R., Andriole, G., Reiter, R.E., Marks, L., Azzouzi, A.-R., and Emberton, M. (2016). Final Results of a Phase I/II Multicenter Trial of WST11 Vascular Targeted Photodynamic Therapy for Hemi-Ablation of the Prostate in Men with Unilateral Low Risk Prostate Cancer Performed in the United States. *J. Urol.* 196, 1096–1104.
- Tardivo, J.P., Del Giglio, A., de Oliveira, C.S., Gabrielli, D.S., Junqueira, H.C., Tada, D.B., Severino, D., de Fátima Turchiello, R., and Baptista, M.S. (2005). Methylene blue in photodynamic therapy: From basic mechanisms to clinical applications. *Photodiagnosis Photodyn. Ther.* 2, 175–191.

Teiten, M.-H., Bezdetnaya, L., Morlière, P., Santus, R., and Guillemin, F. (2003a). Endoplasmic reticulum and Golgi apparatus are the preferential sites of Foscan localisation in cultured tumour cells. *Br. J. Cancer* 88, 146–152.

Thompson, D.O. (1997). Cyclodextrins--enabling excipients: their present and future use in pharmaceuticals. *Crit. Rev. Ther. Drug Carrier Syst.* 14, 1–104.

Thordarson, P. (2011). Determining association constants from titration experiments in supramolecular chemistry. *Chem Soc Rev* 40, 1305–1323.

Tikhomirov, A.M., Shmigol', T.A., Kozhinova, E.A., Kiagova, A.A., Bezdetnaia, L.N., and Potapenko, A.I. (2009). Investigation of aggregates of dyes by the method of resonance light scattering: correction of spectra. *Biofizika* 54, 824–830.

Torchilin, V.P. (2005). Recent advances with liposomes as pharmaceutical carriers. *Nat. Rev. Drug Discov.* 4, 145–160.

Torchilin, V.P. (2010). Passive and active drug targeting: drug delivery to tumors as an example. *Handb. Exp. Pharmacol.* 3–53.

Trachtenberg, J., Weersink, R.A., Davidson, S.R.H., Haider, M.A., Bogaards, A., Gertner, M.R., Evans, A., Scherz, A., Savard, J., Chin, J.L., et al. (2008). Vascular-targeted photodynamic therapy (padoporfin, WST09) for recurrent prostate cancer after failure of external beam radiotherapy: a study of escalating light doses. *BJU Int.* 102, 556–562.

Triesscheijn, M., Ruevekamp, M., Out, R., Van Berkel, T.J.C., Schellens, J., Baas, P., and Stewart, F.A. (2007). The pharmacokinetic behavior of the photosensitizer meso-tetrahydroxyphenyl-chlorin in mice and men. *Cancer Chemother. Pharmacol.* 60, 113–122.

Tromberg, B.J., Orenstein, A., Kimel, S., Barker, S.J., Hyatt, J., Nelson, J.S., and Berns, M.W. (1990). In vivo tumor oxygen tension measurements for the evaluation of the efficiency of photodynamic therapy. *Photochem. Photobiol.* 52, 375–385.

Trushina, O., Novikova, E., Filonenko, E., Chissov, V., and Vorozhtsov, G. (2011). Photosens PDT at the treatment of virus-associated precancer and non-invasive cervical cancer. *Photodiagnosis Photodyn. Ther.* 8, 217.

Uekama, K., and Otagiri, M. (1987). Cyclodextrins in drug carrier systems. *Crit. Rev. Ther. Drug Carrier Syst.* 3, 1–40.

Van Hees, T., Piel, G., Evrard, B., Otte, X., Thunus, L., and Delattre, L. (1999). Application of supercritical carbon dioxide for the preparation of a piroxicam-beta-cyclodextrin inclusion compound. *Pharm. Res.* 16, 1864–1870.

Van Ommen, B., De Bie, A.T.H.J., and Bär, A. (2004). Disposition of ¹⁴C-alpha-cyclodextrin in germ-free and conventional rats. *Regul. Toxicol. Pharmacol. RTP* 39 Suppl 1, 57–66.

Vanlangenakker, N., Vanden Berghe, T., Krysko, D.V., Festjens, N., and Vandenabeele, P. (2008). Molecular mechanisms and pathophysiology of necrotic cell death. *Curr. Mol. Med.* 8, 207–220.

Veenhuizen, R., Oppelaar, H., Ruevekamp, M., Schellens, J., Dalesio, O., and Stewart, F. (1997). Does tumour uptake of Foscan determine PDT efficacy? *Int. J. Cancer* 73, 236–239.

Vemuri, S., and Rhodes, C.T. (1995). Preparation and characterization of liposomes as therapeutic delivery systems: a review. *Pharm. Acta Helv.* 70, 95–111.

de Visscher, S.A.H.J., Melchers, L.J., Dijkstra, P.U., Karakullukcu, B., Tan, I.B., Hopper, C., Roodenburg, J.L.N., and Witjes, M.J.H. (2013). mTHPC-mediated photodynamic

therapy of early stage oral squamous cell carcinoma: a comparison to surgical treatment. *Ann. Surg. Oncol.* **20**, 3076–3082.

Vyas, A., Saraf, S., and Saraf, S. (2008). Cyclodextrin based novel drug delivery systems. *J. Incl. Phenom. Macrocycl. Chem.* **62**, 23–42.

Wagner, A., Denzer, U.W., Neureiter, D., Kiesslich, T., Puespoeck, A., Rauws, E.A.J., Emmanuel, K., Degenhardt, N., Frick, U., Beuers, U., et al. (2015). Temoporfin improves efficacy of photodynamic therapy in advanced biliary tract carcinoma: A multicenter prospective phase II study. *Hepatol. Baltim. Md* **62**, 1456–1465.

Wagnieres, G., Hadjur, C., Grosjean, P., Braichotte, D., Savary, J.F., Monnier, P., and van den Bergh, H. (1998). Clinical evaluation of the cutaneous phototoxicity of 5,10,15,20-tetra(m-hydroxyphenyl)chlorin. *Photochem. Photobiol.* **68**, 382–387.

Wang, X., Deng, L., Cai, L., Zhang, X., Zheng, H., Deng, C., Duan, X., Zhao, X., Wei, Y., and Chen, L. (2011). Preparation, characterization, pharmacokinetics, and bioactivity of honokiol-in-hydroxypropyl- β -cyclodextrin-in-liposome. *J. Pharm. Sci.* **100**, 3357–3364.

Wen, L.Y., Bae, S.-M., Do, J.H., Park, K.-S., and Ahn, W.S. (2011). The effects of photodynamic therapy with Photodithazine on HPV 16 E6/E7 associated cervical cancer model. *J. Porphyr. Phthalocyanines* **15**, 174–180.

West, C.M.L., West, D.C., Kumar, S., and Moore, J.V. (1990). A Comparison of the Sensitivity to Photodynamic Treatment of Endothelial and Tumour Cells in Different Proliferative States. *Int. J. Radiat. Biol.* **58**, 145–156.

Westermann, P., Glanzmann, T.M., Folli, S., Braichotte, D., Forrer, M., Andrejevic-Blant, S., Mach, J.-P., Monnier, P., and Bergh, H. van den (1995). Comparison of the influence of a water-soluble polymer carrier on the tumor localization and biodistribution of mesotetrametahydroxyphenylchlorin (mTHPC) in two animal models. In 5th International Photodynamic Association Biennial Meeting, (International Society for Optics and Photonics), pp. 45–51.

Whelpton, R., Michael-Titus, A.T., Basra, S.S., and Grahn, M. (1996). Distribution of temoporfin, a new photosensitizer for the photodynamic therapy of cancer, in a murine tumor model. *Photochem. Photobiol.* **61**, 397–401.

Yakavets, I., Yankovsky, I., Bezdetnaya, L., and Zorin, V. (2017a). Soret band shape indicates mTHPC distribution between β -cyclodextrins and serum proteins. *Dyes Pigments* **137**, 299–306.

Yakavets, I., Yankovsky, I., Millard, M., Lamy, L., Lassalle, H.-P., Wiehe, A., Zorin, V., and Bezdetnaya, L. (2017b). The alteration of temoporfin distribution in multicellular tumor spheroids by β -cyclodextrins. *Int. J. Pharm.* **529**, 568–575.

Yakavets, I., Lassalle, H.-P., Scheglmann, D., Wiehe, A., Zorin, V., Bezdetnaya, L., Yakavets, I., Lassalle, H.-P., Scheglmann, D., Wiehe, A., et al. (2018a). Temoporfin-in-Cyclodextrin-in-Liposome—A New Approach for Anticancer Drug Delivery: The Optimization of Composition. *Nanomaterials* **8**, 847.

Yakavets, I., Lassalle, H.-P., Yankovsky, I., Ingrosso, F., Monari, A., Bezdetnaya, L., and Zorin, V. (2018b). Evaluation of temoporfin affinity to β -cyclodextrins assuming self-aggregation. *J. Photochem. Photobiol. Chem.* **367**, 13–21.

Yakavets, I., Millard, M., Zorin, V., Lassalle, H.-P., and Bezdetnaya, L. (2019). Current state of the nanoscale delivery systems for temoporfin-based photodynamic therapy: Advanced delivery strategies. *J. Controlled Release* **304**, 268–287.

Yakavets, I.V., Yankovsky, I.V., Khludeyev, I.I., Lassalle, H.P., Bezdetnaya, L.N., and Zorin, V.P. (2018c). Optical Methods for the Analysis of the Temoporfin Photosensitizer

Distribution Between Serum Proteins and Methyl- β -Cyclodextrin Nanocarriers in Blood Serum. *J. Appl. Spectrosc.* *84*, 1030–1036.

Yankovsky, I., Bastien, E., Yakavets, I., Khludeyev, I., Lassalle, H.-P., Gräfe, S., Bezdetnaya, L., and Zorin, V. (2016). Inclusion complexation with β -cyclodextrin derivatives alters photodynamic activity and biodistribution of meta-tetra(hydroxyphenyl)chlorin. *Eur. J. Pharm. Sci. Off. J. Eur. Fed. Pharm. Sci.* *91*, 172–182.

Young, S.W., Woodburn, K.W., Wright, M., Mody, T.D., Fan, Q., Sessler, J.L., Dow, W.C., and Miller, R.A. (1996). Lutetium Texaphyrin (PCI-0123): A Near-Infrared, Water-Soluble Photosensitizer. *Photochem. Photobiol.* *63*, 892–897.

Yow, C.M., Chen, J.Y., Mak, N.K., Cheung, N.H., and Leung, A.W. (2000). Cellular uptake, subcellular localization and photodamaging effect of temoporfin (mTHPC) in nasopharyngeal carcinoma cells: comparison with hematoporphyrin derivative. *Cancer Lett.* *157*, 123–131.

Zappacosta, R., Cornelio, B., Pilato, S., Siani, G., Estour, F., Aschi, M., and Fontana, A. (2019). Effect of the Incorporation of Functionalized Cyclodextrins in the Liposomal Bilayer. *Molecules* *24*, 1387.

Zhang, J., Jiang, C., Figueiró Longo, J.P., Azevedo, R.B., Zhang, H., and Muehlmann, L.A. (2018). An updated overview on the development of new photosensitizers for anticancer photodynamic therapy. *Acta Pharm. Sin. B* *8*, 137–146.

Zhu, Q., Guo, T., Xia, D., Li, X., Zhu, C., Li, H., Ouyang, D., Zhang, J., and Gan, Y. (2013). Pluronic F127-modified liposome-containing tacrolimus–cyclodextrin inclusion complexes: improved solubility, cellular uptake and intestinal penetration. *J. Pharm. Pharmacol.* *65*, 1107–1117.

Zidovetzki, R., and Levitan, I. (2007). Use of cyclodextrins to manipulate plasma membrane cholesterol content: evidence, misconceptions and control strategies. *Biochim. Biophys. Acta* *1768*, 1311–1324.

SCIENTIFIC OUTPUT

SCIENTIFIC OUTPUT

ARTICLES IN PEER-REVIEWED JOURNALS

Yakovets I., Millard M., Zorin V., Lassalle H.-P., Bezdetsnaya L. Current state of the nanoscale delivery systems for temoporfin-based photodynamic therapy: Advanced delivery strategies. *J Control Release*. 2019; 304: 268-287.

Yakovets I., Jenard S., Francois A., Maklygina Y., Loschenov V., Lassalle H.-P., Dolivet G., Bezdetsnaya L. Stroma-Rich Co-Culture Multicellular Tumor Spheroids as a Tool for Photoactive Drugs Screening. *J Clin Med*. 2019; 8(10): E1686.

Mangeolle T., **Yakovets I.**, Lequeux N., Pons T., Bezdetsnaya L., Marchal F. The targeting ability of fluorescent quantum dots to the folate receptor rich tumors. *Photodiagn. Photodyn*. 2019; 26: 150-156.

Maklygina Y., Romanishkin I., Ryabova A., **Yakovets I.**, Bolotina L., Loschenov V. Investigation of the properties of a three-dimensional cell tumor model. *Bulletin of RSMU*. 2018; 6: 14-20.

Millard M., **Yakovets I.**, Piffoux M., Brun A., Gazeau F., Guigner J.-M., Jasniewski J., Lassalle H.-P., Bezdetsnaya L. mTHPC-loaded extracellular vesicles outperform liposomal and free mTHPC formulations by an increased stability, drug delivery efficiency and cytotoxic effect in tridimensional model of tumors. *Drug Deliv*. 2018. 25(1): 1790-1801.

Yakovets I., Lassalle H.-P. Scheglmann D., Wiehe A., Zorin V., Bezdetsnaya L. Temoporfin-in-cyclodextrin-in-liposome – a new approach for anticancer drug delivery: the optimization of composition. *Nanomaterials*. 2018; 8(10): 847-861.

Mangeolle T., **Yakovets I.**, Marchal S., Pons T., Bezdetsnaya L., Marchal F. Fluorescent nanoparticles for the guided surgery of ovarian peritoneal carcinomatosis. *Nanomaterials*. 2018; 8: 572 – 592.

Yakovets I., Lassalle H.P., Yankovsky I., Ingrosso F., Monari A., Bezdetsnaya L., Zorin V. Evaluation of temoporfin affinity to β -cyclodextrins assuming self-aggregation. *J Photochem Photobiol A*. 2018; 367: 13-21.

Yakovets I., Yankovsky I., Khludeyev I., Bezdetsnaya L., Zorin V. Optical Methods for the Analysis of the Temoporfin Photosensitizer Distribution Between Serum Proteins and Methyl- β -Cyclodextrin Nanocarriers in Blood Serum. *J Appl Spectrosc*. 2018; 84: 1030-1036.

Yakovets I., Yankovsky I., Millard M., Lamy L., Lassalle H.-P., Wiehe A., Zorin V., Bezdetsnaya L. The alteration of temoporfin distribution in multicellular tumor spheroids by β -cyclodextrins. *Int Journal Pharm*. 2017; 529: 568-575.

Millard M., **Yakovets I.**, Zorin V., Kulmukhamedova A., Marchal S., Bezdetsnaya L. Drug delivery to solid tumors: The predictive value of the multicellular tumor spheroid model for nanomedicine screening. *Int J Nanomed*. 2017; 12: 7993-8007.

Farrakhova D., **Yakovets I.**, Loschenov V., Bolotina L., Zorin V. Investigation of chlorin photosensitizers distribution in monolayer and spheroid cell cultures. *Biomedical Photonics*. 2017; 6(2): 4-11.

Yakovets I., Yankovsky I., Bezdetsnaya L., Zorin V. Soret band shape indicates mTHPC distribution between β -cyclodextrins and serum proteins. *Dyes Pigm*. 2017; 137: 299–306.

Yankovsky I., Bastien E., **Yakavets I.**, Khludeyev I., Lassalle H.-P., Gräfe S., Bezdetsnaya L., Zorin V. Inclusion complexation with β -cyclodextrin derivatives alters biodistribution and photosensitizing efficacy of meta-tetra(hydroxyphenyl)chlorin. *Eur J Pharm Sci.* 2016; 91: 172-182.

MAJOR ORAL COMMUNUCATIONS

Yakavets I., Lassalle H.-P., Zorin V., Bezdetsnaya L. *Cyclodextrin-based photoactive liposomal nanoparticles for tumor targeting.* 17th International Photodynamic association World Congress, 27 June - 4 July 2019, Boston, USA. 2019;

Yakavets I., Lassalle H.-P., Zorin V., Bezdetsnaya L. *Cyclodextrin-based photoactive liposomal nanoparticles for tumor targeting.* "Light and Life" 2019 ESP-IUPB World Congress, 25-30 August 2019, Barcelona, Spain. 2019;

Yakavets I., Millard M., Lassalle H.-P., Zorin V., Bezdetsnaya L. *Temoporfin-in-Cyclodextrin-in-Liposome nanoparticles for tumor targeting.* *Pharmaceutics & Novel Drug Delivery Systems* 2018, 4-8 October 2018, Moscow, Russia. 2018; 10: 32.

Yakavets I., Lassalle H.P., Bezdetsnaya L., Zorin V. mTHPC-in-cyclodextrin-in-liposome nanodelivery system. 11th European and Global Summit for Clinical Nanomedicine, Targeted Delivery and Precision Medicine (CLINAM), 1-5 September 2018, Basel, Switzerland. 2018; 230. (*short oral communication*)

Yakavets I., Lassalle H.P., Bezdetsnaya L., Zorin V. *Optimization of the composition of liposomal-based hybrid nanoparticles for mTHPC delivery.* 4th International conference Current Trends in Cancer Theranostics, 1-5 July 2018, Trakai, Lithuania. 2018; 74.

Yakavets I., Zorin V.P., Lassalle H.P., Bezdetsnaya L. *Cyclodextrin-based photoactive liposomal nanoparticles for tumor targeting.* 2nd Edition of Global Conference on Pharmaceutics and Drug Delivery Systems, 4-6 June 2018, Rome, Italy. 2018; 26.

Yakavets I., Yankovsky I., Lassalle H.P., Bezdetsnaya L., Zorin V. *Cyclodextrins as nanodelivery system in mTHPC-PDT.* 16th International Photodynamic Association World Congress, 8-13 June 2017, Coimbra, Portugal. 2017; 65.

COMMUNICATIONS PRESENTED BY COLLABORATORS

Farrakhova D., Maklygina Y., Romanishkin I., Ryabova A., **Yakavets I.**, Millard M., Bolotina L., Plyutinskaya A., Karmakova T., Pankratov A., Loschenov V. *Investigation of Ce6 accumulation and distribution in cell cultures of head and neck cancers.* Saratov Fall Meeting 2018: Optical and Nano-Technologies for Biology and Medicine, 23-27 September 2019, Saratov, Russia. 2019.

Millard M., **Yakavets I.**, Lassalle H.P., Piffoux M., Gazeau F., Silva A., Bezdetsnaya L. *Natural nanocarriers-based mTHPC for the photodynamic therapy.* International Conference On Nanomedicine And Nanobiotechnology – ICONAN 2018, 26-28 September 2018, Rome, Italy. 2018; 176.

Millard M., **Yakavets I.**, Lassalle H.-P., Zorin V., Kulmukhamedova A., Bezdetsnaya L. *Nanoparticle-based mTHPC delivery in the photodynamic therapy of cancer.* International Conference Laser Optics (ICLO), Saint Petersburg, Russia, 2018. 2018; 583.

Farrakhova D., **Yakavets I.**, Loschenov V., Bolotina L., Zorin V. *Comparitive accumulation study of chlorin group photosensitizers on monolayer and multicellular tumor spheroids of cell culture*. 2018 International Conference Laser Optics (ICLO), Saint Petersburg, Russia, 2018; 589.

Yankovsky I., **Yakavets I.**, Lassalle H.P., Bezdetsnaya L., Zorin V. *Alteration of temoporfin pharmacokinetics by β -cyclodextrin derivatives*. Applied Nanotechnology and Nanoscience International Conference – ANNIC 2017, 18-20 October, Rome, Italy. 2017; 118-120.

Millard, M., **Yakavets, I.**, Marchal, S., Lassalle, H.-P., Bezdetsnaya, L. *Influence of mTHPC liposomal distribution in multicellular spheroid on the photodynamic therapy efficacy*. Joint Congress of the French and Italian Photochemists and Photobiologists, September 19-22, 2016, Bari, Italy. 2016; 114.

SYNTHESE DES TRAVAUX

DE THESE

SYNTHESE DES TRAVAUX DE THESE

La thérapie photodynamique (PDT) est un traitement alternatif du cancer plus ciblé et moins invasif que les modalités traditionnelles. Au cours des dernières décennies, il a été démontré que la combinaison de médicaments utilisés en PDT (photosensibilisateurs, PS) avec des nano-plateformes de nanomatériaux permet une distribution précise des PS aux tissus cibles améliorant l'efficacité de la PDT. Étant donné que les PS les plus efficaces ont tendance à être des molécules hydrophobes insolubles avec une forte tendance à l'agrégation, leur encapsulation dans des nanovéhicules pourrait améliorer leurs propriétés pharmacocinétiques. De plus, les nanoparticules offrent la possibilité d'un ciblage actif, de libération contrôlée et de thérapies combinées multimodales.

La Temoporfine (mTHPC, nom du médicament : Foscan®), est l'un des PS les plus puissants cliniquement approuvés. Cependant, sa faible solubilité en milieu aqueux rend son administration compliquée. Ainsi, de nombreux travaux ont été réalisés afin de tester les nanoparticules comme systèmes d'administration de la temoporfine. Au cours des 25 dernières années, de nombreuses nanoplateformes comme les complexes d'inclusion, les nanoparticules lipidiques, les polymères et les nanotubes de carbone ont été chargées de temoporfine. Les études montrent que la formulation liposomale permettait de réaliser un ciblage sélectif du médicament qui rendait possible l'optimisation des paramètres pharmacocinétiques, de prévenir l'irritation locale et de réduire la toxicité du médicament, alors que les complexes d'inclusion à base de cyclodextrine modifient la biodistribution de la témporfine.

Aujourd'hui, on observe une certaine saturation dans le développement des nanomatériaux pour l'administration des médicaments. L'assemblage de plus d'un type de nanomatériaux dans une nanoparticule hybride pourrait être considéré comme une stratégie intéressante dans le développement de nonamédicaments (Deljoo et al., 2019; Sailor and Park, 2012; Yakavets et al., 2019). Les nanoparticules hybrides qui contiennent au moins deux nanoparticules distinctes assemblées dans une nanostructure fonctionnelle pourraient avoir des effets curatifs synergiques lorsque les nanomatériaux combinés sont soigneusement sélectionnés. Dans le cas de la mTHPC, nous avons proposé une association «liposomes et cyclodextrine » dans le nanoassemblage "médicament dans cyclodextrine dans liposome" (DCL). Ce DCL pourrait limiter la dissociation des complexes mTHPC/CD, éviter une libération rapide du médicament ainsi qu'améliorer la pénétration des PS dans les tissus tumoraux. Ainsi, nous avons supposé que la mTHPC-DCL pourrait dépasser les limitations de chaque nanostructure individuelle en fournissant un ciblage

passif de la tumeur par les liposomes et une pénétration profonde des complexes mTHPC/CD dans le tissu tumoral.

Les liposomes représentent des nanocapsules phospholipidiques qui pourraient être chargées de composés hydrophobes dans la bicouche lipidique ou de médicaments hydrophiles dans le noyau aqueux interne (Torchilin, 2005). Après environ deux décennies d'études, la formulation liposomale de mTHPC (Foslip[®]) est l'une des NP à base de mTHPC les plus efficaces et les plus étudiées (Reshetov et al., 2013). Les liposomes conventionnels encapsulent près de 8 % (p/p) de mTHPC dans une bicouche lipidique, ce qui permet la solubilisation complète d'une molécule de mTHPC hautement hydrophobe lors son administration. Le Foslip[®] présente une toxicité plus faible dans le noir et pourrait potentiellement cibler passivement la tumeur par effet EPR, améliorant ainsi la sélectivité de la distribution de la mTHPC. De plus, il a été démontré que le traitement Foslip[®]-PDT était plus efficace à des DLI plus courtes de 6 à 15 heures que la DLI de 24 heures pour le Foscan[®] (Reshetov et al., 2013). Toutefois, les liposomes ont une pénétration limitée dans les tissus tumoraux (Gaio et al., 2016; Millard et al., 2018), et libèrent rapidement la mTHPC dans le sang lors de l'interaction avec les composants sériques (Reshetov et al., 2013). En résumé, les liposomes apparaissent comme des nanocages puissantes, qui pourraient être améliorées par l'encapsulation de complexes supramoléculaires nanométriques mTHPC/CD.

Afin d'améliorer le transport de la mTHPC vers le tissu cible et de renforcer son accumulation intra-tissulaire, il a été proposé de coupler deux de ces systèmes de libération indépendants. Ainsi, l'objectif principal du présent travail a été de développer et d'optimiser la nanoconstruction de la molécule chargée de témporfine dans la cyclodextrine dans les liposomes (DCL) afin d'obtenir une combinaison synergique de deux systèmes de libération pour un relargage efficace de la mTHPC dans le tissu tumoral cible. Dans ce but, la complexation de la mTHPC avec des CDs et le comportement de ces complexes dans un modèle 3D de tissu tumoral *in vitro* ont été étudiés. De plus, de nouvelles méthodes d'analyse de la libération de la mTHPC à partir de CD ont été mises au point pour caractériser la structure de la mTHPC-DCL. In fine, la composition des mTHPC-DCL développés a été optimisée en fonction des études sur des modèles tumoraux 2D et 3D *in vitro*.

Les cyclodextrines (CD) ont été largement étudiées comme excipient pharmaceutique unique au cours des dernières décennies et sont encore à l'étude pour de nouvelles applications. Des rapports récents ont démontré la puissance des β -CDs sur des modèles de tumeurs précliniques *in vitro* et *in vivo* comme nanovéhicule de la mTHPC (Yankovsky et al., 2016). Des études approfondies sur les CD en tant qu'agents pharmaceutiques ont démontré que l'effet de la CD dépend fortement de l'affinité de la CD avec le médicament (Stella and

He, 2008). Lorsque nous avons affiné la valeur des constantes de liaison en supposant l'auto-agrégation des molécules de mTHPC, nous avons obtenu des valeurs beaucoup plus élevées que celles déjà rapportées dans la littérature (Bautista-Sanchez et al., 2005; Desroches et al., 2001). Selon nos calculs (Yakavets et al., 2018b), le TM- β -CD complètement méthylé montre la plus forte affinité ($K = 1,1 \times 10^7 \text{ M}^{-1}$) comparé au Me- β -CD ($K = 7,1 \times 10^5 \text{ M}^{-1}$) et au Hp- β -CD ($K = 1,7 \times 10^5 \text{ M}^{-1}$). On pourrait suggérer que la méthylation de β -CDs augmente leur affinité pour la mTHPC, permettant de moduler le comportement des PS dans les milieux biologiques. De plus, l'étude détaillée des propriétés photophysiques des complexes d'inclusion mTHPC/CD a révélé des changements de la forme de la bande de Soret de la mTHPC en fonction du complexe d'inclusion (Yakavets et al., 2017a). Nous avons confirmé, à l'aide de simulations de dynamique moléculaire (Yakavets et al., 2018), que les changements spectraux étaient induits par l'interaction des CD avec les groupes phényle, ce qui entraînait la rotation des substitués phényles (Yakavets et al., 2017a). Il est à noter que l'intercalation de la molécule de mTHPC dans le microenvironnement lipidique n'est possible qu'en conformation planaire, entraînant des changements opposés de la forme de la bande de Soret de la mTHPC. Ainsi, la technique spectrale basée sur la forme de la bande de Soret pourrait être utilisée pour la surveillance du microenvironnement de la mTHPC et pourrait être appliquée pour la détection des complexes mTHPC/CD dans le noyau aqueux des liposomes hybrides.

Comme il a été mentionné plus haut, la méthylation des β -CDs augmente leur affinité avec la mTHPC, ce qui permet de moduler le comportement des PS dans les milieux biologiques. Pour décrire le mécanisme d'altération, nous avons étudié la distribution de la mTHPC dans des sphéroïdes tumoraux multicellulaires 3D en présence de différents types de β -CDs (Yakavets et al., 2017). Nous avons constaté que l'accumulation de mTHPC dans les sphéroïdes dépend fortement du type et de la concentration des CD, comme cela a déjà été signalé pour les cellules monocouches (Yankovsky et al., 2016). En variant les concentrations de β -CDs, nous pourrions augmenter l'absorption de PS dans les sphéroïdes 3D et aussi l'inhiber. Nous avons montré que la β -CD avec une plus faible affinité pour la mTHPC (Hp- β -CD) a permis de tripler la concentration totale de PS, tandis que la Me- β -CD pourrait améliorer l'absorption de mTHPC au maximum 2 fois. Cependant, une constante d'affinité plus élevée de liaison des Me- β -CD à la mTHPC permet de transporter le PS dans les couches cellulaires plus profondes. Nous avons suggéré que la petite taille du complexe d'inclusion (environ 3 nm) ainsi que sa longue durée de vie déterminent le transport du PS dans la profondeur du tissu tumoral. Par ce mécanisme, la mTHPC se redistribue rapidement à partir des protéines sériques aux membranes cellulaires (absorption accrue) et diffuse facilement dans le milieu interstitiel (pénétration accrue). Par conséquent, il a été suggéré que la mTHPC/ β -CDs pourrait améliorer considérablement les propriétés des

liposomes chargés de mTHPC en améliorant la pénétration limitée des liposomes dans le tissu tumoral.

Après toutes les études préliminaires sur la formation du complexe d'inclusion, nous avons commencé à construire des liposomes hybrides. Afin de trouver la composition DCL la plus optimale pour l'administration de la mTHPC, nous avons synthétisé 9 compositions différentes basées sur trois types de β -CD (Hp-, Me- et TM- β -CD) et trois concentrations de charge de PS (Yakavets et al., 2018). La composition lipidique des vésicules DCL a été tirée du Foslip[®], de sorte que les caractéristiques physico-chimiques (taille et charge superficielle) des DCL étaient similaires à celles du Foslip[®]. En utilisant des techniques spectrales, nous avons confirmé la possibilité d'encapsuler la β -CD/mTHPC dans le noyau aqueux interne des liposomes sans détruire les liposomes et sans redistribution inattendue de la mTHPC dans la bicouche lipidique. Selon nos données, plus de 85% de la mTHPC était lié aux CDs à l'intérieur des liposomes. Nous avons également abordé la question de la stabilité colloïdale de la mTHPC-DCL grâce aux données de déstabilisation des liposomes en présence de β -CDs (Hammoud et al., 2019; Piel et al., 2006; Puskás et al., 2006). Selon les données de diffusion dynamique de la lumière, la stabilité colloïdale des DCL dépend du rapport de charge de la mTHPC: β -CD et du type de β -CD. Ainsi, les DCL ayant la charge de mTHPC la plus élevée basée sur le β -CD méthylé présentent une stabilité colloïdale pendant plus de 3 mois. Nous avons supposé que le facteur clé de la déstabilisation des DCLs était la concentration de molécules libres β -CD dans le noyau aqueux, qui éliminent les composants lipidiques formant des complexes d'inclusion (Fatouros et al., 2001; Szente and Fenyvesi, 2017; Uekama and Otagiri, 1987).

En ce qui concerne le criblage des mTHPC-DCLs dans la culture cellulaire en monocouche d'adénocarcinome du côlon HT29 et des sphéroïdes tumoraux multicellulaires 3D, nous avons révélé le rôle crucial de la concentration de charge de la mTHPC sur l'absorption intracellulaire. Les mTHPC-DCL à charge unique ont démontré une meilleure pénétration et distribution dans les sphéroïdes tumoraux, mais l'accumulation totale était significativement inférieure à celle du Foslip[®] en raison de la liaison de la mTHPC hautement compétitive avec les CD, les protéines sériques des membranes liposomales et les cellules. Ainsi, nous avons amélioré les mTHPC-DCL en les chargeant dans la bicouche lipidique comme c'est le cas pour le Foslip[®]. Les caractéristiques physico-chimiques ainsi que la stabilité colloïdale des DL-DCL n'ont pas été modifiées par rapport aux mTHPC-DCL. La charge de concentrations élevées de mTHPC dans la bicouche lipidique a entraîné un quenching de fluorescence et a été confirmée par spectroscopie. Dans l'ensemble, 70% de la mTHPC était liée dans la bicouche lipidique et 30% du PS était encapsulé dans le noyau aqueux interne avec des β -CDs, ce qui était très proche pour les prévisions théoriques. De

cette façon, les DL-DCL fournissent une accumulation cellulaire appropriée de PS dans les cultures cellulaires 2D et 3D. Cependant, en ce qui concerne l'objectif principal qui était d'augmenter la capacité de pénétration de la mTHPC dans les tissus tumoraux, nous avons principalement concentré nos études sur le modèle de sphéroïdes multicellulaire. Nous avons démontré une amélioration significative de la distribution de la mTHPC grâce à l'utilisation de la nanoconstruction TD. Les cellules des sphéroïdes traités par TD ont accumulé de façon presque homogène la mTHPC, ce qui a été confirmé par cytométrie de flux et microscopie de fluorescence, tandis que le MD a montré une distribution de la mTHPC principalement à la périphérie des sphéroïdes ainsi que Foslip[®]. Nous avons supposé que l'affinité extrêmement élevée de la mTHPC pour TM- β -CD conduit à la formation de complexes d'inclusion à vie longue capables de transférer la mTHPC en profondeur du tissu tumoral. Ainsi, nous avons pu détecter des complexes d'inclusion de la mTHPC/TM- β -CDs dans le milieu de culture après une incubation de 24 heures avec des sphéroïdes, alors que les complexes de Me- β -CD ont une durée de vie plus courte, entraînant une pénétration limitée de la mTHPC dans les sphéroïdes.

Néanmoins, les avantages des DL-DCL en tant que système d'administration de la mTHPC n'ont pas été suffisants pour améliorer l'efficacité PDT dans le sphéroïde tumoral multicellulaire *in vitro* ainsi que chez les souris ayant subi une xénogreffe tumorale *in vivo*. Malgré l'amélioration de la distribution de la mTHPC dans les sphéroïdes, la mort cellulaire induite par la TPD dans les sphéroïdes traités par TD et MD était similaire à celle de Foslip[®]. De même, chez les souris xénogreffées de tumeurs, le délai de croissance tumorale moyen était de 30 jours pour la TD ainsi que pour le Foslip[®]. Nos études en cours portent sur différents paramètres expérimentaux permettant l'optimisation de la DL-DCL dans des modèles précliniques. L'une des solutions possibles est l'incorporation dans les liposomes d'un composant favorisant la libération de nanoshuttles CD après stimulation.

La présente étude a confirmé l'avantage des mTHPC-DCL à double charge par rapport aux formulations liposomales de mTHPC classiques (Foslip[®]) en termes de pénétration dans les tissus tumoraux. Dans l'ensemble, les vésicules lipidiques de type matryoshka proposées qui libèrent des complexes mTHPC/CD illustrent un équilibre optimal entre la stabilité plasmatique et la libération efficace de PS.

ABSTRACT

Photodynamic therapy (PDT) is an alternative cancer treatment which offers a more targeted and less invasive treatment regimen compared to traditional modalities. Temoporfin (mTHPC, medicinal product name: Foscan[®]), is one of the most potent clinically approved PS. However, its poor solubility in aqueous medium caused several complications of its administration. The present study is aimed at the development of drug-in-cyclodextrin-in-liposome (DCL) nanoparticles by coupling two independent delivery systems: cyclodextrin/mTHPC inclusion complexes and liposomal vesicles to improve the transport and penetration of mTHPC to the target tissue. The formation of inclusion complexes between cyclodextrins and mTHPC was studied in detail. Based on these data, single and double loaded mTHPC-DCLs have been prepared, optimized and characterized. It was demonstrated that mTHPC-DCLs are stable and almost all mTHPC is bound to β -CDs in the inner aqueous liposome lumen. The influence of DCLs on mTHPC accumulation, distribution and photodynamic efficiency was studied in human adenocarcinoma HT29 cellular monolayer and spheroid models. Using 3D multicellular HT29 tumor spheroids we demonstrated that trimethyl- β -CD-based DCL provides homogenous accumulation of mTHPC across tumor spheroid volume thus supposing optimal mTHPC distribution.

Key-Words : Photodynamic therapy, mTHPC, cyclodextrins, binding constants, drug-in-cyclodextrin-in-liposomes, multicellular tumor spheroids.

RESUME

La thérapie photodynamique (PDT) est un traitement alternatif du cancer plus ciblé et moins invasif que les modalités traditionnelles. La Temoporfine (mTHPC, nom sous forme médicamenteuse : Foscan[®]), est l'un des PS les plus puissants cliniquement approuvés. Cependant, sa faible solubilité en milieu aqueux a provoqué plusieurs complications lors de son administration. La présente étude vise à mettre au point des nanoparticules constituées d'une molécule anticancéreuse couplée à la cyclodextrine intégré dans un liposome (drug-in-cyclodextrin-in-liposome, DCL) en couplant deux systèmes d'administration indépendants : les complexes d'inclusion cyclodextrine-mTHPC et les vésicules liposomales pour améliorer le transport et la pénétration de la mTHPC dans le tissu cible. La formation de complexes d'inclusion entre les cyclodextrines et la mTHPC a été étudiée en détail. Sur la base de ces données, des mTHPC-DCL à simple et double charge ont été préparées, optimisées et caractérisées. Il a été démontré que les mTHPC-DCL sont stables et que presque tous les mTHPC-DCL sont liés à β -CDs dans la lumière aqueuse interne des liposomes. L'influence des DCLs sur l'accumulation, la distribution et l'efficacité photodynamique de la mTHPC a été étudiée dans des modèles cellulaires en monocouche et sphéroïde multicellulaires 3D d'adénocarcinome de pharynx humain (HT29). En utilisant des sphéroïdes, nous avons démontré que le DCL à base de triméthyl- β -CD fournissait une accumulation homogène de la mTHPC dans tout le volume des sphéroïdes tumoraux, suggérant ainsi une distribution optimale de la mTHPC.